Faculdade de Ciências do Mar e do Ambiente
UNIVERSIDADE DO ALGARVE

Sediment Dynamics and Tidal Inlet Relocation in Mixed-Energy Settings: The case of Ancão Inlet (Algarve - Portugal)

by

Ana Vila Concejo

Dissertação apresentada à Universidade do Algarve para obtenção do grau de Doutor em Ciências do Mar, especialidade em Oceanografia.

FARO, 2003

Para Brad, por todo.

Para mis padres, Michel y Teté, por su apoyo.

NOTE: *The main parts of this thesis correspond to scientific papers that were published or are being published in international scientific journals included in the citation index. However, for the structure of the thesis, all the methods are compiled in Chapter 4 and the results, discussions and conclusions are in Chapters 5, 6, 7 and 8.*

Abstract

The main aim of this thesis is to study the sedimentary dynamics of mixed energy tidal inlets on different time scales (from hours to decades) as well as to analyse inlet relocation as a coastal management tool. The field studies were carried out in the Ria Formosa, a multi-inlet barrier island system located in southern Portugal.

Long Term Studies: The four natural inlets of the Ria Formosa were studied for the period between the 1940's and 1996. Inlet width and position of the inlet channel were determined using a series of vertical aerial photos and charts. The objective was to determine the association between inlet migration patterns and different hydrodynamic conditions, major storms and engineering interventions. Results indicate that natural inlet opening and evolution were mainly affected by three factors: (a) the existence of sub-embayments (western and eastern) inside the system, (b) exposure to wave energy, and (c) inlet efficiency. Two distinctive eastward migration patterns were found by analysing the correlation coefficient (r) between inlet width evolution and inlet migration and by the comparison of the shape of the curves fitted to the inlet migration behaviour. Typical migration of the high-energy flank is characterised by an initial stage of readjustment, with low migration rates, followed by a stage of high eastward migration rates, up to a limiting position. Inlet width remains reasonably constant during the entire migration cycle, thus the correlation between inlet width and position is very low. Typical inlets on the low-energy flank are formed by barrier breaching during major storms and produce, initially, very wide inlets. Eastward inlet migration on the low-energy flank follows a natural logarithmic curve where channel migration is accompanied by strong constructional processes on the updrift barrier. Due to subsequent inlet width reductions, the correlation between inlet width and position is significant.

Medium Term Studies: A monitoring program, including the acquisition of a series of topo-bathymetric surveys and oblique aerial photos, has been carried

out at Ancão Inlet since its artificial opening in June 1997. The results (morphologic and volumetric) were analysed with relation to the prevailing oceanographic conditions. This allowed the development of a conceptual evolutionary model for the natural evolution of artificially opened inlets with 4 stages: Stage 1 is the artificially opened inlet; Stage 2 represents the inlet after reaching dynamic equilibrium for the channel and while it is developing the deltas; Stage 3 is the *mature migrating inlet*; and Stage PS (Post-Storm) is the inlet situation after high-energy conditions. Transition between stages 1 to 3 is a continuous process with intermediate sub-stages. Transition to Stage PS is a discrete phenomenon, caused by high-energy events, after which the inlet continuously changes back to the previous stage.

Short Term Studies: Three sediment transport studies using tracers were performed at Ancão Inlet. The objectives of the experiments were to determine and understand the sediment transport pathways and magnitudes on the updrift margin of an inlet. In order to apply the traditionally used Space Integration Methodology to the tracer experiments, some adaptations had to be made. The division of the study area into morphologically defined sectors was found to be a key factor for the applicability of tracers in such a complex area. Therefore, 4 sectors were defined: Sector A representing the straight part of the updrift beach; Sector B being the upper area of the swash platform; Sector C being the lower area of the swash platform; and Sector D representing the inner parts of the inlet margin. The integrated study of all data (wind, waves, currents, tracer distribution and topographic evolution) led to the determination of the sediment pathways. Three tidal stages (TS), associated with distinctive sediment transport patterns, were found to occur at the inlet margin during each tidal cycle: TS1 implies flooding currents, and thus, transport towards the inside of the inlet area, both on the swash platform and the inner parts of the inlet area; during TS2 flooding currents transporting sediments towards the inlet occur on the swash platform whilst the interaction of the flooding currents with the flood delta produces the development of an anticlockwise internal gyre (IG) that results in ebbing currents occurring in the inner inlet margin; TS3 implies ebbing transport both in the inner margin and the swash platform. Evidence of the existence of a clockwise external gyre (EG) on the swash platform was found. A semi-quantitative conceptual model was developed in order to explain the sediment transport pathways and magnitudes that a known mass of sediment would follow after arriving at the swash platform. It was found that the areas with the

largest sediment accumulation were Sector B and C, whilst almost no sediment was retained in Sector D which underwent strong erosive processes. According to the model only 48% of the initial mass of sediments are still in the system after two tidal cycles. It is hypothesised that sediment losses are due to sediment transport towards the ebb delta and to sediment by-passing occurring from the ebb delta to the downdrift beach through swash bar processes. The herein defined conceptual model represents a useful tool that could be applied to other tidal inlets under similar conditions, facilitating sediment budget studies around tidal inlets.

Inlet Relocation Assessment: Two inlets were relocated in the Ria Formosa and were the subject of a monitoring program that included the acquisition of quantitative (topo-bathymetric surveys) data. The data obtained from the monitoring program were analysed together with the wave climate and then compared with historical information on the natural inlets, in order to assess the degree of success of the relocation actions. One of the relocations studied, Ancão Inlet, was considered to be successful even though an initial unexpected behaviour produced some material damage to property. On the contrary, the relocation of Fuzeta Inlet, did not have the expected results and the new inlet was effected by the same problems as the old one.

It was found that the most important factor for a relocation action to succeed is the correct choice of the location of the opening. A theoretical procedure to enhance the possibilities of relocation success is suggested: (1) Hydrodynamic studies are needed in order to determine if the present conditions are similar to the historical ones. (2) The position for the inlet opening is chosen according to the hydrodynamic conditions but there are other factors to be taken into account, i.e., the historical migration paths and typical inlet width of the natural inlet; the hydrodynamics of the backbarrier; the morphology of the backbarrier and, for multi-inlet barrier island systems, the proximity to adjacent inlets. (3) Once the position is chosen, environmental impact studies should be made in order to assess the risk of the relocation for the ecosystems of the area. Only if the environmental impact studies are favourable, should a relocation action be performed.

Resumo

O objectivo principal desta tese é o estudo da dinâmica sedimentar em barras de maré de ambientes mistos a várias escalas temporais (de horas a décadas) assim como analisar a utilidade da relocalização de barras como uma ferramenta de gestão costeira. Os trabalhos de campo foram efectuados na Ria Formosa, um sistema de ilhas barreira com múltiplas barras, localizado no Sul de Portugal.

Estudos de Longo Termo: Foram estudadas as quatro barras naturais da Ria Formosa para o período compreendido entre a década de 1940 (data incerta) e 1996. As larguras e posições das barras foram determinadas com recurso a fotografias aéreas verticais e a cartas náuticas. O objectivo deste trabalho foi determinar a relação entre os padrões de migração das barras e as diferentes condições hidrodinâmicas, ocorrência de tempestades de alta energia e intervenções de engenharia costeira. Os resultados obtidos indicam que os processos de abertura e evolução natural das barras foram afectados principalmente por três factores: (a) a existência de sub-sistemas lagunares (ocidental e oriental), (b) a exposição à agitação incidente, e (c) a eficiência da barra. Pela análise do coeficiente de correlação (r) entre a largura e a localização das barras, e pela comparação da forma das curvas de ajuste com as curvas de migração das barras, foram determinados dois padrões típicos de migração para oriente. A migração típica do flanco de alta energia está caracterizada por uma fase inicial de reajuste, com taxas de migração baixas, seguida de uma fase de migração para oriente, com elevadas taxas de migração, até atingir uma posição limite. A largura da barra permanece razoavelmente constante durante todo o ciclo de migração, e portanto, a correlação entre a largura e a localização da barra é muito baixa. As barras do flanco de baixa energia são tipicamente formadas através da rotura da ilha barreira, durante tempestades de alta energia sendo geralmente muito largas na fase inicial. A curva de migração para oriente destas barras, segue um padrão de logaritmo natural, onde a migração do canal da barra é acompanhado por processos de construcção muito significativos na margem a barlamar da barra. Devido

às subsequentes reduções da largura da barra, a correlação entre a largura e a localização da barra é significativa.

Estudos de Médio Termo: A Barra do Ancão foi relocalizada em Junho de 1997, e tem sido monitorizada através de medições topo-batimétricas e de fotografias aéreas oblíquas. Os resultados (morfológicos e volumétricos) foram analisados junto com as condições oceanográficas, o que permitiu o desenvolvimento de um modelo conceptual para a evolução de barras relocalizadas. Este modelo tem 4 fases de evolução: A Fase 1 caracteriza a barra após a sua relocalização; a Fase 2 representa a barra depois do canal ter atingido o equilíbrio dinâmico, e quando os deltas de enchente e de vazante ainda estão em desenvolvimento; a Fase 3 corresponde à *barra migratória madura*; e a Fase PS resulta da resposta da barra a uma tempestade de alta energia. A transição entre as fases 1 a 3 é um processo contínuo que envolve sub-fases intermédias. A transição para a Fase PS é um evento discreto, causado por uma tempestade de alta energia, após a qual, a barra evoluirá de forma contínua para a fase anterior à tempestade.

Estudos de Curto Termo: Foram efectuadas três campanhas de estudo de transporte sedimentar com recurso a luminóferos (traçadores fluorescentes) na Barra do Ancão. Os objectivos destas campanhas foram compreender e determinar os padrões e magnitudes do transporte sedimentar na margem a barlamar de uma barra de maré. Devido às características da área de estudo, nomeadamente a sua morfologia não rectilínea e a existência de correntes bidireccionais, foi necessário efectuar uma adaptação do método tradicional (*"Space Integration Method"*). Verificou-se que a divisão da área de estudo em sectores definidos morfologicamente foi um factor chave na aplicação de luminóferos numa área complexa. Assim, foram definidos 4 sectores: O Sector A representa a parte rectilínea da praia a barlamar da barra; O Sector B é a parte mais elevada da *swash platform*; O Sector C representa a parte baixa da *swash platform*; O Sector D é representativo das partes internas da margem a barlamar da barra. O estudo integrado de todos os dados (incluindo dados de vento, ondas, correntes, distribuição de luminóferos e evolução topográfica) permitiu a determinação dos padrões de transporte sedimentar. Verificou-se a existência de três fases dentro do ciclo de maré (TS), associadas a diferentes padrões de transporte sedimentar: TS1 implica a existência de correntes de enchente, e portanto, transporte sedimentar para as partes internas da margem a barlamar da barra, quer desde a *swash platform*, quer desde os sectores internos; durante a fase TS2, as correntes de enchente transportam sedimento desde a *swash platform* para as partes internas da barra.

Simultaneamente, devido à interacção das correntes de enchente com o delta de enchente, desenvolve-se um giro interno, no sentido antihorário (IG) que produz correntes de vazante nos sectores internos da margem a barlamar da barra; a fase TS3 implica transporte de vazante quer nos sectores internos, quer na *swash platform*. Ainda durante esta fase, verificou-se a existência de um giro externo, no sentido horário, na zona da *swash platform*. A análise dos resultados permitiu o desenvolvimento de um modelo conceptual semiquantitativo para explicar os padrões e as magnitudes do transporte sedimentar que uma massa conhecida de sedimento seguiria caso chegasse à zona de estudo. Verificou-se que os sectores com a maior acumulação de sedimento foram o Sector B e o Sector C, enquanto que o Sector D apresentou forte erosão. Segundo este modelo, só o 48% da massa inicial de sedimento mantém-se no sistema após dois ciclos de maré. Adicionalmente, é sugerido que as perdas de sedimento correspondem ao transporte sedimentar para o delta de vazante e aos processos de transposição sedimentar através de *swash bars*. O modelo conceptual definido nesta tese representa uma ferramenta que poderia ser aplicada a outras barras de maré de características similares, facilitando os estudos do balanço sedimentar em áreas donde existam barras de maré.

Avaliação da relocalização de barras: Duas das barras da Ria Formosa (Barra do Ancão e Barra da Fuzeta) foram relocalizadas. Desde a sua abertura foram objecto de programas de monitorização sobre tudo através de medições topo-batimétricas. Os dados assim obtidos foram analisados em conjunto com os dados da agitação marítima, e foi efectuada a comparaçãoda sua evolução com o comportamento histórico das barras naturais. Esta comparação foi feita com o objectivo de avaliar o grau de sucesso das acções de relocalização. A relocalização da Barra do Ancão foi considerada uma intervenção bem sucedida, mesmo considerando que o inesperado comportamento inicial produziu alguns danos materiais. Pelo contrário, a relocalizaçãoda Barra da Fuzeta não teve os resultados esperados, mostrando, a barra nova, os mesmos problemas que causaram a relocalização da barra antiga.

Verificou-se que o factor mais importante a ter em conta para o sucesso de uma acção de relocalização, é a escolha adequada do local da abertura artificial. Como resultado dos estudos efectuados, é proposto um procedimento teórico para melhorar as possibilidades de sucesso de uma relocalização: (1) O estudo do hidrodinamismo da zona é importante para determinar se as condições hidrodinâmicas actuais são semelhantes às históricas. (2) O local de abertura da barra deverá

ser escolhido, não só em função das condições hidrodinâmicas, mas também de outros factores como, por exemplo, a largura do canal e os padrões históricos de migração da barra; o hidrodinamismo da zona lagunar; a morfologia da laguna; e, para sistemas de multiplas barras, a proximidade das barras adjacentes. (3) Uma vez decidido o local de abertura da barra nova é preciso avaliar os riscos ecológicos associados à relocalização, portanto deverão ser efectuados os devidos estudos de impacte ambiental. A relocalização só deverá ser efectuada caso os resultados dos estudos de impacte ambiental sejam favoráveis.

Contents

List of Figures

List of Tables

Notation

ϵ	Surf scaling parameter (Guza and Inman, 1975).
ξ_b	Surf similarity parameter (Battjes, 1974).
η_{dtr}	Daily tidal range.
η^*_{dtr}	Maximum tidal range.
θ_p	Mean wave direction at peak period.
ρ_s	Sand density.
Ω	Tidal prism.
A_c	Cross-sectional area of the inlet throat.
A_{Ri}	Area represented by each sampling point in tracer experiments.
B	Inlet channel width in Gerritsen and Dunsbergen (1998) stability equation.
d	Distance between the FT injection point and the location of the FT_C in tracer experiments.
d_L	Distance between the injection point and the FT_{CL} in tracer experiments.
EG	External gyre (sediment transport paths on the swash platform).
F_{mi}	Multiplying factor used to extrapolate the results of a sample to the entire represented area in tracer experiments.
FT	Fluorescent tracers.
FT_C	Total cloud centroid (vertical integration of FT_{CL}) in tracer experiments.
FT_{CL}	FT cloud centroid for each layer in tracer experiments.
$FT_{injected}$	Mass of FT injected in the study area in tracer experiments.
h	Height of the samples in tracer experiments.
H_s	Significant wave height.

IG	Internal gyre (sediment transport paths on the swash platform).
k	Radius of the sample (corer or container) in tracer experiments.
L_1	Loss of sediments after 1 tidal cycle, t=1 (semi-quantitative conceptual model for sediment transport at the swash platform).
L_2	Losses of sediment at t=2 (semi-quantitative conceptual model for sediment transport at the swash platform).
L_2B	Losses of sediment due to the reworking from sector B (semi-quantitative conceptual model for sediment transport at the swash platform).
L_2C	Losses of sediment due to the reworking from sector C (semi-quantitative conceptual model for sediment transport at the swash platform).
L_2D	Losses of sediment due to the reworking from sector D (semi-quantitative conceptual model for sediment transport at the swash platform).
LTS1	First low tide sampling in tracer experiments.
LTS2	Second low tide sampling in tracer experiments.
MD_{LEV}	Maximum number of days with continuous '*Levante*' conditions.
M_2C	Mass of sediment that is reworked from Sector C for stage 2 of the model (semi-quantitative conceptual model for sediment transport at the swash platform).
M_2D	Mass of sediment that is reworked from Sector D for stage 2 of the model (semi-quantitative conceptual model for sediment transport at the swash platform).
M_A	Known mass of sediment arriving at the western limit of the swash platform at t=0 (semi-quantitative conceptual model for sediment transport at the swash platform).
M_i	Mass of remaining FT in each representative area in tracer experiments.
M_L	Mass of remaining FT for each layer in tracer experiments.
M_{Si}	Mass of FT found in each sample in tracer experiments.
M_T	Total mass of FT remaining in the study area in tracer experiments.
MSL	Mean sea level.
n	Number of FT grains found in each sample in tracer experiments.
NOL	Natural opening location for a tidal inlet.

P	Deep water incident wave power.
P_n	P normalised with the predicted tidal data.
$PRFT$	Percentage of remaining FT in tracer experiments.
$PRFT_1$	Percentage of remaining FT at t=1 (semi-quantitative conceptual model for sediment transport at the swash platform).
$PRFT_2$	Percentage of remaining FT at t=2 (semi-quantitative conceptual model for sediment transport at the swash platform).
Q	Sediment transport rate.
r	Pearson-r correlation coefficient.
SB_1	Percentage of remaining FT in Sector B at t=1 (semi-quantitative conceptual model for sediment transport at the swash platform).
SB_2	Percentage of remaining FT in Sector B at t=2 (semi-quantitative conceptual model for sediment transport at the swash platform).
SC_1	Percentage of remaining FT in Sector C at t=1 (semi-quantitative conceptual model for sediment transport at the swash platform).
SC_2	Percentage of remaining FT in Sector C at t=2 (semi-quantitative conceptual model for sediment transport at the swash platform).
SD_1	Percentage of remaining FT in Sector D at t=1 (semi-quantitative conceptual model for sediment transport at the swash platform).
SD_2	Percentage of remaining FT in Sector D at t=2 (semi-quantitative conceptual model for sediment transport at the swash platform).
t	Time.
T_p	Peak wave period.
TS1	Tidal stage 1.
TS2	Tidal stage 2.
TS3	Tidal stage 3.
$tan\ \beta_{bf}$	Profile slope for the beach face.
$tan\ \beta_{sp}$	Profile slope for the swash platform.
V_{ebb}	Sand volume of the ebb-tidal delta.
V_{FT}	Average grain volume of the FT in tracer experiments.
$V(FT_C)$	Total velocity of the FT_C in tracer experiments.

$V(FT_{CL})$	Velocity of displacement of the tracer centroid for each layer in tracer experiments.
V_{Ri}	Representative volume for each sample in tracer experiments.
V_S	Sample volume in tracer experiments.
V_{max}	Maximum tidal velocity.
X_i	X co-ordinate for each sampling point in tracer experiments.
$X(FT_C)$	X co-ordinate for each FT_C in tracer experiments.
$X(FT_{CL})$	X co-ordinate for each FT_{CL} in tracer experiments.
Y_i	Y co-ordinate for each sampling point in tracer experiments.
$Y(FT_C)$	Y co-ordinate for each FT_C in tracer experiments.
$Y(FT_{CL})$	Y co-ordinate for each FT_{CL} in tracer experiments.
Z_o	thickness of the active layer (area given by the average cross-shore profile of mixing depth) in tracer experiments.
Z_{oi}	Mixing depth for each corer sample in tracer experiments.
Z.H.	Hydrographic Zero, Portuguese datum located 2 m below mean sea level.

Acknowledgements

It goes without saying that a PhD cannot be done without the help of many people. I guess that this becomes even more true when the thesis is made in a foreign country and written in a foreign language.

I especially want to thank my supervisors João M. Alveirinho Dias and Óscar M. Cerveira Ferreira for their invaluable support. Their support has been essential, both their professional and scientific advice and also the friendship they both have given to me since my arrival in March 1998.

I want to thank Brad for more or less everything. He is everything I ever wanted. His love, care, support and patience (especially during the last months of the writing) have been essential for me to be able of finishing this PhD. Thank you for your love and for being so good to me. On the professional side, he has discussed with me every part of my work, giving me really useful suggestions. He also has helped me with some of the data analyses, especially with Matlab, and he has come to the field with me all of the times that were needed. Also, he is the person that has read, I don't know how many times, all of my work and has helped me with the English and for that he deserves at least a medal! Also, he is the one who taught me how to use LaTeX, the software I have used to write this thesis.

Working at CIACOMAR has been a gratifying experience. Despite the isolation, we are too far from Gambelas, we have managed to make of the place a good working space. I thank all the people that have shared the office with me, especially to Ana Matias because she has done it for a very long time and, aside from the interesting discussions about coastal processes, we have become very good friends. Thanks also to André and Brad that have been as patient as Matias during these last months when I was lost, stressed and probably unbearable. The three of them, together with Tiago and Óscar, form the littoral group I belong to, and they have been going to the fieldwork all the time in order to

save my time to write this thesis. I thank them for that. Large thanks also go to the rest of the good people that works or have worked there. Also, I want to thank Rui Taborda and Paolo Ciavola for their help and advice. Paolo is now a great friend and I thank him for that.

I want to thank my parents, Michel and Teté for the education, love and support they have given to me over all of these years. My sisters have also been there, to fight or to laugh, but always giving me love and support. Also to Josele and, of course, Miguelito. This acknowledgement extends to the rest of my family, too numerous to be named here, but with an special mention to both my grandmas, Tere and Matilde. Also to the Australian family, I do not get to see them very often but they are great.

Irene Alejo, from Vigo University, encouraged me to do post-graduate studies; for that, and for being a good friend, I want to thank her. Also, I want to thank Javito, from Cádiz University, because he is the one that sent me the announcement for the INDIA fellowship that I had when I first came to the University of Algarve. The decision to move to Faro was made with the help of my family, Irene Alejo and also my very good friends Ana García and Patricia Quintas. I thank Ana (por los nuestros!) and Patri for the friendship; it has been very important for me.

The support, kindness and friendship that all the people showed me when I arrived here is something that I will never forget and that I will be always grateful for. All of these people made sure that I was not alone and tried their best to make me feel good. Learning the language was tough (and sometimes funny) and slow, but with the help of everybody (special mention goes to Carla and Ana Matias!), I passed from Galician to Portunhol and finally, to Portuguese. Carla was a good friend from the beginning and I really enjoyed the two years we spent sharing the crazy house at Montenegro.

The work for the INDIA project was a really interesting (and intense) experience. I had never worked in a big project and the INDIA project was big and had too many deadlines. Also, through the long search, many times for impossible material/equipment, and innumerable days and nights making fieldwork at the inlet, I made some very good friends (that I want to thank for their help and friendship) like Roos, Axel, Robert, Paul, Jon, Mark... and a very special one, Brad, my husband, that has been making me happy ever since.

I also want to thank all the people that helped during the INDIA intensive

fieldwork campaigns. Tracer campaigns, like the ones we did, imply many people and we made three campaigns in three months. I thank Patrícia Silva for spending her time (and eyes) counting the samples from AMI.1-1. Special thanks also to Nuno Lourenço and Miguel Castro for making a team with me to develop the automatic system for tracer counting. The FENIX system really made my life easier.

The Parque Natural da Ria Formosa kindly supplied the first topo-bathymetric maps, both from Ancão (June 1997) and Fuzeta (July and August 1999) Inlets. The Ancão surveys of August 1997 and April 1998, were made in collaboration with the Direção Regional do Algarve (DRA). I want also to thank Custódio Contreiras and his team for their availability to work at any time and under any meteorological conditions (except rain!) in the topo-bathymetric surveys that were made both at Ancão and Fuzeta inlets. Armando, Silvério and Capela, from the PNRF drove the boat in all of the Ancão surveys, and many times worked extra-time only to fit with the tides. Sr. Zé drove the boat for the Fuzeta surveys. The first campaigns at Fuzeta Inlet were organised and made first by Célia Duarte and then by Catarina Sá-Pires. I only organised those that were made during the year 2001.

For the topo-bathymetric surveys, many of my friends and colleagues got a prism and went, literally, running on the deltas and beaches, and thus, became a part of our own and special *Delta-Force*. I want to thank all of them because I know it is tough physical work and also because they did it only to help me. I also thank the oceanography students that came to help me in the last campaigns; I hope that the experience was as useful for them as it was to me.

I thank also Tim Kana and Bill Cleary for supplying me with information about other relocation actions that were performed in the USA. This information has been very useful for the analysis of my results.

I also want to thank all my friends, those that are here and those that are all over the world. You are very important to me. My friends here in Portugal have become almost a part of my family. Special thanks to the Spanish crew (and aggregates) for speaking in Spanish and allowing my brain a little rest, also for the great moments that we have spent together. Thank you to all the people that have shared a Thursday at Havana Bar, and/or a weekend in Zambujeira do Mar.

Financial support for this thesis has been partially supplied by several projects:

The INDIA (INlet Dynamics Initiative: Algarve) project from the European Marine Science and Technology program (MAST3-CT97-0106).

The CROP (Cross-shore Processes in contrasting Environments) from the Fundação para a Ciência e a Tecnologia de Portugal (PDCTM/MAR/15265/99).

Several protocols between the CIACOMAR-CIMA-IMAR and the Instituto de Conservação da Natureza de Portugal (ICN) through the Parque Natural da Ria Formosa (PNRF):

- Monitorização da Barra Nova do Ancão (1997-1998).
- Monitorização da Barra Nova da Fuzeta (1999-2000).
- Monitoirzação das Barras do Ancão e da Fuzeta (2001).

Wave and tidal data between 1997 and 2001 was supplied by the Instituto Hidrgráfico de Portugal.

Some of the data that was used for the analysis of the short-term AMI campaigns was obtained, under the framework of the INDIA project, by other INDIA partners:

- The University of Amsterdam acquired and processed the wind data that was used for the analysis of the short-term AMI campaigns.
- BODC (British Oceanographic Data Centre) acquired and processed the wave data from the Triaxys buoy.

Chapter 1

Introduction

"Tell us a story!" said the March Hare.

"Yes, please do!" pleaded Alice.

"And be quick about it," added the Hatter, "or you'll be asleep again before it's done."

Lewis Carroll, *"Alice in Wonderland."*

Barrier islands are very complex and delicate systems that have constantly been an important focus of attention for researchers all around the world. Due to natural and anthropogenic factors such as sea level rise, variations in sediment supply, storm events, dune occupation or coastal engineering actions, some of these systems are showing serious problems in maintaining their natural characteristics and consequently, their coastal dynamic equilibrium. For this reason, many studies are being carried out in order to gain a better knowledge and understanding of these complex systems, including the inlets which separate the islands since they are often the most dynamic part of the system. Besides their environmental importance in exchanging water from restricted backbarrier areas, and keeping the dynamic equilibrium of the coastal system, coastal inlets often play an important role in navigation representing the only access to some harbours or coastal populations. As a consequence, many papers have been recently published focusing on the subjects of inlet evolution and behaviour (i.e., Hicks and Hume, 1997; Ranasinghe *et al.*, 1998; Stauble, 1998; Williams *et al.*, 1998; Marden and Cleary, 1999; Johnsen *et al.*, 1999; Morang, 1999; Ranasinghe and Pattiaratchi, 1999; FitzGerald *et al.*, 2001; Williams *et al.*, 2003). Motivation for most of these studies results from a need for improving the knowledge of natural and artificial inlet evolution, since a great number of inlets have direct and indirect impacts on regional economy (navigation, aquaculture, etc.). Some papers are based on inlet evolution monitoring and their results can be helpful in the planning of future coastal management (i.e., Kana and Mason, 1988; Cialone *et al.*, 1999; Forbes and Solomon, 1999; Galgano and Leatherman, 1999).

Due to the natural and anthropogenic factors mentioned above, many tidal inlets have undergone significant hydrodynamic changes. These hydrodynamic changes have implied: faster migrating rates, an unexpected migration (i.e., Forbes and Solomon, 1999), realignment of the channel making navigation difficult (i.e., Hands and Shepsis, 1999) or threatening a coastal population (i.e., Kana and Mason, 1988). Tidal inlets can also represent a hazard to neighbouring areas since they induce strong shoreline variations; these hazardous situations become worse when the tidal inlet is a migrating one.

Traditional engineering solutions to tidal inlet coastal hazards are hard pro-

tection techniques such as inlet stabilisation by jetties. The jetties are intended to make navigation safer and channel maintenance cheaper. However, such structures have severe environmental problems and imply a high aesthetic impact (Pilkey and Wright, 1988). One of the main environmental problems associated with jetties is the interruption of the longshore sediment transport. Long jetties extending thousands of metres into the sea may trap and retain millions of cubic metres of sand on the upcoast side (i.e., Penland, 1979; Pilkey and Neal, 1980; C.E.R.C., 1984).

It has been only recently that coastal managers have started to use a soft protection engineering technique that, when applied to migrating inlets, involves the artificial opening of a new tidal inlet along the historic migration path of the inlet. The old inlet is then artificially closed or it is left open and will eventually close when the new inlet captures the entire tidal prism. A secondary benefit of inlet relocation is the release of sediment from the abandoned inlet that allows the shoals on the ebb-tidal delta to move onshore and naturally nourish the downdrift beach (Kana, 2003). Once the inlet is relocated, the degree of success depends on: (1) the hydrodynamic efficiency of the new inlet to remain open and (2) that the new inlet is not causing the same problems as the old one. However, even in a successful relocation, the new inlet is likely to start migrating downdrift and therefore, some time later (typically decades), it will reach the same position and will start to cause the same problems as before the relocation. A new relocation will be needed once the relocated inlet has again reached the problematic position.

Inlet relocation is a soft protection management tool that permits the protection of the coastal zone without implying a large environmental impact. The concept of this approach is to work with natural processes, rather than confronting nature (www.coastalhazards.wcu.edu, 2002). It simply reproduces, when done correctly, the natural evolution of a migrating inlet. However, it has not been widely used. There are only a few examples where inlet relocation has been undertaken. The oldest record of inlet relocation, found in the literature, corresponds to the relocation of Tubbs Inlet (North Carolina, USA) (www.coastalhazards.wcu.edu, 2002). The relocation of Tubbs Inlet was completed in 1969/70 and since then, the inlet has been migrating in the opposite direction to its historic migration trends (Dr. W.J. Cleary, Personal Communication, 2003). No publications were found regarding the evolution of this relocated inlet.

The case of Captain Sam's Inlet (South Carolina, USA) is probably the best known since several publications have been made after its relocation (i.e., Ma-

son, 1986; Kana and Mason, 1988; Kana and McKee, 2003). According to these authors Captain Sam's is a small mesotidal inlet that was relocated in February 1983. The relocation was undertaken because the migration of the inlet plus the realignment of the channel was threatening a coastal population. The relocation was successful and no damages occurred: the relocated inlet was no longer threatening the coastal population. However, by 1995 the inlet was again in the same position where it had been before the relocation (CSE, 1995). Therefore, the inlet was successfully relocated for the second time in April 1996 (CSE, 2001). A comprehensive analysis of the relocations made at Captain Sam's Inlet is given in Kana and McKee (2003).

Inlet relocation has been recently used in Portugal. The relocated inlets were Ancão and Fuzeta inlets (in 1997 and 1999 respectively), both located in the Ria Formosa barrier island system (on the southern coast of Portugal). The results of these relocations are presented and evaluated in Chapter 6 and Chapter 8 of this thesis.

Most recently, Mason Inlet (North Carolina, USA) was threatening a coastal population (Cleary, 2002) and was relocated in March 2002 (Broders, 2002; Erickson *et al.*, 2003). The relocation was paid for by property owners who have agreed on a 30-year maintenance dredging commitment, which enables them to re-dredge the inlet up to 9 times in the next 30 years if it starts to move outside a defined corridor (Broders, 2002). During the first year after the relocation, the location of Mason Inlet has been mostly stable, thus not representing a threat to the property; however, it has been acting as a sediment trap and therefore undergoing infilling processes (Erickson *et al.*, 2003). Cleary and FitzGerald (2003) made a study of the changes induced by the relocation finding a significant increase in tidal prism. As a consequence of the inlet being flood dominated, they predicted further infilling of the inlet. Moreover, their estimations predict that once the sand from the former ebb-tidal delta is reworked and transported downdrift, the shoreline immediately downdrift of the new inlet will be likely to experience erosion.

Some other inlet relocations are presently being considered, for example, Kraus *et al.* (2003) provide the details about the hypothetical relocation of Fire Island Inlet (New York, USA). Cleary *et al.* (2003) explain the future relocation of the ebb channel (not the entire inlet) for Bogue Inlet (North Carolina, USA).

The study of the sediment budget in inlet areas is a key element for the successful planning and execution of any engineering interventions. According to Rosati and Kraus (1999) inlets increase the complexity of sediment budgets because sediment transport magnitudes and pathways are difficult to define due to the combined effect of tidal currents (ebb and flood), and waves over a complex bathymetry. Therefore improving the knowledge of sediment transport inside inlet systems is needed in order to provide a better understanding of their evolution.

According to Allen (1988) sediment tracer studies apparently provide the best information on nearshore transport. Sediment transport studies using fluorescent tracers have been very important in the development of sediment transport theories that are nowadays widely used by coastal scientists and engineers. It was in the 1960's that the international scientific community started to use fluorescent coating or paints on sand in order to perform sediment transport studies. The work of, for example, Zenkovitch (1969), Abecasis *et al.* (1962), Yasso (1965), Yasso (1966) and Ingle (1966) can be considered as pioneering in a technique that in the following decades became widespread all around the world. Since then, sediment tracer studies have been widely used for the study of sediment transport on straight beaches (i.e., Komar and Inman, 1970; Komar, 1977; Kraus *et al.*, 1982; Kraus, 1985; Michel, 1997; Ciavola *et al.*, 1997a, 1998). The results from these and other studies (not using tracers) were then used for the development of empirical formulae to calculate longshore transport (i.e., C.E.R.C., 1984; Kamphuis *et al.*, 1986). However, sediment tracer techniques have also been applied to more complex systems such as swash platforms (Oertel, 1972), a tidal inlet (Penland, 1979), submarine sand banks (Collins *et al.*, 1995), swash bars on swash platforms (Balouin, 2001) and harbours (Ferreira *et al.*, 2002), and provided useful information on sediment transport.

Aims of the Study

The main aim of this thesis is to study the sedimentary dynamics of mixed energy tidal inlets at different time scales (from hours to decades) as well as to analyse inlet relocation as a coastal management tool. This thesis represents a scientific contribution to two of the areas of knowledge about mixed energy tidal inlets that presently have a lack of data and results: (a) Inlet relocation and (b) Sediment pathways and magnitudes at tidal inlets.

The main parts of this thesis correspond to scientific papers that were published or are being published in international scientific journals included in the citation index. However, for the structure of the thesis, all the methods are compiled in Chapter 4 and the results, discussions and conclusions are in Chapters 5, 6, 7 and 8.

Outline

The studies were made for the natural inlets of the Ria Formosa barrier island system (Southern Portugal) and were specially focused on two relocated inlets: Ancão and Fuzeta inlets. For achieving the above mentioned objectives, this thesis is structured as follows:

- A general review of tidal inlet dynamics is given in Chapter 2. A brief review of the main studies that have been performed on tidal inlets is presented. Results concerning tidal inlets with similar characteristics to those studied in this work are emphasised.
- The study area is presented in Chapter 3. A brief review of the main characteristics of the natural inlets of the Ria Formosa barrier island system is given. Special emphasis is applied to the two relocated inlets.
- The methodology used both for acquiring the data and for analysing them is explained in Chapter 4.
- Long term studies. Historical data is important in order to analyse the present behaviour of tidal inlets. Therefore, a study of the recent evolution (∼1945-1996) of the natural inlets of the Ria Formosa was made. This study is presented in Chapter 5.
- Medium term studies. The evolution of Ancão Inlet in the two years that followed its relocation is presented in Chapter 6. A conceptual model with the stages of a relocated inlet of similar characteristics to Ancão Inlet is given in this chapter.
- Short term studies. Tracer studies were performed on the updrift margin of Ancão Inlet. The results obtained for the sediment transport pathways and magnitudes are presented in Chapter 7. A semi-quantitative conceptual model that explains the sediment transport on the updrift margin of a tidal inlet is also presented in this chapter.

- Relocation assessment. In Chapter 8 a general assessment of the relocation actions that were carried out in the Ria Formosa is presented. Data presented is comprised of the inlet evolution over four years for Ancão Inlet and two years for Fuzeta Inlet. A schematic with the theoretical procedures to follow in order to perform a relocation is also presented.
- The general conclusions regarding all the analyses performed are summarised in Chapter 9.
- A bibliographic list of the references cited in this thesis is given in Chapter 10.
- A list of publications and technical reports that were produced under the framework of this thesis is presented in Chapter 11.
- The topo-bathymetric maps corresponding to Ancão and Fuzeta inlets are in Appendix A.

Chapter 2

A review of tidal inlet dynamics

"Still round the corner there may wait
A new road or a secret gate;
And though I oft have passed them by,
A day will come at last when I
Shall take the hidden paths that run
West of the Moon, East of the Sun."

J.R.R. Tolkien *"The Lord of the Rings."*

A general review of tidal inlet dynamics is presented in this chapter. Due to their environmental and economic importance, tidal inlets have been the object of many investigations for many years all around the world. Due to the large number of studies, the main results concerning tidal inlets with similar characteristics to the ones of the Ria Formosa barrier island system are highlighted in this chapter.

Tidal inlets are openings in the shore line through which water penetrates the land, thereby providing a connection between the ocean and bays, lagoons or marsh and tidal creek systems (FitzGerald, 1996). The main channel of a tidal inlet is maintained by tidal currents (Escoffier, 1940). According to FitzGerald (1996) the second part of this definition distinguishes tidal inlets from open embayments or rock-bound passage-ways where there is little or no mobile sediment. However, according to the same author, one side of the inlet may be bedrock outcrops or a bedrock headland. According to Huntley and Nummedal (1978) tidal inlets are complex regions whose continually changing morphology is the result of the interaction of wave and tidal forces acting on the nearshore sediments. Tidal inlets are also the key environments in the behaviour of coastal lagoons, since inlets condition sediment, salinity, nutrients, pollutant and organism dispersal between the lagoon and the ocean (Isla, 1995).

A significant part of the world's coastline consists of barrier island systems (Bakker and de Vriend, 1995). Barrier islands occur in greatest abundance where broad low-relief coastal plains lie adjacent to the inner shelf and they constitute almost 12% of the world's coastline (Glaeser, 1978). The morphology of barrier islands is influenced by a number of factors including mode of formation, sediment supply, sea-level rise, and wave and tidal processes (FitzGerald *et al.*, 1984). According to FitzGerald *et al.* (1984) when the supply of sediment is sufficient to maintain the barrier system the primary control of its general morphology is the hydrographic regime of the region.

Hayes (1979) made a study of barrier island morphology as a function of tidal and wave regime. Through the application of the tidal range classification of Davies (1964) to the study of shoreline morphology, Hayes (1979) found five general categories of shoreline and established their relation with the presence

or absence of barrier island systems and tidal inlets. However, it is important to note that the Hayes (1979) classification was made assuming a constant and moderate wave climate, thus, studying the effects of the variation in tidal range for a given area with moderate wave climate.

The five categories of the Hayes (1979) classification system are:

(1) The microtidal coast (mean tidal range <1 m) is characterised by long, narrow and rather straight barriers with widely spaced inlets.

(2) The low-mesotidal coast (mean tidal range is 1-2 m) is characterised by increasing numbers of tidal inlets with washovers diminishing. It is a coast of mixed tidal and wave energy but with waves dominant (Davis and Hayes, 1984). Tidal inlets, that occur infrequently along the coast, typically have large flood deltas, but due to the wave dominance, ebb deltas are small or absent (FitzGerald, 1996) and have a slightly arcuate shape (FitzGerald *et al.*, 2001). These inlets are usually small (widths <200 m) with shallow main channels (depths <6 m) (FitzGerald *et al.*, 2001).

(3) The high-mesotidal coast (mean tidal range 2-3.5 m) has abundant tidal inlets, large ebb tidal deltas and drumstick barriers. It is also a mixed-energy coast but tides are dominant (Davis and Hayes, 1984). Tidal inlets comprise a significant portion (>15%) of the shoreline and ebb deltas are well formed and strongly influence wave refraction patterns along the inlet shoreline (FitzGerald, 1996). According to the same author, the presence of flood deltas, in these conditions, is dependent on the amount of open water area in the backbarrier (i.e., more open water provides more room for flood delta development).

(4) The low-macrotidal coast (mean tidal range 3.5-5 m) may have some wave-built bars but barriers are not developed.

(5) The macrotidal coast (mean tidal range >5 m) has numerous tidal-current formed ridges and extensive tidal flats and marshes.

According to Davis and Hayes (1984), the above mentioned classification by Hayes (1979) uses tidal ranges that tend to develop similar morphologies through a spectrum of wave climates. Also, the classification is generally restricted to coastal areas with moderate wave energy. The length of barriers along an island chain can be correlated to tidal range and wave energy (Hayes, 1979) because

these factors and others, notably bay area, control the size and number of tidal inlets (FitzGerald, 1988).

2.1 Inlet Morphology

Tidal currents are responsible for the continual removal of sediment that is transported towards the inlet from the adjacent shores (FitzGerald, 1996). The sand carried into the bay mostly by the flood tidal currents forms one or more flood-tidal deltas and sediment transported seaward by the ebb discharge forms the ebb-tidal delta (i.e., Isla, 1995; FitzGerald, 1996). Tidal range and wave action are the main processes responsible for the shape of the deltas (Isla, 1995).

In Figures 2.1 and 2.2 the main components of a tidal inlet are presented. According to Davis (1996) there are basically three major parts to a tidal inlet:

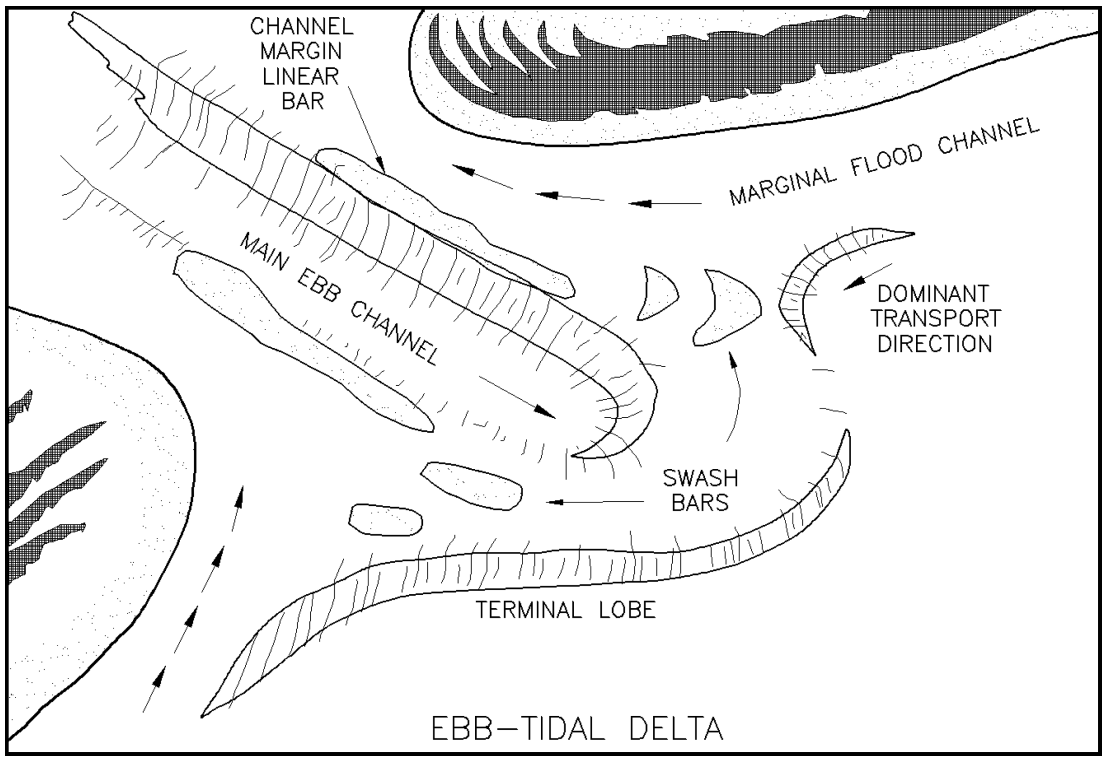

Figure 2.1: Morphology of a tidal inlet, from Seabergh (2002), after Hayes (1980).

(1) The inlet throat. This corresponds to the channel between the adjacent barrier islands and through which the tidal flux passes. The dimensions of this opening are dependent on the area of the enclosed bay and the tidal range (Leatherman, 1988). A cross-section of the throat typically reveals an

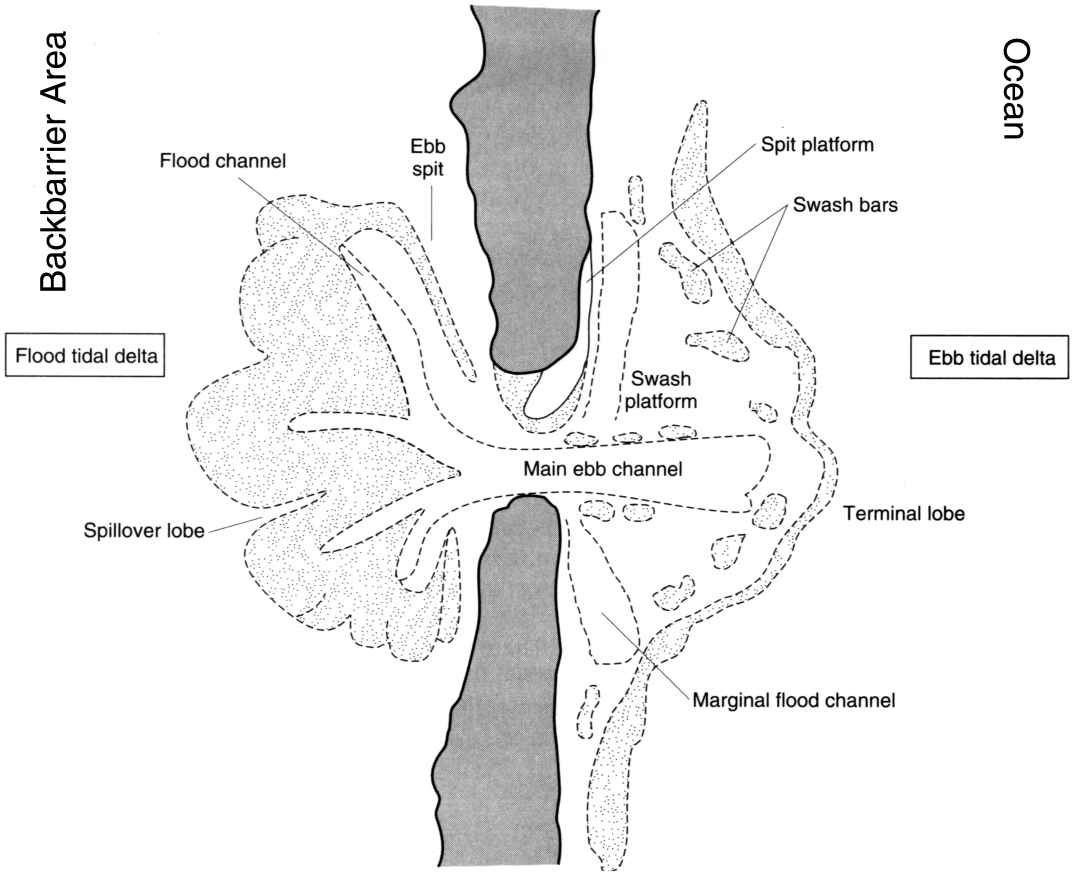

Figure 2.2: Morphology of a tidal inlet, from Davis (1996).

asymmetrical shape, normally being deeper on the side that corresponds to the direction of the net longshore sediment transport (Davis, 1994). Sand transport in the main channel is dominated by ebb currents (Dyer and Huntley, 1999).

(2) The ebb-tidal delta. Ebb-tidal deltas are accumulations of sand which front tidal inlets and are formed by the interaction of tidal- and wave-generated currents (Smith and FitzGerald, 1994). According to Huntley and Nummedal (1978) the most prominent feature of an ebb tidal delta is a broad relatively deep central channel, terminating on the seaward side with a deltaic fan of sediment often many kilometres offshore. This channel is the continuation of the ebb channel, or main channel of the inlet. This channel is flanked on either side by linear bars, and broad sheets of sand known as swash platforms on which shoreward migrating swash bars are commonly observed (Huntley and Nummedal, 1978).

(3) The flood-tidal delta. This delta is usually larger than the ebb delta

since the bay (or backbarrier area) is a relatively low energy environment (Leatherman, 1988). The flood delta of a migrating inlet normally migrates with the inlet, however, it usually leaves behind some portion of the sediment accumulated by the delta. According to Leatherman (1988) once an inlet closes or migrates downdrift, the abandoned flood-tidal delta, or the parts of it remaining after the migration, serve as platforms upon which salt marshes can develop.

According to FitzGerald (1988) tidal inlets not only trap sand temporarily on their deltas, but they also are responsible for the longer term loss of sediment due to sand transport into the backbarrier environment or deposition at prograding inlet channels.

According to the literature (i.e., Hayes, 1975; Davis, 1996), the shape of flood-tidal deltas are generally fan- or horseshoe-shaped with a broad ramp that slopes up to the surface on the landward end. This ramp is a shallowing continuation of the inlet channel and carries sediment to the tidal delta during flooding tides. When the tidal range is at least 1.5 m (as in the Ria Formosa), the ebbing tides are deflected around the lobes of the flood delta, producing a sand body with at least a modest amount of relief. The outer part of the tidal delta is smoothed by the ebbing currents, which carry some sediment and deposit it in the form of ebb spits, and breaches may form in the high part of the flood delta forming spillover lobes. The overall configuration of the flood delta resembles the outline of a horseshoe (Figure 2.3).

According to Davis (1996), ebb-tidal deltas exhibit greater variation than flood deltas because they are exposed to open water waves. Assuming that a substantial sediment supply is available, the controlling factors of the size and shape of the ebb-tidal delta are the tidal currents and their interaction with wave-generated processes. The three general types of ebb deltas are tide-dominated, mixed energy and wave-dominated. The tide-dominated ebb deltas tend to protrude into the sea essentially shore-normal with well developed sand bars along the margins. The mixed energy ebb deltas have a generally smoothed and arcuate sandbar (also called the Terminal Lobe), and the wave-dominated ebb deltas have very little sediment accumulated at all. According to Morang and Parson (2002) the ebb-tidal delta is formed by the following components (see Figure 2.2):

- A main ebb channel, scoured by the ebb currents.

- Linear bars that flank the main channel, the result of wave and tidal current interaction.
- A terminal lobe, located at the seaward end of the ebb channel and the adjacent barrier islands.
- Swash platforms, which are sand sheets located between the main ebb channel and the adjacent barrier islands.
- Swash bars that form and migrate across the swash platforms because of currents generated by breaking waves.
- Marginal flood channels, which often flank both updrift and downdrift barriers.

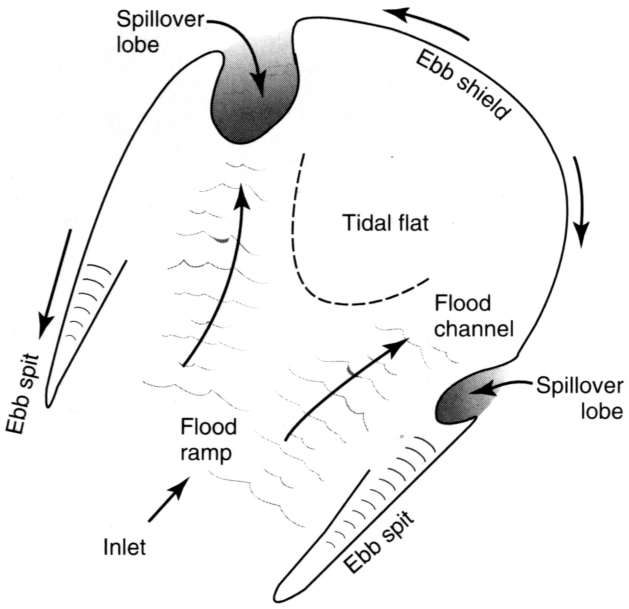

Figure 2.3: Morphology of a flood-tidal delta, from Davis (1996), after Hayes (1975).

Ebb-tidal deltas are shaped by the ebb currents issuing from the inlet mouth and modified by wave action, they rely on the sand being transported seaward and deposited when the flow diverges (Dyer and Huntley, 1999). Figure 2.4 shows the four general types of ebb-delta according to the balance of currents (Oertel, 1988 *in* Morang and Parson, 2002). Morang and Parson (2002) affirmed that, with some modifications, these models could apply to most inlets. According to Buonaiuto and Kraus (2003) the slopes on ebb deltas typically do not exceed 4-6°, with seaward slopes being 1-2° steeper than the landward slopes.

Sediment transport patterns on the ebb delta were studied by Oertel (1972) and Smith and FitzGerald (1994). According to Oertel (1972) the interaction between waves and currents appears to be the most important factor for the sediment budget of an ebb-tidal delta: Waves commonly 'break' at points of interference with currents creating wave bores that travel shoreward. Thus, sediment being transported seaward by tidal flow is diverted landward in gyral-paths by wave bores. The resultant 'sediment gyres' are dynamic sediment traps which cause accumulations of sand on swash platforms (Oertel, 1972). Smith and FitzGerald (1994) studied the sediment transport patterns of the ebb-tidal delta of an ebb-dominated inlet, finding that the movement of sand within the ebb delta is characterised by two sediment circulation gyres involving the main channel and adjacent swash platforms. The same authors calculated the sediment transport rates and found that more sand was being circulated in the sediment gyres than bypassing the inlet.

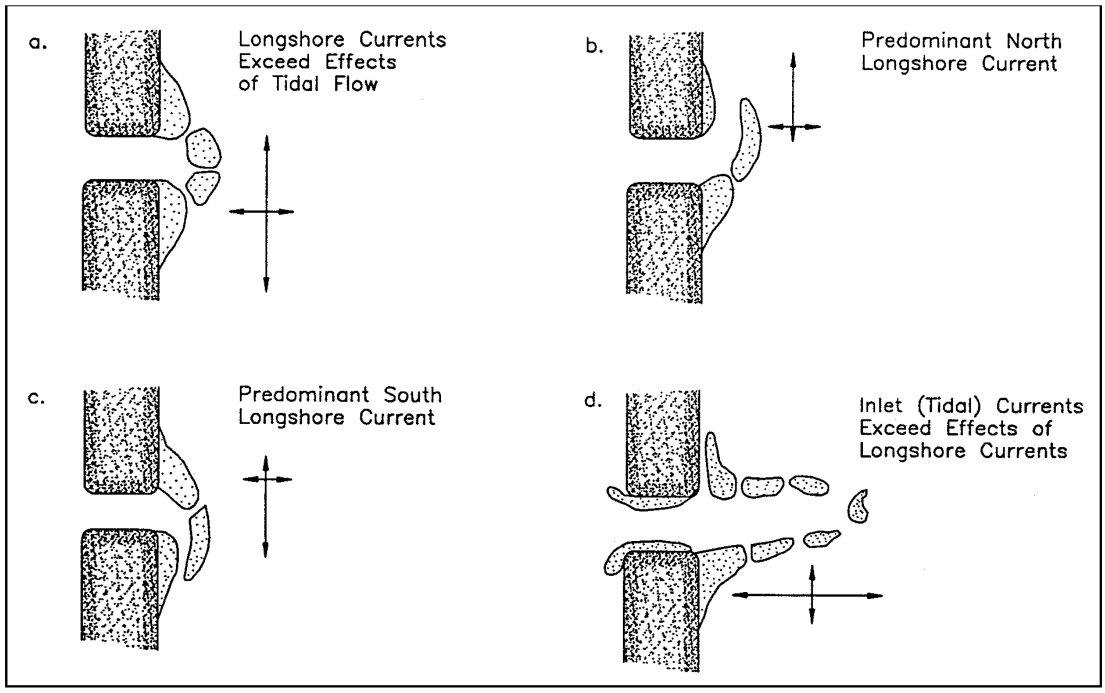

Figure 2.4: Four different shapes of ebb-tidal deltas, modified by the relative effects of longshore versus tidal currents. (From Oertel, 1988 *in* Morang and Parson, 2002).

2.2 Sediment Bypassing

An inlet acts as a complete or partial barrier to longshore sediment transport (Leatherman, 1988). Depending on equilibrium conditions, an inlet may trap sand or naturally by-pass a large portion of the sediment in the littoral drift system (Leatherman, 1988). Inlet sediment bypassing is the process by which sediment moves from the updrift to the downdrift side of the inlet, involving the inlet channel and ebb-tidal delta (FitzGerald *et al.*, 2001). According to the same author, sand enters the main inlet channel along the beach by wave action or through marginal channels by tidal currents and additional sand is transported into the inlet by flood-tidal and wave-generated currents over the shallow swash platform that flanks both sides of the inlet. Under normal or non-storm conditions, sand in the inlet channel is moved in a net seaward direction and is ultimately deposited in the terminal lobe, where the wave current interaction ultimately produces the landward transport of the sand across the swash platform or along the periphery of the ebb delta toward the adjacent beaches (FitzGerald *et al.*, 2001).

FitzGerald *et al.* (2001) made a revision of the natural mechanisms of sediment bypassing at tidal inlets (due to tide- and wave-generated transport). According to these authors, inlet sediment bypassing is the process by which sediment moves from the updrift to the downdrift side of the inlet, involving the inlet channel and ebb-tidal delta. The following mechanisms, described by FitzGerald *et al.* (2001) are based on the work of Bruun and Gerritsen (1959), Bruun (1966), FitzGerald (1982), FitzGerald (1988) and Morang and Parson (2002), and relate to non-stabilised inlets.

(1) Stable Inlet Processes. A stable inlet is one that has a stable inlet throat (non migrating) and a stable main ebb channel position through the ebb-tidal delta. The stability of the inlet is usually related to the channel being anchored in a substrate resistant to erosion. Bypassing at these inlets occurs through the formation, landward migration, and attachment of large bar complexes to the downdrift shoreline (see Figure 2.5). The time frame for these bars (formed by coalescence of swash bars) to form and migrate onshore is highly variable but usually takes from 4 to 10 years.

(2) Ebb-Tidal Delta Breaching. This occurs at tidal inlets that have stable throat positions, but whose main channels cyclically migrate downdrift.

The dominant direction of longshore transport at these sites produces a preferential accumulation of sediment on the updrift side of the ebb-tidal delta. The sediment accumulation causes a downdrift deflection of the main channel that produces hydraulic inefficiency of the inlet. The breaching process can occur gradually over a period of 6 to 12 months or catastrophically during a single storm when the discharge of flood waters increases the scouring effects of the ebb currents. The breaching process commonly results in the bypassing of a large portion of the ebb delta sand. Some of this sand fills the old channel, while the rest forms a subtidal or intertidal bar complex that migrates onshore ultimately attaching to the landward beach (see Figure 2.5). These bars are identical to the ones described for the Stable Inlet Processes and contain equal or greater volumes of sand. The entire process takes from 5 to 10 years to complete. Gaudiano and Kana (2001) documented and analysed the episodic welding of bar complexes onto the downdrift beach at nine inlets in South Carolina (USA).

(3) Inlet Migration Spit Breaching. Sand transported along the beach and deposited in a tidal inlet constricts the inlet throat decreasing the flow area. Therefore, according to the Escoffier (1940) stability concept, the constriction causes an increase in current velocity which leads to greater scouring of the inlet channel and re-establishment of the equilibrium channel cross-sectional area. Because longshore transport along most coasts adds sand predominantly to one side of the inlet, the opposite side erodes preferentially causing the inlet to migrate (Jonhson, 1919). This migration mechanism can be observed in Figure 2.5. The rate of migration is then dependent on sediment supply, wave energy, tidal current strength, and composition of channel banks. As an inlet migrates, it leaves behind a series of curved beach ridges that define the updrift spit.

(4) Outer Channel Shifting. This mechanism is similar to Ebb-Tidal Delta Breaching, but it is limited to the seaward end of the main channel and involves smaller volumes of sand. The inner portion of the main channel remains in a fixed position while the outer channel is deflected downdrift because of preferential accumulation of sand on the seaward, updrift side of the swash platform. The bypassed sand moves onshore as a large swash bar that is usually smaller than those produced by Ebb-Tidal Delta Breaching processes but still may contain large amounts of sediment.

(5) Spit Platform Breaching. At most migrating inlets, the updrift spit is fronted by a large intertidal spit platform. The platform may extend from 100 to more than 1,000 m into the inlet producing a highly asymmetric channel configuration. Large quantities of sand are bypassed when a new channel is breached through the spit platform. Spit accretion and downdrift extension of the spit platform increase the length of the inlet channel, thereby decreasing flow efficiency between the ocean and the backbarrier. Weidman and Ebert (1993) studied this type of bypassing in Massachusetts (USA) and proposed a conceptual model explaining the cyclic occurrence as the result of interrelated morphological, tidal and climatic controls.

(6) Wave Dominated Inlets. At wave dominated inlets, where the ebb delta is small, shallow, and close to the inlet mouth, the waves transport sand along the periphery of the delta especially at high tide. This transport of sand occurs in the same manner as that in the surf and breaker zones. Sediment bypassing at these inlets occurs continuously.

In their final remarks FitzGerald *et al.* (2001) emphasised that even at inlets where sand bypassing occurs in the form of large bars, additional sand is moved to the downdrift shoreline in a continuous mode. The relative magnitude of this process as compared to bar migration varies from inlet to inlet. Also, FitzGerald *et al.* (1984) in a study of sediment bypassing in the East Frisian Islands (Germany) found that the bypassing and welding of large sand bars can strongly control the shape of the barrier islands.

Kana *et al.* (1999) proposed a mesoscale conceptual model for mixed energy settings describing shoreward migration of a large bar (Ebb-Tidal Delta Breaching). It is based on what they call a 'sediment loop' where sediment is exchanged between the ebb delta and the beach. The transport loop is initiated as sediment enters the main channel. Ebb flows, which tend to dominate in mixed energy inlets, shift excess sediment offshore to the ebb-tidal delta. If prolonged winds and waves move parallel to the coast, the delta sediments are transported towards the downdrift sections of the ebb-tidal delta. Variations in wave direction can affect an imbalance between wave- and current-generated transport, therefore onshore transport (bypassing) or offshore transport (delta growth) will be favoured. When onshore transport occurs, a portion of the ebb-tidal delta (excess sediment) is freed to move shoreward under incident waves. The 'transport loop' is completed when the shoal bypass to the adjacent shoreline is complete.

The sequence of ebb-tidal delta changes that may trigger the bypass of a shoal is shown in Figure 2.6.

Additionally Jaffe et al. (1997) found that aside from the nearshore bypassing processes described above, there was an offshore bypassing primarily caused by wind-driven coastal currents during large storms and hurricanes in the Isles Dernieres in Louisiana (USA).

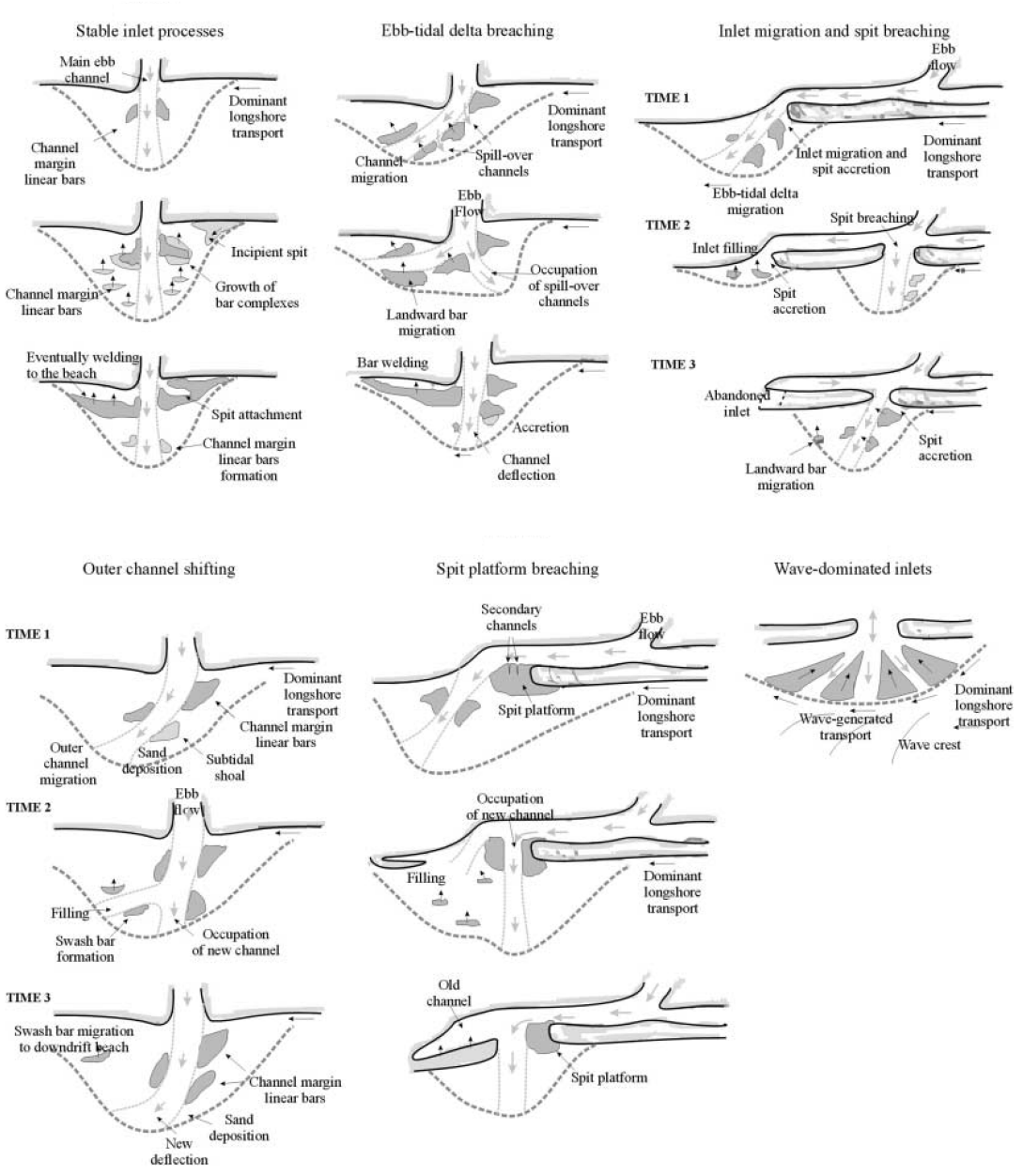

Figure 2.5: Conceptual models of inlet sediment bypassing established by FitzGerald *et al.* (2001).

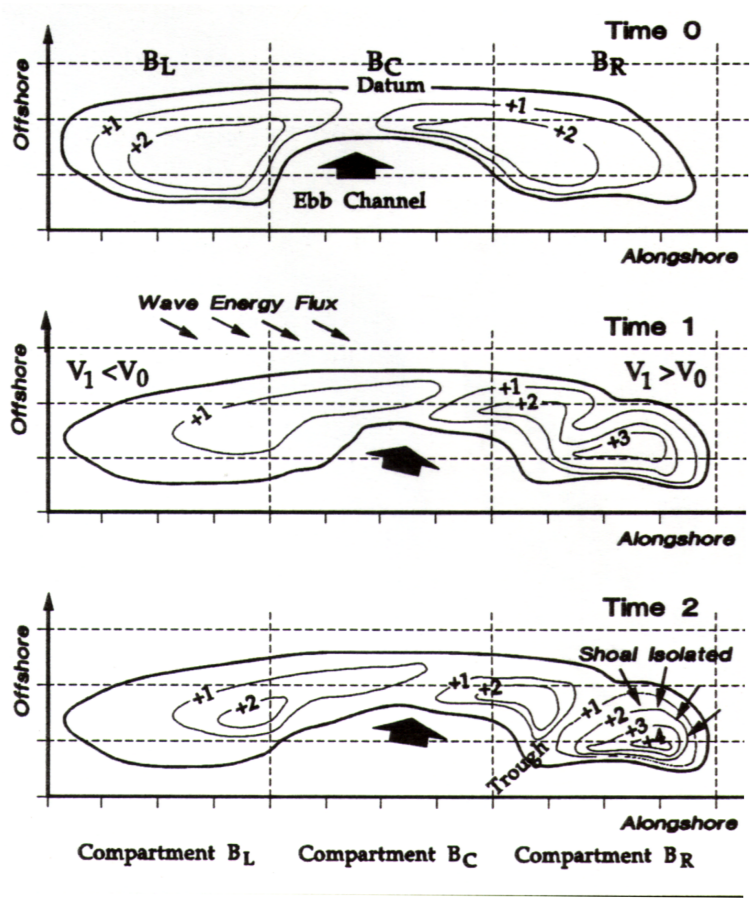

Figure 2.6: Sequence of ebb-tidal delta changes that may trigger shoal bypass events. Initially the delta is symmetric (Time 0) with equal volumes (V) and similar swash platforms elevations in the left and right compartments (B_L and B_R, respectively). At Time 1, excess sediment has accumulated in B_R under the influence of a net longshore transport. By Time 2, multiple shoals at higher elevation develop in B_R under more frequent wave breaking, leading to isolation of and eventual release from the delta of the highest, most remote, bar. From Kana *et al.* (1999).

2.3 Inlet Stability

Inlet stability is divided into locational stability, a state in which the inlet remains in a fixed position and does not experience any significant migration, and geometrical stability, a state in which the inlet dimensions and general shape remain relatively constant, experiencing only small deviations through time (Mason, 1986; Salles, 2001). The geometrical stability is the stability against closure (Dean, 1999) that characterises the capacity of an inlet to remain open under natural conditions (no jetties and no dredging). Therefore, inlets can be considered stable in terms of their location, their geometry or both. Geometrically stable inlets are those that have the ability to return to their initial configuration after a disturbance (Hume and Herdendorf, 1992).

Inlet stability is related to the strength of the longshore current versus the tidal jet flushing capacity (Leatherman, 1988). According to Nummedal and Fisher (1978) several investigations of process-response characteristics of tidal inlets have demonstrated that the geometry of an inlet entrance and the associated sand shoals (including both deltas) depends upon three major environmental factors: (1) the tidal range, (2) the nearshore wave energy, and (3) the morphology (relief) of the back-barrier bay.

Nummedal and Fisher (1978) affirmed that the relative magnitudes of factors (1) and (2) control, to a large extent, the inlet stability. The tidal range controls one of the main parameters for inlet hydrodynamics: the tidal prism (Ω). The tidal prism is the amount of water exchanged in a given area during the tidal cycle, it is defined as the product of the tidal range and the area of the backbarrier bays that are served by the inlet (i.e., Davis, 1994).

The third factor controls the degree of velocity asymmetry through the inlet gorge (Nummedal and Fisher, 1978). Large tidal amplitude to channel depth ratio causes relatively shorter floods (flood dominance), and the existence of tidal flats can produce longer rising tide and stronger ebb currents (ebb dominance), if the intertidal storage is large enough to overcome the effects of time-variable channel geometry (Salles, 2001). The existence of salt-marshes in the backbarrier produces a large variation in water surface area during the tidal cycle that tends to develop ebb-dominant flow (Nummedal and Fisher, 1978). According to Walton (2002) if the duration of the falling tide exceeds that of the rising tide leading to a larger peak flood current (higher cross-sectional averaged peak flood velocity), the system is referred to as flood dominant or flood asymmetric. And if the duration

of the falling tide is shorter than that of the rising tide leading to a stronger peak ebb current, the system is referred to as ebb dominant or ebb asymmetric.

Flood-dominance has a tendency to transport sediment landward, with the consequent development of important flood deltas and the gradual shoaling of the channels (Aubrey, 1986) being therefore associated with long-term instability of the inlet (Salles, 2001). Ebb-dominant inlets have the tendency of exporting material to the outer deltas, and, depending on the amount of sediment deposited during flood and slack by the tidal currents and the wave action, may be associated with increased chances of stability (Salles, 2001). However, the classification of an area as ebb or flood dominated has to be made carefully. Lessa (2000) stated that extreme tidal events should be taken into account for the final classification into ebb or flood dominated. This author found that, for areas that are flood dominated during most of the time, sediment transport during episodes of ebb-dominance under extreme tidal events (only a few times over a year) can overwhelm the more frequent flood dominant transport.

According to O'Brien (1971), the first analytical approach to the hydrodynamic regime of tidal inlets at sandy coasts was given by Brown (1928). Escoffier (1940) published one of the most commonly used relationships for the study of the stability of tidal inlets. His work was based on the results from Brown (1928) and relied on the calculation of the mean velocity of peak tidal currents, also called maximum velocity in the literature (i.e., O'Brien, 1971; Dean, 1999; Salles, 2001). According to Escoffier (1940) the maximum velocity for a stable (geometrical and/or locational stability) inlet, that is assumed to have the same absolute value on flooding and ebbing, should be around 1 m/s.

Empirical stability relationships have been used to characterise the stability of tidal inlets. One of the most widely used is the relationship between the cross-sectional area of the inlet throat (A_c) and the tidal prism (Ω). O'Brien (1969) was one of the first authors to propose a relationship between these two parameters, he found two different relationships for inlets with no jetties (Equation 2.3.1) and for jettied inlets. For the purposes of this work, only stability relationships related to inlets with no jetties are presented. Therefore,

$$A_c = 2 \cdot 10^{-5} \cdot \Omega \tag{2.3.1}$$

where the Ω corresponds to average spring tides and is measured in cubic feet (ft^3) and A_c is measured in square feet (ft^2) and is referred to the mean sea

level (MSL). According to Dean (1999) the relationship given by O'Brien (1969) provided a good fit for inlet systems with Ω ranging approximately from 10^8 to 10^{11} ft^3.

Jarret (1976, in Dean 1999) extended the tidal prism cross-sectional area correlation including 162 inlets with and without jetties on the Atlantic, Gulf and Pacific Coasts of the USA. The best least squares fit for all entrances with one or no jetties was found to be (A_c in m^2 and Ω in m^3):

$$A_c = 5.77 \cdot 10^{-5} \cdot \Omega^{0.95} \tag{2.3.2}$$

More recently, several authors (i.e., Hume and Herdendorf, 1993; Michel, 1997) have tried to refine these expressions for their application to other inlets in New Zealand and France respectively. Hume and Herdendorf (1993) used A_c-Ω relationships to characterise and classify estuary entrances.

Gerritsen and Dunsbergen (1998) incorporated the width of the channel (B, in metres) into the stability equations finding two expressions, one theoretical (Equation 2.3.3) and one empirical (Equation 2.3.4) for the Dutch North Sea Inlets, for semi-diurnal tidal conditions. For both equations A_c and Ω are in m^2 and m^3 respectively):

$$A_c = 1.42 \cdot 10^{-3} \cdot \Omega^{\frac{3}{4}} \cdot B^{\frac{1}{4}} \tag{2.3.3}$$

$$A_c = 8.0 \cdot 10^{-4} \cdot \Omega^{0.8} \cdot B^{0.2} \tag{2.3.4}$$

According to O'Brien (1969) on any sandy coast affected by wave action, the waves will tend to drive sand into the inlet whereas the tidal currents will tend to maintain some equilibrium area by scouring the sand from the inlet into the bay or seaward. Therefore, Dean (1999) explains that it should be a maximum tidal velocity (V_{max}) that is the velocity required to maintain the equilibrium flow area. For semidiurnal regimes where the tidal cycle is ~45,000 s:

$$V_{max} \approx 3.5 \ ft/s \approx 1 \ m/s \tag{2.3.5}$$

The A_c-Ω relationships imply that an increase in Ω will induce erosion in the tidal inlet as a consequence of increased stress by stronger currents, thereby increasing the value of A_c (Hofstede, 1999). Furthermore, Walton and Adams

(1976) proposed an empirical relationship between the sand volume of the ebb-tidal deltas (V_{ebb}) and Ω. An increase of Ω induces a higher sediment transport to the ebb delta, therefore increasing V_{ebb}:

$$V_{ebb} = 13.8 \cdot 10^{-5} \cdot \Omega^{1.23} \tag{2.3.6}$$

where V_{ebb} is in cubic yards (yd^3) and Ω is in cubic feet (ft^3).

Multiple tidal inlets are a particular case where a single embayment communicates with the ocean through more than one tidal inlet. The stability of such systems depend in part on factors not found in single inlet systems (Salles, 2001). According to the same author, morphological changes in a given inlet are likely to modify the hydrodynamic behaviour in the inlet and its 'area of influence' inside the lagoon, which in turn may affect the hydrodynamics at other inlets and in other areas of the lagoon. Van de Kreeke (1985) expanded the analysis of Escoffier (1940) to include the interaction of multiple inlets, concluding that most multiple inlet systems are unstable. Therefore one or more of the inlets will eventually close (Van de Kreeke, 1985). However, Aubrey *et al.* (1993) found that multiple inlet stability analysis could not be calculated using the same area for each inlet. Moreover, Escoffier's linear approach does not permit the introduction of the hydrodynamics of the embayments into the stability analysis. Finally, Aubrey *et al.* (1993) applied numerical models for tidal propagation and dissipation along the embayment, and found that some multi-inlet systems can be stable on a decadal time scale.

Other authors (i.e., Salles, 2001; Smith, 2001; Huang *et al.*, 2002) have performed further investigations into multiple inlet stability and hydrodynamics. Salles (2001) focused his investigation on the tidal hydrodynamics of the Ria Formosa barrier island system, through the study of the historic and present conditions as well as the application of numerical models. He found that the hydrodynamic interaction between inlets servicing a single embayment, and the capacity of the system to adjust to inlet disturbances by transferring large proportions of the tidal prism from one inlet to another, and by modifying the residual flow and sediment transport patterns, contribute to keeping multiple inlets open.

2.4 Final Remarks

A general review of the knowledge of tidal inlet dynamics has been given in this chapter. However, it is important to note that the majority of the studies of tidal inlets have been made for the eastern coast of the USA. There are also some investigations done on the barrier island systems of northern Europe, namely the Frisian Islands, but they are not as numerous. In any case, the wave and tidal conditions, both on the east coast of the USA and northern Europe, cannot be considered as representative of all barrier islands in the world. Therefore, more studies, encompassing all the relevant aspects of tidal inlet morphology, bypassing or stability, are needed at other barrier systems worldwide in order to correct the present skewness of the knowledge.

Additionally, it can be said that inlet relocation is considered as a useful tool that requires further studies and investigations in order to improve the success of its future application.

Chapter 3

Study Area

"At that time Macondo was a village of twenty adobe houses, built on the bank of a river of clear water that ran along a bed of polished stones, which were white and enormous, like prehistoric eggs. The world was so recent that many things lacked names, and in order to indicate them it was necessary to point."

Gabriel García Márquez, *"One Hundred Years of Solitude."*

The Ria Formosa is a multi-inlet, barrier island system located in southern Portugal (Figure 3.1). It consists of two peninsulas and five islands that extend over 50 km. Connection between the ocean and the backbarrier area is made through six tidal inlets. According to Andrade (1990), the backbarrier area consists mainly of salt marsh and small sandy islands covering 8.4×10^7 m^2 and comprising a complicated pattern of tidal channels and creeks.

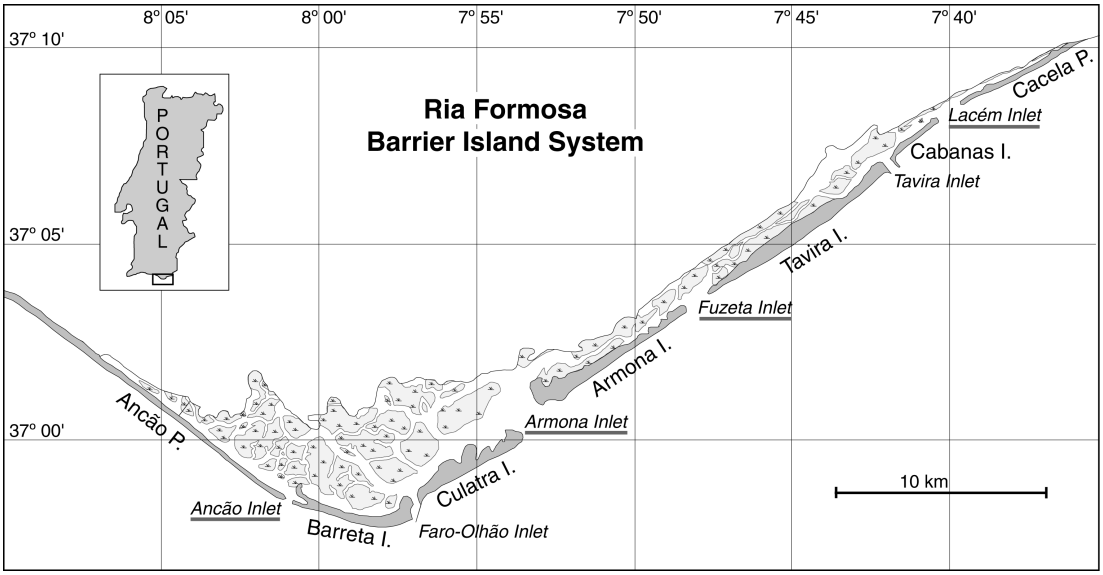

Figure 3.1: Map showing the Ria Formosa barrier island system and its location inside Portugal. The names of the natural inlets are underlined.

3.1 Forcing Mechanisms

3.1.1 Climatic Setting

The wind patterns in the study area vary on a daily time scale (Cunha, 1957; Faria *et al.*, 1981). According to these authors, the winds are typically weak and from the north during the night, changing to the southwest or south during the morning. In the afternoon the winds usually turn to the southwest or west increasing their speed. According to the same authors, calm periods usually occur during the beginning of the morning or the beginning of the night.

Wind data for Faro Airport between 1970-1980 was obtained from IM (1991). According to these data, the dominant winds are with a northerly component (43% of the time, including NE, N and NW) during winter and with a westerly component (61% of the time, including SW, W and NW) during summer. The percentage of '*Levante*' events (E-SE winds) was typically higher in winter (25%) than in summer (18%). In terms of wind speed, there are not significant differences in the average values for winter (13.32 km/h) and for summer (13.27 km/h). However, the maximum average velocities during winter (17.53 km/h for SW winds) are higher than the maximum average velocities during summer (15.93 km/h for W winds). Strong winds ($>$ 36 km/h) occur 35 days per year in Faro (67% of the time from W-SW) and only 2 days per year in Tavira (Cunha, 1957, 1985). Very strong winds ($>$ 55 km/h) typically occur 5 days per year in Faro and none in Tavira (Cunha, 1957). Storms are more frequent in Faro than in Tavira, with an average of 8 and 6 storms per year respectively (Faria *et al.*, 1981).

In terms of rainfall, the Ria Formosa can be considered as a semi-arid area (Faria *et al.*, 1981; Cunha, 1985). According to Cunha (1985), who analysed data between 1941 and 1970, there is an increase in the rainfall from the west to the eastern areas of the Ria Formosa, the average annual values ranging between 450 mm and 590 mm. According to Machado (1980), who analysed data between 1948 and 1967, the maximum number of consecutive days with no rain was 188 for Faro and 160 for Tavira. The same author established that the maximum number of consecutive days with rainfall was 14 for Faro and 23 for Tavira. According to Matias (2000), who used the values given by Faria *et al.* (1981), 85% of the annual rainfall occurs between October and March.

3.1.2 Oceanographic Setting

Tides in the area are semidiurnal, average ranges, determined using tidal predictions from IH (years 1990 to 1999, see 9), are 2.8 m for spring tides and 1.3 m during neap tides, however, maximum ranges of 3.5 m can be reached. Salles (2001) made an extensive study of the tidal constituents in the Ria Formosa barrier island system, finding a strong distortion of the tide within the lagoon (i.e. reduction of tide amplitude and creation of phase lags due to friction). However, according to the same author, there is no definite trend of the tidal distortion as a function of the distance to the inlets.

Wave climate in the area is moderate to high (Ciavola *et al.*, 1997a). According to C.Costa (1994), who made an analysis of the wave data for the period between September 1986 and December 1993, average values for significant wave height (H_s) and peak period (T_p) are smaller in summer (H_s=0.78 m; T_p=7.1 s) than in winter (H_s=1.15 m; T_p=9.2 s), indicating the higher frequency of swell conditions. Incident waves are normally from the W-SW, representing 68% of the total, although '*Levante*' (E-SE wind) events occur often in the area, producing E-SE waves that represent 29% of the total (C.Costa, 1994). The average wave conditions for the study area according to C.Costa (1994) are shown in Table 3.1. Storms in the study area correspond to events with H_s greater than 3 m (Pessanha and Pires, 1981). M.Costa (1994), using the same data as C.Costa (1994), concluded that the highest storm frequency occurs in the period between November and January. For H_s values between 3 and 4 m, SE storms are more frequent than SW storms, while for H_s larger than 4 m, SW storms are more frequent (M.Costa, 1994). Pires (1998) established the return periods for the main directions using directional data from the years 1986 to 1995, and concluded that for the same return period, SW storms exhibit higher H_s values than SE storms; a storm with H_s=5.7 m would have a return period of 5 years for SW conditions, while for SE conditions the return period would be 100 years or more. Costa et al. (2002) found that the most common storms have a persistence between 2 and 5 days, are from the South and have H_s values between 3 and 5 m.

Net littoral drift and longshore currents in this area are typically from west to east. Several authors (Granja *et al.*, 1984; Consulmar, 1989 *in* Bettencourt, 1994; Andrade, 1990; Bettencourt, 1994) have presented estimations of net littoral drift values for several parts of this region. Results from these estimations are very different, mostly due to different data sources and methods used. Val-

Table 3.1: Typical oceanographic conditions in the study area (after C.Costa, 1994). H_s= Mean Significant Wave Height, T_p= Mean Peak Period.

	H_s (m)	T_p (s)	Directions (%)				
			W	SW	S	SE	E
SUMMER	0.78	7.1	56.8	13.4	2.2	23.8	2.7
WINTER	1.15	9.2	42.8	21.2	1.9	26.9	6.9
ANNUAL	0.92	8.0	51.5	16.3	2.1	25.0	4.2

ues obtained by the authors above range between a minimum of 6,000 m^3/year obtained by Andrade (1990), and a maximum of 300,000 m^3/year (Consulmar, 1989 *in* Bettencourt, 1994).

3.2 The Ria Formosa: General view

The Ria Formosa, that is part of a natural park, shows some atypical characteristics for a barrier island system including: (1) it is not located on a coastal-plain coast (Pilkey *et al.*, 1989); (2) the maximum spring tidal range (around 3.5 m) is close to the upper limit of mesotidal coasts, which represents the upper limit for the occurrence of barrier islands according to the classification of Hayes (1979) and due to these relatively high tidal ranges, the lagoon side of the islands are modified by the erosive effect of spring tides (Pilkey *et al.*, 1989): and, finally, (3) it is one of the few barrier island systems in the world with a triangular shape (Bettencourt, 1994). The origin of the Ria Formosa is not clear, however, Pilkey *et al.* (1989) established the holocenic landform migration to be in agreement with the classical shoreface transgression model. According to the same author, the islands probably originated as spits connected to a cape; these spits were detached when the shoreline retreat accelerated in response to the sea level rise over the lip of the platform. According to Salles (2001) the general shape and morphologic evolution of the barrier island results from (1) the geological origin and evolution of the system, and its response to relative sea-level rise (thousands of years), (2) the exposure to different wave and current conditions on either side of the system (years), and (3) from the effects of storms (weeks/days).

The cuspate shape of the Ria Formosa system produces two areas differentiated in terms of exposure to wave action. The west flank is more energetic, being under the direct influence of the dominant wave conditions, while the east flank

is only directly exposed to the '*Levante*' conditions. A brief resume of the characteristics of the natural inlets (Ancão, Armona, Fuzeta and Lacém, see Figure 3.1) in the Ria Formosa is given in this section.

The west flank typically has only one tidal inlet although at various times in the past has had up to three tidal inlets (Weinholtz, 1964; Esaguy, 1986a). Ancão Inlet (Figure 3.2) is a small migrating inlet that has an average width of 300 m (Vila *et al.*, 1999). Several authors have described the behaviour of this inlet as having a cyclic eastward migration (Weinholtz, 1964; Esaguy, 1986a; Dias, 1988; Pilkey *et al.*, 1989; Vila *et al.*, 1999), although other authors have interpreted its behaviour as erratic movements with no defined directions or cyclic behaviour (Andrade, 1990; Salles, 2001). Eastward migration rates found in the literature are very variable, ranging from tens of metres per year (Pilkey *et al.*, 1989; Bettencourt, 1994) to an extreme value of 170 m/year (Granja *et al.*, 1984). Average historical values for inlet width were also examined by several authors and were found not to have very strong variations. Values obtained by Esaguy (1986a) ranged from 200 m to 250 m, which are comparable to the average values found by Salles (2001). According to Andrade (1990), the inlet is ebb-dominated. Ancão Peninsula and Barreta Island are narrow (in the vicinity of Ancão Inlet), consisting of one single dune ridge that can reach heights of 7 m (above MSL).

The east flank presently has five inlets, although the number of inlets has varied over time. Two of the inlets on this flank, Faro-Olhão Inlet and Tavira Inlet (see Figure 3.1) were artificially opened and stabilised with jetties in 1929-1955 (Esaguy, 1984) and 1927-1985 (Esaguy, 1987), respectively.

Armona Inlet (Figure 3.2) is considered to be the only naturally stable (in terms of location) inlet of the system (i.e., Weinholtz, 1964; Dias, 1988; Pilkey *et al.*, 1989). Bettencourt (1994) proposed that the locational stability of Armona Inlet was related to the existence of a paleochannel in the same position, however, this hypothesis has never been validated through corer sampling in the area. Armona Inlet has occupied the same position through recent centuries although its width has varied significantly (Weinholtz, 1964; Andrade, 1990; Salles, 2001). According to Esaguy (1984) and Dias (1988), during the last century, its width has narrowed by approximately 2,500 m, from 4,300 m in 1873, to 1,850 m in 1983. The same authors explained that narrowing of the inlet was mostly related to the growth of the eastern tip of Culatra Island, since its growth rates were similar to the inlet narrowing rates. As a consequence of the rapid growth, the eastern part of Culatra Island contains low dune areas with high overwash susceptibility

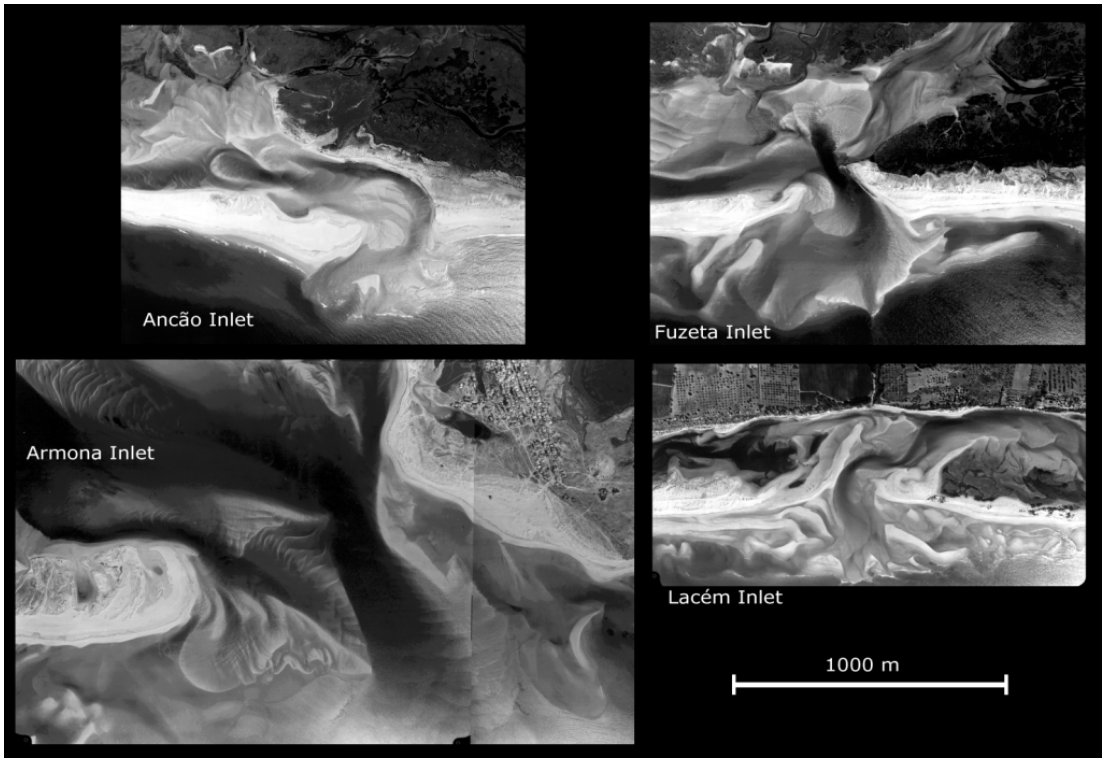

Figure 3.2: Vertical aerial photos showing a view of the natural inlets of the Ria Formosa barrier island system in 1996.

(Andrade *et al.*, 1998; Garcia *et al.*, 2002) that under high energy conditions could lead to barrier breaching. Due to its width, this inlet has a very complex morphology and often consists of two or more channels.

Fuzeta Inlet (Figure 3.2) shows a clear pattern of cyclic easterly migration (Weinholtz, 1964; Esaguy, 1985; Dias, 1988; Pilkey *et al.*, 1989; Andrade, 1990; Salles, 2001). Eastward migration rates were variable, ranging from 30 m/year (Andrade, 1990) to 344 m/year (Esaguy, 1984). The typical width of this inlet varies from a hundred to two thousand metres, consisting, on occasions, of two channels. According to Andrade (1990), Fuzeta Inlet is ebb-dominated. Armona and Tavira islands, in the vicinity of the inlet, do not have very high dune ridges thus, overwash susceptibility is quite high (Andrade *et al.*, 1998), especially at the western tip of Armona Island.

Lacém Inlet (Figure 3.2) typically opens over a wide area during storms because Cabanas Island is easily inundated. Dias (1988) explains that Cabanas Island corresponds to the eastern part of Tavira Island, and that it was separated with the artificial opening of Tavira Inlet. According to the same author, this island was completely destroyed by major storms in 1941 and in 1961, however

in 1962 it had already recovered, having a length of 100 m. Therefore, accretion processes on Cabanas Island are fast and cause eastward inlet migration as well as inlet narrowing (Dias, 1988; Pilkey *et al.*, 1989). Typical widths for this inlet range from thousands to hundreds of metres and a double channel can exist.

3.3 The Soft Engineering Programme

Since 1997 the Ria Formosa has undergone an extensive engineering programme in order to recover the dynamic equilibrium of the system and to decrease the associated natural hazards (Ramos and Dias, 2000; Dias *et al.*, 2003). This programme included soft protection techniques such as inner channel dredging, beach and dune replenishment and the relocation of two of the inlets (Ancão and Fuzeta inlets, see Figure 3.1). The main reasons for the relocations were that both inlets were undergoing infilling processes and meandering of the main channel. Therefore, it was decided that their relocation in a western position would improve their hydrodynamic efficiency and avoid the existing problems that were making navigation difficult and restricting water exchange through the inlets. Both of the inlet relocations were monitored by the CIACOMAR (Centre for the Study of Coastal and Marine Environments from the University of Algarve) team under a special protocol with the Instituto de Conservação da Natureza (Portuguese Institute of Nature Conservation) through the Ria Formosa Natural Park. The results from the monitoring programs can be found in Dias *et al.* (1998), Dias *et al.* (2000) and Vila-Concejo *et al.* (2001).

3.3.1 Ancão Inlet

Ancão Inlet was relocated on the 23rd June 1997 some 3,500 m west of its position in 1996. Through the dredging of 200,000 m^3 of sediment (mostly sand) an initial channel of around 2 m depth (relative to Z.H.; Portuguese Hydrographic Zero, 2 m below MSL) and 96 m width (between dune cliffs existing on both margins of the inlet, hereafter referred as cliffs) was created. Dredging of the inlet was only undertaken until the establishment of a connection between the sea and the lagoon (Figure 3.3), with the erosion due to tidal currents being responsible for the channel enlargement. Part of the 200,000 m^3 of sediment dredged for the inlet opening was placed in the innermost western end of the inlet channel, to protect existing houses. The remainder was placed in front of

Barreta Island, to avoid rapid migration and to enhance the longshore drift that would, eventually, close the old inlet of Ancão where no engineering actions were performed.

Several studies have been performed at Ancão Inlet since its relocation. According to Ciavola *et al.* (2000a), Salles (2001) and Williams *et al.* (2003), the new Ancão Inlet, after the relocation, was ebb-dominated. According to Morris *et al.* (2001) it shows characteristics of both a tidal (well defined deep main channel and marginal flood channels) and a wave dominated inlet (relatively small ebb delta), being tide dominated most of the time. Morris *et al.* (2003) found that under the Davis and Hayes (1984) energy classification system, the modal state of the area (41% of the time) was mixed energy (tide dominated).

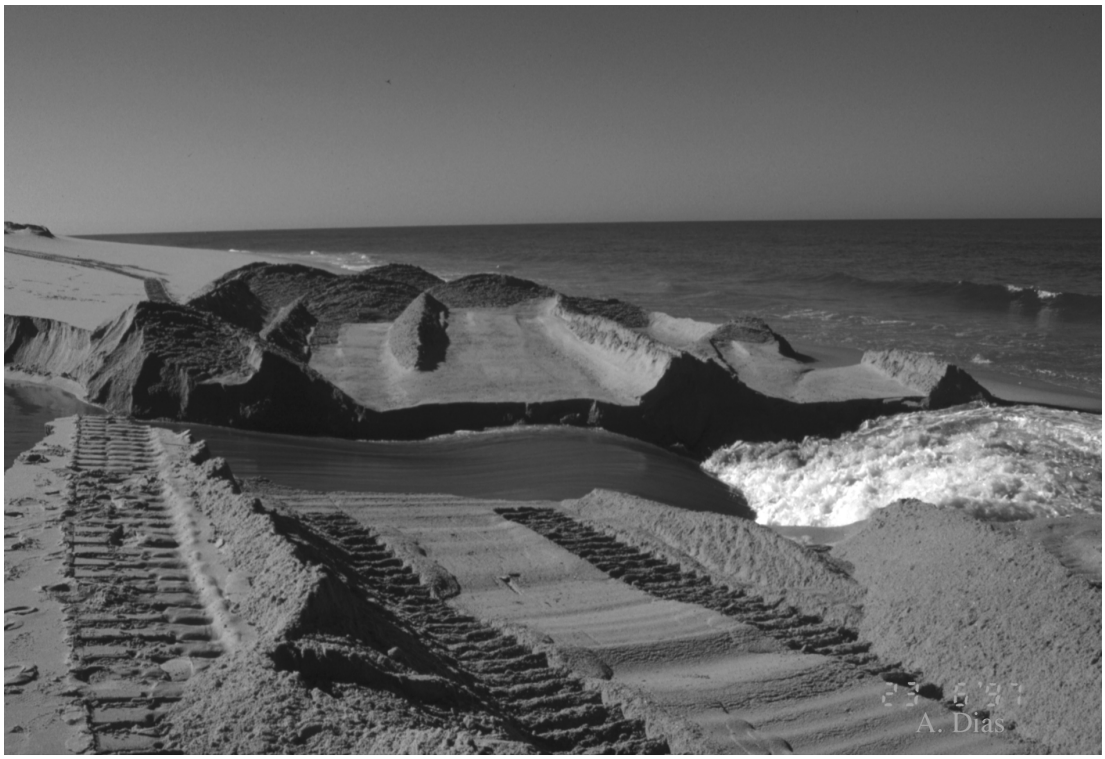

Figure 3.3: Photo showing the opening of the relocated Ancão Inlet.

Figure 3.4 shows a vertical aerial photo taken in April 1999 where the main morphological features (see Section 2.1), as well as the main sediment transport patterns, of the inlet can be observed. In Figure 3.5 the situation in July 2001 is shown. The main sediment transport patterns are still the same but the inlet has already migrated, the ebb-tidal delta shows a larger volume and sediment bypassing can be better observed. Also, the locations of two fixed points (A and B) can be observed in both figures. The location of the dune cliffs in 1999 of

both Ancão Peninsula and Barreta Island are also marked (as dashed lines) in Figure 3.5. It can be seen that between 1999 and 2001 large erosion occurred on Barreta Island, where in 1999 there were dunes with an elevation above mean sea level (MSL) of 6 m, in 2001, according to Matias (Personal Communication, 2003) there is a strongly overwashed area with elevations about 3.5 m (MSL).

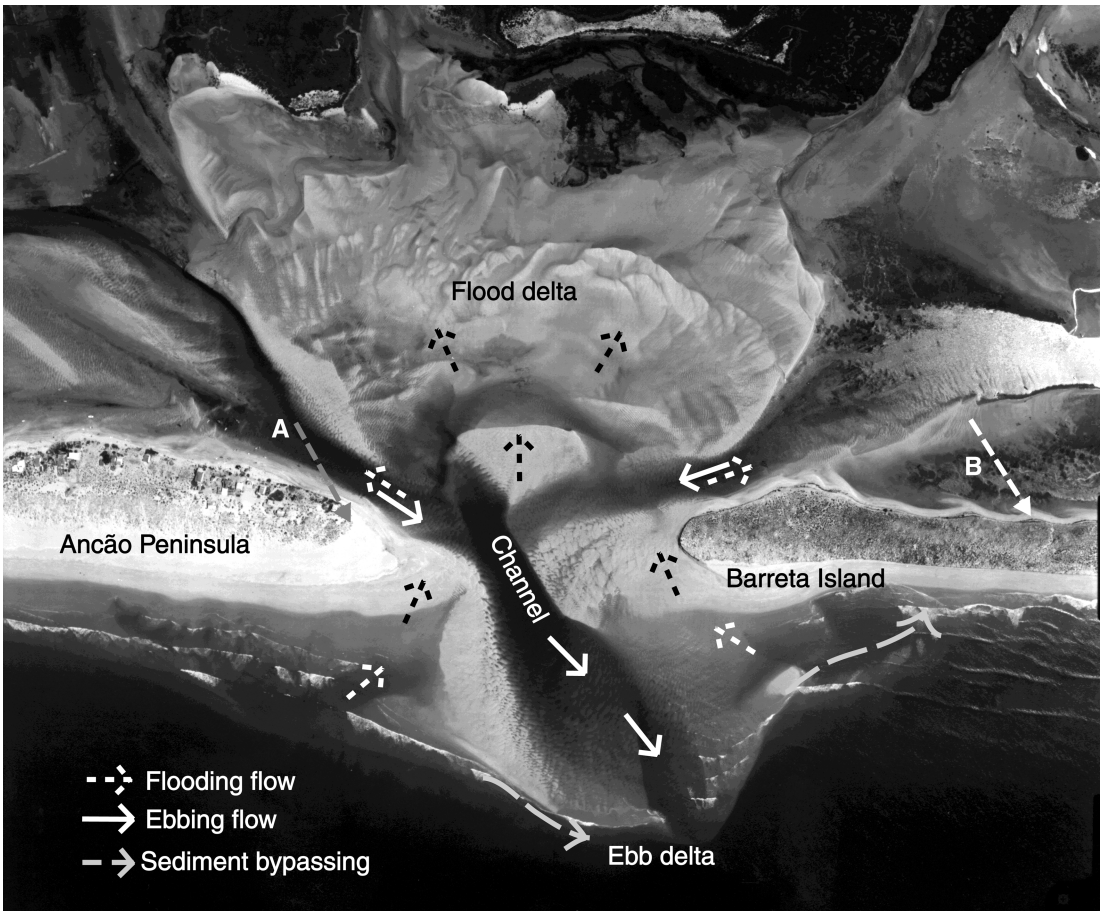

Figure 3.4: Vertical aerial photo showing Ancão Inlet in April 1999. Both deltas and the channel are shown. The main sediment transport patterns are also marked: flooding, ebbing and bypassing. Location of A and B refer to stable reference points (After Vila-Concejo *et al.*, 2001).

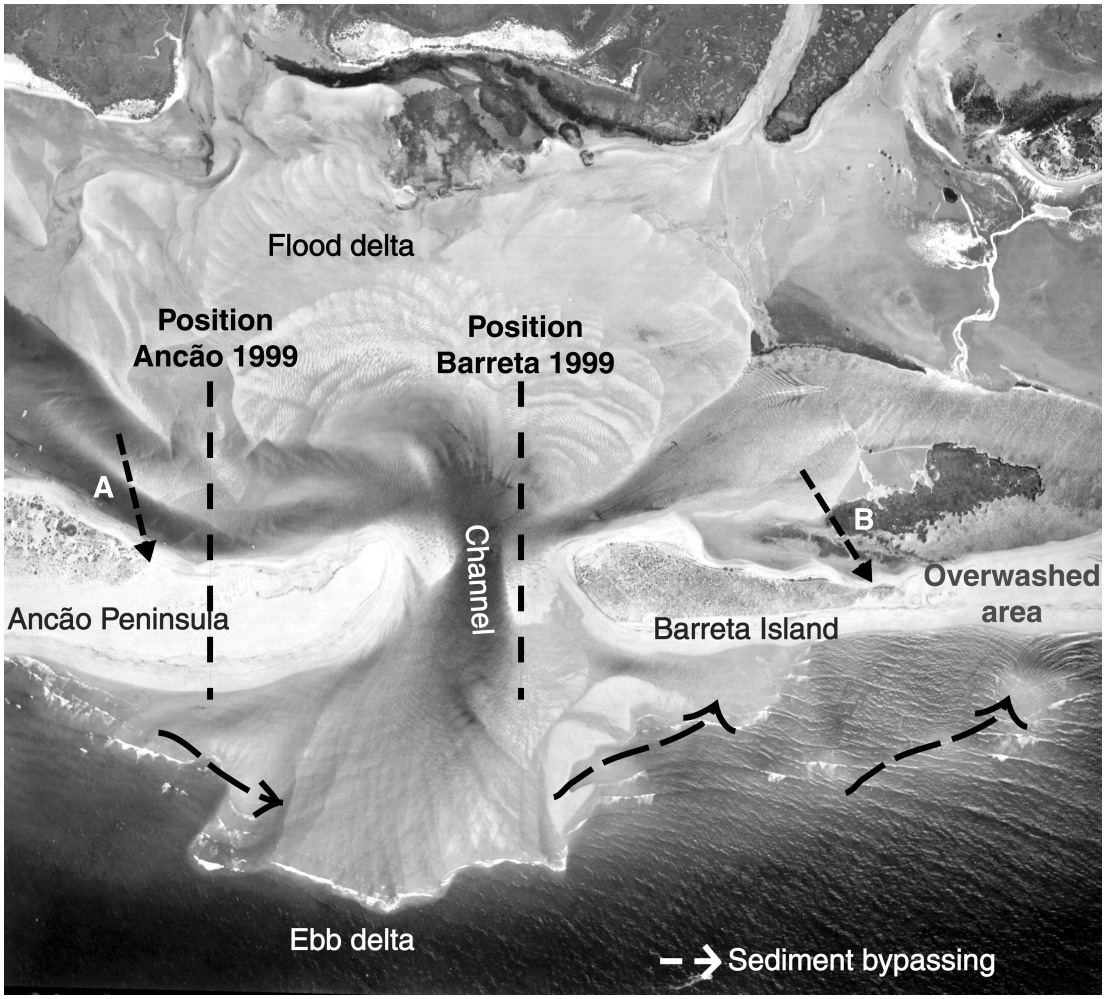

Figure 3.5: Vertical aerial photo showing Ancão Inlet in August 2001. Both deltas and the channel are shown. The position of the inlet in 1999 is also shown. Location of A and B refer to stable reference points (After Vila-Concejo *et al.*, 2001).

3.3.2 Fuzeta Inlet

Fuzeta Inlet was relocated on the 18th July 1999 some 800 m west of its position in 1996 (Figure 3.6). As in the case of Ancão relocation, the dredging was only performed until a connection between the ocean and the lagoon was established. The sediment dredged in the inlet opening was then used to close the existing old inlet. Due to infilling processes, some dredging was performed in the inner channels adjacent to Fuzeta Inlet in August and November 1999 as well as in January and May 2000.

Figure 3.6: Photo showing the relocation of Fuzeta Inlet.

The conditions of the old Fuzeta Inlet can be observed in Figure 3.7. The main morphological features are shown as well as the main sediment transport patterns. It can be seen that due to the meandering of the channel, the main ebbing is not direct with the subsequent low efficiency in water exchange. Figure 3.8 shows the relocated Fuzeta Inlet in 2001. The location of Fuzeta Inlet was already very close to that of 1999 and meandering of the channel can still be observed. However, some sediment by-passing can be observed in 2001.

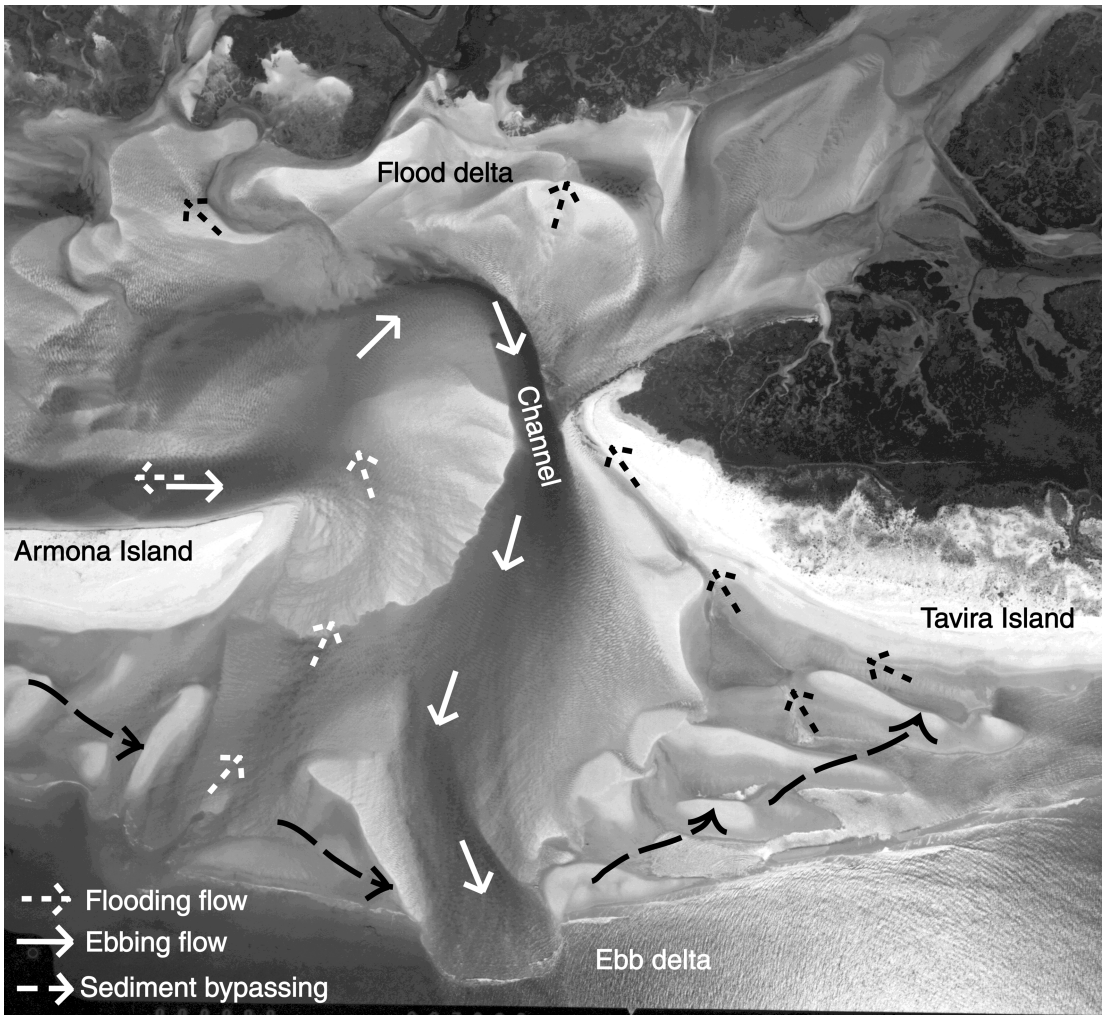

Figure 3.7: Vertical aerial photo showing the old Fuzeta Inlet in April 1999 (before relocation). Both deltas and the channel are shown. The main sediment transport patterns are also marked: flooding, ebbing and bypassing. (After Vila-Concejo *et al.*, 2001).

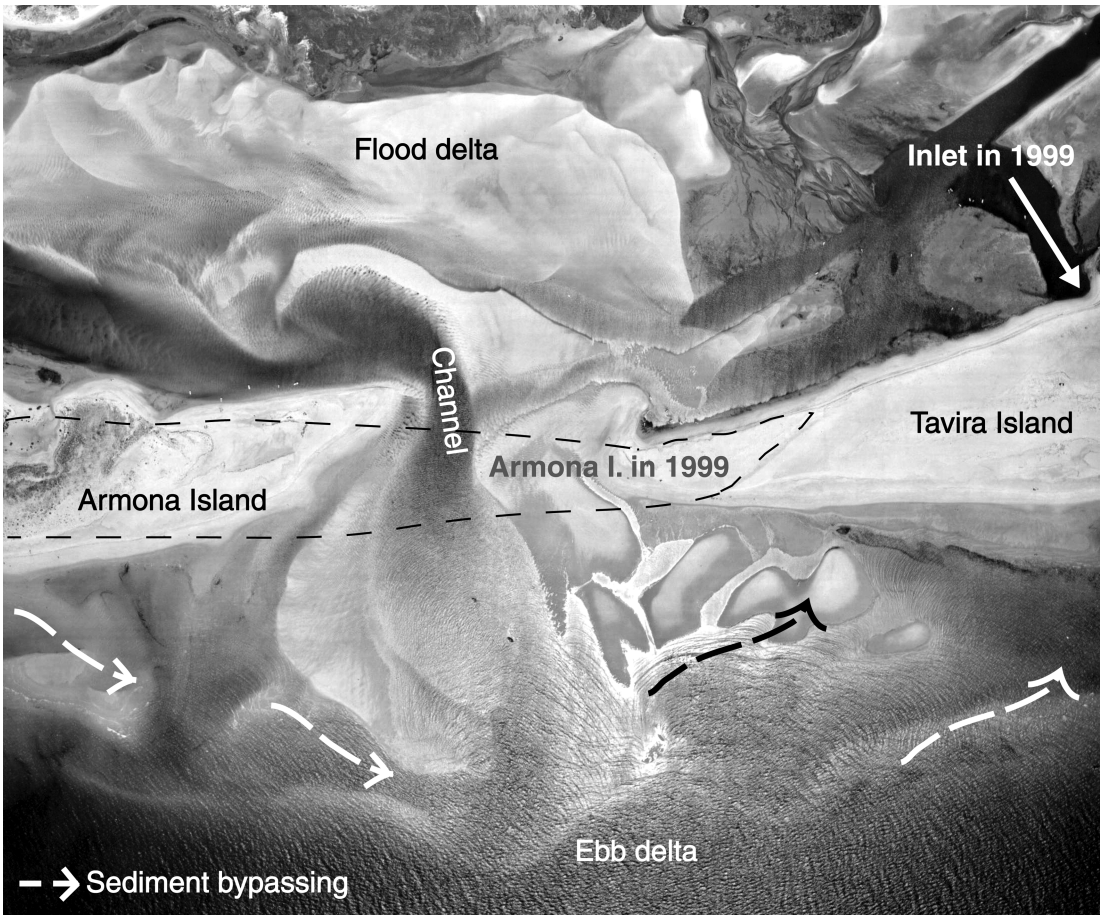

Figure 3.8: Vertical aerial photo showing Fuzeta Inlet in August 2001. Both deltas and the channel are shown, as well as the sediment bypassing patterns. The position of the old Fuzeta Inlet in 1999 is also shown with a dashed line. (After Vila-Concejo *et al.*, 2001).

Chapter 4

Methods

"Consider, Sir," answered Sancho, "that those which appear yonder, are not giants, but windmills; and what seem to be arms are the sails, which, whirled about by the wind, make the millstone go."

"One may easily see," answered Don Quixote, "that you are not versed in the business of adventures: they are giants; and, if you are afraid, get aside and pray, whilst I engage with them in a fierce and unequeal combat."

Miguel de Cervantes, *"Don Quixote."*

4.1 Long Term Studies

Long term studies correspond to the historical analyses performed for all the natural inlets of the Ria Formosa barrier island system (Figure 3.1) during the second half of the 20th century.

Inlet width and position were determined for Ancão, Armona, Fuzeta and Lacém inlets for the period between the 1940s and 1996. This period was chosen (a) because it corresponds to the period for which quality information (vertical aerial photos, charts, maps and documents) is available; and (b) because as mentioned in Section 3.3, since 1997 the Ria Formosa barrier island system has undergone an extensive engineering programme.

To determine inlet width, the minimum width at the inlet gorge was measured using the high tide marks as reference for vertical aerial photos, identified as the darker area on the sand, and the mean sea level isobath, when using charts or maps. Comparison of inlet width measurements using different levels is problematic and can introduce errors related with the slope of the inlet margins. An error analysis was performed taking into account the slopes of the inlet margins on both flanks of the system: Ancão Inlet was used for the west flank, and Lacém inlet was taken as representative of the east flank. Computations of distance between different isobaths, mean sea level (MSL) isobath *versus* typical high tide isobaths (taken as 2 m above MSL), were made using the data from both of the flanks. Since the slope of the inlet margins is steeper on the western flank than on the eastern one, the results of error analysis provided an average error of 40 m for the west flank, and 80 m for the eastern one, when comparing data referred to different isobaths (i.e., charts *versus* photos). Since the large majority of the computed inlet width changes are in the order of hundreds to thousands metres, the method used here provides good long term estimations, showing the important reductions or increases in inlet width.

Inlet position was determined in each case by measuring the distance, along a fixed line following the orientation of the coast, from an arbitrary reference point

to the centre of the main inlet channel. Positions were then converted such that they refer to a point located 10 m west of the initial position of the inlet in the 1940s. Reference points for each studied inlet are shown in Figure 4.1. In the case of double channel inlets, a morphologic criteria was applied, that is, measuring both channels (Armona Inlet) or choosing the final remaining channel (Lacém Inlet).

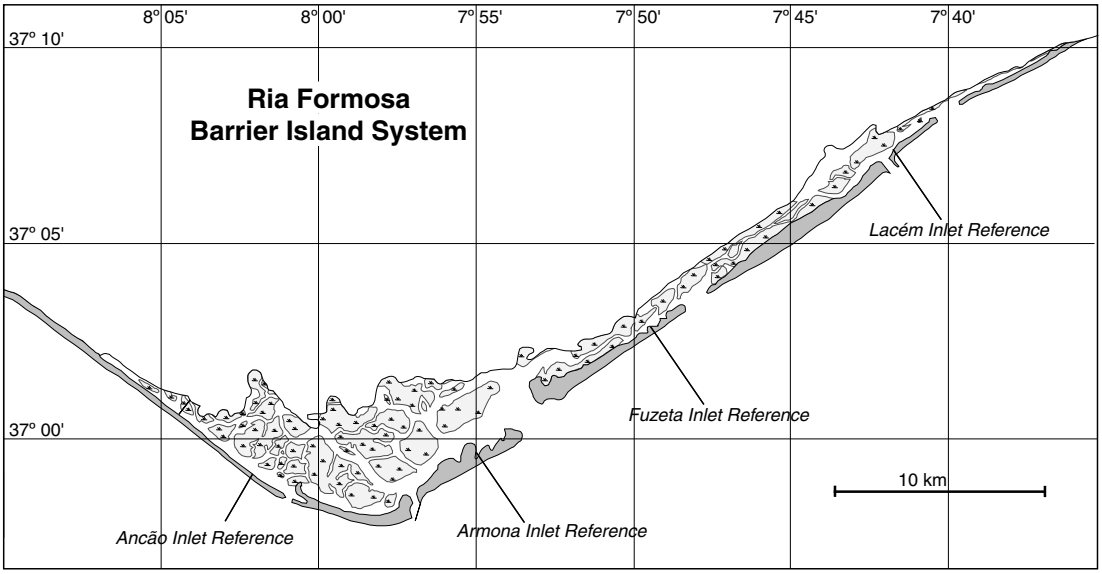

Figure 4.1: Location of the reference points used for the inlet migration studies for each natural inlet in the Ria Formosa barrier island system.

Data sources consisted of a series of aerial photos (see Table 4.1) and one navigation chart published in 1982 by the Portuguese Instituto Hidrográfico (IH), showing Ancão Inlet conditions in 1979-80 (scale: $1:15,000$).

Table 4.1: Coverage and scale of vertical aerial photos used for this study.

Year	Ancão Inlet	Armona Inlet	Fuzeta Inlet	Lacém Inlet	Scale (approximate)
∼1945*	yes	yes	yes	no	$1:20,000$
1969	no	yes	yes	no	$1:25,000$
1972	yes	no	yes	yes	$1:7,000$
1976	yes	yes	yes	yes	$1:25,000$
1985	yes	yes	yes	yes	$1:15,000$
1989	yes	yes	yes	yes	$1:10,000$
1996	yes	yes	yes	yes	$1:8,000$

*Exact date for these aerial vertical photos is unknown.

Complementary data, published by other authors, were used when possible to provide a better coverage of the studied period (see Table 4.2). Data for double channel inlets were only employed if the morphologic criterion was coincident with the one used in this study. Consequently, no additional data were utilised for Armona Inlet and results from Salles (2001) were not used for Lacém Inlet. Andrade (1990) data were not employed because his criteria was not explicit, and his values are remarkably different from those obtained from this and other studies, even for the same years. Other authors obtained their data using fixed lines, that (even if they are also alongshore) possibly have a different orientation from the one used here. An error analysis was performed taking into account the angle of orientation of the line (α), as well as the distance to the reference point (d). A function of error (e) was obtained ($e = 0.0002 \cdot d \cdot \alpha^2$), providing an average error of 30 m for differences between 0.5° and 15° and d between 50 m and 5,000 m, with maximum values of 170 m. Thus, comparison of data provided by other authors introduces an extra error to data accuracy. However, the main aim of the study is focused on determining long period trends rather than specific or short period changes. Therefore, accuracy of the data used is considered to be sufficient for long term trend determination, since inlet position changes are normally in the order of hundreds to thousands of metres.

Table 4.2: Years from which data from other authors were used at specified inlets.

Inlet	Salles (2001)	Esaguy (1985)	Esaguy (1986a)	Esaguy (1986b)
Ancão	1951, 1964	—	1950, 1965, 1978, 1979	—
Fuzeta	1951, 1964	1944, 1955, 1962, 1982, 1984	—	—
Lacém	—	—	—	1950, 1962

Correlation coefficients (Pearson-r, hereafter termed r) between inlet width and channel position were calculated to define possible interdependency between these parameters.

To obtain a better definition of each inlet migration pattern, curve fitting of the inlet evolution over time was undertaken. This involved studying the polynomial or logarithmic relationship between inlet position and time. Comparison of migration patterns between inlets was then made using these curves. However, it should be noted that fitted curves were not calculated with the purpose of predicting future behaviour of the studied inlets, thus they are only applicable in

the positions interval given by the data.

Inlet evolution (width and position) results were then analysed by comparison with engineering actions undertaken in the system (i.e. inlet stabilisation) as well as with storm records obtained from bibliographic sources.

4.2 Medium Term Studies

Medium term studies correspond to the monitoring studies that were performed at Ancão and Fuzeta inlets after their respective relocations. Ancão inlet was monitored from its opening in June 1997 until July 2001. Fuzeta Inlet monitoring was undertaken from the relocation that was performed in July 1999 until August 2001.

4.2.1 Forcing Mechanisms

Offshore wave data were recorded by a directional Wave-Rider buoy placed by IH offshore of Santa Maria Cape (see Figure 3.1) at a location (36°54.3'N, 07°53.9'W) in a depth of 93 m. Records were obtained for every 20 minutes every 3 hours, except during storm periods when data were recorded every half hour. Daily maxima for the study period were available for use in this study. A characterisation of the wave climate of the area was made using these data.

The first two years of Ancão Inlet

To obtain an annual characterisation, data was averaged (including significant wave height, H_s; peak period, T_p; and mean wave direction at peak period, θ_p) for each year and for the whole study period. Wave propagation using a model could not be performed due to the lack of a detailed bathymetric map covering all of the area from the inlet to the wave-rider buoy off Santa Maria Cape. Hourly tidal predictions were used to obtain the tidal characterisation of the study area.

To obtain a relationship between the oceanographic conditions and the inlet evolution, a characterisation of the periods between surveys was done using the wave data averages (H_s, T_p and θ_p), the percentage of '*Levante*' episodes as well as MD_{LEV} (the maximum number of days with continuous '*Levante*' conditions), and the maximum, minimum and average tidal ranges. Since important morphologic changes in inlets are frequently related to the most energetic episodes,

an analysis of energy changes through time was performed. In order to obtain a characterisation of the most energetic periods, average values of H_s, T_p and θ_p were calculated for the 10 most energetic days (with highest H_s) of each of the periods between surveys. Correlation coefficients (Pearson-r) were calculated in order to define possible interdependency between the oceanographic conditions and the inlet evolution. However, only correlations that were significant with more than a 95% of confidence were used in this study.

The entire study period: 1997-2001

Daily maxima between July 1997 and November 2001 were available for use in this study. Values of maximum H_s and their associated T_p and θ_p were used. Linear wave theory was applied to provide an estimation of the deep water incident wave power (P). Morris *et al.* (2001) found that the combination of high tidal levels and storm events was a key factor for explaining the evolution of Ancão Inlet. Therefore, following the methodology used by Morris *et al.* (2001) the wave power P was normalised with the predicted tidal data to obtain the normalised wave power P_n such that:

$$P_n = P(\eta_{dtr}/\eta^*_{dtr}) \tag{4.2.1}$$

where P is the wave power, η_{dtr} is the daily tidal range and η^*_{dtr} is the maximum tidal range. Thus at spring tides $P_n \sim P$ and at neap tides $P_n \sim 0.3P$. According to Morris *et al.* (2001) this parameter conveniently reflects the enhanced erosion potential during high spring tides without totally negating the possibility of some erosion occurring during storm conditions at lower tidal range, when wave set-up can be significant. The P_n thereby calculated was then partitioned according to the direction of the waves: W-SW for those with θ_p>180° and E-SE ('*Levante*') for θ_p<180°.

4.2.2 The Inlets

Topobathymetric Maps

Topo-bathymetric surveys were periodically performed at both inlets from the inlet opening until the summer of 2001. Table 4.3 shows a list of the surveys performed at each inlet. The first survey performed at Ancão Inlet, courtesy of the Ria Formosa Natural park, only covers a part of the area of the dredged channel. Values from this survey will be used to set the original conditions of Ancão Inlet; however, the measurements made in August 1997 will be considered as the *initial conditions* because the survey of June 1997 does not cover the entire inlet area.

Table 4.3: List of the topo-bathymetric surveys that were performed at each inlet.

	Ancão Inlet	Fuzeta Inlet
Jun-97	yes	–
Aug-97	yes	–
Apr-98	yes	–
Jul-98	yes	–
Oct-98	yes	–
Dec-98	yes*	–
Jan-99	yes*	–
May-99	yes	–
Jul-99	yes	yes
Aug-99	no	yes
Nov-99	yes	no
Dec-99	no	yes
Jan-00	yes*	no
Feb-00	no	yes
Mar-00	yes*	no
Jun-00	yes	no
Jul-00	no	yes
Sep-00	yes	no
Oct-00	no	yes
Jan-01	yes	no
Apr-01	yes	yes
Jun-01	no	yes
Jul-01	yes	no
Aug-01	no	yes

*No ebb delta data was measured due to wave conditions.

Each survey was undertaken over two days during spring tide conditions. Tide

tables from IH (IH, 1997, 1998, 1999, 2000, 2001) were used to determine the days where the surveys were to be made. One of the days was used to measure the intertidal and supratidal areas using a total station. The other day, using a boat with an echo sounder, was dedicated to measurement of the subtidal areas. Positioning of the boat was done using a total station, thus avoiding the need for tidal correction in data processing. The intertidal area was also surveyed by boat, when possible, during high tide in order to obtain duplicate points for control of accuracy, and to allow a connection between bathymetric and topographic measurements. Spacing of the measured points was regular over most of the area. However, as suggested by Hicks and Hume (1997), a closer spacing was used in the areas where morphological variations were more dramatic (i.e. sand bars, inlet channel).

The measurements were complemented with a series of oblique aerial photographs taken, when possible, at the same time as the field measurements. A series of topo-bathymetric maps was created using the data (see Appendix A). Through comparison of these maps it is possible to compute volumetric changes as well as to study the inlet channel evolution.

Volumetric Evolution

The volumetric studies included individual quantitative calculations for each of the main morphologic features of the inlet. The methodology used for the study of the volumetric evolution is an adaptation of the 'Ebb-Shoal Edge Method' presented by Stauble (1998). This author described this methodology for the study of an ebb delta, and proposed the definition of a polygon around it. Volume calculations were done above one horizontal plane defining the base of the morphology. The accuracy of the Stauble (1998) method relies on the design of the polygons such they cannot include any area corresponding to other morphologic features. However, this methodology did not seem to be very suitable for migrating inlets as dynamic as Ancão or Fuzeta inlets. The adaptation used in this study consisted of the definition of 3 areas, larger than the morphologies to be studied (Figure 4.2), where volumetric computations were made using fixed vertical levels (defined with morphological criteria) as limits for the different inlet features (Figure 4.3). It is important to note that these areas do not necessarily define separated physical systems or sedimentological units, they are specific regions of interest that take into account different morphological features whilst making optimal use of the available data. For area F (Flood delta area) it was

assumed that the entire area above 0.5 m Z.H. (F> 0.5) would correspond to flood delta evolution, and below that level (F< 0.5) to the inner channels. For areas C (Channel area) and E (Ebb delta area), it was assumed that changes below 1 m Z.H. would correspond to the inlet channel (C< 1) and the ebb delta (E< 1) evolution respectively, whilst differences above that level (C> 1, E> 1) would correspond to changes on the adjacent beach.

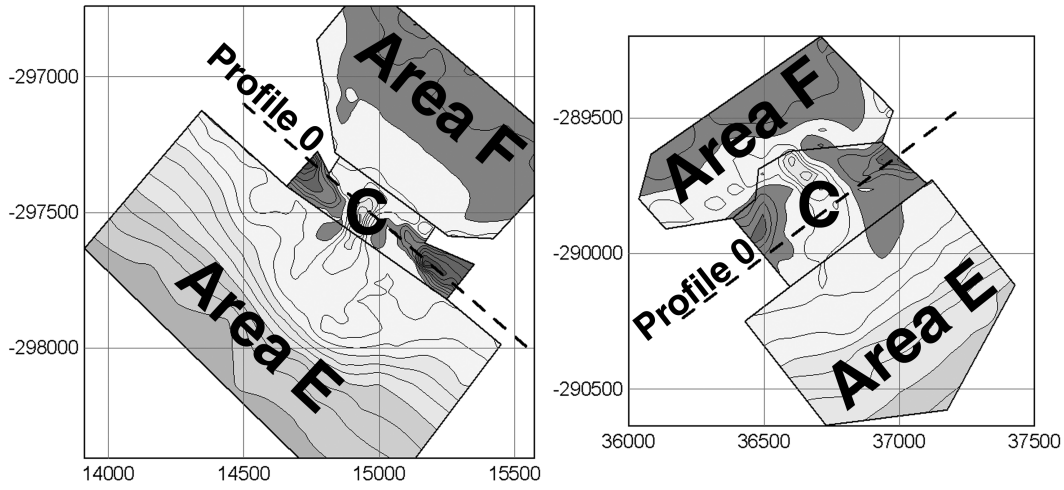

Figure 4.2: Generic areas (F, C and E) defined for volumetric calculations and location of Profile 0 for (a) Ancão Inlet and (b) Fuzeta Inlet.

Measured data for area F were not available during the first year of the evolution of both inlets; the first time that the flood delta was measured was July 1998 for Ancão Inlet and July 2000 for Fuzeta Inlet (see Appendix A, Figures A.3 and A.19). Thus, following the 'Residual Method' described by Stauble (1998), an interval of values was calculated for flood delta accumulation (F> 0.5) during this period. For this purpose three factors were taken into account: extent of the flood delta area one year after the inlet opening; field observations of the sand wedge forming the flood delta; and values of subsequent flood delta erosion. Using these data an approximated initial volume of the delta was calculated (using the area and dimensions of the sand wedge) such that it was larger than the subsequent erosive processes. However, it was not possible to define an interval of values suitable for the evolution of the inner channels (F< 0.5) during the first year. Nevertheless, due to the previous existence of salt marsh areas and tidal creeks in the backbarrier area, volumetric variations in the inner channels are expected to be orders of magnitude smaller than those related to flood delta formation.

The sum of the three partial areas (F, E and C) define the herein named *Total*

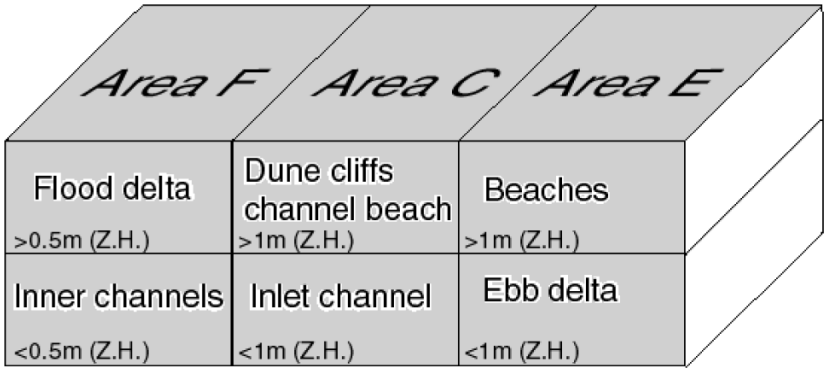

Figure 4.3: Schematic representation of limits and morphologies defined for volumetric calculations.

Area. Volumetric evolution of this larger area was computed in order to have a general idea of the evolution of the entire inlet during the study period. It is important to note that areas defined for the study of the inlets were selected as a function of data point reliability in each survey, however, they are as large as possible given this constraint.

The advantages of the method presented here are: (1) it is possible to use generic areas bigger than the morphology to be studied, and therefore migration does not necessarily imply redefinition of the generic area; (2) a *Total Area* defined by the sum of all the small generic areas provides a control mechanism over the calculations; (3) analyses are not only made for the main morphologic features but for all the inlet parts located inside the *Total Area*. The main disadvantage resulting from the use of this method is that the volume below a horizontal plane does not provide directly the volume of the specified morphologic feature. However, changes in the computed volume provide the evolution of the morphology within the given area.

In order to determine the average vertical error produced by the method, an analysis of the subtidal region located between 6 and 8 m depth was performed. According to Andrade (1990) the closure depth for this area is 6 m (Z.H.), so it was expected that the selected area would show no significant variations. The average vertical error obtained for this area ($\sim$13 cm) was then extrapolated to the entire study area (*Total Area*), providing a maximum error of 65,000 m^3. The main sources of error in the subtidal area are related to the wave conditions during the survey where the movement of the boat implies tilting of the echo sounder and of the prism. However, it is important to point out that vertical errors due to wave conditions are unlikely to occur with the same trend, i.e. always overestimating. To determine vertical errors it would have been optimal to use

the points located in the intertidal area where both topographic and bathymetric measurements were taken. However, these points were not taken in exactly the same locations and as a consequence they could not be used for analysing vertical accuracy but rather were used to provide data quality assessment.

Grid spacing is a function of the original spacing of the data points. Thus, the possibility of errors due to differences in grid spacing was also investigated. Volumetric calculations were performed using different grid spacing for the same data points. Maximum differences in volume were found to be around 4,000 m^3 for the *Total Area*, which can be considered as negligible when compared with errors associated with vertical accuracy.

Inlet Channel Evolution

Inlet channel evolution was studied in two different ways: (1) the inlet throat was defined for each map in order to analyse inlet width at mean sea level (MSL), maximum depth and cross-sectional area (A_c) below MSL; and (2) a longshore profile (Profile 0 in Figure 4.2) was defined in order to analyse inlet migration by defining the changes of the location of the channel axis along the profile.

The tidal prism (Ω) was calculated using the cross-sectional area according to the empirical relationship given by O'Brien (1969) (see Equation 2.3.1). This parameter (Ω) is known to be a good indicator of inlet efficiency.

4.3 Short Term Studies

As part of the INDIA project intensive field campaign, three experiments (AMI.1, AMI.2 and AMI.3) were planned and performed at the easternmost spit of Ancão Peninsula, on the western shore of Ancão Inlet (Figure 3.1). The main objectives were to identify, understand and, when possible, quantify the sediment transport patterns and processes that were occurring on the updrift margin of Ancão Inlet. The identified processes were then analysed together to develop a semi-quantitative conceptual model of the sediment paths and magnitudes. The particular objectives of each campaign are explained individually in Section 4.3.2 together with the setting of the experiments.

4.3.1 Forcing Mechanisms

Two bi-axial electromagnetic currentmeters (EMCMo and EMCMn) were tested and prepared in the laboratory and were used in all the field campaigns. Acquisition frequency used for the EMCMo was 1.6 Hz whilst acquisition frequency for the EMCMn was 16 Hz. These instruments were not self-logging and thus they were hardwired to a PC logging continuously. For the AMI.3 campaign the University of Ferrara deployed its RUNTI system (Ciavola *et al.*, 2000a,b) with one bi-axial electromagnetic currentmeter (EMCMr) and one pressure transducer (PTr). These instruments were self-logging and data was collected as 20 minute bursts at 4 Hz every half an hour. Details of the position of each sensor are given in Section 4.3.2.

Other data used in this study were obtained under the framework of the INDIA project (Williams *et al.*, 1999, 2003): (1) Wind data was obtained *in situ* by the University of Amsterdam between the 12th of January and the 26th March 1999; (2) Off-shore wave data was obtained from a Triaxys wave-rider buoy that was temporarily deployed (between the 13th January and the 25th March) with co-ordinates 36°58.0'N and 08°00.1'W, in a depth of 25 m. Records were obtained every hour. Where there were gaps in buoy records, data was obtained from the wave-rider buoy of IH (see Section 4.2.1).

4.3.2 Setting of the experiments

An irregular grid was defined for the study area according to the morphologic and hydrodynamic characteristics at the time (Figure 4.4). It is important to note that the grid was defined to the east of the westernmost injection point because of the hydrodynamic conditions, waves and currents were eastward directed. This grid was used for topographic measurements and sample collection for all the experiments. Names were given to the profiles using the distance of their origins to a reference profile (Profile 0, P0). Distance between profiles was 50 m in the straight part of the area (P0 to P400), while radial profiles were defined for the inlet margin with a spacing of 10 m between profile origins (P410 to P500). The profiles P520 to P650 were located on the inner beach, spacing between these profiles was variable ranging from 10 to 50 m.

For the preparation of the fluorescent tracers (FT) the methodology given by Ciavola *et al.* (1998) was followed: sediment from the study area was collected

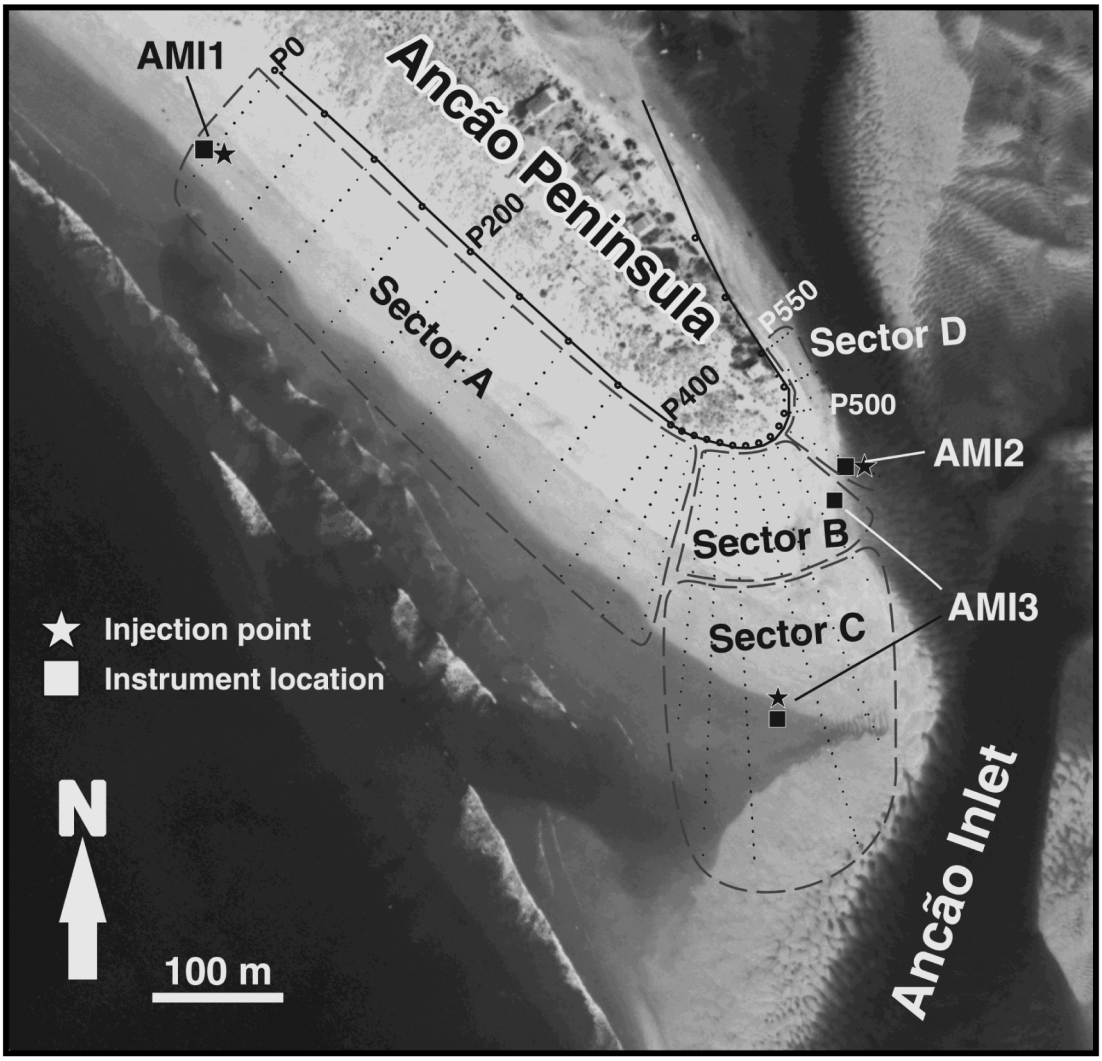

Figure 4.4: Aerial photo of the study area showing the profiling/sampling grid as well as the instrument and injection locations for each campaign. Sectors dividing the study area (A, B, C and D) are also shown.

before each experiment, it was washed with fresh water to eliminate the salt, dried, dyed with orange fluorescent ink (Atomlac Industrie Glycero Orange Fluo) and dried again. The sand was then sieved, eliminating grains with diameter larger than 2 mm in order to remove aggregates that could have formed during the dying process. A sample from the FT was taken to compare it with the natural sand from the study area. Before placing the FT in the field, they were washed with sea-water and a small amount of detergent to lubricate the grains, to avoid the transport of the tracers as a floating layer. As mentioned above, samples were collected along the established grid (Figure 4.4). The area where the samples were to be collected was determined, prior to each sampling, by

detecting the presence of FT using a portable UV light. Shore-normal spacing between the samples along a profile was between 10 and 60 m, depending on the total length of the profile, the spacing being larger on the longer radial profiles located on the sand spit. Sampling was undertaken during the first and second low tides after tracer deployment. Sample collection consisted of shallow cores (∼30 to 40 cm) that were then sectioned into 5 cm samples. Semi-surficial samples, using small containers of 10 cm depth, were taken in areas covered with water or when dispersion of the tracers was expected to be too high. When available, a boat was used for taking submarine samples in the adjacent areas using a Van Veen grab.

AMI.1

The objectives of this campaign were to determine the sedimentary transport patterns of the updrift beach and the inputs of sediment from the beach into the inlet area, quantifying the percentages of sediment either moving towards the backbarrier area or going towards the ebb-delta area.

The AMI.1 campaign was undertaken between the 20th and the 22nd January 1999. The FT, 300 kg, were placed on the lower beach face at P0 (Figure 4.4) on the first low tide of the 20th January. Topographic profiles were measured under low tide conditions on the 22nd using a total station. Deployment of both the EMCM's was carried out at the same time as the placement of the FT. EMCMn was deployed on the lowest part of P0 (Figure 4.4) and EMCMo was deployed close to P500. In both cases, the axis orientation was chosen to measure longshore and cross-shore currents along the beach and at the inner areas. Due to technical problems EMCMo did not acquire any data during this campaign, therefore, its position is not marked in the figure. Elevations above the bed for EMCMn were 10 cm for the first recorded tide and 12.5 cm for the second tide. The first low tide sampling (LTS1) was carried out on the night of the 20th January (AMI.1-1), corer samples were collected along the sampling grid from P0 to P420. The second low tide sampling (LTS2) was undertaken on the morning of the 21st January (AMI.1-2), corer sample collection was performed between P150 and P520. After the sectioning of the cores a total of 930 samples were obtained, 418 of which correspond to AMI.1-1 and 512 to AMI.1-2.

AMI.2

The objectives of this campaign were to determine the sedimentary exchange at the western edge of the inlet and the interactions with both the oceanic and internal beaches, the channel and the ebb delta.

The AMI.2 campaign was undertaken between the 17th and the 19th February 1999. The FT, 100 kg, were placed on the lower part of P490 (Figure 4.4) on the second tide of the 17th February. Topographic measurements of beach profiles were carried out between profile P400 and P550 on the 18th February under low tide conditions. Both EMCM's were deployed, at the same time as the FT, on the lowest part of the inlet margin, on P490 (Figure 4.4), close to the FT injection point. Orientation of the currentmeter axes was: longshore, vertical for EMCMo, and longshore, cross-shore for EMCMn. Elevations above the bed for EMCMo and EMCMn were respectively 31.5 and 34 cm for the first recorded tide and 47 and 48 cm for the second one. Both the EMCM's were higher for the second tide in order to avoid burial due to sand wave movement. The LTS1 was carried out on the morning of the 18th February (AMI.2-1), corer samples were collected between P430 and P520, and a total of 527 samples were obtained after the sectioning of the cores. Additionally, 22 submarine samples were taken from the channel and from the area located in front of the swash platform. The LTS2 was undertaken on the night of the 18th February (AMI.2-2), large dispersion of the FT was expected, and thus 93 semi-surficial samples were collected between P400 and P550. In total, 620 samples were collected during AMI.2.

AMI.3

The objectives of this campaign were to determine the sedimentary exchanges between the swash platform, the western shore of the inlet, the inlet channel and the beach.

The AMI.3 campaign was carried out between the 18th and the 20th March 1999. During the second low tide of the 18th March, 290 kg of FT were placed between P450 and P460, on the swash platform that connects the inlet margin with the ebb delta (Figure 4.4). Due to the coarse nature of the sediments on the swash platform, FT were not sieved for AMI.3. Topographic measurements of the profiles was performed between P350 and P600 on the 18th March. Both the EMCM's were deployed, at the same time as the FT, on the lowest parts of the inlet margin between P480 and P490. Axis orientation was: longshore,

vertical for EMCMn, and longshore, cross-shore for EMCMo. Elevations above the bed for EMCMn and EMCMo were respectively 40 and 18 cm for the first recorded tide and 37 and 44 cm for the second tide, the large variations being due to sand wave migration in the area of deployment. The RUNTI system was deployed on the swash platform close to the FT injection point (Figure 4.4). Axis orientation of EMCMr was to measure longshore and cross-shore currents. The LTS1 was undertaken with cores on the morning of the 19th March (AMI.3-1) between P440 and P500 giving a total number of samples after sectioning of 487. Additionally, 30 submarine samples were taken in the channel and in front of the swash platform using a boat. The LTS2 was carried out on the night of the 19th March between profiles P400 and P540 (AMI.3-2). Due to the expected high dispersion of FT semi-surficial samples were collected, giving 99 samples. In total, 586 samples were collected during AMI.3.

4.3.3 Data Analyses

Forcing Mechanisms

Due to the orientation of the Ancão Peninsula (see Figure 3.1 and 4.4), it is important to note that the shore normal directions are given by 52°N (onshore) and 232°N (offshore). Therefore this axis will be used as the limit between mechanisms that would force the sediment to be transported in a general eastward direction, towards the inlet area (from 52°N to 232°N) or in a general westward direction, away from the inlet area (from 232°N to 52°N). For example, winds, waves or currents coming from a southerly direction would force the sediments to be transported away from the inlet, thus causing transport in a general westward direction.

Wind data corresponding to the days of the experiments were obtained and processed by the University of Amsterdam under the framework of the INDIA project. Data used here corresponds to average wind speed and direction taken every half an hour during the time of the experiments.

The Instituto Hidrográfico (IH) provided the predicted hourly tidal elevation data. For AMI.3, tidal elevation data every 30 minutes was obtained from the PTr data at the RUNTI location.

Offshore wave data from the Triaxys buoy was used for AMI.1 and AMI.2. Due to a technical problem with the buoy, the IH buoy offshore Santa Maria Cape

was used for AMI.3. Wave parameters used for this study were H_s, T_p and θ_p.

During AMI.3 *in situ* wave data were obtained from the PTr. Spectral analysis was used for computing the wave parameters at the RUNTI location, according to methods described in Ciavola (1999).

Data quality control was performed on all currentmeter data files (EMCMo, EMCMn and EMCMr), eliminating files with no reliable/usable data. Data files were then filtered to eliminate high frequency peaks that could be a source of error. Current velocity averages were calculated over 15 minutes sample bursts for EMCMo and EMCMn, and over 30 minutes for EMCMr. The velocity and direction of the resultant current was calculated for every burst.

Topography

Topographic profiles were obtained, and data quality control was performed on the topographic data, prior to the analyses. Topographic maps were generated using the surveys. The interpolation method was linear krigging and spacing of the interpolation nodes was adjusted as a function of the distance between measured points. The morphologic and volumetric evolution of the easternmost spit of Ancão Peninsula was obtained by comparison of the maps.

The profile slopes were calculated for the beach face ($tan\ \beta_{bf}$) on the profiles located on the oceanic beach; and for the swash platform ($tan\ \beta_{sp}$) on those profiles located on the oceanic side of the inlet margin (P430 to P460). The Surf Scaling Parameter (ϵ) (Guza and Inman, 1975) was used to define whether the profile was reflective or dissipative. The Surf Similarity Parameter (ξ_b) Battjes (1974), also known as the Iribarren Number, was calculated in order to determine the breaking type of the incident waves. Breaking wave heights used for the calculation of ξ_b were obtained *in situ* by visual observation. Calculations of the above mentioned parameters on the profiles located on the swash platform and at the inlet margin were not made because at these locations the influence of the bi-directional tidal currents cannot be neglected, and thus these parameters would not have a physical meaning.

Tracer counting: The FENIX system

A total of 2,136 samples were obtained overall during the AMI campaigns, therefore there were too many to consider manual counting as an efficient methodology (in terms of expended time and effort). Therefore, an automatic system for FT counting was developed, the FENIX system. The system consisted of a high-resolution digital camera mounted on a frame where the samples were photographed, in the dark, under a UV light. The pictures were then analysed using a GIS (Geographic Information System) programme that counted the FT grains present in every sample by using an image analysis algorithm. Prior to each counting, a calibration of the FENIX system had to be made. For this, a fixed amount of sand from the study area (20 g), the blank sample with no FT, was photographed and processed. This was done to obtain the background fluorescent properties of the sediments. Following that, known amounts (in grams) of FT were added to the blank sample and each was also photographed and processed. From this, a calibration curve providing the mass of FT present in each sample was determined (Figure 4.5). In this case, the calibration curve was obtained through a linear fit (straight line) because the relationship between the number and the mass of FT is expected to be linear. Results from the FENIX system were carefully compared with those obtained from manual counting, namely AMI.1-1, and the results of that comparison were satisfactory.

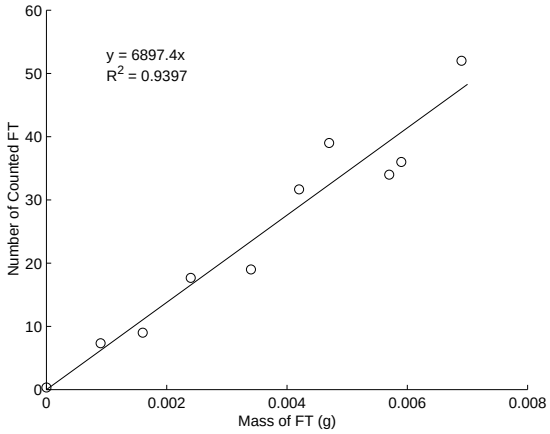

Figure 4.5: FENIX calibration curve (linear fit) used for AMI.1 campaign (After Vila-Concejo *et al.*, 2003b).

Tracers

Grain-size analyses were performed in order to compare the natural sand from the study area with the FT. Grain-size parameters (mean and sorting) were calculated according to the methodology described by Folk and Ward (1957) using the computer program GRADISTAT (Blott and Pye, 2001).

FT grains present in the LTS1 of AMI.1 (AMI.1-1) were manually counted under a UV lamp. The FENIX system was developed and used for the rest of the samples. Due to differences in grain-size, and shell content, the system was properly calibrated for each campaign. The number of FT grains for 100 g of sample was then computed in order to generate maps of distribution of the tracers.

The definition of FT mass centroids was obtained applying the Space Integration Method (SIM). This method has been widely used for the application of tracer techniques to determine longshore transport (e.g., Komar and Inman, 1970; Kraus *et al.*, 1982; Madsen, 1987; Ciavola *et al.*, 1997a, 1998). Some variations were made to the method described by Ciavola *et al.* (1998) to facilitate its applicability to such a complex system as the updrift margin of an inlet.

Co-ordinates (X_i, Y_i) are assigned to each sampling point, using the topographic data as a basis and linear interpolation and trigonometry to calculate the co-ordinates in between topographic points. The area represented by each sampling point (A_{Ri}) is then computed as a function of the distance to the surrounding sampling points. Taking into account that not all the cores reached the same sampling depth, and thus there are variations in the distance to the surrounding sampling points, different areas are calculated for each corer for every 0.05 m layer. Once the A_{Ri} is computed, it is possible to calculate the representative volume (V_{Ri}) for each sample,

$$V_{Ri} = A_{Ri} \cdot h \tag{4.3.2}$$

where h is the height of the samples, $h = 0.05$ m for corer samples and $h = 0.10$ m for semi-surficial samples taken with plastic containers.

The sample volume (V_S) is then defined as:

$$V_S = \pi \cdot k^2 \cdot h \tag{4.3.3}$$

where k is the radius of the sample (corer or container).

A multiplying factor (F_{mi}), that will be used to extrapolate the results of a sample to the entire represented area, is then obtained for each sample by dividing the representative volume (V_{Ri}) by the sample volume (V_S),

$$F_{mi} = V_{Ri}/V_S \tag{4.3.4}$$

The mass of FT in each sample (M_{Si}) is calculated as,

a. For manually counted samples, the number of FT grains in each sample (n) is multiplied by the sand density (ρ_s, 2,650 kg/m^3, for quartz sand), and the average grain volume, V_{FT} (estimated as the volume of a sphere whose diameter equals the mean grain size of the FT):

$$M_{Si} = n \cdot \rho_s \cdot V_{FT} \tag{4.3.5}$$

b. M_{Si} is directly obtained with the FENIX system by applying the linear fit.

The mass of remaining FT in each representative area (M_i) is calculated by multiplying the mass of tracer sand found in each sample (M_{Si}) by the multiplying factor (F_{mi}),

$$M_i = M_{Si} \cdot F_{mi} \tag{4.3.6}$$

The mass of remaining FT for each layer (M_L) is then calculated by the summing of all the M_i obtained for each sample within a determined layer,

$$M_L = \sum M_i \tag{4.3.7}$$

The total mass of FT remaining in the study area (M_T) is then calculated by summing of all the M_L obtained for each studied layer,

$$M_T = \sum M_L \tag{4.3.8}$$

With this, the percentage of remaining FT ($PRFT$), also called the percentage of recovery (i.e., Madsen, 1987; Ciavola *et al.*, 1997a, 1998; White, 1998), in the

study area, which according to White (1998) should be, at the least, between 60% and 80% to be considered as a successful campaign, can be calculated,

$$PRFT = M_T \cdot 100/FT_{injected} \tag{4.3.9}$$

The co-ordinates of the FT cloud centroid (FT_{CL}) for each layer are then calculated as a weighted average of the co-ordinates of each sample, using the percentage of M_i ($\%M_i$) represented by each sample with relation to the M_L as the weighting factor,

$$\%M_i = M_i \cdot 100/M_L \tag{4.3.10}$$

Therefore, the location of a FT_{CL} is calculated for each studied layer,

$$X(FT_{CL}) = \sum (X_i \cdot \%M_i)/100 \tag{4.3.11}$$

$$Y(FT_{CL}) = \sum (Y_i \cdot \%M_i)/100 \tag{4.3.12}$$

The velocity of displacement of the tracer centroids can be calculated for each layer by dividing the distance (d_L) between the injection point and the FT_{CL}, by the time between the two low tides, in this case 12.5 h (45,000 s). A velocity is then obtained for the FT cloud centroid of each layer,

$$V(FT_{CL}) = d_L/45,000 \tag{4.3.13}$$

The vertical integration of FT_{CL} is then calculated by the weighted average of the co-ordinates of each FT_{CL}. For this purpose, the percentage of FT present in each layer ($\%M_L$) in relation to the total mass of FT found in all the layers (M_T) is used as the weighting factor,

$$\%M_L = M_L \cdot 100/M_T \tag{4.3.14}$$

$$X(FT_C) = \sum (X(FT_{CL}) \cdot \%M_L)/100 \tag{4.3.15}$$

$$Y(FT_C) = \sum (Y(FT_{CL}) \cdot \%M_L)/100 \tag{4.3.16}$$

The total velocity of the FT_C is then calculated by dividing the distance (d) between the FT injection point and the location of the FT_C by the time between the two considered low tides, (45,000 s),

$$V(FT_C) = d/45,000 \tag{4.3.17}$$

Velocities of displacement were only calculated for the LTS1 of AMI.1, as it is the only experiment that was undertaken on a fairly straight area with uni-directional longshore currents. The rest of the experiments were undertaken on the swash platform with the combined action of longshore and bi-directional tidal currents (ebb and flood). Therefore, the distance found between the FT_C and the injection point in these experiments is not considered to be representative of the trajectory of the FT, thus velocity calculations were not made.

To calculate the volume of transported sand, it is necessary to calculate the mixing depth, that is the thickness of the moving layer where the grains of sediment are subjected to vertical and lateral movements caused by wave action and by the superimposed longshore currents (Kraus *et al.*, 1982). For this study the mixing depth for each corer sample (Z_{oi}) was calculated according to the methodology proposed by Kraus *et al.* (1982), Kraus (1985) and Ciavola *et al.* (1997b) as the interval within beach cores where 80% of the FT was found. An average cross-shore profile of sand mixing depth was obtained by calculating the mean mixing depth for the samples located at the same cross-shore position along the beach. The sediment transport rate (Q) is a function of the total velocity ($V(FT_C)$) and the thickness of the active layer Z_o, which is the area given by the average cross-shore profile of mixing depth. Therefore, it was only calculated for the LTS1 of AMI.1:

$$Q = V(FT_C) \cdot Z_o \tag{4.3.18}$$

To study the sedimentary patterns at the inlet, four sectors were defined according to the morphology of the study area (Figure 4.4). Sector A (P0 to P420) represents the straight part of the updrift beach, velocities are assumed to be uni-directional and thus, transport velocities can be calculated by the approach explained above. Sector B (P430 to P480, until 100 m from the head of the profiles) represents the upper part of the swash platform located on the eastern-most part of Ancão Peninsula that connects the peninsula with the ebb delta; this sector is naturally separated by a tidal channel from the lower part of the

swash platform. Sector C (P430 to P480, seaward of 100 m from the head of the profile) represents the lower part of the swash platform. Sector D (P490 to P650) represents the inner part of the western shore of Ancão Inlet. Sectors B, C and D are characterised by the existence of bi-directional tidal currents thus, transport velocities cannot be computed. A FT_{CL} was calculated for each sector and a FT_C was then calculated for each sector by an average weighted with the percentages of FT found in each layer within the sector following the methods described above.

Chapter 5

Long Term Studies: Recent evolution of the natural inlets of the Ria Formosa barrier island system

"Ocean, if you were to give, a measure, a ferment, a fruit
of your gifts and destructions, into my hand,
I would choose your far-off repose, your contour of steel,
your vigilant spaces of air and darkness,
and the power of your white tongue,
that shatters and overthrows columns,
breaking them down to your proper purity."

Pablo Neruda, *"The Wide Ocean, Canto General."*

This chapter is partially published by the Coastal Education and Research Foundation:

Vila-Concejo, A., Matias, A., Ferreira, Ó., Duarte, C., Dias, J.M.A., 2002. Recent evolution of the natural inlets of a barrier island system in Southern Portugal. *Proceedings of International Coastal Symposium, 25th - 29th March 2002*, Templepatrick, Northern Ireland. *Journal of Coastal Research*, SI(36), 741-752.

5.1 Results

5.1.1 Ancão Inlet

Ancão Inlet (Figure 3.2) evolution in terms of width and evolution is shown in Figure 5.1. During the study period, this inlet experienced two eastward migration cycles: Ancão-1 and Ancão-2. The opening date of Ancão-1 Inlet is unknown, however, in 1941 a major storm was recorded in the area (Weinholtz, 1964; Esaguy, 1985, 1986a,b; Andrade, 1990) and thus the opening of an inlet at a position close to that recorded for ∼1945 could have occurred. Sometime between 1972 and 1976, a new inlet (Ancão-2) opened at a western position, close to the one of ∼1945 (Figure 5.1). There are no certainties about the exact date of the opening of Ancão-2 Inlet. However Pita and Carvalho (1987) indicated, using hindcast predictions, the occurrence of a very large storm in January 1973. For a short period two inlets co-existed, one at its final stage and the other one at its beginning.

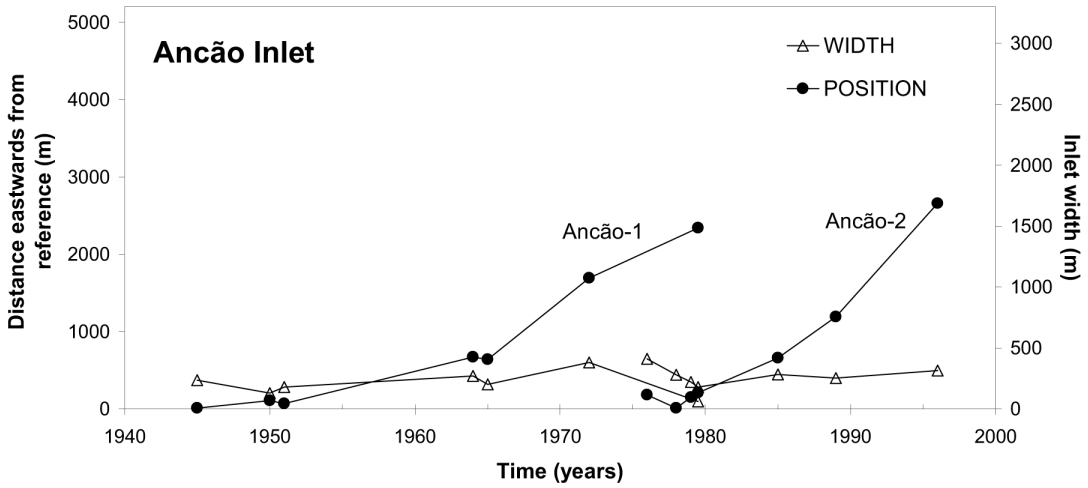

Figure 5.1: Inlet width and displacement evolution of Ancão Inlet between ∼1945 and 1996.

With the exception of the last stage of Ancão-1, where the inlet was almost completely infilled, inlet width did not exhibit strong variations during the study period (Figure 5.1). Average width, not taking into account the last stage of Ancão-1, was found to be 260 m. Maximum inlet width was 410 m reached by Ancão-2 in 1976.

Migration trends were similar for both cycles (r=0.981, significant with 99% of confidence), with the inlet showing an initial stage of readjustment, characterised by low migration rates, followed by a stage of high eastwards migration rates, until a limiting position about 2,700 m from inlet initial position was reached. The Ancão-2 migration cycle was, however, more rapid than the Ancão-1 cycle. Average migration rates were close to 40 m/yr for Ancão-1 and 100 m/yr for Ancão-2. Maximum migration rates occurred in the last stages of inlet evolution with 210 m/yr for Ancão-2. The temporal length of the migration cycle for Ancão Inlet appears to be in the order of 30-40 years.

There is no significant relationship between inlet migration and inlet width evolution. Correlation coefficient values between these parameters are very low, -0.051 for Ancão-1 and 0.163 for Ancão-2. Thus, channel migration and inlet width evolution appear to be independent processes for this inlet, with the inlet width being reasonably constant at all evolutionary stages.

Curve fit values for both cycles of inlet migration are shown in Table 5.1. The best fit for both Ancão migration patterns was found to be a second order polynomial function.

5.1.2 Armona Inlet

Armona Inlet (Figure 3.2) had two channels for the entire study period, both of which appear to have had equal hydrodynamic importance. Due to this, both channels were measured in order to study inlet evolution: Armona W and Armona E. The evolution of the position of both channels as well as inlet width evolution is shown in Figure 5.2.

Inlet width decreased during the study period, with the exception of a small increment of 200 m between 1989 and 1996. Average rates of inlet width decrease were about 30 m/yr for the entire study period, reaching a maximum of about 50 m/yr for the periods ∼1945-1976 and 1985-1989.

Migration rates were calculated separately for both channels, Armona W and

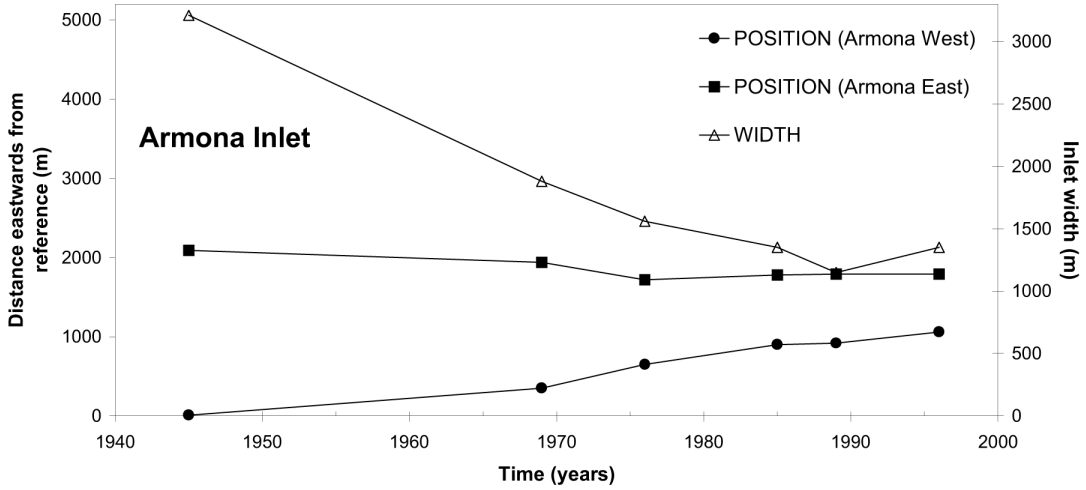

Figure 5.2: Inlet width and displacement evolution of Armona Inlet between ∼1945 and 1996.

Armona E. Eastwards migration occurred for Armona W with an average eastern migration rate of 22 m/yr, and a maximum of 43 m/yr between 1969 and 1976. Armona E showed a first stage of westerly migration with an average migration rate of 19 m/yr. Since 1976, the position of the eastern channel of Armona Inlet has shown little variation. Therefore, and essentially due to the eastward displacement of Armona W, the separation between the channels decreased during the study period. The comparison of the evolution of both channels showed an inverse r of -0.866 that is significant with 95% of confidence.

The correlation between channel position and inlet width was calculated for both channels. It was observed that the decrease of inlet width was inversely related to the migration of Armona W (r=-0.923, significant with 99% confidence) and positively related to the westward displacement of Armona E (r=0.912, significant with 95% confidence).

The best curve fit for both channels was found to be a second order polynomial function, shown in Table 5.1.

5.1.3 Fuzeta Inlet

Fuzeta Inlet (Figure 3.2) width evolution and channel positions through the study period are shown in Figure 5.3. The date of the opening of Fuzeta Inlet is not known, although its western position in 1944, suggests it may have formed

during the major storm of 1941.

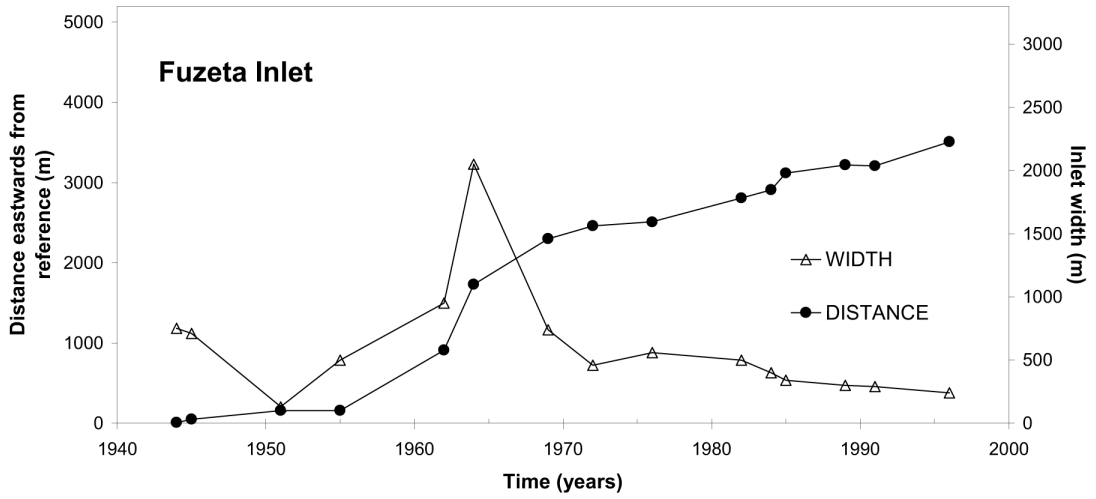

Figure 5.3: Inlet width and displacement evolution of Fuzeta Inlet between ∼1945 and 1996.

Inlet width showed strong variation during the study period, with an average width for the entire period of approximately 600 m. However, three stages can be distinguished:

(a) Between 1944 and 1951 inlet width decreased from 750 m to 130 m.

(b) Between 1951 and 1964 the width increased dramatically to a maximum of 2,050 m.

(c) Between 1964 and 1996 inlet width decreased to 240 m in 1996.

The most important inlet width change occurred between 1962 and 1969 with an initial increase rate of 550 m/yr, followed by a decrease of 260 m/yr. During this period, inlet morphology became more complex, with the existence of two channels. Salles (2001) interpreted maximum inlet width in 1964 as the result of the opening of an inlet west of Fuzeta during a major storm in March 1961 (Weinholtz, 1964; Esaguy, 1986b), and the merging of both inlets in the period between 1962 and 1964 due to natural processes.

Inlet position (Figure 5.3) showed an eastward migration for the entire study period. Three migration stages can also be distinguished:

(a) Between 1944 and 1955 migration rates were low (average migration rate was 19 m/yr).

(b) Between 1955 and 1964 migration rates were high, with an average of 259 m/yr.

(c) Since 1964 until 1996 there was a period of moderate eastward migration with an average rate of 63 m/yr.

The average migration rate for the entire study period was 82 m/yr. The maximum migration rate between 1962 and 1964 (410 m/yr) was possibly associated with the merging of the two inlets.

Correlation between inlet width and channel position was calculated for two periods, before and after the width peak of 1964. Between 1944 and 1964 there was a positive correlation (r=0.892, significant at the 95% confidence level) and between 1969 and 1996 there was an inverse r of -0.924 (significant at the 99% confidence level).

Two different curve fits for the migrating behaviour were calculated for the periods before and after the maximum width. For the period between 1944 and 1964 (Fuzeta-a) the best fit was given by a second order polynomial function (see Table 5.1), while the second period (Fuzeta-b) showed a logarithmic behaviour (Table 5.1). Several authors (Esaguy, 1985; Andrade, 1990; Salles, 2001) found 3,500 m to be the maximum distance migrated by Fuzeta Inlet. Therefore, in 1996, Fuzeta Inlet was near its eastern limit position.

5.1.4 Lacém Inlet

Lacém Inlet (Figure 3.2) was opened by the 1941 major storm (Esaguy, 1986b). Data on inlet width evolution and channel migration is shown in Figure 5.4. The inlet channel showed an eastward migration for the entire study period. Inlet width showed some strong variations, with a generally decreasing trend.

The average width of Lacém Inlet was approximately 1,240 m for the entire study period, with a maximum recorded for 1962 (2,800 m), probably due to the major storm described by Weinholtz (1964) and Esaguy (1986b) that affected the study area in early 1961. A second high inlet width value was observed in 1976 (2,230 m), probably caused by the same storm that opened Ancão-2 Inlet. Until 1976 Lacém Inlet showed 2 channels; merging of the channels caused a strong decrease in inlet width between 1976 and 1985. Lacém Inlet width was still decreasing between 1985 and 1996, however, at much lower rates.

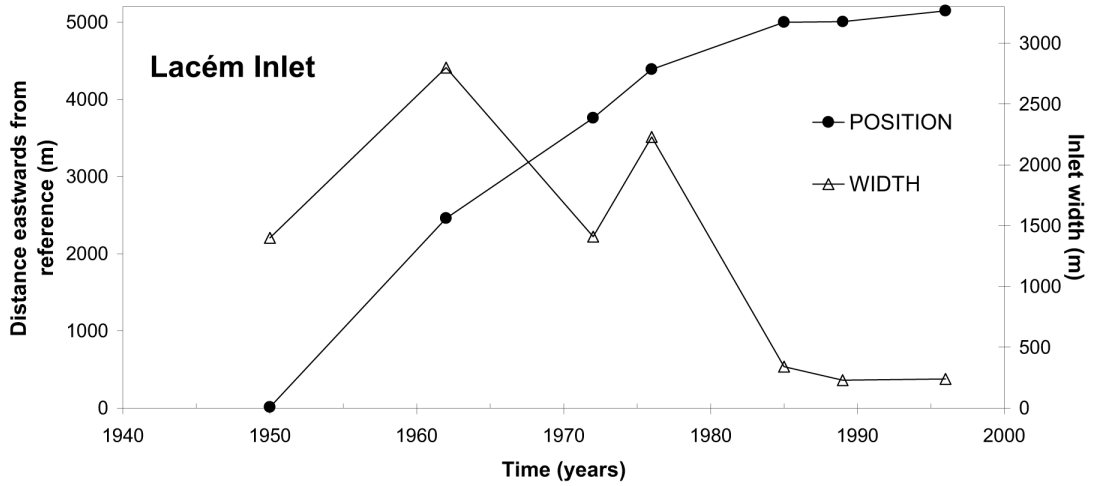

Figure 5.4: Inlet width and displacement evolution of Lacém Inlet between ∼1945 and 1996.

The eastward migration rate of Lacém Inlet had an average value of 97 m/yr. However, migration rates were much higher between 1950 and 1976, with a maximum of 204 m/yr between 1950 and 1962. The minimum migration rate occurred between 1985 and 1989.

Due to the existence of initial width variations, the correlation between inlet width and channel migration was not calculated for the entire study period. Between 1950 and 1972 a correlation coefficient was not calculated due to the existence of only 3 data points with strong changes. However, between 1976 and 1996 there was a significant inverse correlation (r=-0.983 at 95% confidence level) that shows interdependence between inlet width evolution and channel migration.

The best curve fit for Lacém Inlet migration was found to be a natural logarithmic curve, whose function is given in Table 5.1. This function describes reasonably well the behaviour of the inlet channel during the study period. The limit location that defines the end of Lacém Inlet eastward migration on Cacela Peninsula is unknown.

Table 5.1: Details of curve fits obtained for the inlet migration patterns. A second order polynomial fit is used for all inlets, except for Fuzeta-b and Lacém, to express inlet position (P_{inlet}, in metres) in terms of time (t, in years), i.e. $P_{inlet} = a \cdot t^2 + b \cdot t + c$. For Fuzeta-b and Lacém inlets a natural logarithmic curve is used, i.e. $P_{inlet} = a \cdot ln(t) + b$. Determination coefficients (R^2) indicate the percentage of behaviour defined by the curve fit.

Inlet	Coefficients			R^2
	a	b	c	
Ancão-1	2.16	-26.68	103.70	0.983
Ancão-2	5.54	-12.25	-0.29	0.998
Armona W	0.10	-15.44	-86.65	0.974
Armona E	0.15	-15.35	2173.00	0.825
Fuzeta-a	6.57	-111.40	442.78	0.942
Fuzeta-b	1820.6	-3901.2	—	0.960
Lacém	3141.0	-7161.0	—	0.988

5.2 Discussion

5.2.1 Natural versus stabilised inlets

Hydrodynamic studies carried out by Salles (2001) indicate a division of the Ria Formosa barrier island system into 3 hydrodynamically quasi-independent sub-embayments: (a) the western sub-embayment, including Ancão, Faro-Olhão and Armona inlets; (b) the central sub-embayment, including Fuzeta and Tavira inlets; and (c) the eastern sub-embayment, only including Lacém Inlet. However, Andrade (1990) found that Tavira and Lacém inlets were part of the same sub-embayment. It is possible that at the beginning of the study period this could have been the case, however, with the migration of Lacém Inlet this connection would have become less obvious. Given the study period presented here, Lacém is considered to be included in the same sub-embayment as Fuzeta and Tavira inlets. Thus, a western (with Ancão, Faro-Olhão and Armona inlets) and an eastern sub-embayment (with Fuzeta, Tavira and Lacém inlets) are considered. This hydrodynamic division has important implications for the explanation of the effects caused by the artificial opening and stabilisation of both Faro-Olhão and Tavira inlets. Following this division, the artificial opening of Faro-Olhão Inlet (1929-1955) could have had significant consequences for Ancão and Armona inlets, whilst the opening and stabilisation of Tavira Inlet (1927-1985) could have had significant consequences for Fuzeta and Lacém inlets.

Stabilisation of the Faro-Olhão Inlet was completed in 1955 (Esaguy, 1984). In Figure 5.1 it is seen that Ancão Inlet did not experience any significant changes during the first stages of the study period. Andrade (1990) found that Ancão Inlet is only connected with the rest of the system during late flooding or early ebbing stages of the tide. This hydrodynamic semi-independence of Ancão Inlet could have minimised the consequences of the opening and stabilisation of Faro-Olhão Inlet.

The effects of Faro-Olhão Inlet on Armona Inlet have been studied by Esaguy (1984). According to this author, Armona Inlet decreased its width between 1873 and 1983 at an average rate of 20 m/yr and a maximum of 50 m/yr for the period between 1950 and 1977, with this maximum being related with the stabilisation of Faro-Olhão Inlet. Data presented here (see Figure 5.2), show that average decrease rates were about 30 m/yr for the entire study period reaching two maxima of 50 m/yr for the periods ∼1945-1976, which can be directly related

to the stabilisation of Faro-Olhão Inlet, and 1985-1989, whose relationship with these engineering actions is not clear. The works at Faro-Olhão Inlet enhanced an ongoing process, i.e. the reduction of Armona's Inlet width, a process ongoing since the end of the 19th century but which was highly accelerated. Another factor to be taken into account is that Faro-Olhão Inlet was dredged at a location where another inlet had existed before (Esaguy, 1986b). The former inlet (Bispo Inlet), opened in 1861, was almost completely infilled when the construction of Faro-Olhão Inlet begun (Salles, 2001). This may have minimised the consequences of the engineering works.

Tavira Inlet (Figure 3.1) was artificially opened for the first time in 1927, and closed soon after the opening (Esaguy, 1987). In 1936 it was artificially re-opened and stabilised but it closed again by 1950 (Esaguy, 1987). It was re-opened again in 1961 (after the March storm) and in 1985 it was finally dredged and stabilised (Esaguy, 1987). Consequences of the 1961 re-opening of Tavira Inlet in Fuzeta and Lacém inlet evolution are not obvious in Figures 5.3 and 5.4, however, the spacing of the data does not allow differentiation between the consequences of the re-opening and those caused by the 1961 storm. The 1985 stabilisation does not seem to have had important consequences for Fuzeta or for Lacém inlet evolution. It is unrealistic to assume that Tavira Inlet opening and stabilisation in a multi-inlet system did not produce any strong consequences in the neighbouring inlets. However, it is important to note that the hydrodynamic efficiency of Tavira Inlet is very low, representing a very low percentage (about 4%) of the total tidal prism of the system (Andrade, 1990). Thus, its opening did not cause a strong influence on the hydrodynamics of the neighbouring inlets.

5.2.2 Migration trends

According to the results presented here, two main types of migration patterns can be distinguished inside the Ria Formosa barrier island system. Ancão Inlet represents migration where the updrift margin of the inlet is built approximately at the same rate as the downdrift margin is eroded (Figure 5.5a). Both the ebb and the flood deltas migrate at approximately the same rate as the inlet channel (Pilkey *et al.*, 1989), and inlet width is almost constant and therefore independent of inlet migration, except during the last stages of inlet closure (Figure 5.1). Migration patterns for Ancão Inlet showed an initial stage of readjustment, with low migration rates, followed by a stage of high eastwards migration rates, until it

reached a limit position (about 2,700 m from inlet initial position). Lacém Inlet represents the second type of migration, where channel migration is accompanied by strong constructional processes on the updrift barrier, and consequently, by inlet width reductions (Figure 5.5b). This particular form of migration was first described by Pilkey *et al.* (1989) and exists at wide inlets formed by large storms that completely eroded portions of the updrift barrier. Inlet position with time at Lacém Inlet followed a natural logarithmic migration pattern accompanied by inlet width reduction, with the exception of the occurrence of large storm, when inlet width increased (Figure 5.4).

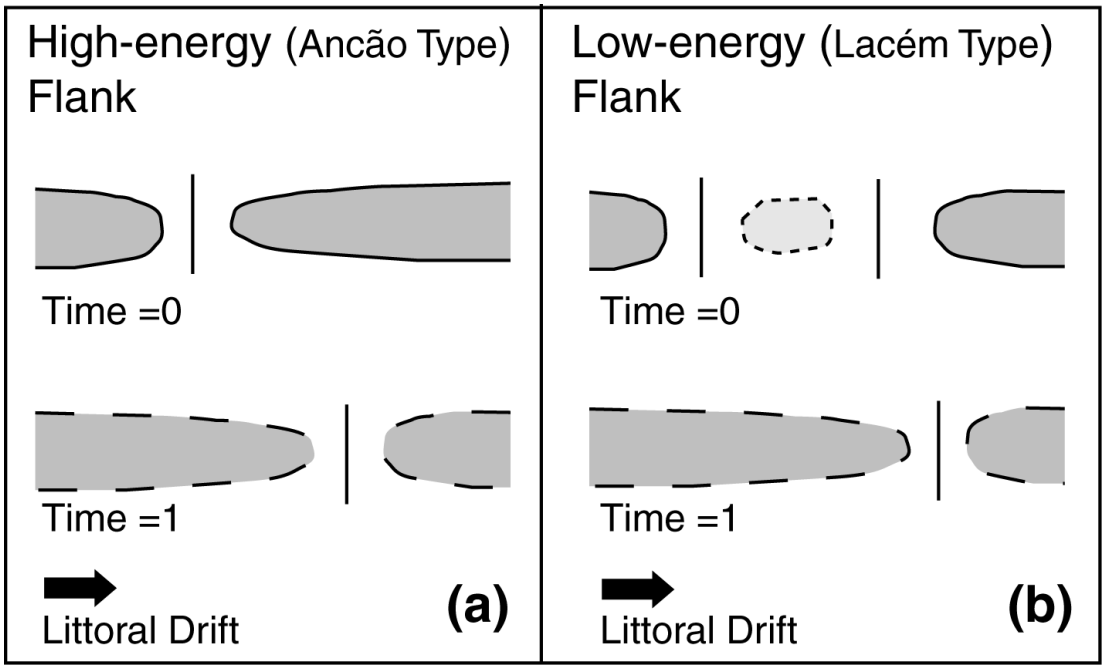

Figure 5.5: Typical inlet migration patterns determined for the natural inlets in the Ria Formosa barrier island system. (a) Represents the Ancão type of migration, typical of the high-energy flank. (b) Shows the Lacém type of migration, typical for the low-energy flank.

Differences between these two migration patterns are due to several reasons:

(a) Incident wave energy is much greater on the west flank and decreases towards the east, Cacela Peninsula being the least energetic area of the system (Andrade, 1990).

(b) Barriers located updrift from the inlets in the east flank have lower dune areas that present a high degree of overwash susceptibility (Andrade *et al.*, 1998) and thus, destruction of large portions of these barriers is more likely to occur on the east flank of the Ria Formosa.

However, these factors do not completely explain the different migration patterns obtained in this study.

Fuzeta Inlet is a mixed case where the inlet started with a pattern similar to the one observed for Ancão (see Figure 5.5a), however, as consequence of a major storm event, a large portion of Armona Island was eroded and Fuzeta Inlet became very wide. Since that time, the migration pattern observed for this inlet has been logarithmic and therefore, similar to that observed for Lacém Inlet (see Figure 5.5b). It appears that the destruction of the easternmost tip of Armona Island after the 1961 storm caused the change in the migration pattern. Pilkey *et al.* (1989) explained Fuzeta Inlet migration as occurring in a series of 'jumps', as a new inlet would open during a storm at a short distance east of the former position. Data presented here do not show evidence of the migration occurring by 'jumps', nevertheless, some 'jumps' may have occurred without effecting the long term migration patterns of the inlet. An inlet 'jump' would help to explain the very high migration rates found for the period 1962-1964. Consequences of the 1973 storm, that possibly opened Ancão-2 and caused a peak in Lacém Inlet width, on Fuzeta Inlet are not obvious in Figure 5.3. Overwash susceptibility in the vicinity of Fuzeta Inlet is not as high as around Lacém Inlet, and the maximum width of Lacém Inlet after the 1961 storm was much greater than the one recorded for Fuzeta Inlet. Thus, the energy required to erode Fuzeta Inlet margins and increase its width is greater than that needed to erode Lacém Inlet margins.

Armona Inlet represents a peculiar case. As explained previously, narrowing of the inlet has been an ongoing process since at least 1873 (Esaguy, 1984). As shown in Figure 5.2, the two Armona channels are converging. Esaguy (1984) stated that once both of the channels have merged, the remaining channel would get deeper and start an eastward migration similar to that described for Ancão Inlet. Data presented in this study do not show any evidence to supporting this theory, which can only be verified in the future, after the merging of the channels. However, it seems to be possible that Armona Inlet, like the other natural inlets located on the east flank, was formed during a major storm (perhaps in the last century) that eroded most of Culatra Island. Inlet migration (Armona W) due to updrift barrier re-construction, such as occurs at Lacém Inlet (see Figure 5.5b), is an ongoing process, showing slower rates that the other inlets with this type of migration pattern, i.e. Lacém Inlet and the second phase of Fuzeta Inlet.

5.3 Conclusions

A study of the evolution of the four natural inlets of a multi-inlet barrier island system was presented in this chapter. Both natural variations of the hydrodynamic forcing factors, and variations caused by engineering interventions, namely the artificial opening and stabilisation of two inlets on the east flank of the system, were taken into account.

The consequences of the artificial opening and stabilisation of an inlet are mainly related to three factors: (a) the existence of sub-embayments inside the system that constrain the number of natural inlets that will be under the influence of the engineering interventions; (b) the exposure to wave energy that affects inlet behaviour; and (c) the location of the artificial inlet within the system that determines its hydrodynamic efficiency.

Two sub-embayments were defined within the Ria Formosa barrier island system, the western sub-embayment including Ancão, Faro-Olhão and Armona inlets, and the eastern sub-embayment, including Fuzeta, Tavira and Lacém inlets. Data presented in this chapter showed that Ancão Inlet, due to its quasi-independency within the western sub-embayment, did not show any observable variations in its behaviour after the opening and stabilisation of Faro-Olhão Inlet. However, the width of Armona Inlet, which had been decreasing since the end of the 19th century, started to decrease at much higher rates, thus losing some of its hydrodynamic efficiency. It is believed that the consequences of the opening and stabilisation of Faro-Olhão Inlet were not greater because it was performed in a former inlet position. Due to the low hydrodynamic efficiency of Tavira Inlet, analyses performed for Fuzeta and Lacém inlet showed no directly related variations in their behaviour after the opening and stabilisation of Tavira Inlet.

Results presented in this study showed that long term inlet migration patterns are eastward for the whole system. Two very well differentiated migration patterns were found for this system (see Figure 5.5): one for the high-energy (west) flank, and one for the low-energy (east) flank of the system. Migration patterns were found by analysing the relationships between inlet width evolution and inlet migration as well as by comparison of the shape of the curve fits. Typical migration for the high-energy flank is characterised by an initial stage of readjustment, with low migration rates, followed by a stage of high eastward migration rates, until reaching a limit position. Inlet width stays reasonably constant during the entire migration cycle, thus Pearson-r coefficients (r) between

inlet width and position are very low. Typical low-energy flank inlets are formed by barrier breaking during a storm, giving large values of inlet width during the initial stage. Migration patterns for the low-energy flank follow the trend of a natural logarithmic curve, where strong construction processes on the updrift barrier accompany channel migration. As a consequence, inlet width generally decreases with the migration, and values of r between inlet width and inlet migration are generally significant. Due to the high overwash susceptibility of inlet margins on this flank, inlet width could increase during large storms.

Chapter 6

Medium Term Studies: The first two years of Ancão Inlet

"[...] even in his most artificial creations, nature is the material upon which man has to work; certain spots will persist in remaining surrounded by the vassals of their own especial sovereignty, and will raise their immemorial standards among all the 'laid-out' scenery of a park, just as they would have done far from any human interference, in a solitude which must everywhere return to engulf them, springing up out of the necessities of their exposed position, and superimposing itself upon the work of man's hands."

Marcel Proust, *"In Search of Lost Time. 1.-Swan's Way."*

This chapter is partially being published by Elsevier:

Vila-Concejo, A., Ferreira, Ó., Matias, A., Dias, J.M.A.. The first two years of an inlet: sedimentary dynamics. *Continental Shelf Research* (in press).

6.1 Results

6.1.1 Oceanographic conditions

The average offshore wave conditions at Santa Maria Cape (see Figure 3.1) for the entire study period (June 1997 to July 1999) are shown in Table 6.1. As can be observed in the Table, annual averages of mean H_s and T_p showed higher values during the first year of inlet evolution than during the second year. Although the dominant wave direction (θ_p) was from the W during 57% of the time, average direction was from the SW for the entire period (Table 6.1).

Table 6.1: Averaged offshore wave conditions at Santa Maria Cape wave-rider buoy during the first two years of Ancão Inlet evolution.

		H_s (m)	T_p (s)	θ_p (°)
1st year	Winter	1.31	9.54	206.7
	Summer	0.80	6.53	224.2
	Annual	1.06	8.03	215.4
2nd Year	Winter	0.79	8.76	217.7
	Summer	0.70	6.49	223.1
	Annual	0.75	7.63	220.4
Total		0.9	7.83	217.9

Seasonal variations were studied using the definitions of maritime winter (October to March) and maritime summer (April to September) that are commonly used on the Portuguese coast. Both years showed higher values of mean H_s and T_p in winter than in summer (Table 6.1). The summer to winter increment of average H_s and T_p registered during the first year was much larger than the second year (see Table 6.1). The first year of inlet evolution was much more energetic than the second: mean H_s values for the first year summer (0.8 m) were found to be almost the same as those during the second year winter. Storms during the first year were found to occur 7.5% of the time (96% during maritime winter);

during the second year, this percentage decreased to 1.2% (100% during maritime winter).

Wave and tidal data results for the periods in between surveys are shown in Figure 6.1. MD_{LEV} (Figure 6.1a) had maximum values for the period before the April 1998 survey (36 days) and before the October 1998 survey (10 days). The percentage of '*Levante*' events showed some variations, reaching a maximum ($\sim$40%) in the period between October and December 1998. Tidal ranges were very similar during the periods considered (Figure 6.1b), however, some variations in tidal range appeared to exist between December 1998 and January 1999 (a minimum in the maximal tidal range, and a maximum in the minimum tidal range) that were due to the short duration of the period (2 weeks). Therefore, these tidal variations are considered artificial and will not be taken into account for further analyses.

Results obtained by calculating the averages of H_s, T_p and θ_p for the 10 most energetic days of each period are also shown in Figure 6.1c. As can be seen, the most energetic events in the area (corresponding to the period before the April 1998 survey) were from the southwest ($270° < \theta_p < 180°$). Mean direction obtained for the 10 most energetic days was from '*Levante*' ($180° < \theta_p < 90°$) only in the periods before the December 1998 and May 1999 surveys. As expected, T_p seemed to increase for higher values of H_s. The highest and the lowest values for T_p and H_s were registered for waves from the southwest.

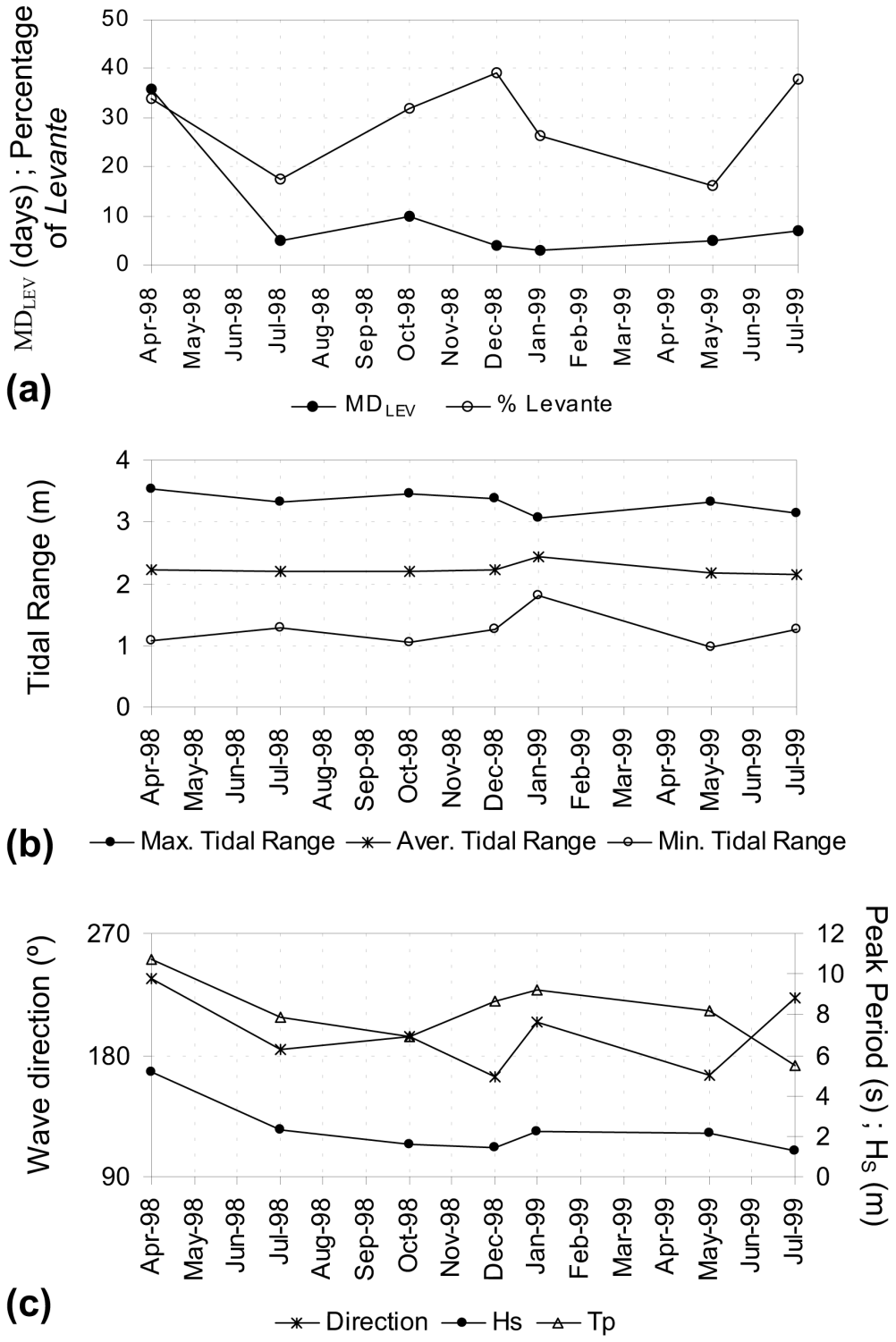

Figure 6.1: Summary of wave and tidal conditions during the first two years of Ancão Inlet: (a) Maximum number of days with continuous '*Levante*' conditions (MD_{LEV}) and the percentage of '*Levante*' conditions; (b) Maximum, average and minimum tidal range (m) for each period considered; and (c) Average values for the 10 most energetic days, significant wave height (H_s), and peak period (T_p) are shown on the right axis, the left axis shows the direction (θ_p) in degrees.

6.1.2 Inlet Channel

Inlet Throat

According to the bathymetric survey undertaken in August 1997 the new Ancão Inlet had a cross-sectional area below mean sea level (A_c) at inlet throat of about 310 m^2. An increment of almost 400 m^2 occurred between August 1997 and April 1998 (Figure 6.2a) leading to an A_c of 700 m^2. After April 1998, A_c decreased slowly reaching values of 640 m^2 and 530 m^2 in July and October 1998 respectively. The maximum value for A_c was 750 m^2 in December 1998, a rapid decrease (130 m^2) occurred between this survey and January 1999 (Figure 6.2a) and after that time A_c showed smaller variations having values between 580 m^2 (May 1999) and 670 m^2 (July 1999). No significant values (over 95% of confidence) of Pearson-r (r) were found between A_c evolution and the parameters representing the oceanographic conditions.

Inlet width (MSL) evolution at inlet throat is also presented in Figure 6.2a, a strong increment (150 m) occurred between August 1997 and April 1998 when width at inlet throat reached 240 m. After that, variations in inlet width were smoother reaching a minimum value of 220 m in October 1998 and a maximum of 400 m in May 1999. Between May and July 1999, variations in width at inlet throat were negligible. Strong interdependency was found between inlet width evolution (Figure 6.2a) and H_s of the 10 most energetic days (Figure 6.1c) of each period, providing a Pearson-r coefficient value of 0.941 which is significant with 99% of confidence. However, since April 1999, most of the inlet width variance was related to changes in the downdrift margin of Ancão Inlet. Thus, relating to eastwards migration processes that were probably related with the dominant SW direction found for most of the most energetic days of each period.

Maximum channel depth at inlet throat is also represented in Figure 6.2a. Equilibrium values for maximum channel depth were realised soon after opening (3.8 m and 4.4 m in August 1997 and April 1998 respectively). The average value for inlet maximum depth was 4.3 m for the entire study period, variations in inlet maximum depth at channel throat were generally small (Figure 6.2a). However, in December 1998 and July 1999, inlet depth increased by more than 2 m, reaching on both occasions depths over 5.3 m. Significant values of Pearson-r correlation coefficients were not found when comparing the evolution of maximum channel depth at inlet throat with forcing mechanisms.

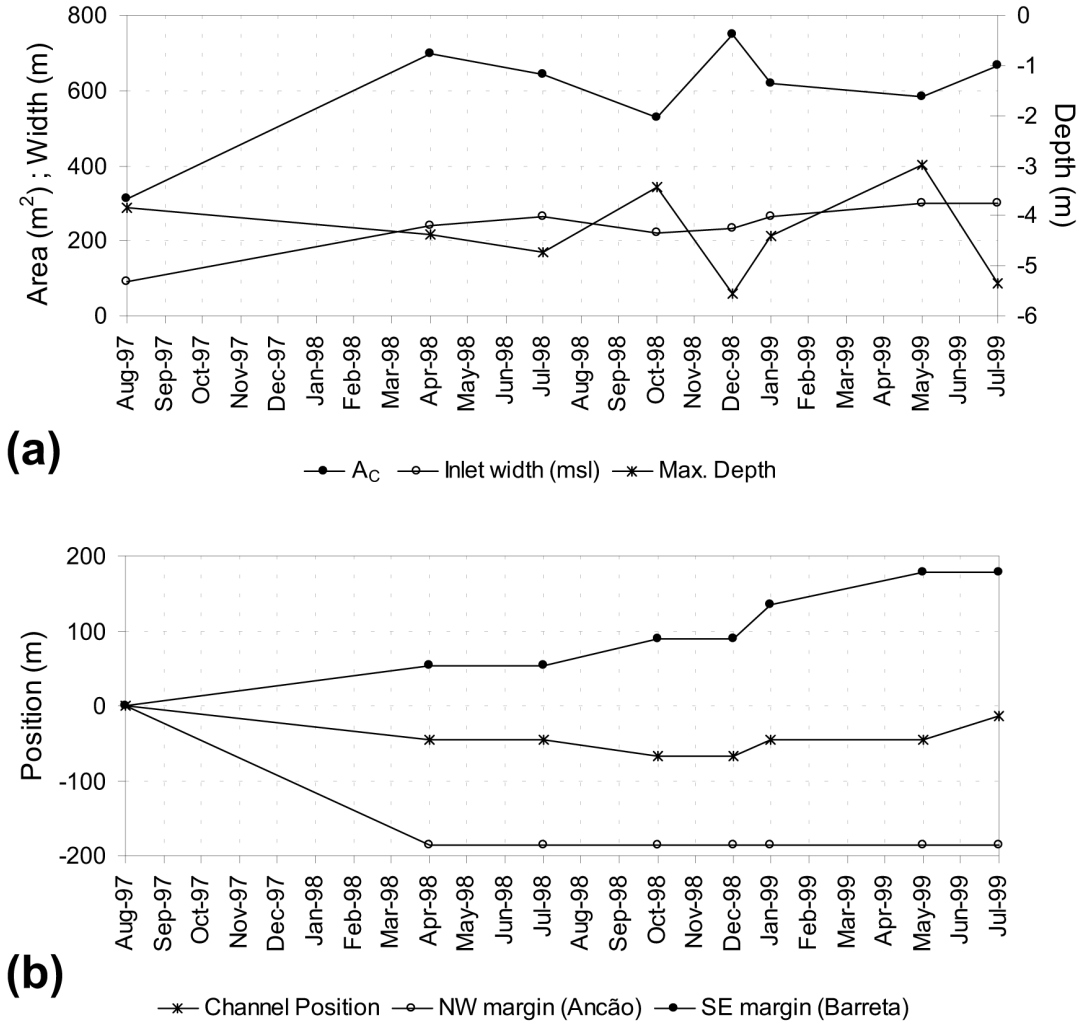

Figure 6.2: Inlet channel evolution between August 1997 and July 1999. (a) Evolution at inlet throat: inlet cross-sectional area below MSL (A_c in m^2) and channel width (m) are shown on the left axis; channel maximum depth (m) is shown on the right axis. Depth is referred to the Portuguese Hydrographic Zero (2 m below MSL). (b) Evolution at Profile 0: Position of inlet channel, and both margins of the inlet through time. Note that negative values represent positions west of the position in August 1997.

Inlet migration and associated processes

Inlet channel position, computed using Profile 0 (see Figure 4.2), also changed during the first two years of the inlet evolution (Figure 6.2b). Following historical data, it was expected that after some initial readjustments the inlet would start to migrate eastwards. This did not occur and between the opening and April 1998 an unexpected movement towards the west of about 80 m was found. Alongshore

dune cliff retreat at the channel western margin (Ancão Peninsula) due to channel migration was approximately 190 m between August 1997 and April 1998 (Figure 6.2b). Westward movement of the deepest point of the channel continued until October 1998, with a net movement of 101 m. In January 1999, the expected downdrift migration began, with a total eastward movement up until July 1999 of about 52 m. As a consequence, inlet channel position in July 1999 was still 50 m to the west of the observed position at opening. Downdrift migration of the channel implied the subsequent alongshore dune cliff erosion of the SE margin of the inlet, Barreta Island. Figure 6.2b also shows that inlet position changes did not occur in a continuous way, since during some of the periods included in this study there was no movement or migration. Pearson-r coefficient values showed inverse interdependency (r=-0.792 with 95% of confidence) between inlet channel position (Figure 6.2b) and MD_{LEV} (Figure 6.1a); meaning that an increment in MD_{LEV} would imply westward displacement of the inlet (negative values).

6.1.3 Volumetric evolution

Volumetric computations were performed for the period between August 1997 and May 1999. Three areas were defined to analyse the volumetric evolution of the study area (Figure 4.2). Volume changes determined during the analysed period for each area can be found in Table 6.2. No significant values of Pearson-r coefficient were found between volumetric evolution and forcing parameters.

Partial Evolution: Area F

F>0.5 (flood delta): Using the geometric/morphologic approach (based on the criteria of Stauble, 1998) an accumulation between +125,000 and +200,000 m^3 was computed for the flood delta during the first year of inlet evolution (August 1997 to July 1998). During the second year (July 1998 to May 1999), some erosion occurred in this area (-79,600 m^3). Most of the erosion on the flood delta occurred between October and December 1998, coincident with an observed retreat of the front part of the delta. In total, an accumulation between +45,400 and +120,400 m^3 occurred on the flood delta during the first two years of inlet evolution.

As can be observed in Table 6.2, the only two erosive episodes took place, between October and December 1998, and between January and May 1999, these

erosive episodes were possibly related to the direction of the waves during the 10 most energetic days of each period, given that these periods were the only ones when the 10 most energetic days showed a '*Levante*' direction (see Figure 6.1c).

F<0.5 (inner channels): As has been stated previously, it was not possible to define the evolution of the inner channels during the first year. In the second year, between July 1998 and May 1999, a small net accumulation of +28,800 m^3 occurred. Except for the period between October 1998 and January 1999, this area did not show very strong volumetric variations (Table 6.2). During that period, an erosion between October and December 1998 was followed by the accumulation that occurred between December 1998 and January 1999. The erosive episode was possibly related with the '*Levante*' conditions during the 10 most energetic days (Figure 6.1c).

Partial Evolution: Area C

C>1 (dune cliffs and inlet margins): During the first year of inlet evolution this partial area showed a very severe erosion of -315,100 m^3 mainly due to the channel enlargement (Table 6.2). In the second year, this erosion was less dramatic with a value of -39,600 m^3. The overall erosion was -354,700 m^3. The strongest erosion period was found to be between August 1997 and April 1998 (-283,100 m^3), induced by the significant enlargement of the inlet channel (about 150 m in inlet width at MSL and almost 400 m^2 in A_c below MSL, see Figure 6.2a). A small accumulation of +18,600 m^3 occurred between July and October 1998, due to the development of a sand spit on the end of Ancão Peninsula possibly related with the low-energy conditions registered for this period (see Figure 6.1c).

C<1 (inlet channel): The evolution of this area is marked by relatively small volumetric changes. During the first year an erosion of -14,400 m^3 was found. The strongest erosion during this period was coincident with the most significant enlargement of the inlet channel, between August 1997 and April 1998 (-18,000 m^3). In the second year, a small erosion of -3,000 m^3 occurred, this relatively small value was indicative of volumetric stability for the inlet channel. Between October 1998 and January 1999 strong variations occurred in the inlet channel, with an erosion of about -30,000 m^3 (until December 1998) followed by accretion of approximately +24,000 m^3 (until January 1999). These strong variations were possibly related to the '*Levante*' conditions registered for the 10 most energetic days of the period between October and December 1998 (Figure 6.1c). During

the first two years of inlet evolution a net erosion of -17,400 m^3 occurred.

Partial Evolution: Area E

E>1 (beaches): Erosion of -66,900 m^3 occurred during the first year of inlet evolution. After the strong erosion that occurred in the first year of the study period, this area became almost stable, with an observed net erosion of only -1,800 m^3 during the second year (Table 6.2). The total erosion over the whole study period was -68,700 m^3.

E<1 (ebb delta): Between August 1997 and July 1998, this area underwent an accumulation of +612,200 m^3. Accumulation between August 1997 and April 1998 was approximately the same as that for the period between April 1998 and July 1998 (around +300,000 m^3). During the second year, an accumulation of +39,600 m^3 was found. Total accumulation for the two years was +651,800 m^3.

Total Evolution

Not all the surveys covered the entire study area. Therefore, detailed volumetric changes for the *Total Area* were only calculated for the period between July 1998 and May 1999 (second year of inlet evolution). Nevertheless, an approximation to the values of the *Total Area* during the first year was made. An interval of accumulation between +340,800 m^3 and +415,800 m^3 was calculated for the *Total Area* during the first year of inlet evolution. Although the evolution of the inner channels (F<0.5) is not included in these computations, it appears that the volumetric evolution of the inner channels would have been orders of magnitude smaller than that which occurred in other areas related to delta formation and channel enlargement. During the second year, a smooth erosion of -55,600 m^3 occurred in the *Total Area* which, given the accuracy of the data, is considered as being not significant implying volumetric stability and thus dynamic equilibrium for the second year. From August 1997 to May 1999, the *Total Area* experienced an estimated accumulation of between +285,200 m^3 and +360,200 m^3 (no data for F<0.5 during the first year).

Yearly volumetric changes in the analysed generic areas, and their associated vertical differences, are shown in Table 6.2 and in Figure 6.3. Coinciding with the development of the main inlet features, the volumetric variations were more dramatic during the first year of inlet evolution. In Figure 6.3a the following can be

observed: (1) strong accumulation due to ebb delta development; (2) significant retreat of the shoreline and erosion of backshore and dunes due to inlet readjustments, with vertical erosion up to 12 m; and (3) infilling of the artificially opened channel associated with the westward migration of the inlet channel that was due to the MD_{LEV} values mentioned above. During the second year of inlet evolution, volumetric variations were of less importance (see Table 6.2) indicating a certain degree of equilibrium in the system. In Figure 6.3b it can be appreciated that the single strong vertical variation was due to the eastward migration of the inlet channel, accompanied by the subsequent readjustments of the ebb delta. Summing the absolute volumetric changes (the values of erosion and accumulation) for each generic area it was found that absolute volumetric changes during the first year (between 1,133,600 m^3 and 1,208,600 m^3) were about 7 times greater than those occurring in the second year (163,600 m^3). This suggests that Ancão Inlet reached a state of dynamic equilibrium by the end of the first year of its evolution. This is confirmed by the existence of well developed flood and ebb deltas as well as sand spits at both sides of the inlet in July 1998 (see Appendix A, Figure A.3).

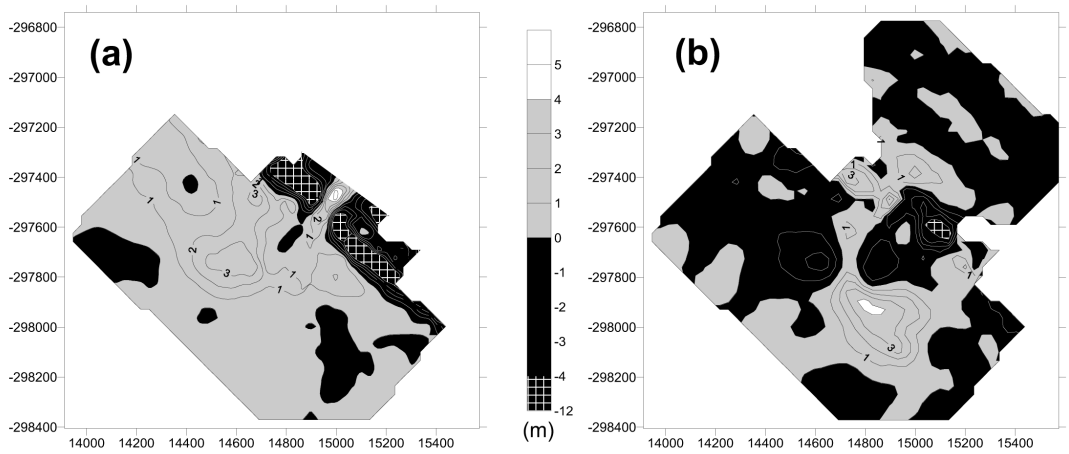

Figure 6.3: Isopach contour map showing yearly vertical evolution (m) of the *Total Area*, during the first year (a) and the second year (b) of the evolution of Ancão Inlet.

Table 6.2: Volumetric evolution of the main morphologic areas of Ancão Inlet system (in 10^3 m^3).

		AREA F		AREA C		AREA E	
		F>0.5	F<0.5	C>1	C<1	E>1	E<1
1st	Aug97-Apr98	—	—	-283.1	-18.0	-51.4	+305.1
Year	Apr98-Jul98	—	—	-32.0	+3.6	-15.5	+307.1
	Annual	+(125-200)	—	-315.1	-14.4	-66.9	+612.2
	Jul98-Oct98	+20.3	+10.6	+18.6	-6.3	+7.5	+12.1
2nd	Oct98-Dec98	-158.1	-46.6	-1.6	-29.6		
Year	Dec98-Jan99	+100.6	+51.7	-52.9	+24.4	-9.3	+27.5
	Jan99-May99	-42.4	+13.1	-3.7	+8.5		
	Annual	-79.6	+28.8	-39.6	-3.0	-1.8	+39.6
Net values over two years		+(45.4-120.4)	+28.8	-354.7	-17.4	-68.7	+651.8

6.2 Discussion

In this section a conceptual model of the natural evolution of an artificially opened inlet is presented that was developed based on the results of the monitoring program of Ancão Inlet . The evolution of Ancão Inlet with relation to the stages of this conceptual model as well as to oceanographic forcing mechanisms is then discussed. Finally, the conceptual model is applied to another artificially opened inlet.

A schematic of the conceptual model is presented in Figure 6.4. Stages 1 to 3 represent inlet formation and evolution under non-storm wave conditions. Transition between these stages is a continuous phenomenon with intermediate sub-stages. Stage 1 (Figure 6.4a) shows the inlet immediately after its opening, the inlet channel is narrow with steep artificial dune cliffs on both margins. Forcing parameters, tides and waves, then cause the enlargement of the channel and equilibrium values for A_c are reached, thus beginning Stage 2 of inlet evolution. During Stage 2 (Figure 6.4b), the inlet is acting as a sediment trap providing sediment for the formation of sand spits on both sides of the channel and development of both deltas indicating sediment transport in and out of the inlet. The end of Stage 2 is reached when both deltas reach volumetric dynamic equilibrium. Stage 3 (Figure 6.4c) represents the *mature migrating inlet*, where the inlet is no longer acting as a sediment trap allowing some bypassing to occur. Downdrift migration of the channel is now accompanied by updrift spit growth and the migration of both deltas that can become asymmetric. Stage PS (Post-Storm) shows the situation after high-energy conditions (Figure 6.4d). Transition to Stage PS is a discrete phenomenon, caused by high-energy events, after which the inlet will follow a continuous change back to the previous stage.

In August 1997, almost two months after its opening, Ancão Inlet was still showing immature characteristics such as a narrow channel with steep margins (see Appendix A, Figure A.1). Values for A_c were small (Figure 6.2a) thus, following the relationships given by O'Brien (1969) the tidal prism captured by the new inlet was equally small. Ebb and flood deltas were not yet developed, however, curvature of the isobaths indicates the formation of embryonic deltas (see Appendix A, Figure A.1). All of these characteristics are shown in Figure 6.4a, corresponding to Stage 1 of the conceptual model.

After the initial stage it was expected that Ancão Inlet would undergo modifications caused by the forcing parameters that would lead towards dynamic

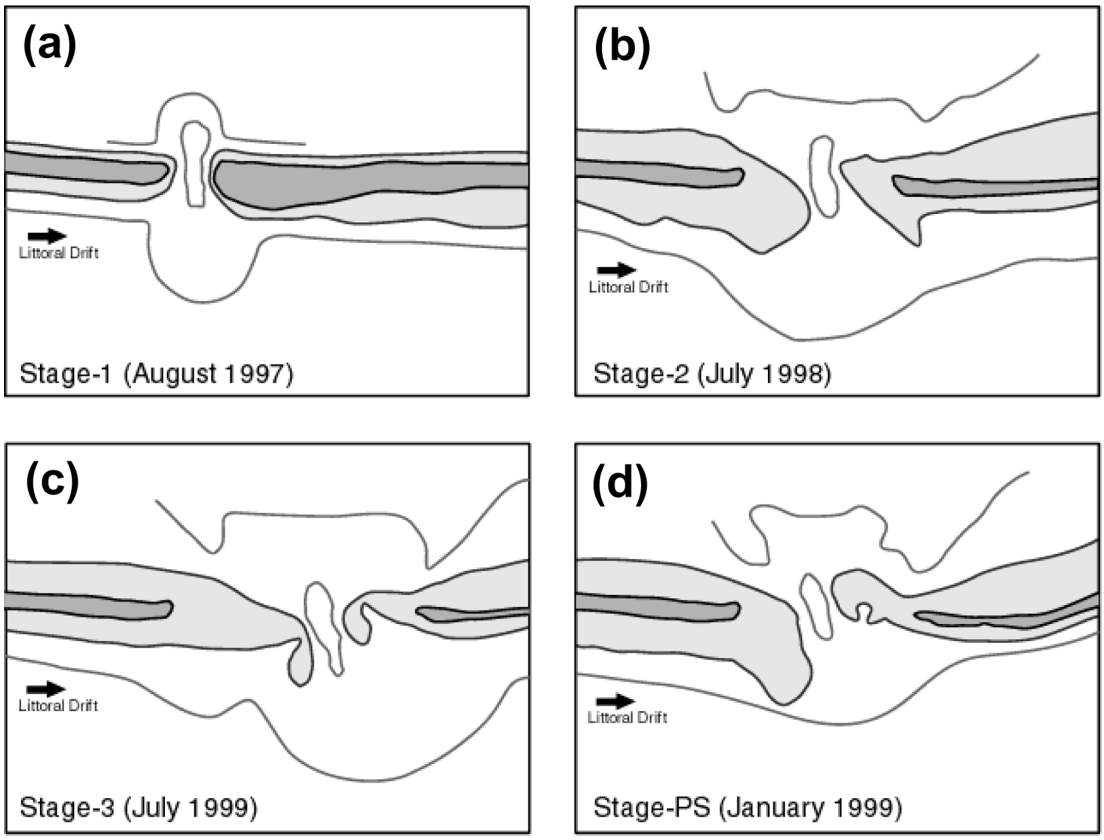

Figure 6.4: Schematic representation, based on Ancão Inlet maps, of natural inlet evolution stages after its opening. (a) Stage 1 represents the situation immediately after the inlet opening; (b) Stage 2 corresponds to a developed inlet after reaching dynamic equilibrium; (c) Stage 3, represents the situation of a *natural* inlet after migration induced by normal longshore drift; and (d) Stage PS shows inlet features after high-energy conditions.

equilibrium. After its opening Ancão Inlet started to increase its width and A_c, meaning that there was a corresponding increase in the tidal prism that was being captured from the old inlet which led finally to its closure by February 1998. The main increment in both inlet width at MSL and A_c occurred between August 1997 and April 1998 (reaching 240 m and 700 m^2 respectively), further variations in these parameters were of much less importance (Figure 6.2a). Simultaneously, volumetric variations of the inlet channel (C<1, see Table 6.2) were also more dramatic for the period between August 1997 to April 1998, becoming much less dramatic after that period. Thus, it can be said that by that time, the new Ancão Inlet had captured the entire tidal prism that corresponded to the former inlet, reaching dynamic equilibrium for the inlet channel and thus, entering Stage 2 of the conceptual model.

The formation of the ebb and flood deltas, as a result of sediment being transported by tidal currents across the inlet channel, did not occur until some months after the inlet channel reached dynamic equilibrium in July 1998 (Table 6.2 and Appendix A, Figure A.3). In Figure 6.3a and Table 6.2 the strong accumulative processes that led to the development of both deltas can be seen. Development of the ebb delta is an important factor for the inlet to reach its dynamic equilibrium because its shallow nature provides a natural breakwater for the landward inlet shorelines (FitzGerald, 1988). In April 1998 the Ancão ebb delta was not yet completely developed (see Appendix A, Figure A.2). Development of the flood delta was slower than the development of the ebb delta, a fact that could be due to the ebb tidal current dominance in the main channel. Ebb tidal dominance is a consequence of the existence of salt marsh areas and tidal creeks in the back-barrier area (Nummedal and Fisher, 1978). Ciavola *et al.* (2000a) showed ebb dominance for the inner area of the western margin of the inlet and Williams *et al.* (2003) demonstrated the ebb dominant nature of the inlet under spring tide conditions. In Figure A.4 (Appendix A) the development of both deltas can be observed. As a consequence, Ancão Inlet reached the end of Stage 2, one year after its artificial opening (Figure 6.4b), indicating dynamic equilibrium with respect to the development of the inlet channel and both ebb and flood deltas.

According to historical data given in the literature(i.e., Weinholtz, 1964; Granja *et al.*, 1984; Esaguy, 1986a) and to data presented in Chapter 5, it was expected that Ancão Inlet would start an eastward migration cycle after some of the initial readjustments were concluded. However, eastward migration did not start until January 1999 (Figure 6.2b). Instead, a significant abnormal westward migration (Figure 6.2b) occurred between August 1997 and April 1998 (45 m), with a less important westward displacement occurring between July and October 1998 (20 m). Westward movements of the channel can be related to the '*Levante*' conditions that occurred during the periods considered (Figure 6.1a), when the percentage of '*Levante*' episodes was quite high. However, it has been seen that the values of MD_{LEV} seemed to be determining the westward displacement of the channel. During these periods, the two largest values for MD_{LEV} were reached, four times larger for the first period, when maximum westward movement occurred. Thus, there is a relationship between the abnormal westward inlet migration and the prevailing oceanographic conditions, namely the MD_{LEV} that showed significant correlation values with inlet channel position. To support the hypothesis of the importance of the values of MD_{LEV}, it can be seen in

Figure 6.1a that periods with high percentage of '*Levante*' episodes (October to December 1998, and May to July 1999), did not imply any westward displacements of the inlet channel (Figure 6.2b). Westward displacement of the channel in this particular case is not likely to be related to the high-energy events but rather to persistent '*Levante*' conditions. The absence of the protection given by a developed ebb delta in the period between August 1997 and April 1998 probably increased the effects of the large values of MD_{LEV}.

Inlet channel migration through time did not occur in a continuous way (Figure 6.2b), rather the highest displacement rates depended on the occurrence of high-energy conditions. The eastward displacement of the inlet channel in January 1999 (see Figure 6.2b) occurred after a period of extreme high-energy conditions, the wave climate for the 10 most energetic days of the period (Figure 6.1c) consisted of high-energy SW conditions. Morris *et al.* (2001) analysed the relationship between oceanographic conditions (including waves and tides) and inlet changes such as channel migration and dune cliff retreat using video image data. The authors found that stronger variations occurred when high-energy conditions were coincident with higher tidal sea levels. However, significant inlet migration can also be associated with non-storm wave energy conditions. FitzGerald *et al.* (2001) explained inlet migration (using the work of Escoffier (1940) and Johnson (1919), the later *in* FitzGerald *et al.*, 2001) as a sequence deposition of sediment on the updrift side of the inlet that causes constriction of the flow, then as a consequence, current velocity increases leading to a greater scouring on the downdrift side of the inlet re-establishing the equilibrium cross-sectional area. This pattern of evolution can be observed in Figure 6.5 which shows the eastward migration of the channel from January to July 1999. Sediment accumulation on the updrift side of the inlet channel was observed in May 1999 for the deepest sections of the channel producing the reduction in its depth. The migration sequence (the inlet channel moved about 30 m) was completed in July 1999 with the scouring of the downdrift side of the deepest parts of the inlet channel.

During the second year of inlet evolution, since the inlet channel and deltas were already inside equilibrium values, inlet processes that occurred were not directly related to the artificial character of the inlet opening. Prevailing oceanographic conditions during the second year consisted of low-energy SW waves, causing eastward migration processes in the study area. Ancão Inlet showed Stage 3 (Figure 6.4c) characteristics in May and July 1999, although, due to the low-energy incident wave conditions, eastward inlet migration was not very

rapid (see Appendix A, Figures A.7 and A.8). In July 1999 the channel position was still 50 m to the west of the original dredged channel position in June 1997. Stage 3 is the *mature migrating inlet* meaning that the inlet has stable values of A_c and fully developed deltas that migrate with the channel. The relatively low volumetric changes during the second year (Table 6.2 and Figure 6.3b) indicate that the inlet was no longer acting as a sediment trap and thus, bypassing processes seemed to be occurring. Downdrift erosion on Barreta Island due to lack of bypassed sediments was not observed during the second year of inlet evolution, thus continuous sediment bypassing (FitzGerald *et al.*, 1984) seemed to be occurring. Simultaneously, the data in Appendix A suggests that some bypassing could have occurred as episodic shifting of the outer channel (FitzGerald *et al.*, 2001); however, due to the lack of data coverage of the ocean side of the inlet in December 1998 and January 1999, this can only be observed in the period between May and July 1999 (see Appendix A, Figures A.7 and A.8). As mentioned above, in Stage 3, the eastward migration of the channel is accompanied by delta migration, in Appendix A ebb delta asymmetry due to eastward inlet migration can be observed. After reaching Stage 3, the eastward migration of Ancão Inlet and the associated bypass processes are expected to continue following the historical trends. Thus, according to data from Esaguy (1986a) and from Chapter 5 of this thesis the eastward migration should continue at relatively high rates, until reaching a limiting position where the reduction in tidal prism will lead to the infilling of the inlet channel.

Stage PS in the conceptual model represents the situation of the inlet after a SW storm (Figure 6.4d), transition to this stage can occur from any of the other stages. Post-storm conditions at Ancão Inlet in January 1999 were also studied using video monitoring techniques by Morris *et al.* (2001). Results obtained with regard to inlet margin evolution and inlet channel response, were similar to those presented here. Under high-energy conditions, littoral drift is higher than under non-storm conditions, thus an overloading of the inlet by-pass capabilities occurs producing sediment accumulation on the updrift margin of the inlet (Morris *et al.*, 2001). High-energy incident waves produce the partial destruction of the ebb delta, allowing the direct impact of waves on the shoreline and the subsequent destruction of the outermost parts of the sand spit. Sediment transport towards the backbarrier area occurs from the ebb delta as well as from both sides of the inlet, producing the infilling of the inlet channel and the inland displacement of its deepest part. In Figure A.6 (Appendix A) it can be observed that, in January

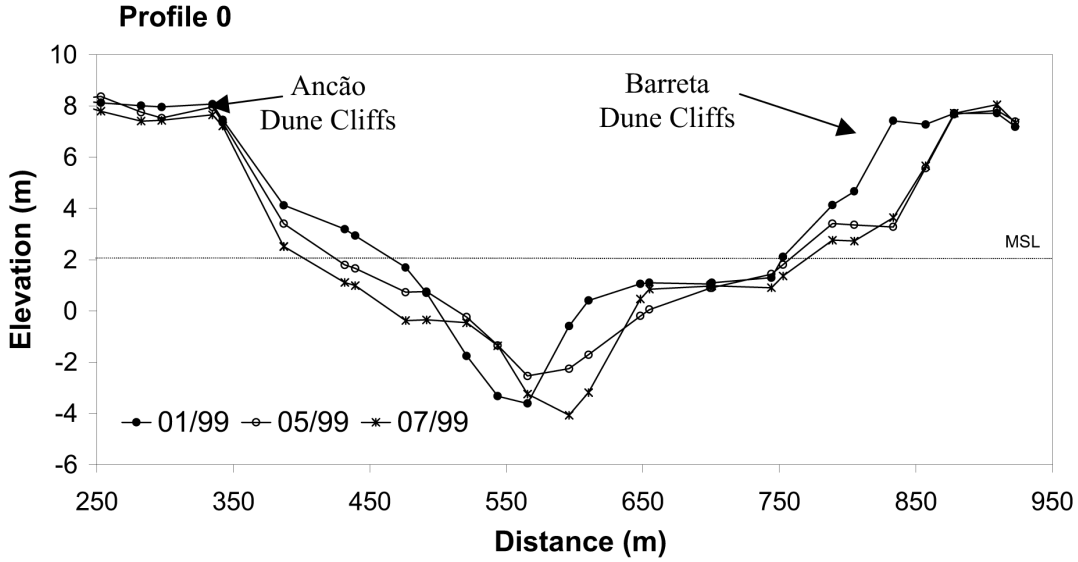

Figure 6.5: Cross section evolution of Profile 0, showing inlet migration between January and July 1999. Elevations refer to Portuguese Hydrographic Zero (2 m below MSL).

1999, the deepest part of the inlet channel had migrated towards the interior of the lagoon, causing a decrease in A_c (Figure 6.2a). Strong accumulation on the flood delta (Table 6.2) and morphology of the recurved sand spit located on the westernmost extreme of Barreta Island (Appendix A, Figure A.6) seem to be evidence of the existence of transport towards the lagoon. Wave data during this period show that on New Years day, a few days before the January 1999 survey, there was a high-energy SW storm with H_s=3.9 m. It seems clear that during this storm, the incident waves transported the sediment eroded from Barreta dune cliffs towards the lagoon, and caused the landward migration of the deepest part of the inlet channel. Simultaneously, it can be observed in Figure A.6 (Appendix A) that in January 1999 the updrift sand spit located on the easternmost extreme of Ancão Peninsula was wider and shorter, indicating a strong accumulation of sediments carried by the longshore drift and the erosion of the outer part due to incident waves.

High-energy conditions from '*Levante*' have different effects on Ancão Inlet than those of SW storms, being of much less importance. There were only two periods for which the direction of the 10 most energetic days was from '*Levante*': between October and December 1998 and between January and May 1999 (Figure 6.1c).Wave conditions in terms of T_p and θ_p were very similar for both periods, however, values of H_s were different, being higher for the period between January

and May 1999 (Figure 6.1c). Erosion of the flood delta occurred only during these periods (Table 6.2), and was almost 4 times larger for the period between October and December 1998. However, observed effects of high-energy '*Levante*' events on other inlet features were different on both occasions. Flood delta erosion between October and December 1998 was accompanied by the erosion of the inner channels and of the inlet channel (Table 6.2) providing an important increase in A_c. Between January and May 1999 flood delta erosion occurred with accumulation in both the inlet channel and the inner channels (Table 6.2). Therefore, although there seems to be a relationship between high-energy '*Levante*' events and flood delta erosion, it would appear that there are other factors that control the effects of such events. It is hypothesised that one of these factors could be the position and shape of the ebb delta, however, due to the lack of data coverage on the ocean side of the inlet in December 1998 and January 1999 this hypothesis cannot be proved with the data available for this study.

Mason (1986) and Kana and Mason (1988) studied the natural evolution of Captain Sam's Inlet (South Carolina, U.S.A.), a small mesotidal inlet that was artificially relocated in February 1983 Mason (1986). Thus, within the framework of the conceptual model presented here, at that time it was in Stage 1. Opening procedures were similar to those used for Ancão Inlet, however in this case the old inlet was artificially closed whilst the old Ancão Inlet (Figure 3.2) closed naturally about 8 months after the opening of the new one. For Captains Sam's Inlet the dynamic equilibrium in inlet width and A_c, 210 m^2 (Mason, 1986) was reached about 7.5 months after the opening (Kana and Mason, 1988) therefore entering Stage 2 of the conceptual model. This time period is slightly shorter than the one found for Ancão Inlet, where Stage 2 was achieved by April 1998, 10 months after the opening (A_c reaching 700 m^2). It is hypothesised that a relationship exists between the time taken by the inlet to reach dynamic equilibrium and whether or not the old inlet is closed artificially: artificial closure of the old inlet allows the new inlet to achieve dynamic equilibrium earlier. For the Ancão Inlet case, the artificial closing of the old inlet would have provided the new inlet with a higher tidal prism than if it remained open and as a consequence the inlet channel would possibly have reached the dynamic equilibrium earlier.

Although both inlets were artificially opened they are not directly comparable due to some differing characteristics such as the smaller size of Captain Sam's Inlet, with a maximum width at MSL of 101.3 m at the throat of the inlet and an equilibrium A_c of 210 m^2, Mason (1986). Tidal range and incident wave energy

at Captain Sams Inlet are also smaller with an average tidal range of 1.7 m and average incident waves of 0.5 m (Mason, 1986). Another difference between these two inlets is related to the availability of space in the backbarrier area. Whilst Ancão Inlet has space and develops a reasonably large flood delta, Captain Sams Inlet does not have sufficient space in the backbarrier area to develop a significant flood delta.

Ancão Inlet reached the end of Stage 2 one year after its opening, the volumetric changes being less dramatic during the second year. By June 1985 (2 years and 4 months after the opening) the ebb delta volume at Captain Sams Inlet had not reached equilibrium values but it was under development (Mason, 1986), thus it seemed to still be in Stage 2. It is assumed that the larger tidal ranges and A_c at Ancão Inlet facilitated ebb delta formation, and thus assisted in the inlet achieving the end of Stage 2.

6.3 Conclusions

The evolution of Ancão Inlet was monitored using a simple survey technique, allowing a comprehension of medium-term natural inlet evolution processes for the first two years after its artificial opening.

Volumetric calculations for inlet evolution were performed using a method that has the advantage of permitting the definition of generic areas for volumetric studies larger than the morphologies to be studied; thus allowing the study of a migrating inlet without periodic redefinitions of the generic areas.

A conceptual model with four evolutionary stages was determined for the evolution of the artificially opened Ancão Inlet (see Figure 6.4): Stage 1 represents the inlet immediately after its artificial opening; Stage 2 is the inlet after reaching dynamic equilibrium for the channel and until the deltas are fully developed; Stage 3, after reaching volumetric equilibrium, represents the *mature migrating inlet*; Stage PS is the inlet after high-energy conditions.

Ancão Inlet was in Stage 1 in June 1997. Transition to Stage 2 included inlet channel enlargement until reaching equilibrium values (April 1998). During Stage 2, the inlet was acting as a sediment trap while developing both flood and ebb deltas. Ancão Inlet reached the end of Stage 2 one year after the opening (July 1998). Transition to Stage 3 occurred during the second year, reaching the *mature migrating inlet* stage by May-July 1999. Only on one occasion, after

high-energy SW storm conditions, did Ancão Inlet show Stage PS characteristics (January 1999). After reaching Stage PS, Ancão Inlet characteristics reverted to a transitional stage between Stages 2 and 3 after a period of fair weather conditions.

The conceptual evolutionary model referred to in this chapter was determined from the evolution of Ancão Inlet. However, it seems to be applicable to other inlets with similar origin and characteristics such as Captain Sam's Inlet (South Carolina, USA).

Chapter 7

Short Term Studies: Tracer studies on the updrift margin of Ancão Inlet

"But, he thought, I keep them with precision. Only I have no luck anymore. But who knows? Maybe today. Every day is a new day. It is better to be lucky. But I would rather be exact. Then when luck comes you are ready."

Ernest Hemingway, *" The Old Man and the Sea."*

This chapter is partially being published by Elsevier:

Vila-Concejo, A., Ferreira, Ó., Ciavola, P., Matias, A., Dias, J.M.A.. Tracer studies on the updrift margin of a complex inlet system. *Marine Geology* (under review).

7.1 Results

7.1.1 AMI.1

Forcing Mechanisms

In Figure 7.1 the forcing mechanisms measured during AMI.1 are shown. Average values obtained during the periods in between FT deployment and LTS1 (AMI.1-1) or LTS1 and LTS2 (AMI.1-2) are in Table 7.1.

Wind conditions are shown in Figure 7.1a. The afternoon of the 20th January was characterised by light SE winds that soon turned to S increasing their speed (maximum of almost 12 m/s at 4 am). After that time, the wind turned to SW-W and rapidly decreased its strength to values lower than 5.5 m/s.

During the afternoon of the 20th January wave conditions at the Triaxys buoy location consisted of SW swell with T_p close to 12 s (Figure 7.1b) and small H_s (0.6-0.7 m) (Figure 7.1c). After the low tide (23 h) T_p decreased to 5-7 s (Figure 7.1b), probably due to the influence of the strong winds measured at that time (Figure 7.1a), θ_p was still SW (Figure 7.1b), showing that the influence of the southerly wind was not enough to change the θ_p offshore. H_s increased to 2 m during the high tide, coincident with the maximum speed measured for the wind, and then decreased to values close to 1.5 m for the rest of the campaign (Figure 7.1c). Incident angles were small and whilst T_p for AMI.1-1 was twice the value for AMI.1-2, H_s for AMI.1-1 was half the value for AMI.1-2 (Table 7.1).

EMCMn values for AMI.1 are shown in Figure 7.2a, and average values can be found in Table 7.1. Resultant currents computed for EMCMn are shown in Figure 7.2b. During the first recorded tide the direction of the resultant currents was between 180° and 232°N, thus sediment transport in a general eastward direction, towards the inlet area, could be expected. Resultant velocities were increasing towards the end of the recording time (maximum values close to 0.4 m/s). The second tide showed more dispersion of the directions of the resultant currents

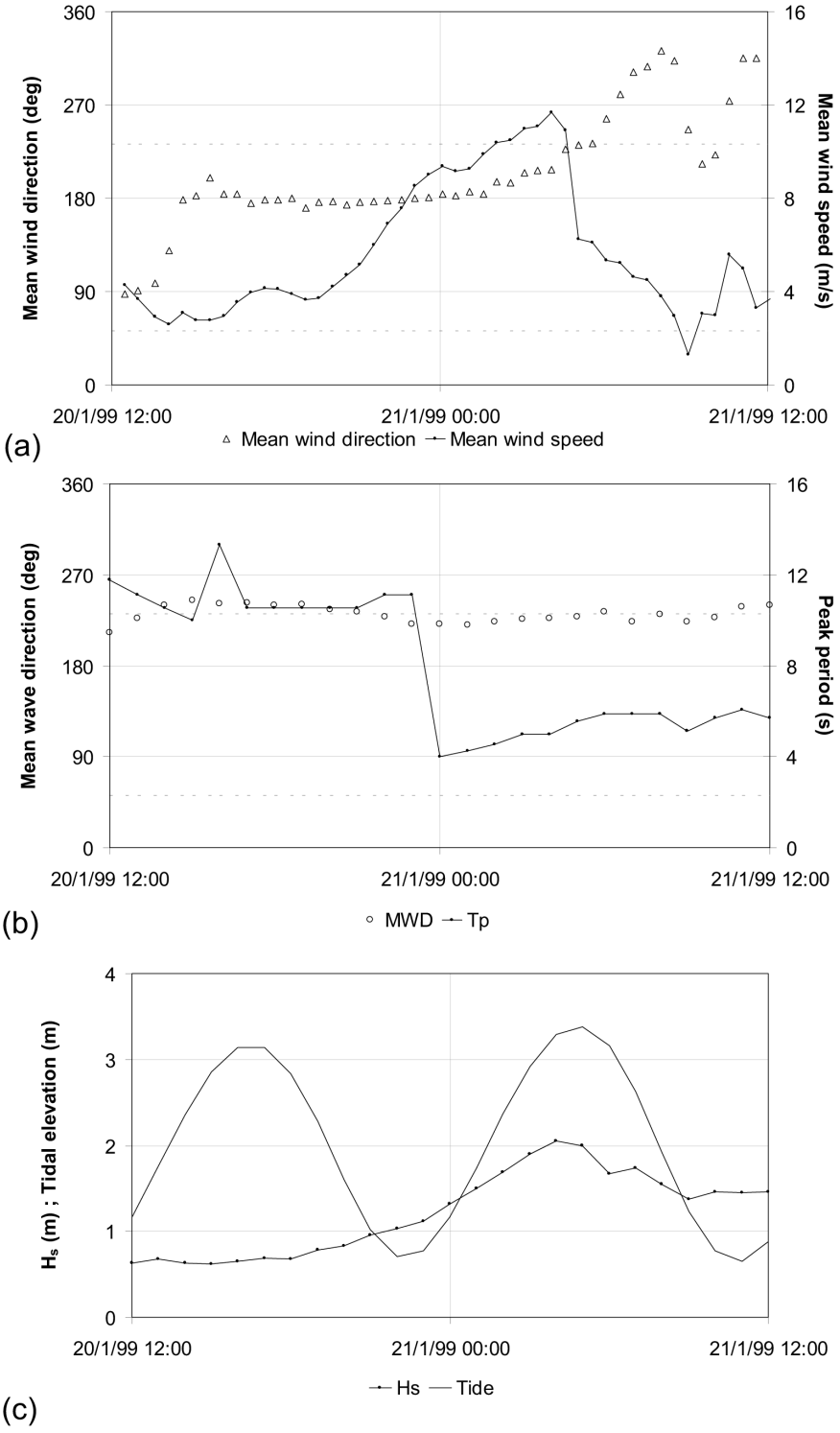

Figure 7.1: Forcing mechanisms during AMI.1. (a) Mean wind direction (°) and Mean wind speed (m/s); (b) Mean wave direction (θ_p, °) and Peak period (T_p, s); (c) Significant wave height (H_s, m) and tidal predictions (m). The dashed lines show the onshore and offshore directions (232° and 52° respectively).

being mostly offshore and westwards directed at the beginning of the tide (maximum values were smaller than 0.5 m/s, average was 0.4 m/s). This is due to the influence of S winds (Figure 7.1a), that were stopping the eastward transport caused by the SW waves (Figure 7.1b) and inducing a general westward direction in the longshore currents. With the turning of the wind (Figure 7.1a) the resultant currents started to run in a general eastward direction, reaching current velocities between 0.4 and 0.6 m/s with an average value close to 0.5 m/s.

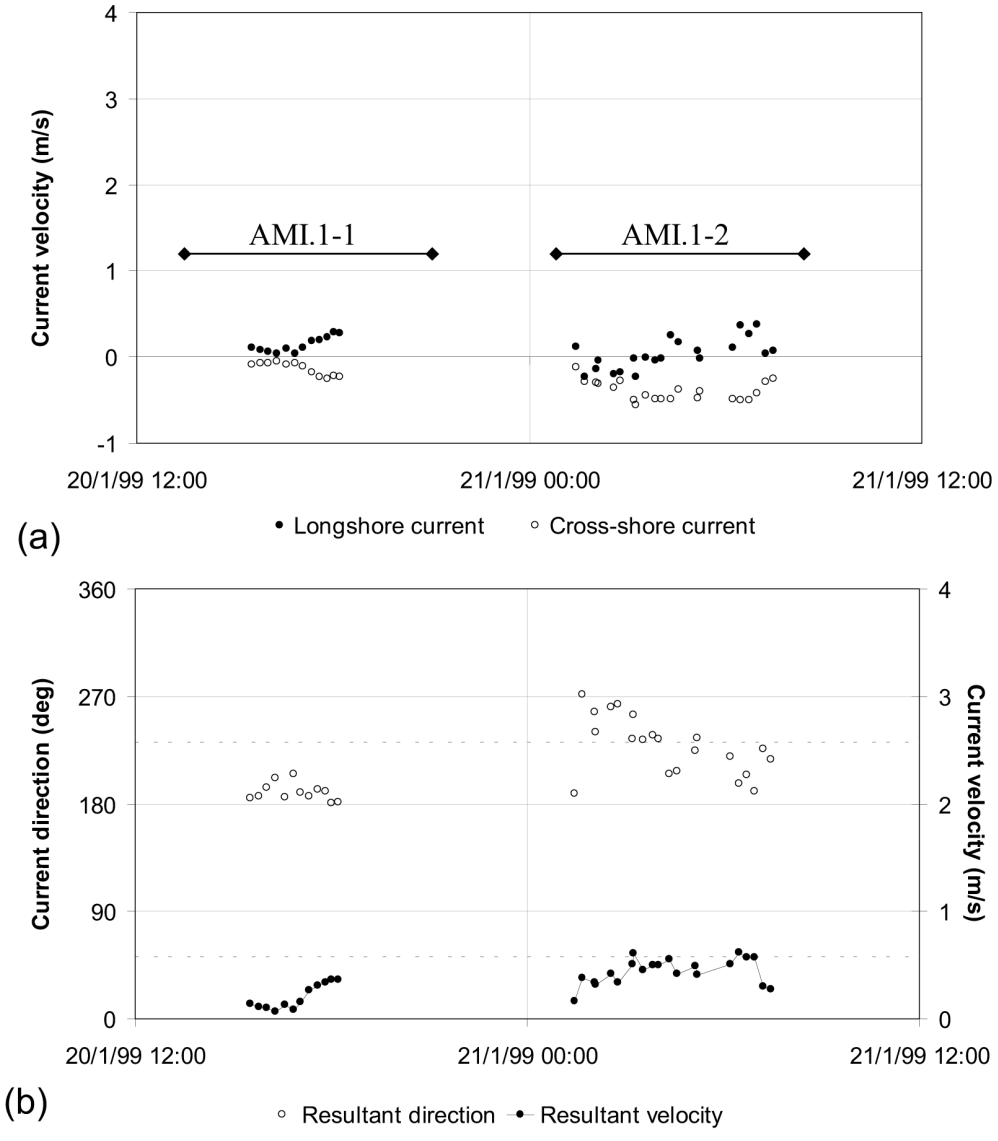

Figure 7.2: Currentmeter data from EMCMn during AMI.1: (a) velocity (m/s) of longshore and cross-shore currents (positive values mean south-eastward and offshore, negative values mean north-westward and onshore); (b) velocity (m/s) and direction (°) of the resultant currents. The dashed lines show the onshore and offshore directions (52° and 232° respectively).

Topography

Some representative topographic profiles are shown in Figure 7.3. Surf Scaling Parameter (ϵ) calculations for the beach face showed an intermediate beach whose slope decreases from P0 ($tan\ \beta_{bf}$=0.09 and ϵ=4.1) towards the inlet ($tan\ \beta_{bf}$=0.05 and ϵ=15 for P400), thus becoming less reflective. Surf Similarity Parameter (ξ_b) calculated for the beach face showed plunging waves, decreasing its value towards the inlet (from 0.9 for P0 to 0.5 for P400) and, thus, gradually changing to values closer to those of spilling waves. The average slope calculated for the swash platform was 0.006, thus very dissipative conditions with spilling waves were occurring. These results are related with the existence of the inlet, the inlet channel interrupts the littoral drift producing sand accumulation on the updrift shore of the inlet and creating the ebb-tidal delta that protects the inlet area from the incident waves.

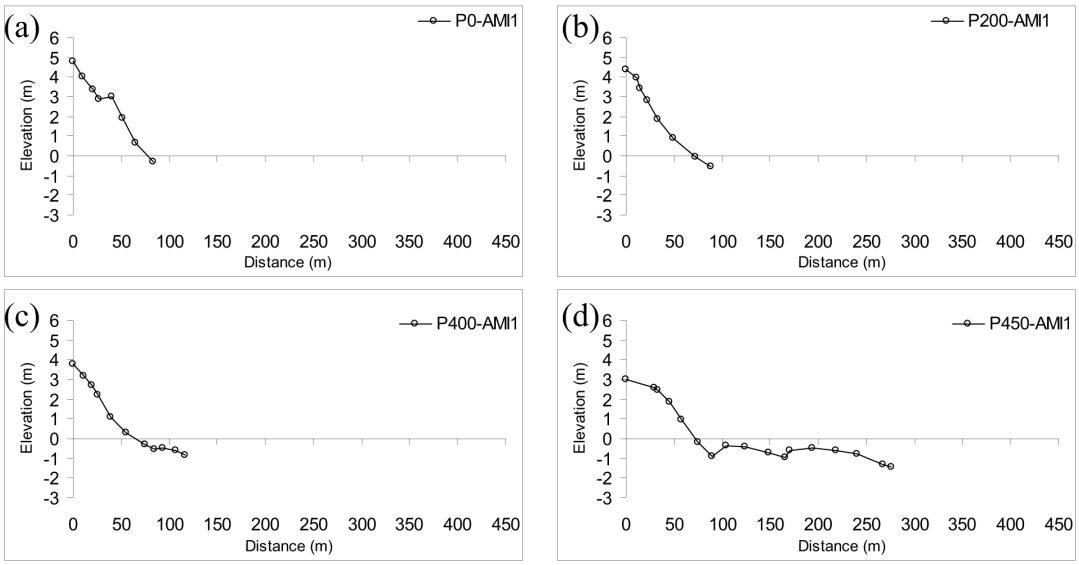

Figure 7.3: Topographic profiles obtained during AMI.1: (a) P0; (b) P200; (c) P400; and (d) P450. Elevation is referenced to mean sea level (MSL).

Tracers

The grain-size comparison of the natural sand with the painted sand (FT) is shown in Table 7.2. Mean grain-size decreased and the sorting improved after the painting; this is probably due to the sieving process that while taking out the aggregates formed during the painting process, also removed some other elements (such as shells) whose size was very different from the mean grain-size.

Analyses of the samples of AMI.1-1 provided the maps shown in Figure 7.4, the eastward sediment transport induced by the nearshore currents (Figure 7.2) caused the distribution of the FT to be entirely located on the straight part of the beach (Sector A). The percentage of remaining FT ($PRFT$) during this first sampling was found to be 83%. Most of the FT (90%) were found in the upper layers of the study area (Figure 7.4a and b), thus indicating no burial of the tracers. FT contents in the lower layers (Figure 7.4d and e) were inferior to 1% of the $PRFT$. Average mixing depth was 5.4 cm, reaching maximum values on the beach face (9.6 cm). Also, by comparison with Figure 7.3, it can be seen that most of the transport took place on the beach face of the study area. The $V(FT_C)$ (vertical integration of the FT velocities found for every layer, see Section 4.3.3) was found to be 4.10×10^{-3} m/s, thus providing eastward sediment transport values of about 950 m^3 for that tide (1,820 m^3/day). The cloud centroid (FT_C) was located 177 m from the injection point in a position close to P200, at 60 m distance from the head of the profile.

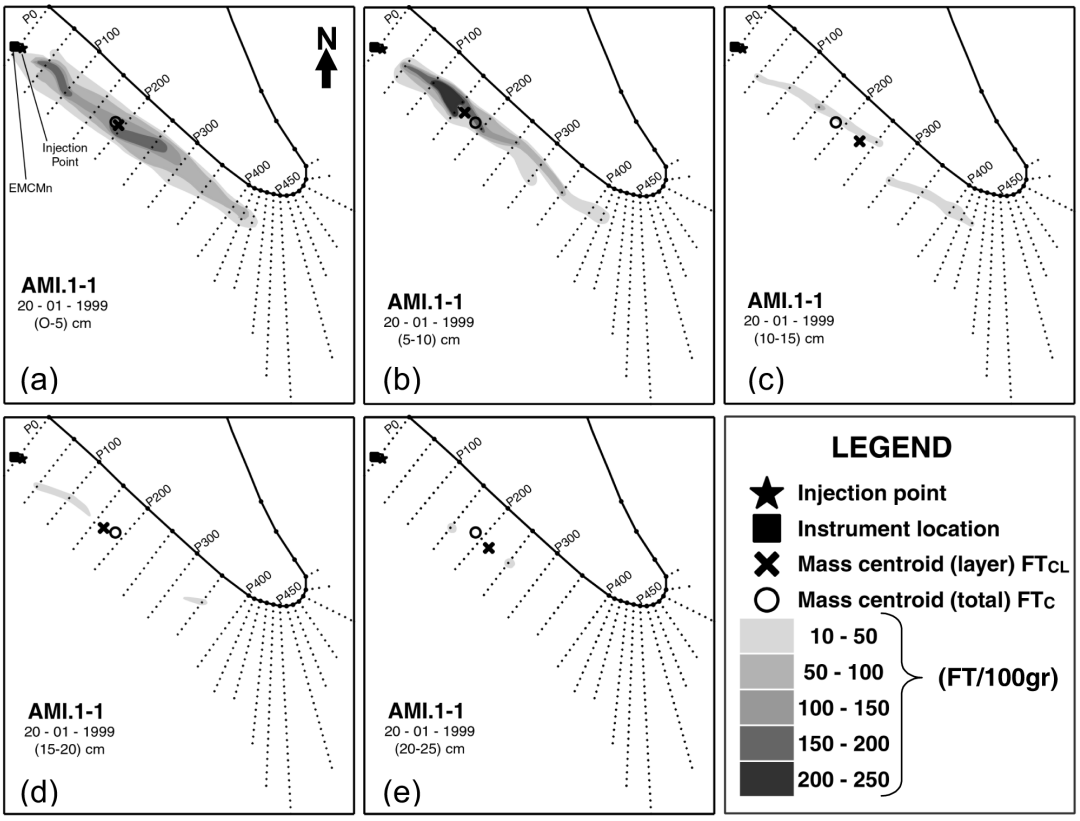

Figure 7.4: FT distribution maps for the analysed layers of LTS1 of AMI.1. Locations of the total (FT_C) and partial (FT_{CL}) mass centroids are shown for each layer: (a) 0-5 cm; (b) 5-10 cm; (c) 10-15 cm; (d) 15-20 cm; and (e) 20-25 cm.

Maps obtained for AMI.1-2 sampling collection are shown in Figure 7.5. $PRFT$ was calculated giving a value of 67%, meaning that 67% of the injected FT was still remaining after 2 tidal cycles. Despite the dispersion in the direction of the currents measured for that tidal cycle (see Figure 7.2), sediment transport was eastward directed and reached the western shore of the inlet. However, and possibly related with the forcing mechanisms measured at the beginning of the experiment, burial of the FT occurred; a decrease in FT contents was found from the surface to 15 cm depth (Figure 7.5a, b and c), 55% of the FT were found in these 3 layers. However, FT contents increased for the lower layers (Figure 7.5d and e) and the FT distribution patterns for AMI.1-2 at 20 cm depth (Figure 7.5d) were found to be very similar to those found for AMI.1-1 at 5 cm depth (Figure 7.4a). Thus only the upper layers (until 15 cm depth) were used to make the analyses. Most of the tracers remained in Sector A (73%), Sector C had 16.4% of the remaining FT and percentages of 8.5% and 2.1% were found respectively in sectors B and D. FT_{CL} calculated for Sector A (Figure 7.5a, b and c) showed higher eastwards transport velocities for the lower layers.

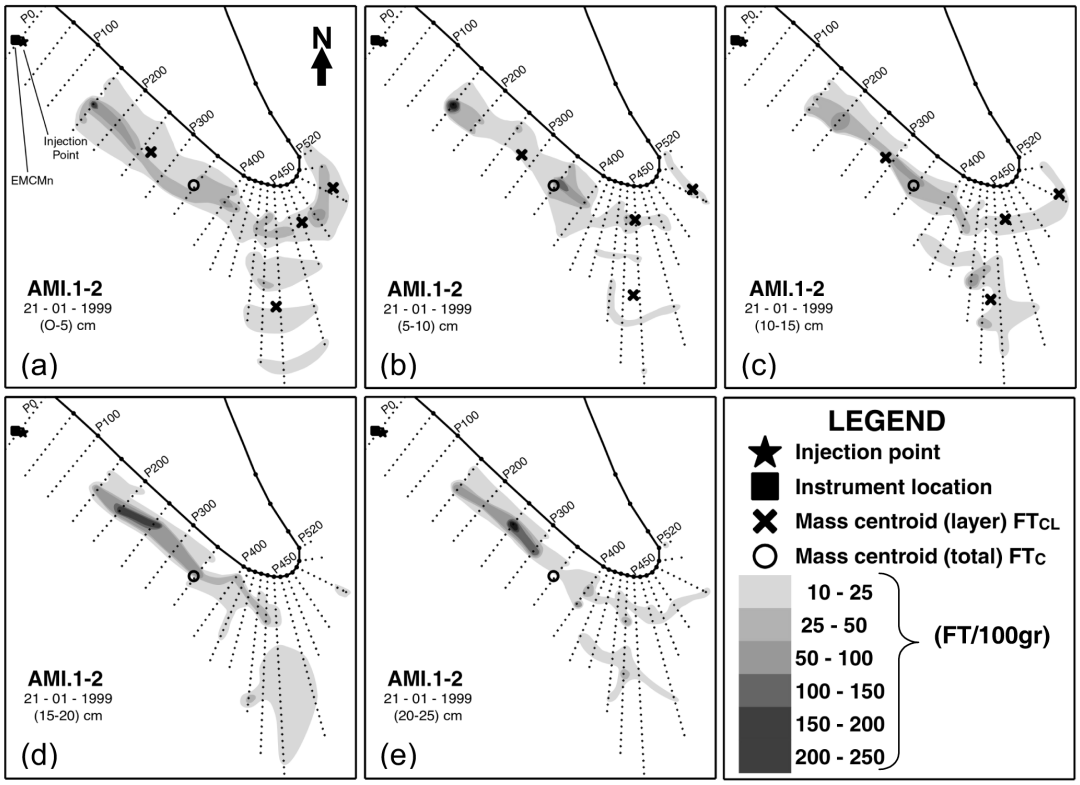

Figure 7.5: FT distribution maps for the analysed layers of LTS2 of AMI.1. Locations of the total (FT_C) and partial (FT_{CL}) mass centroids are shown for each layer: (a) 0-5 cm; (b) 5-10 cm; (c) 10-15 cm; (d) 15-20 cm; and (e) 20-25 cm. FT_{CL} were not calculated for (d) and (e) due to FT burial.

Table 7.1: Average values obtained for the forcing mechanisms measured for each campaign. Positive signs for currents mean south-eastward longshore currents, onshore cross-shore currents and upward vertical currents. Negative signs imply north-westward longshore currents, offshore cross-shore currents and downwards vertical currents.

	Wind Speed (m/s)	Wind Dir. (°N)	H_s (m)	T_p (s)	θ_p (°N)	Longshore current velocity (m/s)			Cross-shore current velocity (m/s)			Vertical current velocity (m/s)		
						EMCMn	EMCMo	EMCMr	EMCMn	EMCMo	EMCMr	EMCMn	EMCMo	
AMI.1-1	4.4	153	0.8	10.9	233	0.14	–	–	-0.14	–	–	–	–	
AMI.1-2	7.0	236	1.6	5.2	227	0.03	–	–	-0.40	–	–	–	–	
AMI.2-1	2.3	250	0.4	10.5	268	0.60	0.89	–	0.04	–	–	–	-0.23	
AMI.2-2	2.3	210	0.5	5.3	161	0.61	0.70	–	0.05	–	–	–	-0.04	
AMI.3-1	1.7	267	0.7	10.9	259	0.40	0.32	0.33	–	0.16	0.33	0.01	–	
AMI.3-2	2.7	210	0.6	11.2	256	0.46	0.40	0.26	–	0.17	0.26	0.01	–	

Table 7.2: Grain-size parameters obtained for the sediment samples taken before (sand) and after (FT) dying with fluorescent paint. Grain-size is expressed in mm.

Campaign		Mean (mm)	Sorting
AMI.1	sand	0.47 Medium Sand	Moderately well sorted
	FT	0.40 Medium Sand	Well sorted
AMI.2	sand	0.47 Medium Sand	Moderately well sorted
	FT	0.55 Coarse Sand	Moderately well sorted
AMI.3	sand	0.82 Coarse Sand	Moderately sorted
	FT	1.01 Very Coarse Sand	Moderately sorted

7.1.2 AMI.2

Forcing Mechanisms

Wind data is shown in Figure 7.6a, and average values for each period can be found in Table 7.1. During the first hours of the 18th February the wind direction was from NW, rotating afterwards to N and NE, during this time the wind was always less than 4 m/s. About 6 am on the 18th February the wind rotated to E-SE increasing its velocity to a maximum of 7 m/s, after that, the wind continued its rotation towards SW-W and finally N at the same time that its velocity was decreasing to less than 2 m/s.

Wave direction at the Triaxys buoy location was from the W until before noon on the 18th February (Figure 7.6b). T_p during that period showed values of 10-11 s and H_s values (Figure 7.6c) were low. In the afternoon of the 18th February, θ_p changed to SE (Figure 7.6b) registering maximum H_s of 0.6 m (Figure 7.6c), T_p during that time showed mostly low values (Figure 7.6b). Average values of H_s, T_p and θ_p with relation to the periods AMI.2-1 and AMI.2-2 are shown in Table 7.1.

Data obtained by EMCMo and EMCMn showed that longshore tidal currents were mostly eastward directed (Figure 7.7a and b) and showed similar patterns, average values for AMI.2-1 and AMI.2-2 are in Table 7.1. Vertical currents measured by EMCMo (Figure 7.7a) showed very weak values, however, during the peak of the eastward tidal current on the first recorded tide, a downwards directed current with maximum values of 0.7 m/s was measured. This is probably related with the existence of large bedforms (megaripples with average wavelengths and heights of about 3 m and 0.3 m respectively) that were observed in the area. Vertical currents during the second tidal cycle were negligible (Figure 7.7a). Differences observed between the longshore tidal current velocities measured by EMCMo and EMCMn can also be related with the bedforms mentioned above. Resultant currents calculated for EMCMn are shown in Figure 7.7c. Both recorded tides showed similar patterns starting with weak flooding currents (maximum 0.2 m/s). Ebbing currents started 2.5-3 hours before the high tide slack having low velocities (maximum 0.2 m/s). Ebb current velocities started to increase after the high tide slack and strong ebbing currents (up to 1.5 m/s) started about 1 hour after the high tide slack and lasted for 1.5-2 hours. After that, ebbing currents became weaker with velocities less than 1 m/s.

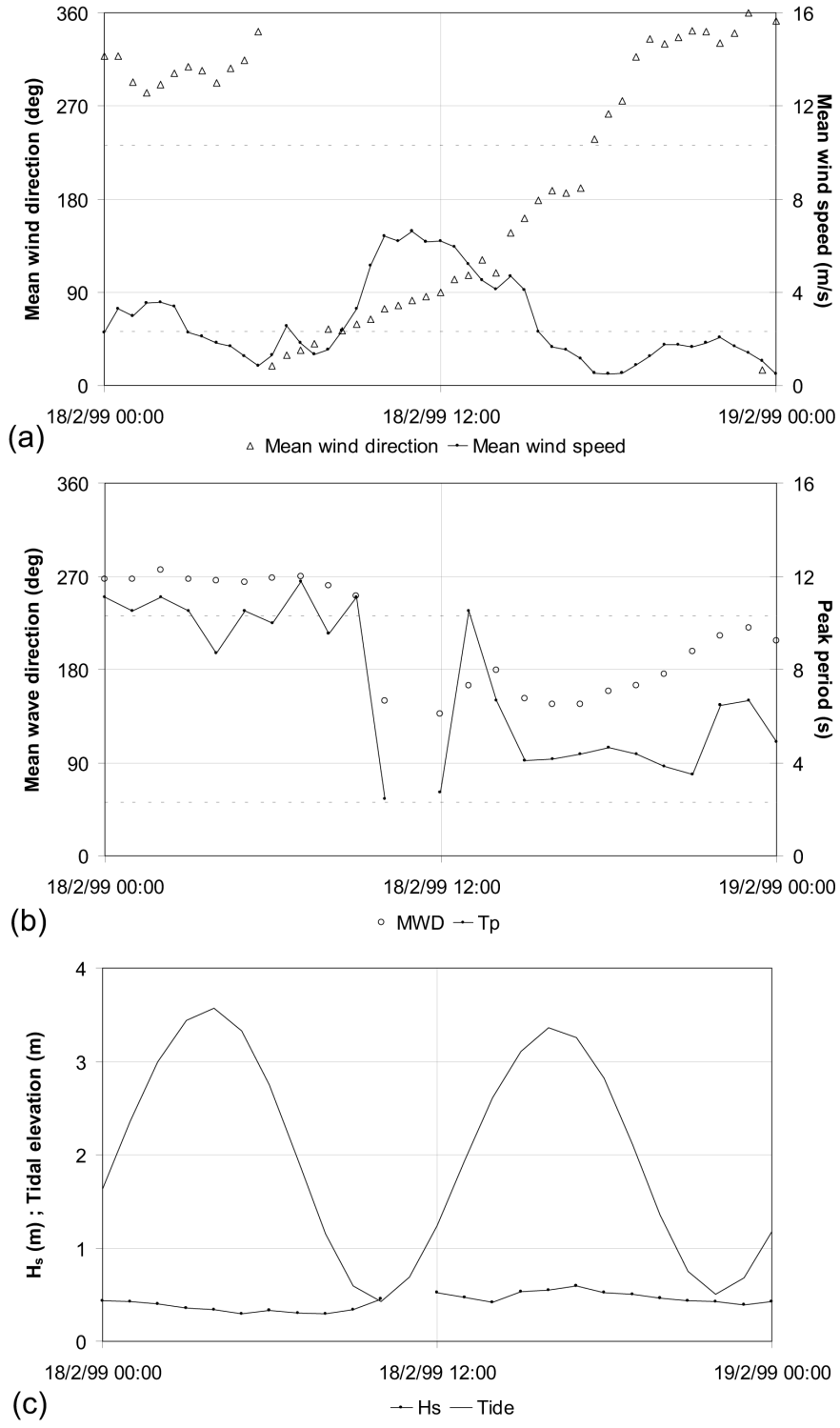

Figure 7.6: Forcing mechanisms during AMI.2. (a) Mean wind direction (°) and Mean wind speed (m/s); (b) Mean wave direction (θ_p, °) and Peak period (T_p, s); (c) Significant wave height (H_s, m) and tidal predictions (m). The dashed lines show the onshore and offshore directions (232° and 52° respectively).

Topography

Topographic profiles measured during AMI.2 were from P400 to P550 because most of the transport occurred on the western shore of Ancão Inlet under tidal inlet effects. Surf Scaling and Surf Similarity parameters on the beach face were only calculated for P400 (representing the part of the study area where influence of bi-directional tidal currents was minimum) giving the following values: $tan\ \beta_{bf}$=0.1; ϵ=3.6; and ξ_b=0.9. Therefore, the beach was in an intermediate state (very close to reflective values) under the influence of plunging waves, thus indicating that some accumulative processes, due to the low energy waves measured in February 1999 might have occurred since AMI.1. Some representative topographic profiles taken during AMI.2 are shown in Figure 7.8. Beach face slope gave values from 0.04 (P430) to 0.19 (P490). The profiles located on the swash platform (P430 and P450) had less steep slopes than the rest due to sediment accumulation. However, as a consequence of berm development P450 had, in this campaign, steeper slopes than during AMI.1. P470 and P490 had steep beach faces, however, due to their location the shape of these profiles is more related to tidal currents than to wave action. The average slope obtained for the swash platform ($tan\ \beta_{sp}$) was 0.008, therefore, indicating dissipative conditions and spilling waves.

Tracers

The grain-size comparison of the natural sand with the painted sand (FT) is shown in Table 7.2. Grain-size increased by 0.08 mm that can be considered acceptable for sediment tracers studies. In this campaign the FT showed sorting values that were very similar to those obtained for the natural sand.

FT distribution maps for AMI.2 are shown in Figure 7.9. Distribution patterns for AMI.2-1 are shown in Figure 7.9(a to e), and the distribution patterns obtained for the semi-surficial samples of AMI.2-2 are shown in Figure 7.9f. The $PRFT$ obtained for AMI.2-1 (60%) was lower than that obtained for AMI.1. The injection point and both of the EMCMs were located on the southern edge of Sector D (Figure 4.4). From Figure 7.7 it can be seen that the currents acting on the injection point were ebb tidal currents for the majority of time. Resultant ebb tidal currents had a direction of approximately 140°N, implying transport towards the inlet channel. No burial of the FT was detected, however, vertical mixing processes were quite high during this campaign. The calculated mixing

depth for the swash platform was close to 30 cm, this is probably related with the existence of the mentioned megaripples. Sectors B and C had 43.8% and 55.8% of the remaining tracers; less than 1% of the FT were found in Sector D. No FT were found in the submarine samples taken in the channel area, however some FT were found in the submarine samples taken in front of the swash platform. The FT_C was located on the northern edge of Sector C, on P450. The partial FT_{CL} showed small variations with depth but without following any determined trends.

The distribution map obtained for AMI.2-2 (Figure 7.9f) shows high dispersion, only 13% of the injected FT were still remaining in the study area, the FT_C is almost at the same position as in AMI.2-1 but with a small eastward displacement. Most of the remaining FT were found in Sector C (63.9%), Sector B had 30.8%, Sector A had 4.7% and Sector D had less than 1%.

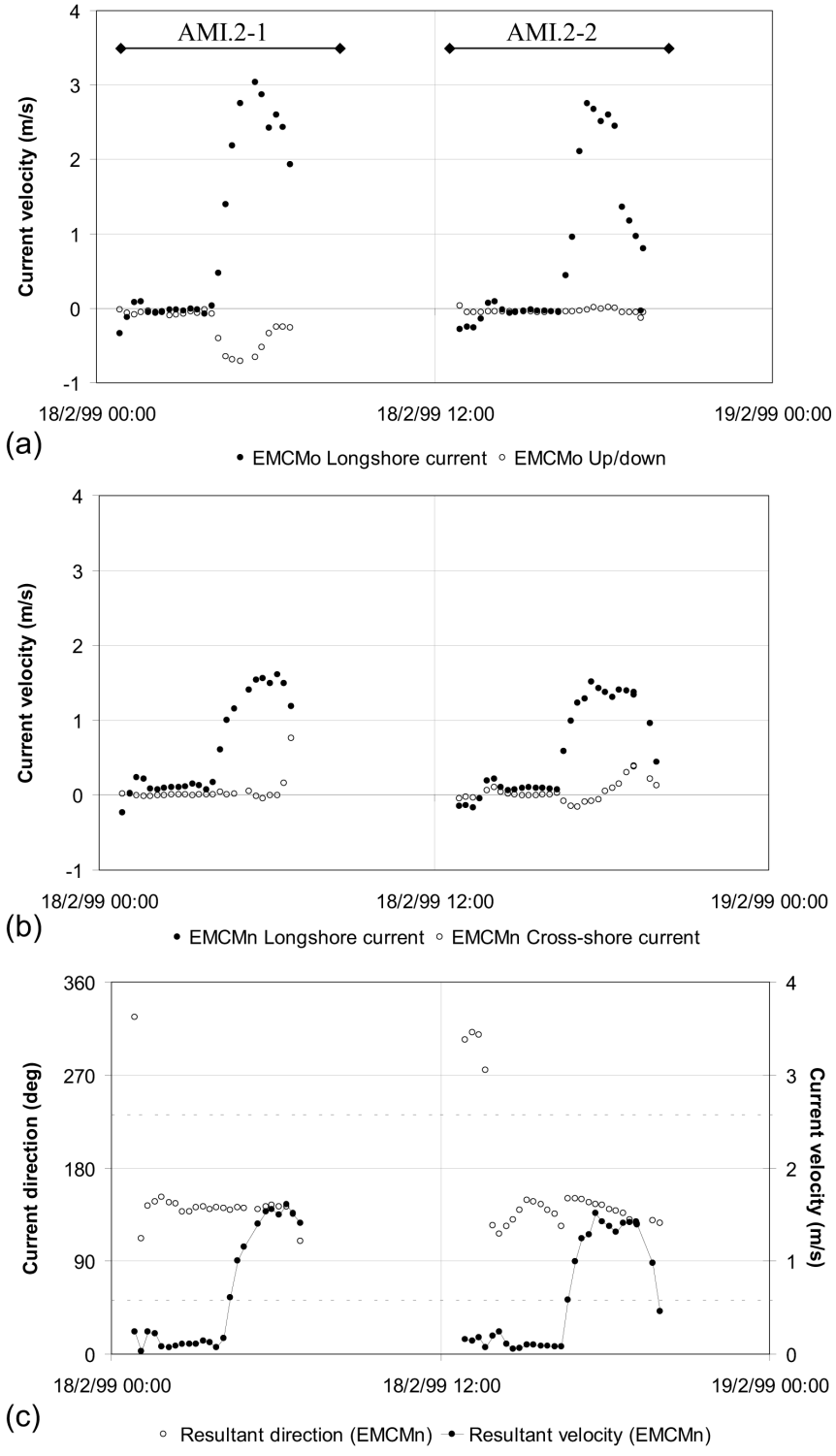

Figure 7.7: Currentmeter data from AMI.2: (a) and (b) show respectively EMCMo and EMCMn current velocity data (m/s) (positive values indicate eastward, upward and northward directions, negative values indicate westward, downward and southward directions). (c) Resultant directions (°) and velocities (m/s) for EMCMn. The dashed lines show the onshore and offshore directions (52° and 232° respectively).

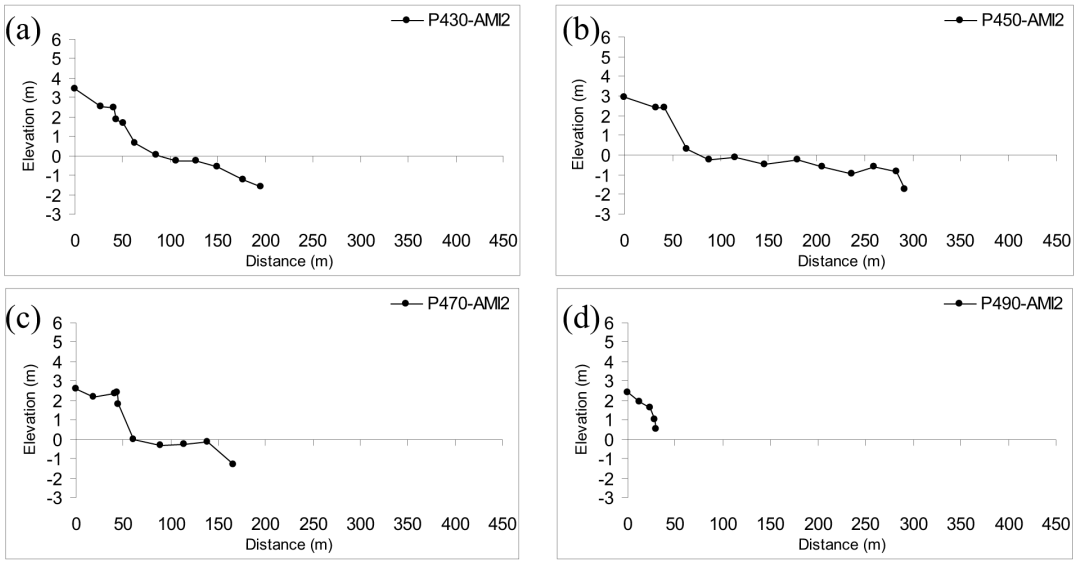

Figure 7.8: Topographic profiles obtained during AMI.2: (a) P430; (b) P450; (c) P470; and (d) P490. Elevation is referenced to mean sea level (MSL).

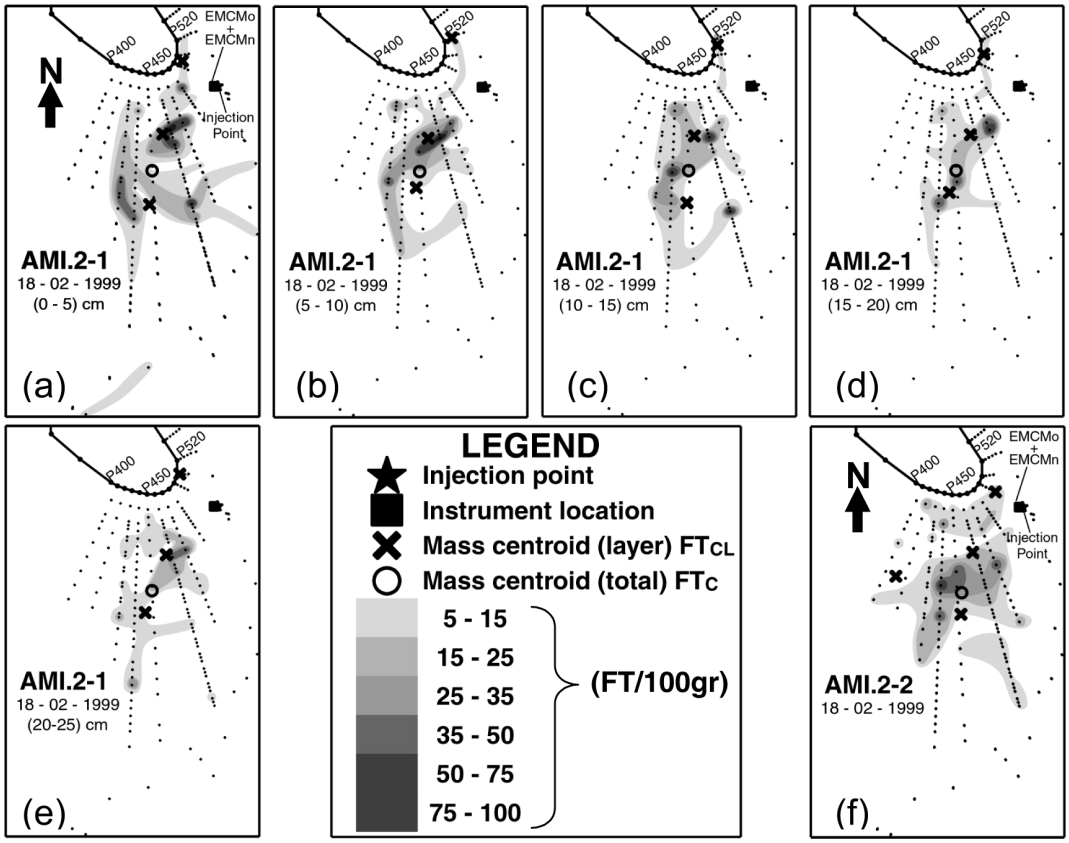

Figure 7.9: FT distribution maps for AMI.2. Locations of the total (FT_C) and partial (FT_{CL}) mass centroids are shown for each layer: (a) LTS1 0-5 cm; (b) LTS1 5-10 cm; (c) LTS1 10-15 cm; (d) LTS1 15-20 cm; (e) LTS1 20-25 cm; and (f) LTS2 semisurficial samples.

7.1.3 AMI.3

Forcing Mechanisms

Wind data for AMI.3 is shown in Figure 7.10a, and average values corresponding to each sample period (AMI.3-1 and AMI.3-2) are in Table 7.1. Wind speed recorded during this campaign was low (less than 4 m/s). Directions rotated from W to NW and N during the first hours of the 19th March. NE winds were measured in the morning and the clockwise rotation to E, SE and S was measured until 16:00 h. After that, the clockwise rotation of the wind indicated SW and W winds.

Wave conditions at the IH buoy location (offshore Santa Maria Cape) are shown in Figure 7.10b and c. During AMI.3, the offshore θ_p was from the W-SW, T_p was 10-12 s (Figure 7.10b) and H_s was small ranging between 0.5 and 0.75 m (Figure 7.10c). Average values for offshore wave conditions for AMI.3-1 and AMI.3-2 are shown in Table 7.1. The pressure transducer deployed with the RUNTI tripod showed that waves at the inlet had T_p values similar to those measured offshore (Figure 7.10b). H_s (RUNTI) was higher than offshore during high tide and lower during low tide (Figure 7.10c). This is related with the natural protection given by the ebb-tidal delta, during low tide the delta is shallow and the waves cannot reach the shore, whilst during high tide the waves can cross the delta due to the increased water depth and reach the shore. Maximum H_s values at the inlet were close to 1 m during the first recorded tide and slightly decreased during the following tides (Figure 7.10c) with average values close to 0.8 m for both tides. It is important to note here that due to the flat morphology of the swash platform the incident waves were already spilling while being measured. Also, as can be observed in Figure 7.10c, the measured tides at the inlet were similar to the predicted tides; however, measured tidal heights were larger than the predicted ones (the maximum difference at high tide was about 0.2 m). There is no data of θ_p at the inlet, however, visual observations indicated SW waves during the field campaign.

Currentmeter data obtained in the internal part of the inlet (EMCMo and EMCMn) are shown in Figure 7.11. Average values corresponding to AMI.3-1 and AMI.3-2 are in Table 7.1. Longshore tidal currents showed similar patterns at EMCMo and EMCMn. Cross-shore tidal currents measured by EMCMo (Figure 7.11a) were mostly northward directed, and reached their maximum values at the same time as the eastward currents but the cross-shore currents had weaker

intensities. Vertical currents showed negligible values (Figure 7.11b). Resultant currents in the internal part of the inlet, computed for EMCMo, showed flooding currents until about 2-2.5 hours before the high tide slack (Figure 7.11c) with maximum velocities of 0.5 m/s for the first tide and 0.4 m/s for the second and the third recorded tides. After that, weak ebbing currents started (0.3-0.4 m/s); during the high tide slack resultant currents are very weak (0.1 m/s). Currents turned back to ebbing directly after the high tide slack increasing their velocity until reaching the maximum velocities (1 m/s) about 1 hour after the high tide slack, maintaining the maximum values for about 2-2.5 hours and then rapidly decreasing.

Currents on the swash platform, measured by EMCMr, are shown in Figure 7.12a. Average values for longshore and cross-shore tidal currents for AMI.3-1 and AMI.3-2 are in Table 7.1. Resultant currents on the swash platform (Figure 7.12b) showed that onshore currents (flooding) reached maximum velocities close to 1 m/s, and lasted until the high tide slack. Offshore currents (ebbing) started after the high tide slack and had weaker velocities (maximum about 0.8 m/s).

From Figure 7.11c and Figure 7.12b it can be seen that there were three stages inside each recorded tidal cycle: (1) until about 2-2.5 hours before the high tide slack, flooding currents occur, with higher flooding velocities on the swash platform; (2) after that and until the high tide slack flooding currents reach their maximum velocity on the swash platform (1 m/s) and simultaneously weak ebbing currents occur in the inner area (max. 0.3 m/s); (3) after the high tide slack, ebbing currents occur in both areas with stronger currents in the internal part, the direction of the ebbing currents on the swash platform (between 270°N and 360°N) indicates westward flow.

Topography

Topographic profiles were undertaken between P350 and P600. Surf Scaling and Surf Similarity parameters for the beach face were only calculated for P400, chosen for being representative of the area where mostly unidirectional currents occur and also because it could be compared with the values obtained for the other field campaigns. Values obtained for the parameters are as follows: $tan\ \beta_{bf}$=0.1; ξ_b=1.7; and ϵ=1.4. Therefore, the beach was in a reflective state under plunging waves, indicating again some accumulation processes in the beach area

close to the inlet shore. Some representative profiles from AMI.3 are shown in Figure 7.13. P430, P450 and P470 show a well developed berm and strong sediment accretion on the lower parts of the profile (including the lower section of the beach face), thus indicating the growth of the swash platform between AMI.2 and AMI.3. The accumulation processes occurred on the lower part of the beach face inducing a less steep slope and as a consequence, the beach face slope values were more dissipative than those obtained for AMI.2, between 0.03 (P450) and 0.09 (P490). Average slope obtained for the swash platform was 0.011, thus it was dissipative under spilling conditions.

Tracers

The grain-size comparison of the natural sand with the painted sand (FT) is shown in Table 7.2. Sediment collected at the swash platform was coarse, therefore to achieve a better similarity between the natural sand and the FT no sieving was performed after the painting. FT were found to be very coarse implying an increment in the mean size of 0.19 mm and both samples were moderately sorted.

The injection point was located in the centre of Sector C (see Figure 4.4). Distribution maps for AMI.3 are shown in Figure 7.14. The maps representing the layers obtained with the corer collection made for AMI.3-1 are in Figure 7.14(a to e) and the one representing the semi-surficial sample collection performed for AMI.3-2 is in Figure 7.14f. The computed $PRFT$ for AMI.3-1 was 62%. Most of the FT were found in Sector C (89.6%) whilst Sector B had 9.8% and Sector D only 0.6%. Some FT were found in the submarine samples collected in front of the swash platform (Figure 7.14a). Vertical mixing of the sediments was very high (mixing depth $\sim$25 cm). For all layers there is an area between Sectors B and C where no FT were found, this area corresponds to tidal channels. The FT_C was found to be in Sector C, about 34 m southwards from the injection point.

The distribution map found for AMI.3-2 (Figure 7.14f) shows high dispersion of the FT as well as a very low concentration. Only 1% of the tracers were still remaining in the study area, 75.4% of them were found in Sector C, 13.6% in Sector B, 8.6% in Sector A and only 2.3% in Sector D.

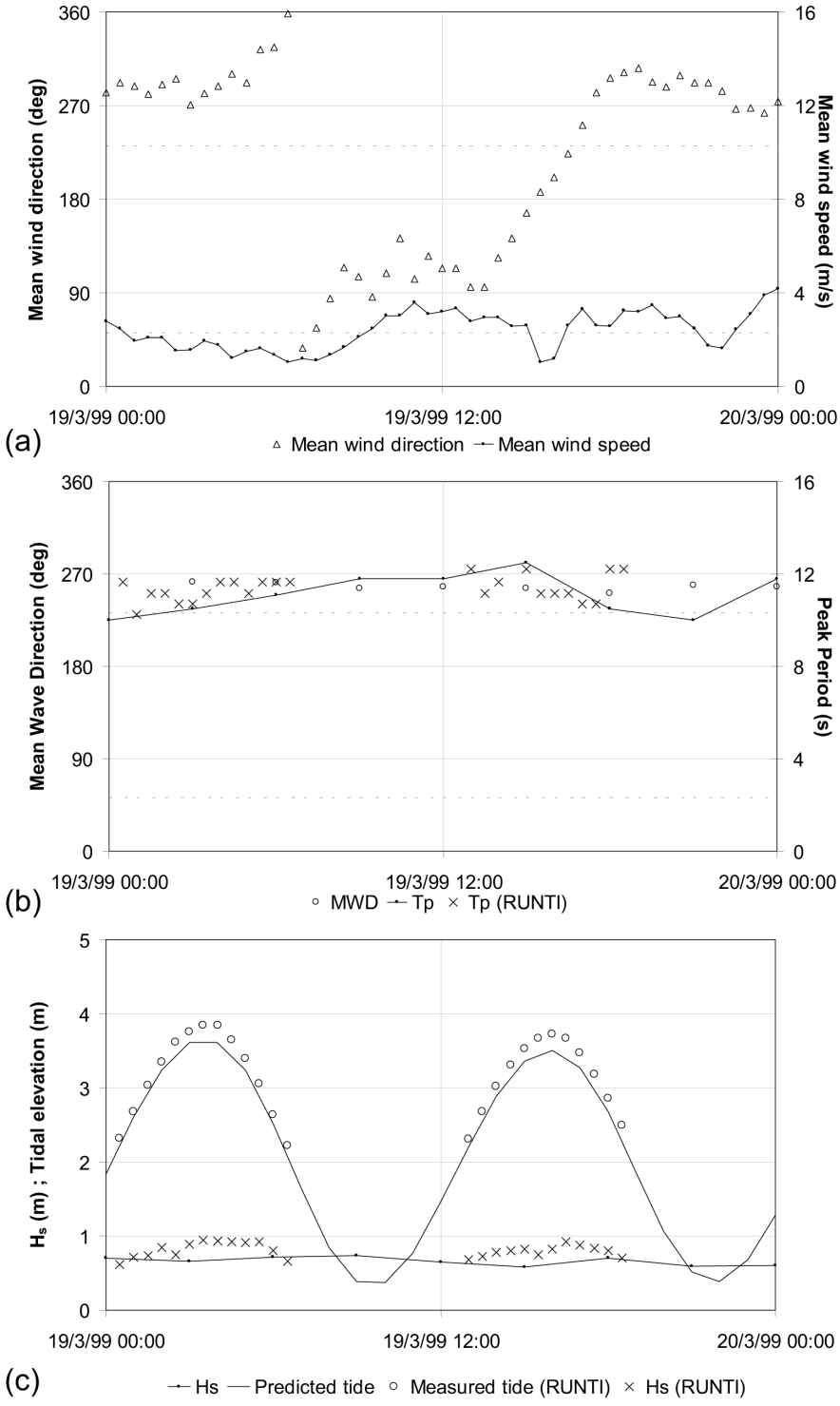

Figure 7.10: Forcing mechanisms during AMI.3: (a) Mean wind direction (°) and Mean wind speed (m/s); (b) Mean wave direction (θ_p, °) and Peak period (T_p, s); (c) Significant wave height (H_s, m), tidal predictions (m) and RUNTI measured tidal elevations (m). The dashed lines show the onshore and offshore directions (232° and 52° respectively).

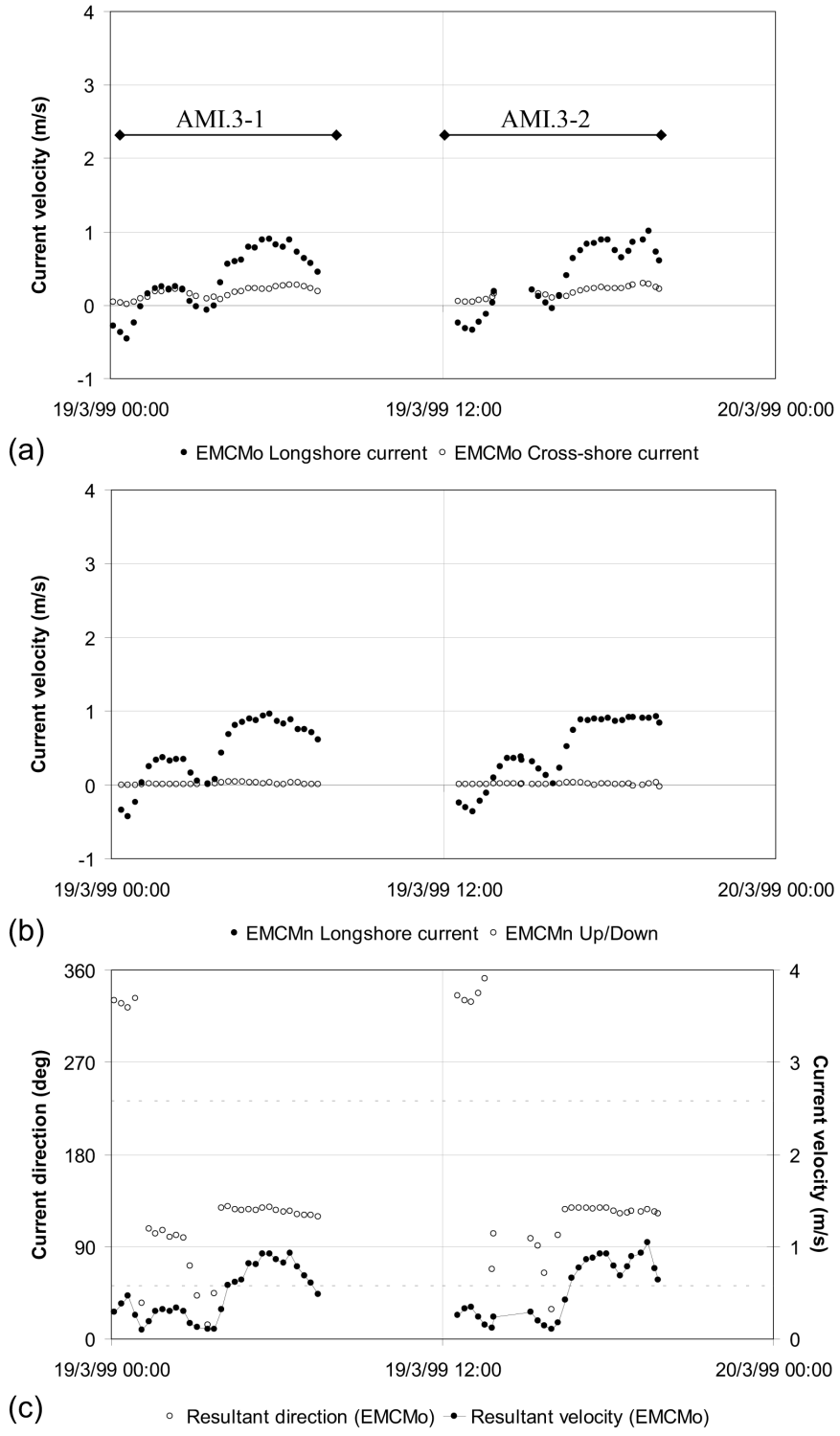

Figure 7.11: Currentmeter data measured by EMCMo and EMCMn at the internal part of the inlet channel during AMI.3. (a) and (b) show respectively EMCMo and EMCMn current velocity data (m/s) (positive values indicate eastward, upward and northward directions, negative values indicate westward, downward and southward directions); (c) Resultant directions (°) and velocities (m/s) for EMCMo. The dashed lines show the onshore and offshore directions (52° and 232° respectively).

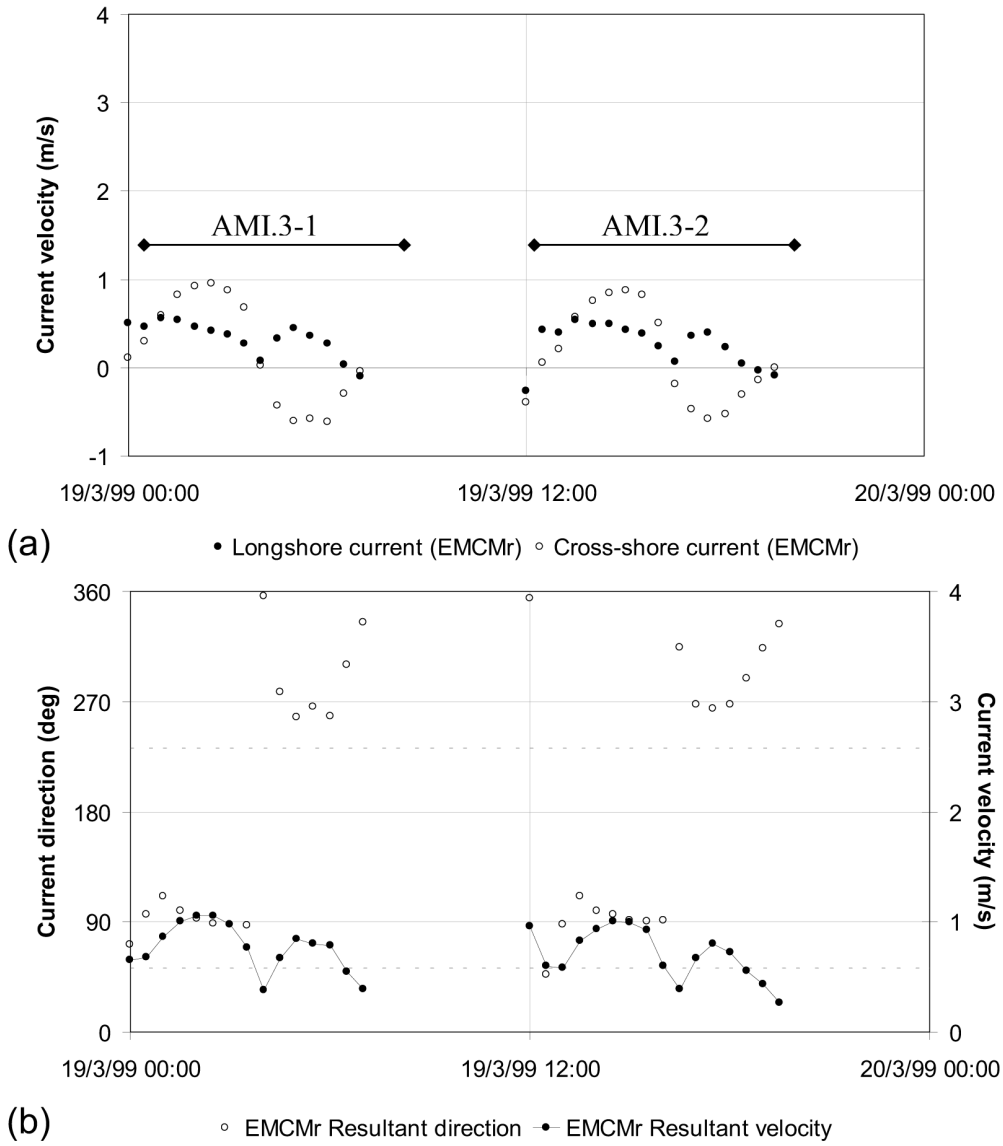

Figure 7.12: Currentmeter data measured by EMCMr at the swash platform for AMI.3. (a) EMCMr current velocity data (positive values indicate south-eastwards and onshore directions, negative values indicate north-westwards and offshore directions); (b) Resultant directions (°) and velocities (m/s). The dashed lines show the onshore and offshore directions (52° and 232° respectively).

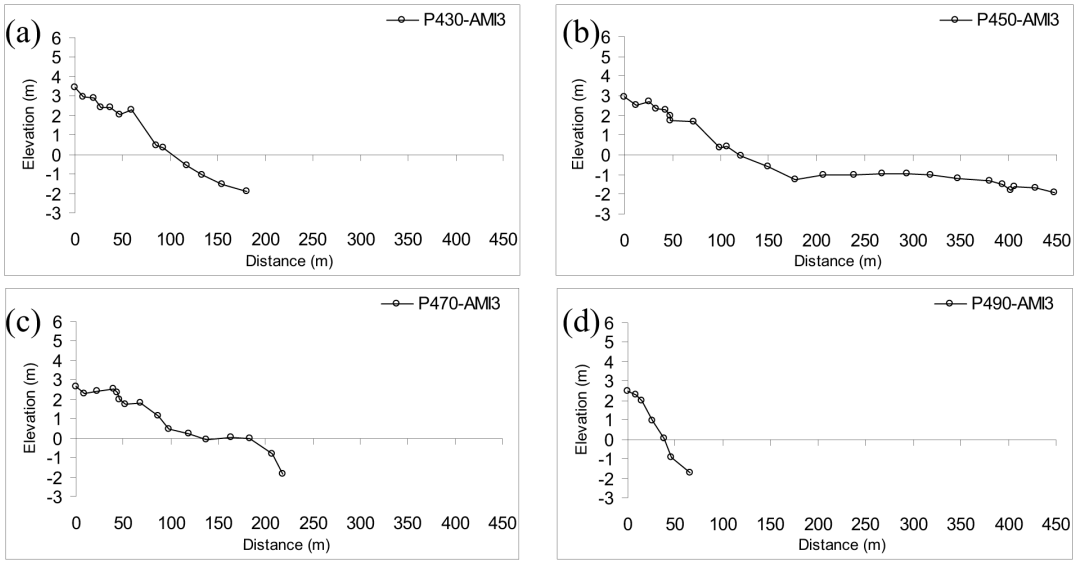

Figure 7.13: Topographic profiles obtained during AMI.3: (a) P430; (b) P450; (c) P470; and (d) P490. Elevation is referenced to mean sea level (MSL).

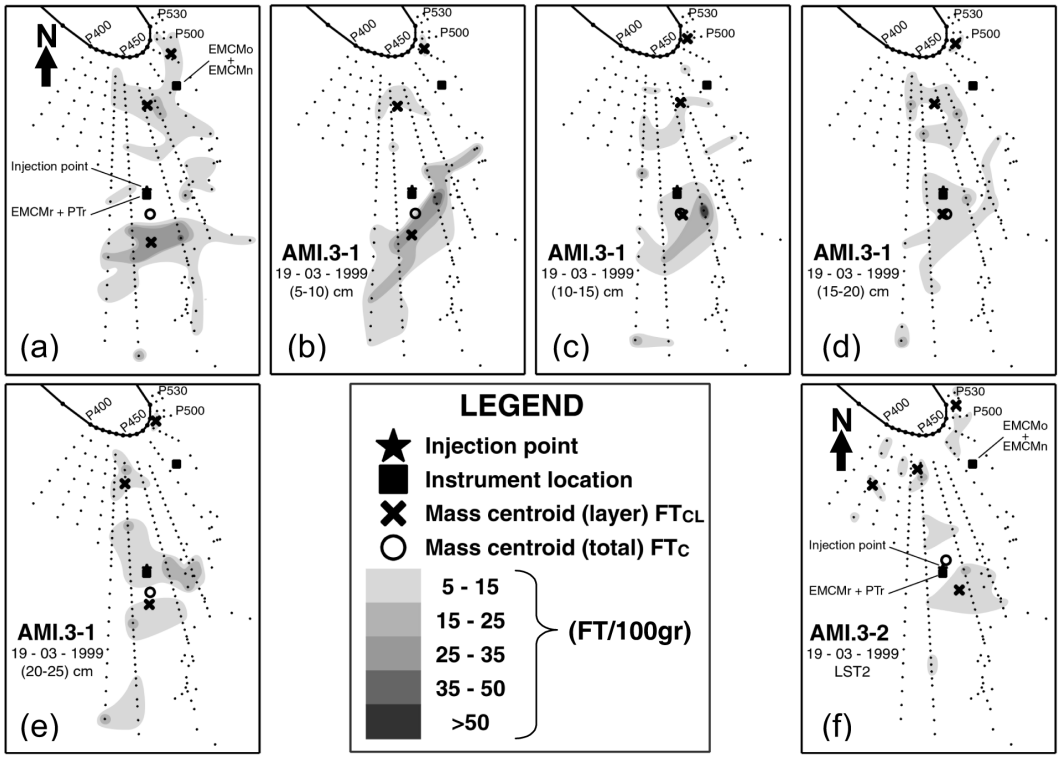

Figure 7.14: FT distribution maps for AMI.3. Locations of the total (FT_C) and partial (FT_{CL}) mass centroids are shown for each layer: (a) LTS1 0-5 cm; (b) LTS1 5-10 cm; (c) LTS1 10-15 cm; (d) LTS1 15-20 cm; (e) LTS1 20-25 cm; and (f) LTS2 semisurficial samples.

7.1.4 General morphologic evolution of the swash platform

Isopach maps showing the topographic vertical variations on the swash platform and adjacent areas are shown in Figure 7.15. From AMI.1 to AMI.2 (Figure 7.15a) it can be seen that strong erosion occurred in the inner parts of the inlet (Sector D) whilst a smooth accumulation was seen for the central parts of the swash platform as well as in the foredune area. The volumetric computations for the total area gave a net erosion of 3,330 m^3. Between AMI.2 and AMI.3 (Figure 7.15b) the erosion seen for the inner part of the inlet was not as strong as between the first two experiments. Accumulation processes were dominant in the central parts of the sand spit and were stronger than between AMI.1 and AMI.2, especially in the southern part of Sector B where over 1 m of accretion was seen, a fact that can also be observed through the comparison of the profiles shown in Figure 7.8 and Figure 7.13. Volumetric computations for the total area gave a net accumulation of 1,880 m^3.

Volumetric changes for the entire period, as well as the FT_C obtained for sectors B, C and D are shown in Figure 7.15c. The volumetric evolution of the swash platform located on the western shore of Ancão Inlet gave a total erosion of -1,450 m^3. The accumulation areas, mostly in Sector B and the northern part of Sector C, show the growth of Ancão Peninsula. Calculation of accumulation rates for these areas gave values close to 210 m^3/tide. The strong erosion in Sector D reached vertical values over 3.5 m, providing erosion rates of 220 m^3/tide.

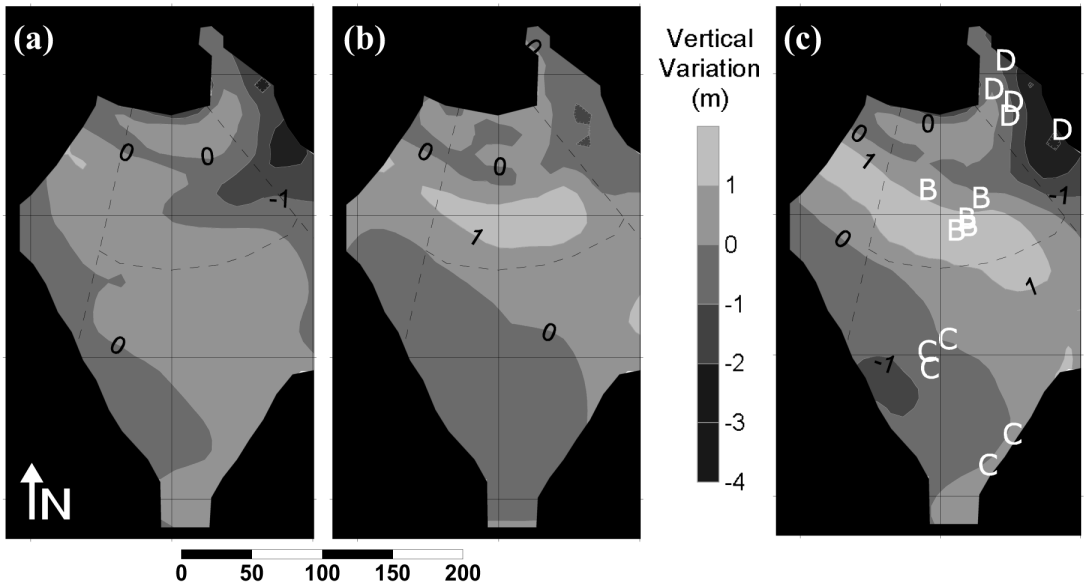

Figure 7.15: Isopach maps of the swash platform located on the easternmost part of Ancão Peninsula showing the vertical variations of the morphology (erosion/accumulation): (a) Variation from AMI.1 to AMI.2; (b) variation from AMI.2 to AMI.3; (c) total variation between AMI.1 and AMI.3. B, C, and D are the total mass centroids (FT_C) obtained for each sector in each campaign.

7.2 Discussion

The work presented here represents an innovative approach to sediment transport studies using tracers in complex environments such as inlet margins. The use of morphologically defined sectors (see Figure 4.4) permitted a semi-quantitative study of the sediment transport paths and magnitudes at the updrift margin of an inlet. The methodology used facilitated the analyses of FT experiments at the updrift margin of an inlet, allowing the definition of sediment transport interactions between different morphologies (e.g. oceanic beach, swash platform, inner beach). However, there are still some restrictions to the use of FT for a complete and quantitative study of sediment transport at inlet margins. According to Madsen (1987) there are three assumptions in FT theory: (1) advection processes dominate diffusion and dispersion; (2) the natural sand from the beach has similar grain-size properties as the FT; and (3) the transport system must be uniform in the longshore direction. The first assumption can only be accepted for Sector A where unidirectional currents largely dominate. The second assumption can be accepted for the three campaigns (see Table 7.2) since the sand to be painted was extracted from the areas where the injection was to be made. The third assumption can be accepted for Sector A, because it is a straight beach and, for the rest of the sectors with some concerns, since they were determined based on the morphology. Bi-directional tidal currents are the main transporting agent for sectors B, C and D. Therefore, for these areas dispersion dominates over advection and it is not possible to calculate, without a large uncertainty, the advection velocities using the tracer results. The use of different colours (i.e., Kraus *et al.*, 1982), deploying one colour during low tide and the other during high tide could facilitate the calculation of sediment advection velocities during ebbing and flooding separately. However, tests with green paint during AMI.2 and other tests made with blue paint, showed that these colours reflect at a very similar wavelength to the shell particles present in the sediments of the study area, making tracer detection in a practical way impossible. As a consequence of these limitations, direct quantification of FT transport can only be made for Sector A. For sectors B, C and D, a semi-quantitative approach based on the definition of sediment transport paths and the transfer between sectors must be established.

7.2.1 Sediment transport paths

According to the literature (i.e., Pilkey *et al.*, 1989; Andrade, 1990; Ciavola *et al.*, 1997a, 1998) and also shown by the data presented in this study, under SW waves the sediment is transported along the updrift beach in a general eastward direction (AMI.1-1, Figure 7.4). Average H_s and T_p for AMI.1-1 was 0.8 m and 8.1 s. The average θ_p was close to 232°N, thus the incident waves had an almost shore-normal approach to the beach, resulting in small incident angles that produced the longshore currents. Sediment transport calculations for AMI.1-1, using the mixing depth calculated along the beach and the weighted velocity of the mass centroid, gave a value of 1,820 m^3/day (950 m^3/tide). Previous studies at a swash bar on the swash platform updrift of Ancão Inlet performed by Balouin (2001) using tracers gave a value of some 370 m^3/day (190 m^3/tide) for the 28th February 1999; offshore wave conditions for that day were SW waves with H_s ranging from 0.8 m to 1.1 m and T_p close to 11 s. From tracer studies performed at Culatra Island (Figure 3.1), Ciavola *et al.* (1997a) calculated values between 200 and 1,200 m^3/day under short period SW waves with average H_s ranging from 0.28 to 0.44 m. According to C.Costa (1994) mean winter values for H_s and T_p at the study area are 1.15 m and 9.5 s respectively and W-SW conditions occur about 64% of the time during winter. Therefore, the SW wave conditions measured during this study and those measured by Balouin (2001) and Ciavola *et al.* (1997a) are inside the expected ranges for SW winter conditions in the study area but slightly inferior to the average values. Thus, it can be said that daily gross littoral drift in the area, for SW winter-calm conditions, ranges from 200 m^3/day to 1,820 m^3/day.

The general morphologic evolution of the swash platform (see Section 7.1.4) showed that sediment accumulation on the swash platform (mostly Sector B) was 210 m^3/tide. Accumulation rates found in this area are in agreement with those obtained by Balouin (2001) for the same area but using different methodology (190 m^3/tide). Therefore, accumulation in Sector B represents about 20% of the gross littoral drift calculated for AMI.1 (950 m^3/tide).

Once the sediment arrives at the inlet area it begins to be subjected to tidal inlet processes such as tidal currents. Results from AMI.1-2 (Figure 7.5) showed that after the second tidal cycle, 73% of the remaining tracers were located in Sector A and 27% entered the area of the swash platform. It should be noted here that the percentage of sediment remaining in Sector A could have been lower if

westward directed currents did not occur during the first stages of AMI.1-2 (see Figure 7.2). Of the FT that entered the swash platform, 31.5% was found in Sector B, 60.7% in Sector C and 7.8% in Sector D. According to the currents measured during this campaign (Figure 7.2) and to the FT distribution maps (Figure 7.5), it seems reasonable to establish direct sediment transport from Sector A to sectors B and C. However, data from this campaign does not allow the establishment of the sediment transport paths to Sector D.

Currentmeter data from AMI.2 and AMI.3 can be used to determine the current patterns on the inner inlet margin (Sector D) and swash platform (Sector C). According to the currentmeter data from AMI.2 and AMI.3 (see Figures 7.7 and 7.11) three tidal stages (TS1, TS2 and TS3) can be defined inside each tidal cycle. TS1 occurs until 2-2.5 hours before the high tide slack, and during this stage, flooding currents occur in both sectors, being stronger in Sector C. TS2 lasts until the high tide slack and during this stage, flooding currents reach their maximum velocity on the swash platform (Sector C, see Figures 7.11c and 7.12b) while weak ebbing currents occur in Sector D (see Figures 7.7c, 7.11c and 7.12b), indicating the possible existence of an anticlockwise current gyre located over Sector D. During TS3, that occurs after the high tide slack, ebbing currents occur in both sectors, being stronger in Sector D (see Figures 7.7c, 7.11c and 7.12b), currents measured in Sector C were westwards directed (Figure 7.12b) that together with the SW incident waves (Figure 7.10b) suggests the existence of a clockwise current gyre.

Sediment transport paths on the swash platform became clearer with the FT results obtained for AMI.2 and AMI.3 (see Figures 7.9 and 7.14). For both campaigns almost no tracers were found close to the injection point, reflecting the highly dynamic nature of the system, and the value of $PRFT$ was close to 60% for the LTS1 of each campaign, which according to White (1998) is inside the range of values considered as 'good'. FT distribution was similar in both campaigns with the maximum FT concentration in Sector C, followed by Sector B, and Sector D where almost no FT were found. Simultaneously, some FT were found in the eastern part of Sector A and in the submarine samples taken in front of the swash platform.

Combining currentmeter and FT data from AMI.2 and AMI.3 the following sediment transport paths are established:

(1) During TS1 the sediments are transported from Sector C and Sector D

towards the inner parts of the inlet system, once the water has reached Sector B, the sediments in this sector are also transported towards Sector D.

(2) During TS2 while flooding currents are still acting in sectors B and C, an anticlockwise circulation gyre, Internal Gyre (*IG*), is established in Sector D producing offshore directed currents in that sector (Figure 7.16a). Therefore, whilst sediments from sectors B and C are transported to the inner parts of the inlet (including Sector D), sediments from Sector D are partially re-circulated due to the influence of the *IG*. The *IG* was visually observed during the fieldwork campaigns but its existence has been confirmed by the analyses of current data during AMI.3. The development of the *IG* (Figure 7.16a) is possibly related with the morphology of the area: while the flood delta is still emerged the flooding currents are constricted to the internal channel located at the back of Ancão Peninsula, once the flood tidal delta is under water the flooding currents that are now more spread interact with the delta and develop an anticlockwise gyre.

(3) During TS3 ebbing currents affect all of the swash platform (towards the ebb jet in the inlet channel for Sector D and westward directed for Sector C), thus the possible explanation for the presence of tracers in sectors A, B and C is the development of a clockwise circulation gyre, External Gyre (*EG*) in the external part of the inlet (Figure 7.16b). Ebbing currents in Sector D are very strong producing sediment removal and consequent erosion, which is in agreement with the results from the morphologic evolution of the swash platform (see Section 7.1.4). The existence of an external gyre (*EG*) on the updrift margin of a tidal inlet has been reported by several authors for inlets in different parts of the world (i.e., Oertel, 1972; Smith and FitzGerald, 1994; Dyer and Huntley, 1999; FitzGerald *et al.*, 2000) and also in previous studies of Ancão Inlet (Williams *et al.*, 2003). According to several authors (i.e., Oertel, 1972; Smith and FitzGerald, 1994) *EG* development (Figure 7.16b) results from wave-current interaction at the terminal lobe of the ebb delta. According to the FT distribution patterns for AMI.2 and AMI.3 (Figures 7.9 and 7.14, respectively), the current velocities at the gyre are high enough to permit sediment re-circulation during a single tidal cycle (e.g. FT found in the eastern part of Sector A for AMI.2 and AMI.3). According to Oertel (1972) the sediment transport capability of the wave bores (onshore directed) is greater than that of the tidal currents (offshore

directed) thus, the *EG* explains the high concentration of FT found in sectors B and C for all the campaigns, and the sediment transport towards sectors A, B and C for AMI.2 and AMI.3. The *EG* also contributes to the explanation of the sediment accumulation found on the central areas of the swash platform that was observed in the medium-term volumetric and morphologic analysis (Figure 7.15).

It is important to note that the sediment transport paths found for the swash platform updrift of Ancão Inlet were very similar for the 3 campaigns. Location of FT_C for sectors B, C and D (Figure 7.15c) was very similar for all the campaigns, the standard deviation of the co-ordinates was calculated providing mean values of 11.8 m, 32.0 m and 17.1 m respectively. FT_C for Sector B shows the lowest variations in its position, in Figure 7.15c it can be seen that the location of FT_C for this sector is coincident with the areas where accumulation processes related with the growth of Ancão Peninsula were occurring. Therefore, under SW winter calm conditions, the sediment transport paths seem to be more dependent of the tidal conditions (that were very similar in all campaigns) and quasi-independent of the waves and wind conditions (that showed some variations in between campaigns). However, it seems reasonable that if not the sediment transport paths, the sediment transport magnitudes under SW winter calm conditions will be greatly influenced by changes in the incident waves, or under the influence of very strong wind. Sediment transport paths are expected to be very different under SE or storm (both from SW and SE) conditions.

A schematic design for the sediment transport paths defined for Ancão Inlet is shown in Figure 7.16. Tidal flooding conditions just before the high tide slack are shown in Figure 7.16a where the *IG* can be observed. The paths are directed towards the internal areas of the inlet, and the transport occurs from Sector A to sectors B and C, and from Sector B to Sector D where part of the transported sediment can be temporarily trapped by the *IG*; sediment transported from Sector C goes directly to the inlet channel and as it travels towards the internal areas, it can also be partially trapped by the *IG*. Sediment transport paths for tidal ebbing conditions are shown in Figure 7.16b, with the approximate location of the *EG*. Under the influence of the incident waves and winds, the longshore currents transport downdrift the sediments in Sector A, from where, still under the influence of the longshore currents, they are transported towards sectors B and C. Simultaneously, strong ebb tidal currents flush the sediments from the internal areas of the inlet towards the ebb jet that reaches the ebb delta. Some of

the sediments transported by the ebb jet are trapped by the *EG* that re-cirulates them towards the easternmost part of Sector A and towards sectors B and C.

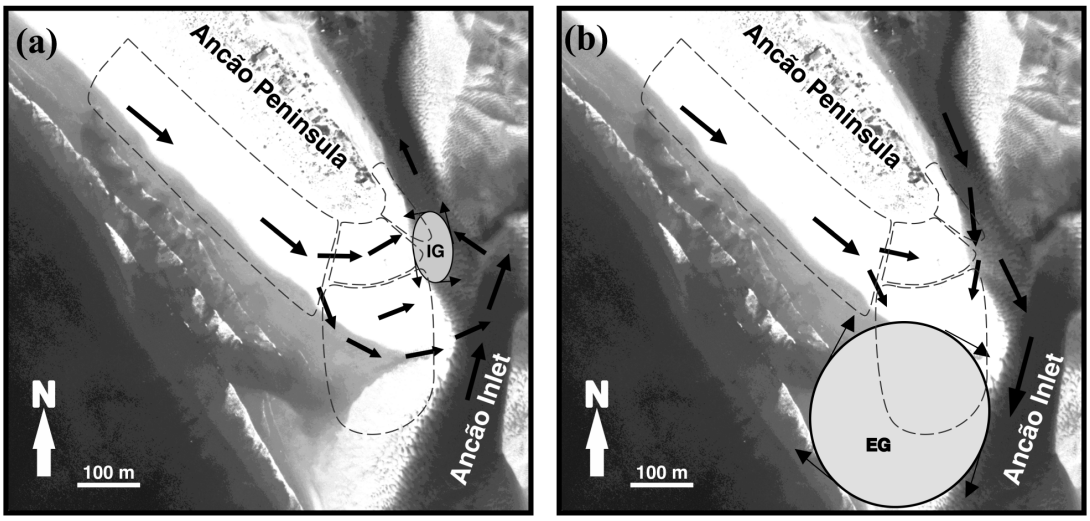

Figure 7.16: Conceptual model for sediment transport paths at the updrift margin of an inlet: (a) flooding conditions and (b) ebbing conditions. Dashed lines show the division between the considered sectors; arrows show the sediment transport pathways; *IG* is the internal gyre; and *EG* is the external gyre.

7.2.2 A semi-quantitative conceptual model for sediment transport at the swash platform

With the results obtained for the three campaigns a semi-quantitative conceptual model can be defined for the sediment transport on the swash platform located on the western shore of Ancão Inlet under SW conditions. However, an analysis of the sediment losses found for the campaigns is needed. Results from sediment loss were found to be very similar for both of the studied tides for AMI.1 (17% and 16% for AMI.1-1 and AMI.1-2 respectively) and for AMI.2 (40% and 47% for AMI.2-1 and AMI.2-2 respectively). However, the two tides studied showed very different percentages of sediment loss for AMI.3 (38% and 61% for AMI.3-1 and AMI.3-2 respectively). Hydrodynamic conditions during the two tides of AMI.3 were very similar, thus the explanation of this difference is probably related with the nature of the sample collection: AMI.3-2 was performed collecting semi-surficial samples with plastic containers. Therefore it could be possible that the FT were completely mixed with the natural sediments or that they were buried during accumulation processes on the platform. As a consequence the values obtained through corer samplings (both LTSs for AMI.1 and the LTS1 for AMI.2 and AMI.3) are considered to be more reliable and are the ones used for sediment transport quantification.

The proposed model is based on the conditions and results found for the AMI campaigns, therefore, the following restrictions are to be taken into account in its application:

(a) Incident waves are from the SW, with average values for H_s ranging from 0.4 to 1.6 m and for T_p from 5.2 to 11.2 s, thus according to C.Costa (1994) correspond to typical calm to moderate SW conditions for the study area, therefore, tide-dominated processes.

(b) Sediment losses found for the tracers are assumed to be real losses of sediment (i.e. sediment is transported outside the study area) and not the result of under sampling (results from AMI.2-2 and AMI.3-2 are not used for the model).

With the combination of the results of the FT analyses from all three campaigns, a semi-quantitative conceptual model was developed for the swash platform. This model has two stages that occur in between consecutive low tides

(beginning of first tide, time 0, t=0; end of first tide and beginning of the second one, time 1, t=1; and, end of the second tide, time 2, t=2) and includes the effect of both the external and the internal gyres determined within this study. Stage 1 occurs between t=0 and t=1 and represents the sediment arrival to the swash platform from the updrift beach. The distribution and loss of sediments inside sectors B, C and D occurs according to the results obtained from the FT analyses for AMI.1-2, such that the sediment injection occurs from Sector A. Stage 2 occurs between t=1 and t=2 and represents the reworking of the sediments inside the swash platform. Results from AMI.2-1 and AMI.3-1 are used to determine the distribution and the losses of sediment, therefore the reworking of the sediments occurs from sectors D and C respectively. The steps of the model are explained in the following paragraphs.

Stage 1: At time t=0 (low tide) a certain amount of sediment (M_A) arrives at the western limit of the swash platform (the limit between Sector A and Sector B). According to results obtained for AMI.1-2, after one tidal cycle (t=1, low tide), the loss of sediments (L_1) is 17% of M_A. Therefore the percentage of remaining FT at t=1 ($PRFT_1$) can be calculated as

$$PRFT_1 = M_A - L_1 \tag{7.2.1}$$

$$PRFT_1 = 0.83 \cdot M_A \tag{7.2.2}$$

This sediment is transported onto the swash platform following the sediment transport paths of Figure 7.16, the following distribution of FT is found: Sector B has 31% (SB_1=0.31 $\cdot$ $PRFT_1$), Sector C has 61% (SC_1=0.61 $\cdot$ $PRFT_1$) and 8% of the FT are in Sector D (SD_1=0.08 $\cdot$ $PRFT_1$).

Stage 2: Stage 2 of the model assumes that the sediment injection is in Sector D (to follow AMI.2-1 patterns) and in Sector C (to follow AMI.3-1 patterns). Therefore the assumption is needed that the sediments remaining in Sector B (SB_1) are directly transported towards Sector D and are reworked from there (Figure 7.16). Simultaneously, the volumetric evolution of the swash platform showed that Sector B acts as a sediment sink and traps approximately 20% of the gross littoral drift (see Section 7.1.4). Therefore, for Stage 2 it is assumed that there are two masses of sediment to be reworked: from Sector D (M_{2D}) is formed by the addition of SD_1 plus the 80% of SB_1, from Sector C (M_{2C}) corresponds to SC_1:

$$\%M_{2D} = SD_1 + (0.80 \cdot SB_1) - L_{2D} \tag{7.2.3}$$

$$\%M_{2C} = SC_1 - L_{2C} \tag{7.2.4}$$

where L_{2C} corresponds to the losses determined for sediment reworking from Sector C for AMI.3-1:

$$L_{2C} = 0.38 \cdot SC_1 \tag{7.2.5}$$

and L_{2D} corresponds to the losses determined for sediment reworking from Sector D for AMI.2-1:

$$L_{2D} = 0.40 \cdot (SD_1 + 0.80 \cdot SB_1). \tag{7.2.6}$$

The quantification of the percentage of remaining tracers at time t=2 is made as follows:

$$PRFT_2 = PRFT_1 - L_2 \tag{7.2.7}$$

where the loss of sediment at t=2 is defined as:

$$L_2 = L_{2B} + L_{2C} + L_{2D} \tag{7.2.8}$$

such that L_{2B} corresponds to losses due to sediment accumulation in Sector B:

$$L_{2B} = 0.20 \cdot S_{B1} \tag{7.2.9}$$

According to AMI.2-1 the distribution of the sediments reworked from Sector D (M_{2D}) is approximately 44% in Sector B, 56% in Sector C and 1% remains in Sector D. According to AMI.3-1, the distribution of the sediments reworked from Sector C (M_{2C}) is 90% remaining in Sector C, 10% in Sector B, and 1% in Sector D. Thus, the total distribution of the sediments in the system is as follows:

$$SB_2 = 0.20 \cdot SB_1 + (0.44 \cdot M_{2D} + 0.10 \cdot M_{2C}) \tag{7.2.10}$$

$$SC_2 = 0.56 \cdot M_{2D} + 0.90 \cdot M_{2C} \tag{7.2.11}$$

$$SD_2 = 0.03 \cdot M_{2D} + 0.01 \cdot M_{2C} \tag{7.2.12}$$

According to the model and assuming a sediment injection in Sector A of M_A=1,000 kg for t=0: after one tide (at t=1) some 830 kg of sediment would still remain in the system, of which 257 kg would be in Sector B, 506 kg would be in Sector C and only 66 kg would be in Sector D. After two tides (t=2) only 477 kg of the sediments injected at t=0 would remain in the system. Distribution at t=2 would be as follows: 102 kg in Sector B, 372 kg in Sector C and less than 1 kg would be in Sector D. Therefore, after two tides only 47% of M_A would remain on the swash platform system and thus, the sediment loss would be 53% of M_A. However, due to the new inputs of sediment provided to the system every tide through the littoral drift, it is important to note that sediment loss in this case, does not correspond to erosive processes. Assuming a constant input of 1,000 kg/tide, after two tides, the sediments to be reworked on the swash platform would be 1,307 kg (477 kg remaining from t=0, plus 830 kg remaining from a new input occurring at t=1). It is important to note that due to the *EG* some of the sediments would be found in Sector A, however, the presented model only takes into account the sediment transport processes on the swash platform.

Loss of sediments can be due to several factors, i.e., accumulation in the ebb/flood delta, inner channels, sediment by-pass or offshore expulsion through the ebb jet. According to Morris *et al.* (2003) and Williams *et al.* (2003) during the time of the fieldwork campaigns Ancão Inlet was in a transitional state (called '*MOR3*'), recovering after post-storm conditions (a large SW storm occurred in December 1998). According to Williams *et al.* (2003) during the '*MOR3*' state, tidal flows are stronger causing the erosion of the flood delta which supplies sediment that is transported offshore to feed the ebb delta and that together with the littoral drift makes possible the restoration of the beach and spits. The existence of an *EG* in a tidal inlet system has been proved by several authors, however, the full extent of such a gyre is known to be variable (Oertel, 1972). The *EG* in the Ancão Inlet system cannot be quantified with the data in this study. However, according to Section 6.1.3 the ebb delta was the only morphologic unit of the inlet that showed continuous accumulation during the first two years of the evolution of Ancão Inlet. Therefore, it seems likely that sediment losses from

the swash platform were transported offshore by the strong tidal flows to feed the ebb delta and that some of them were re-circulated by the *EG* and transported updrift to restore the updrift beach (Figure 7.16b).

Balouin (2001) established that the sediment budget is in equilibrium for the swash platform of Ancão Inlet and that no by-passing processes occurred under fair weather conditions. However, the existence of swash bar complexes migrating from the ebb delta towards the beach on the downdrift side of the inlet that was observed during the fieldwork campaign and afterwards (see Figure 3.4) indicates the existence of sediment bypassing under fair weather conditions. Kana *et al.* (1999) explained this bypassing process as a system where the accumulated sediments on the ebb delta are transported downdrift by the incident waves causing an excess of sediment on the downdrift part of the ebb delta. This sediment excess is then released and moves shorewards under the influence of the incident waves. Additionally, in Section 6.2 it was found that sediment bypassing at Ancão Inlet was occurring in 1999. Therefore, once on the ebb delta, some of the sediments losses from the swash platform could have been transported downdrift under this bypassing method.

The short-term sediment transport patterns found for Ancão Inlet are in agreement with other long-term studies performed at the same area (i.e., Morris *et al.*, 2003; Williams *et al.*, 2003). And also they seem to agree with the general transport patterns that were found for other inlet studies (i.e., Oertel, 1972; Smith and FitzGerald, 1994). The semi-quantitative conceptual model presented here assumes oceanographic and climatologic conditions similar to those measured during the AMI campaigns. It has been developed as a tool to understand what happens to the sediments that arrive at the swash platform from the updrift beach under SW conditions. Therefore other sediment sources, such as the tidal deltas or the inner channels, are beyond the scope of this study and were not taken into account, but could be important. Other sediment transport studies in the area including both deltas and the downdrift beach would be needed to fully understand the sediment transport patterns in the entire inlet system as well as the sediment bypassing mechanisms.

7.3 Conclusions

In recent years, the study of the sediment transport pathways and magnitudes has proved to be a difficult step for the definition of sediment budget in inlet sys-

tems. The division of the study area into morphologically defined sectors was a key step in the successful application of the SIM methodology to such a complex area. Also, the fact of working with a georeferenced co-ordinate system rather than the distances to the injection point traditionally used, increased the reliability and accuracy of the method. Sediment transport pathways were defined, however, sediment transport magnitudes could only be computed for the straight sector of the study area. Gross littoral drift for the study area was 950 m^3/tide.

The combination of the tracer analyses, forcing mechanisms and topographic evolution of the study area permitted the definition of sediment transport pathways. Three tidal stages were differentiated for every tidal cycle (TS1, TS2 and TS3). TS1 occurs from the low tide slack until 2-2.5 hours before the high tide slack, during this time, flooding currents are registered in all of the inlet area. During this stage transport towards the inlet and its inner areas occurs. TS2 occurs after TS1 and implies strong flooding currents occurring on the swash platform while an anticlockwise gyre (internal gyre, *IG*) develops as a consequence of the interaction of the flood delta with the flooding currents (Figure 7.16). During TS2 sediment transport on the swash platform is directed towards the inlet, however, in the inner parts of the inlet ebbing transport can occur due to the re-circulation of the sediments inside the *IG*. TS3 occurs after the high tide slack and ebbing currents are registered both on the swash platform and the inner sectors of the inlet (Figure 7.16). Transport on the swash platform was found to be westwards thus together with the SW incident waves, imply the existence of a clockwise external gyre (*EG*). Sediment transport during this tidal stage is offshore directed in the inner parts of the inlet under strong ebbing currents and westwards directed on the swash platform implying re-circulation of the sediments towards the west and upper parts of the swash platform.

To quantify the sediment transport on the updrift margin of the inlet, the integrated results were used to develop a semi-quantitative conceptual model. Development of the model was made to quantitatively describe the sediment transport pathways and magnitudes followed by a known mass of sediment arriving at the swash platform. Application of the model is restricted to SW winter calm conditions and assumes that the sediment losses are the result of the sediment leaving the system and are not the result of under sampling during the tracer experiments. According to the model, most of the accumulation of sediment occurs on the swash platform whilst the inner sectors of the inlet margin are eroding and thus, do not retain the sediment that arrives there. After one tidal

cycle 83% of the initial mass of sediment remains on the swash platform. The reworking of the same mass of sediments during the following tidal cycle results in only 48% of the initial mass of sediments remaining in the system after two tidal cycles. It is hypothesised that sediment losses are the result of sediment transport towards the ebb delta and that by-pass processes occur from the ebb delta to the downdrift beach though swash bar migration processes.

Chapter 8

Lessons from inlet relocation: Examples from Southern Portugal

"Nantucketers had a good reason to be superstitious. Their lives were governed by a force of terrifying unpredictability – the sea. Due to a constantly shifting network of shoals, including the Nantucket Bar just off the harbour mouth, [...] the simple act of coming to and from the island was an often harrowing and sometimes catastrophic lesson in seamanship."

Nathaniel Philbrick, *"In the Heart of the Sea."*

This chapter is partially being published by Elsevier:

Vila-Concejo, A., Ferreira, Ó., Morris, B.D., Matias, A., Dias, J.M.A., 2003d. Lessons from inlet relocation: examples from Southern Portugal. *Coastal Engineering* (in review).

8.1 Results

8.1.1 Hydrodynamics

With the exception of August 1997, the offshore wave data used for this study had a mean value of 3.4% missing data. Offshore wave data and tidal ranges are shown in Figure 8.1. During most of the study period H_s was less than 3 m (Figure 8.1a) and the T_p was less than 15 s (Figure 8.1b), lower values were obtained in the case of '*Levante*' conditions. As can be seen in Figure 8.1c, the wave climate for the study area can be considered as bi-modal in terms of wave direction. Predominantly, 73% of the time, the offshore direction of the waves was W-SW (θ_p>180°) and '*Levante*' episodes (θ_p<180°) were only registered during 27% of the study period. Figure 8.1d shows the predicted tidal ranges for the study area that were used to normalise the wave power.

The normalised wave power (P_n) for the two main directions (W-SW and '*Levante*') is shown in Figure 8.2. The comparison between Figure 8.2a and Figure 8.2b shows that most of the offshore wave power was from the W-SW. Major W-SW events occurred during the winters of 1997-1998 and 2000-2001 (Figure 8.2a) reaching values of H_s greater than 4 m in both cases (Figure 8.1a). Minor W-SW events occurred in spring 1998 as well as during the winters of 1998-1999 and 1999-2000. '*Levante*' events were scarcer and of shorter duration (Figure 8.2b). The largest '*Levante*' event for the study period occurred in April 2000 (Figure 8.2b) with H_s larger than 3 m (Figure 8.1a). Other high wave power '*Levante*' events occurred in March 1999 and February 2001. During the time of the study there were some other periods that did not have '*Levante*' events with large P_n but had '*Levante*' conditions at a higher occurrence than the rest of the time; i.e. the beginning of the year in 1998 and during winter 1999-2000 (Figure 8.2b).

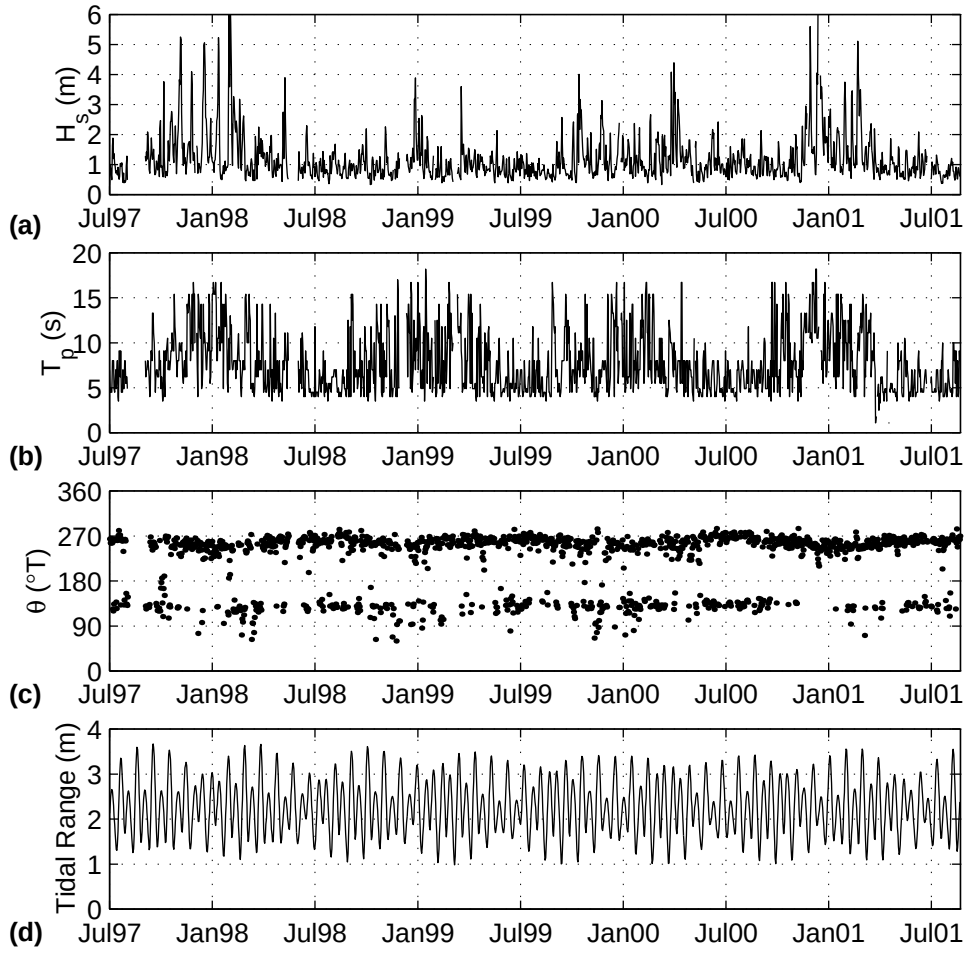

Figure 8.1: Wave and tidal conditions for the study period: (a) Significant wave height (m); (b) Peak period (s); (c) Wave direction at peak period (degrees); (d) Tidal Range (m).

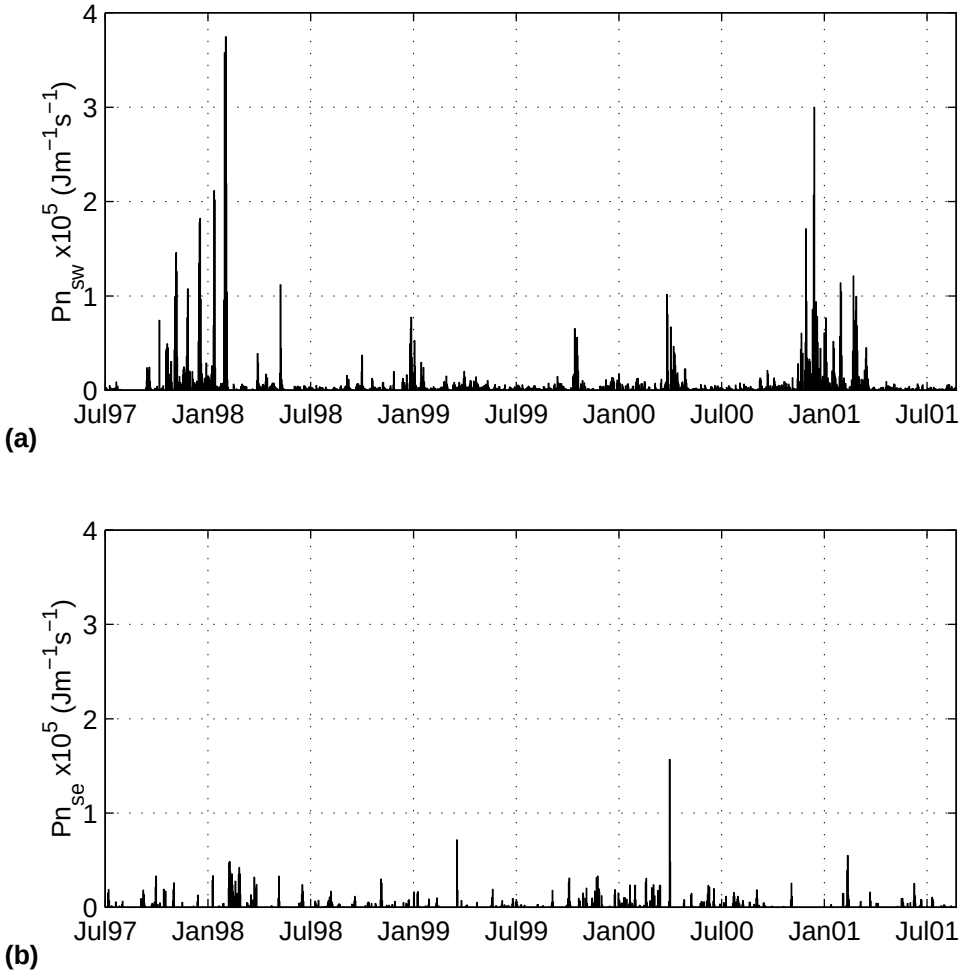

Figure 8.2: Wave power normalised using the tidal range. (a) W-SW direction, (b) E-SE direction.

8.1.2 Evolution of Ancão Inlet

Maps showing the evolution of Ancão Inlet between August 1997 and July 2001 are shown in Appendix A (Figures A.1 to A.16). As can be seen in these figures, after a period of initial readjustments that included flood and ebb tidal-delta formation (July 1998, see Figure A.3), the inlet started its eastward migration (January 1999, see Figure A.6). Migration occurred simultaneously with the building of the updrift spit, therefore, by January 2001 (Figure A.6) a well developed updrift spit can be observed. At the same time, it is possible to see the migration of both deltas occurring with the channel movement (e.g., July 1998, Figure A.3 vs. July 2001, Figure A.16).

Channel Evolution

The evolution of inlet width at inlet gorge is shown in Figure 8.3a. After reaching dynamic equilibrium by April 1998 (see Chapter 6), Ancão Inlet had an average width of 260 m. Maximum inlet width was reached by March 2000 (390 m) and after that, Ancão Inlet channel reduced its width until reaching a minimum value of 125 m by April 2001 (Figure 8.3a). Between April 1998 and September 2000 Ancão Inlet had an average Ω of 9.9×10^6 m^3, showing a maximum Ω of 13.3×10^6 m^3 in March 2000 (Figure 8.3b). A strong decrease in the Ω of Ancão Inlet occurred in the beginning of 2001, reaching a minimum value of 4.5×10^6 m^3 in April 2001. By August 2001 the Ω of Ancão Inlet was still showing low values but slightly higher than in April 2001. The volumetric evolution of Ancão Inlet channel is shown in Figure 8.3 and in Table 8.1. After reaching dynamic equilibrium, the inlet channel showed some small volumetric changes until the channel reached its maximum volume in June 2000 (Figure 8.3c). After that, sedimentary infilling processes in the channel produced the channel minimum volume by January 2001. For the rest of 2001 the channel underwent some changes without recovering its initial volume.

Tidal-Deltas Evolution

One year after the opening (July 1998), the Ancão flood delta had undergone an accumulation of 125×10^3 - 200×10^3 m^3. The accumulative volumetric evolution of the flood delta is shown in Figure 8.4a and Table 8.1. After October 1998 and during 1999 and 2000, the Ancão flood delta had less volume than in July

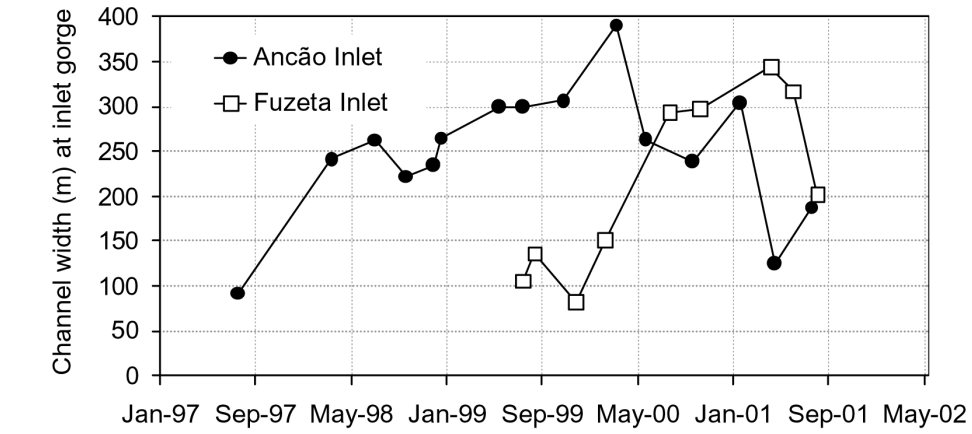

(a)

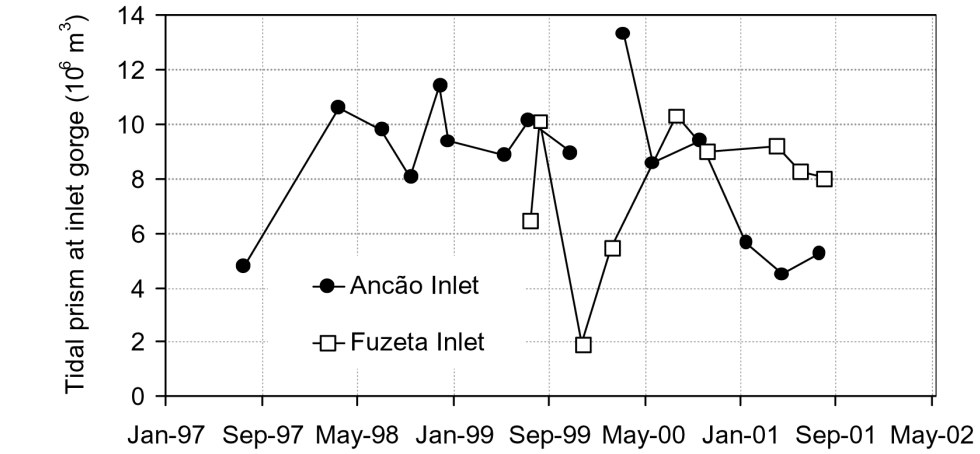

(b)

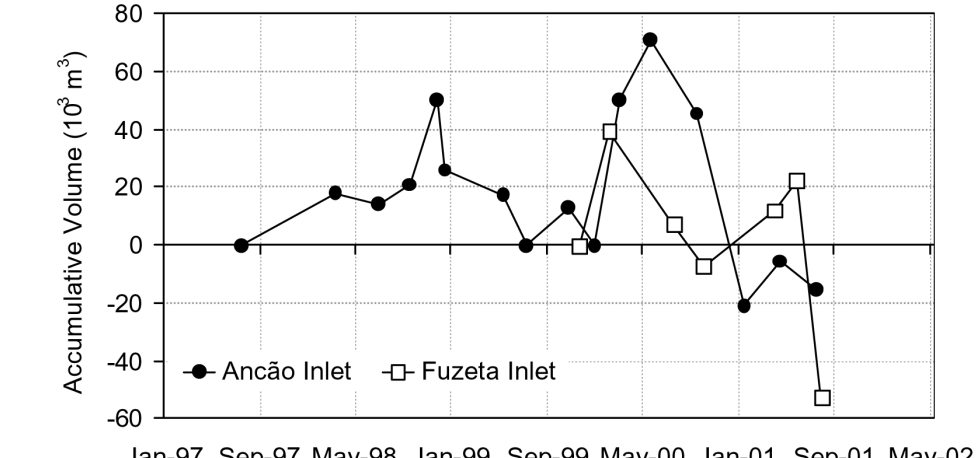

(c)

Figure 8.3: Main parameters related to the inlet channel evolution, (a) channel width at inlet throat (m), (b) Tidal prism (m^3), and (c) accumulative sedimentary volumetric evolution of the channel area (10^3 m^3).

1998 (with a minimum value in December 1998). Accumulative processes during the end of 2000 caused the Ancão flood delta to again reach values similar to that of July 1998 by January 2001, reaching its maximum value in April 2001. Ancão ebb delta (Figure 8.4b and Table 8.1) has been accumulating sediments for the entire study period (1,420×10^3 m^3).

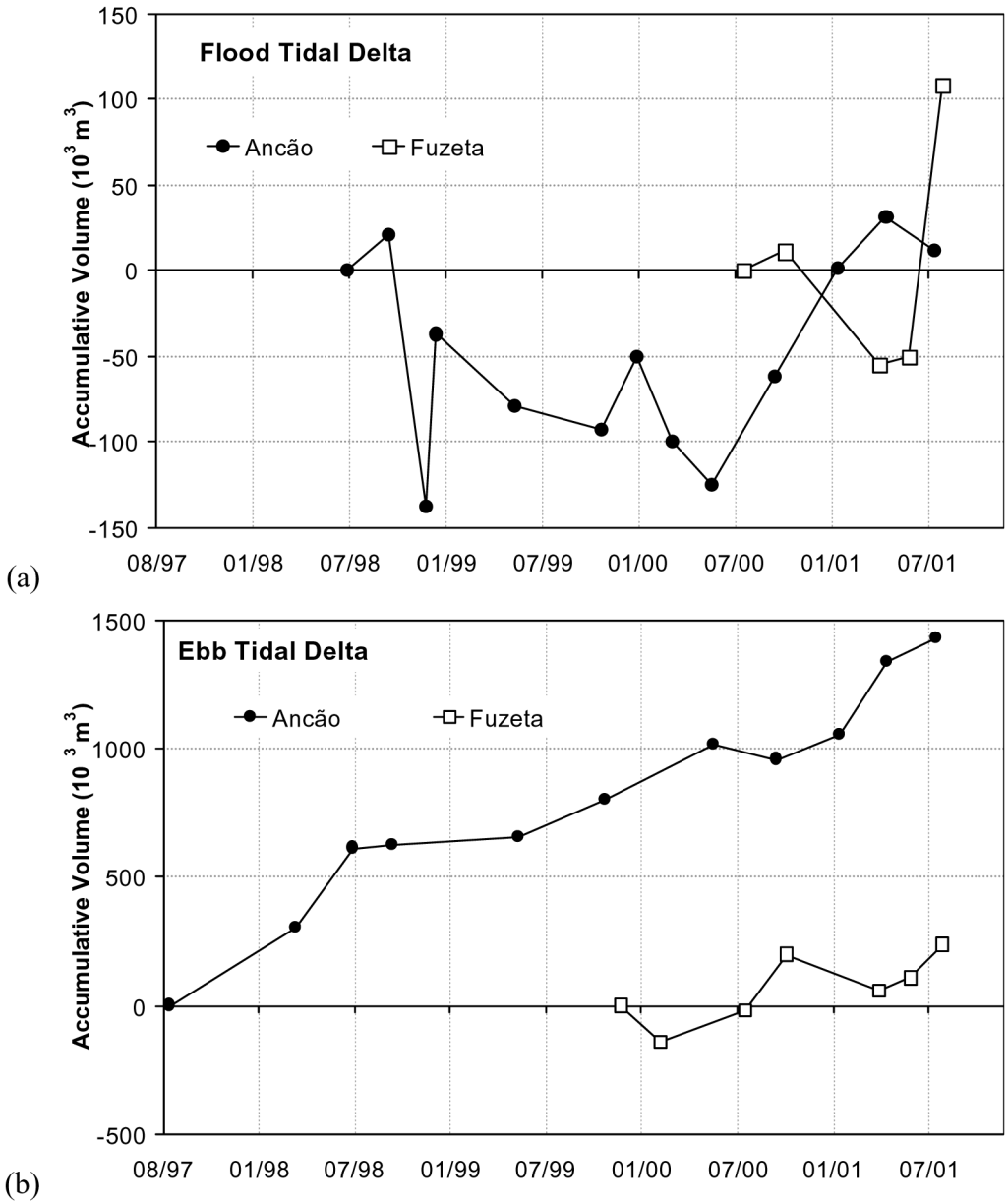

Figure 8.4: Accumulative sedimentary evolution (in ×10^3 m^3) of the (a) flood delta area and (b) the ebb delta area.

Inlet Migration

After some initial readjustment, that included some westward migration, Ancão Inlet started its eastward migration by December 1998 (Figure 8.5), with high migration rates until January 1999 (1.1 m/day). Between July 1999 and September 2000, Ancão Inlet did not show strong migrating movements. However, between September 2000 and April 2001 the inlet migrated 180 m with high migration rates (1.5 m/day between January and April 2001). After April 2001 eastward migration was slower.

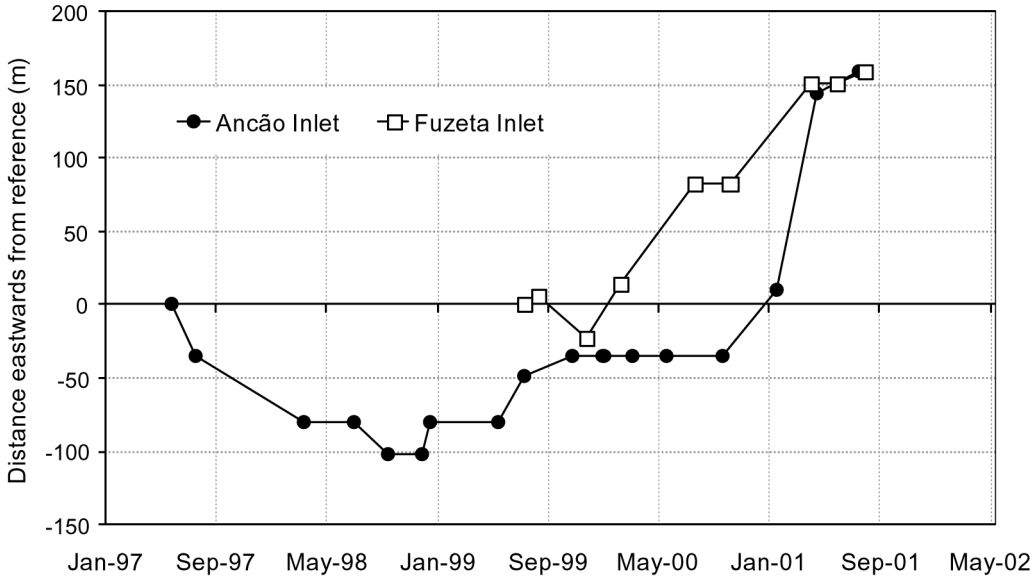

Figure 8.5: Inlet migration. The positions of the deepest points of the channel are referred to an arbitrary point located 10 m to the west from the westernmost position of the channel.

The Effect of Wave Power

The relationship between inlet evolution and the SW wave power (Figure 8.2) seems evident. Under low-energy conditions the inlet, which is ebb-dominated, flushes sediment away from the channel and therefore, reaches its maximum efficiency. On the contrary, under high-energy SW conditions, the sediments are transported towards the inner parts of the inlet thus infilling the channel and producing flood delta growth. Ebb delta erosion under high-energy conditions cannot be distinguished in Figure 8.4b. Moreover, it seems that the increase in

the littoral drift under high-energy conditions is related with ebb delta growth. Simultaneously, the highest migration rates are reached under high-energy SW conditions.

8.1.3 Evolution of Fuzeta Inlet

The evolution of Fuzeta Inlet between December 1999 and August 2001 is shown in Appendix A (Figures A.17 to A.23). Fuzeta Inlet started its eastward migration by December 1999, however, it can be seen that the channel was not very well defined and that infilling processes and meandering of the channel were occurring (December 1999, July 2000, October 2000, June 2001 and August 2001, see Figures A.17, A.19, A.20, A.22 and A.23). The building of the updrift spit, and the migration of both tidal-deltas, occurred at the same time as the channel migration (e.g., July 2000 vs. August 2001).

Channel Evolution

The width of Fuzeta Inlet channel underwent initial readjustments until February 2000 (Figure 8.3a). Inlet width enlargement was rapid from 80 m in December 1999 to 290 m in July 2000, giving an enlargement rate of 0.9 m/day. By July 2000 the width reached similar values to those that, according to several authors (i.e., Esaguy, 1985; Salles, 2001, see Chapter 5) had been registered for the former Fuzeta Inlet for the last 15 years. Therefore, it seems that the channel width of Fuzeta Inlet was reaching dynamic equilibrium values. Average width for Fuzeta Inlet after July 2000 was 290 m. Maximum inlet width was reached by April 2001 (345 m) and after that, a reduction occurred until reaching 205 m by August 2001. Fuzeta Inlet showed strong variations in its Ω (Figure 8.3b) during the first year of evolution, reaching a minimum Ω of 1.9×10^6 m^3 in December 1999. The increase of the Ω after that time caused Fuzeta Inlet to reach its maximum Ω by July 2000 (10.3×10^6 m^3). Between July 2000 and August 2001 the Ω of Fuzeta Inlet underwent small variations, having an average value of 9.0×10^6 m^3. The volumetric evolution of the channel showed strong variations during the first two years of its evolution (Figure 8.3c). An increment in Ω occurred for the periods December 1999 to February 2000 and October 2000 to June 2001. Infilling processes occurred, thus reducing its volume, between February and October 2000 and between June and August 2001.

Tidal-Deltas Evolution

The accumulation at Fuzeta flood delta one year after the opening (July 2000) was 60×10^3 - 95×10^3 m^3. The Fuzeta flood delta underwent some accumulation until October 2000 (Figure 8.4a and Table 8.1). After that, erosive processes caused the flood delta to reach its minimum volume by April 2001. Subsequent accumulative processes caused the Fuzeta flood delta to reach its maximum value by August 2001. Fuzeta ebb delta only showed accumulative processes during the second year of its evolution (Figure 8.4b) giving a net accumulation after two years of 240×10^3 m^3.

Inlet Migration

Initial readjustments implied some westward movement for Fuzeta Inlet (Figure 8.5). However, between December 1999 and April 2001, Fuzeta Inlet showed rapid eastward migration (175 m), reaching maximum rates of 0.5 m/day between December 1999 and February 2000, and 0.4 m/day between February and July 2000 and between October 2000 and April 2001.

The Effect of Wave Power

Fuzeta channel underwent infilling processes and subsequent dredging on the inner channels, thus enhancing the efficiency, until May 2000. After July 2000 the observed variations were less significant than before, therefore, the inlet channel of Fuzeta Inlet had reached dynamic equilibrium. Fuzeta Inlet is flood-dominated and the relationship between inlet evolution and the wave power is not well defined. High-energy or high-occurrence of SE conditions typically produce the infilling of the channel, flood delta growth and accumulation at the ebb delta due to the increase in longshore drift. These conditions also produce the highest migration rates. On the contrary, high-energy SW waves arrive, after a large amount of refraction, at Fuzeta Inlet with such a large incident angle that they do not cause the direct entrance of sediments towards the flood delta, rather they produce the growth of the ebb delta due to larger sediment transport.

Table 8.1: Volumetric evolution of the main morphologic units at Ancão and Fuzeta inlets (10^3 m^3).

	Flood delta	Channel	Ebb delta	Inner channels	Channel beaches	Ocean beaches	Total
ANCÃO INLET							
1st yr.	125/200	-15	610		-315	-65	340/415
2nd yr.	-80	-5	40	30	-40	0	-55
2 YRS.	45/120	-20	650	30	-355	-65	285/360
3rd yr.	-45	-55	360	-85	-20	20	175
4th yr.	140	85	410	75	75	20	805
4 YRS.	140/215	10	1,420	20	-300	-25	1,265/1,340
FUZETA INLET							
1st yr.	60/95	-5	-15		-225	0	-185/-150
2nd yr.	105	60	255	35	50	10	515
2 YRS.	165/200	55	240	35	-175	10	330/365

8.2 Discussion

8.2.1 Evolution towards dynamic equilibrium

According to Chapter 6, there are 4 evolutionary stages (Figure 6.4) in the evolution of relocated inlets with similar characteristics to Ancão Inlet.

Ancão Inlet

The first two years of Ancão Inlet evolution were presented in Chapter 6. According to that Chapter, Ancão Inlet was in Stage 1 in June 1997. Transition to Stage 2 included inlet channel enlargement, reaching equilibrium values in April 1998. During Stage 2, the inlet was acting as a sediment trap while developing both the flood- and the ebb-tidal deltas. Ancão Inlet reached the end of Stage 2 one year after the opening (July 1998). Therefore entering Stage 3 by October 1998, the transition through Stage 3 occurred during the second year, showing full characteristics of a *mature migrating inlet* by May-July 1999. Sediment bypassing was occurring at Ancão Inlet during the second year of its evolution. Only on one occasion, after high-energy SW storm conditions, did Ancão Inlet show Stage PS characteristics (January 1999). The main characteristics and the time that Ancão Inlet spent in each stage are summarised in Table 8.2.

As can be seen from the results, from July 1999 to September 2000, Ancão Inlet was still a *mature migrating inlet*, therefore, in Stage 3. The period from July 1999 to September 2000 is considered a low-energy period. According to several authors (i.e., Morris *et al.*, 2001; Williams *et al.*, 2003, see Chapter 6), most of the migration of Ancão Inlet occurs during high-energy conditions. Therefore, due to the general low-energy conditions (Figure 8.2), inlet migration during this period was small (Figure 8.5) and Ancão Inlet width (Figure 8.3a) and Ω (Figure 8.3b) had maximum values in March 2000. The highest-energy '*Levante*' event occurred in April 2000 and probably induced the decrease of inlet width and Ω that was observed in the following months (June and September 2000). The volumetric evolution of the main morphologic areas also reflects the low-energy conditions.

From September 2000 to April 2001 the study area was under high-energy SW conditions that included some major SW events (Figure 8.2a), while the frequency of occurrence of '*Levante*' conditions was low, with just one '*Levante*' high-energy event in February 2001 (Figure 8.2b). Therefore, in January and April

2001, Ancão Inlet was showing Stage PS characteristics. The high-energy conditions increased the longshore sediment transport and induced sediment transport towards the inner parts of the inlet and rapid eastward migration of the inlet channel. The inlet width increased by January 2001 as a consequence of the SW storms and strongly reduced by April 2001, due to the growth of the easternmost spit of Ancão Peninsula (see Appendix A). The rapid growth of the peninsula and also of the ebb delta (see Figure 8.4b) can be related to the high rates of eastward sediment transport associated with the SW storms. Simultaneously, the infilling of the channel area produced a decrease of the Ω that reached values similar to those at the opening (Figure 8.3b).

July 2001 (Figure A.16) represents a transition from Stage PS back to Stage 3 under calm conditions (Figure 8.2). There is a slight decrease in the volume of the flood delta and some accumulation in the channel and ebb delta (Figure 8.3c and 8.4). Eastward migration occurred but with much lower rates than in the previous months (Figure 8.5); inlet width (Figure 8.3a) and Ω (Figure 8.3b) showed a slight return to its previous values.

Fuzeta Inlet

Fuzeta Inlet was in Stage 1 in July 1999. The first year of its evolution corresponds to the low-energy period mentioned above. The volumetric evolution corresponding to the first year of Fuzeta Inlet was characterised by accumulation on the flood delta and erosion or no significant changes in the rest of the morphological units (see Table 8.1 and Figure 8.3c and 8.4). According to Chapter 6 the transition from Stage 1 to Stage 2 includes inlet channel enlargement until reaching equilibrium values and flood and ebb delta development. Inlet channel width and Ω underwent large increments during the first year. According to the results, Fuzeta Inlet channel reached dynamic equilibrium by July 2000. However, the deltas were not fully developed, the flood delta being more developed than the ebb delta. Therefore, by July 2000 Fuzeta Inlet had not reached the end of Stage 2 but eastward migration had already started.

The second year of evolution of Fuzeta Inlet (July 2000 to August 2001) was characterised by a low-energy summer that had some '*Levante*' events and a very energetic winter with major SW storms (Figure 8.2). The volumetric evolution showed accumulation in all of the main morphological units (Table 8.1) and therefore the entire inlet area was acting as a sediment trap. Both of the

deltas showed accumulation (Figure 8.4) and the inlet channel underwent infilling processes (Figure 8.3c). The major SW storms that occurred during this winter arrived very refracted at Fuzeta Inlet. It seems possible that the incident angle was too large for the waves to pass towards the internal parts of the inlet and change the inlet to Stage PS. However, the energy of the winter events was sufficient to cause some erosion on the ebb delta. The incident SW waves also caused eastward migration and inlet enlargement (Figure 8.3). However, Ω did not show significant variations (Figure 8.3c). After April 2001, the flood delta underwent strong accumulation processes until reaching its maximum volume by August 2001 (Figure 8.4a). The inlet channel underwent small variations until June 2001 and it then underwent infilling processes until August 2001 (Figure 8.3c). The accumulation on the flood delta and the infilling of the channel could be related to the effect of some small '*Levante*' events that pushed the sediments to the inner areas of the inlet. The analysis of the second year of Fuzeta Inlet evolution shows that the ebb delta was already in dynamic equilibrium by October 2000 since only small variations occurred afterwards. The flood delta showed some strong variations after October but since they were related to the high-energy events, the dynamic equilibrium can be accepted for October 2000. Therefore, by October 2000 (15 months after the opening) Fuzeta Inlet reached the end of Stage 2. After that time, Fuzeta Inlet entered Stage 3, thus being considered as a *mature migrating inlet* by April 2001. However, the strong variations in the channel (Figure 8.3) and flood-tidal delta volume (Figure 8.4a) that Fuzeta Inlet underwent after that date, imply that the inlet did not reach a full development as a *mature migrating inlet*. Stage PS was defined as the stage after direct exposure to high-energy conditions. Therefore, Stage PS for Fuzeta Inlet, directly exposed to SE conditions, would be reached after a high-energy SE event. However, Stage PS was never reached by Fuzeta Inlet, probably due to the lack of persistency of the high-energy '*Levante*' conditions. The main characteristics as well as the time that Fuzeta Inlet spent in each evolutionary stage are summarised in Table 8.2.

8.2.2 Evolution according to hydrodynamics

Through the analyses of the evolution it can be seen that there is a strong relationship between inlet evolution and incident wave power and direction. It has been seen that the evolution of Ancão Inlet was different from Fuzeta Inlet. The evolution of Fuzeta Inlet was slower than that of Ancão Inlet, taking a longer time to reach each evolutionary stage (Table 8.2). The main factor determining

the difference in the evolution is related with the inlet position inside the system: while Ancão Inlet is located on the western (high-energy) flank, Fuzeta Inlet is on the eastern (low-energy) flank (see Figure 3.1). The location of the inlet within the system determines not only the exposure to wave action but also some other important factors such as:

(1) The existence of other inlets in a position close to the studied inlets is a key factor not only for the percentage of the total tidal prism that the studied inlet may capture but also for the ebb or flood dominance of the studied inlets.

(2) The backbarrier has tidal channels and creeks that do not have the same hydrodynamic importance, the position of an inlet close to one of the main tidal channels of the backbarrier can be a key factor for tidal inlet efficiency.

(3) The presence of flood deltas in mixed-energy settings is dependent on the amount of open water area in the backbarrier (FitzGerald, 1996), therefore, the position of the inlet inside the system may determine flood delta formation.

(4) The location of an inlet inside the system can also determine the availability of sediments from the littoral drift (important for delta formation).

According to Salles (2001), by the beginning of 1999, the Ria Formosa barrier island system consisted of three hydrodynamically quasi-independent sub-embayments: (1) the western sub-embayment that includes Ancão, Faro-Olhão and Armona inlets; (2) a central sub-embayment including Fuzeta and Tavira inlets; and (3) an eastern sub-embayment with only one inlet, Lacém Inlet. Therefore the hydrodynamics of Faro-Olhão and Armona inlets influence the behaviour of Ancão Inlet, and in the same way, the behaviour of Fuzeta Inlet depends on Tavira Inlet. The same author determined that Ancão Inlet was ebb-dominated and Fuzeta Inlet was flood-dominated. The ebb or flood dominance is related with the rapid formation of a large ebb delta on Ancão Inlet and justifies the slow formation of one on Fuzeta Inlet. However, Ancão's flood delta was also larger than Fuzeta's (Table 8.1). According to FitzGerald (1988) the sand transport into the backbarrier of ebb-dominated inlets occurs primarily during major storm events. On the contrary, flood dominated inlets tend to have sediment constantly transported into the backbarrier area. Ancão's flood delta reached its maximum volume (Figure 8.4a) in the periods that followed the winters with the

most SW wave power (1997-1998 and 2000-2001). Fuzeta's flood delta reached its maximum volume in August 2001 (Figure 8.4a), possibly due to the inland transport of the sediments that arrived in the area due to waves with a high incidence angle during the storms that occurred in the preceding winter. Although Fuzeta's Ω reached equilibrium values by July 2000, the inland sediment transport to the flood delta did not occur until August 2001. Therefore, it seems likely that the sediment supply at Fuzeta Inlet was not sufficient to permit the formation of the flood delta until August 2001. Sediment transport is mainly controlled by wave energy, therefore, the fact of being located on the eastern flank of the system could constrain the availability of sediments for delta construction. Furthermore, Fuzeta Inlet is located immediately downdrift from Faro-Olhão and Armona inlets, the largest inlets in the Ria Formosa (Figure 3.1), that could be acting as sediment traps restraining the amount of sediments that are available to supply Fuzeta Inlet.

Inlet channel evolution also showed differences. While Ancão Inlet channel reached dynamic equilibrium by April 1998 (see Chapter 6), Fuzeta Inlet channel only reached dynamic equilibrium values 12 months after the relocation (Table 8.2). Ancão Inlet channel reached its maximum efficiency by March 2000 (Figure 8.3b), after a period characterised by low-energy SW conditions and high-occurrence of '*Levante*' events (Figure 8.2) where no eastward migration occurred (Figure 8.5). The effects of the major SW events that occurred during the winter 2000-2001 were dramatic for Ancão's inlet channel, inducing infilling processes (Figure 8.3c) and reducing its efficiency by half (Figure 8.3b). Furthermore, the eastward migration of Ancão Inlet during that period reached 1.5 m/day. Fuzeta Inlet channel reached its maximum efficiency by July 2000 (Figure 8.3b). Before that time, the efficiency of Fuzeta Inlet was very low and the inlet was undergoing infilling processes. During that time the eastward migration of Fuzeta Inlet was occurring at a rate of 0.5 m/day. By February 2000, the Fuzeta's efficiency showed some improvement, probably related to the preceding low energy conditions. Between February and July 2000 there were no SW events but the highest energy '*Levante*' event of the study period (April 2000) occurred. It is possible that the '*Levante*' event produced the enlargement of the channel, acting as a catalyst for improving the efficiency of Fuzeta's inlet channel. Therefore, major '*Levante*' events do not seem to affect Fuzeta Inlet in the same way as major SW events affect Ancão Inlet.

Table 8.2: Summary of the main characteristics and evolutionary stages for Ancão and Fuzeta inlets. The time taken by the inlets to reach each evolutionary stage is shown in brackets.

			STAGE 1		STAGE 2	STAGE 3	STAGE PS
	Direct wave exposure	Dominance	Relocation date	Channel equilibrium	Dynamic equilibrium	*mature migrating inlet*	
Ancão	SW	Ebb	Jun-97	Apr-98 (10months)	Jul-98 (12months)	Oct-98 (15months)	Jan-99 Jan-01 Apr-01
Fuzeta	SE	Flood	Jul-99	Jul-00 (12months)	Oct-00 (15months)	Apr-01 (21months)	N.E.*

*N.E.- No evidence during the study period.

8.2.3 Relocation assessment

Except for the period related with the major SW events of the winter 2000-2001, Ancão Inlet was more efficient than Fuzeta Inlet (Figure 8.3b). Furthermore, as can be seen in Table 8.2, it reached Stage 2 in a shorter period and, 15 months after its opening, it had already reached the beginning of Stage 3 (see Chapter 6). It seems obvious that Ancão Inlet captured a larger percentage of the Ω of its embayment than the one that Fuzeta Inlet captured in the central embayment of the system, or that the western sub-embayment has a larger Ω than the central one. In Chapter 5 an extensive analysis of the historical evolution (from ∼1945 to 1996) of both Ancão and Fuzeta inlets is presented. The historical positions of Ancão and Fuzeta inlets are plotted in Figure 8.6 together with the positions measured for the relocated inlets during the study period.

Ancão Inlet was relocated in a location were it had never existed during the period ∼1945 to 1996 (Figure 8.6). It was opened some 1,000 m westwards of the 'natural opening location' (*NOL*) found for that period, where the inlet had opened naturally twice in the last 50 years (see Chapter 5). The Ancão Peninsula is a popular area where many houses were built during the last 40-50 years, some of them without license from the council. Therefore, in order to preserve the safety of the houses and expecting eastward migration, the relocation place was chosen directly to the east of the easternmost houses of the Peninsula. In order to prevent future problems, the authorities of the Ria Formosa Natural Park expropriated these houses (that were illegal). During the readjustment period, when the inlet migrated to the west, several electricity poles and two of the houses were destroyed by the inlet. The eastward migration started afterwards with high migration rates. At present, Ancão Inlet has not yet reached the *NOL* and it seems that the Ω has decreased considerably. The existence of an internal current gyre on the western margin of Ancão Inlet (see Chapter 7) has caused the destruction of two more houses causing severe damage to a third one. The *NOL* corresponds to an area of Barreta Island that, at present, is a low and narrow sector that is subject to overwashing processes (see overwashed area in Figure 3.5). It is expected that as soon as the inlet reaches the *NOL* the eastward migration will occur at very high rates due to the fragility of that sector.

Fuzeta Inlet was relocated only 800 m from its position in 1996. The relocation position was again chosen in order to preserve the safety of the houses that exist on that part of Armona Island. Therefore it was opened eastward of the easternmost

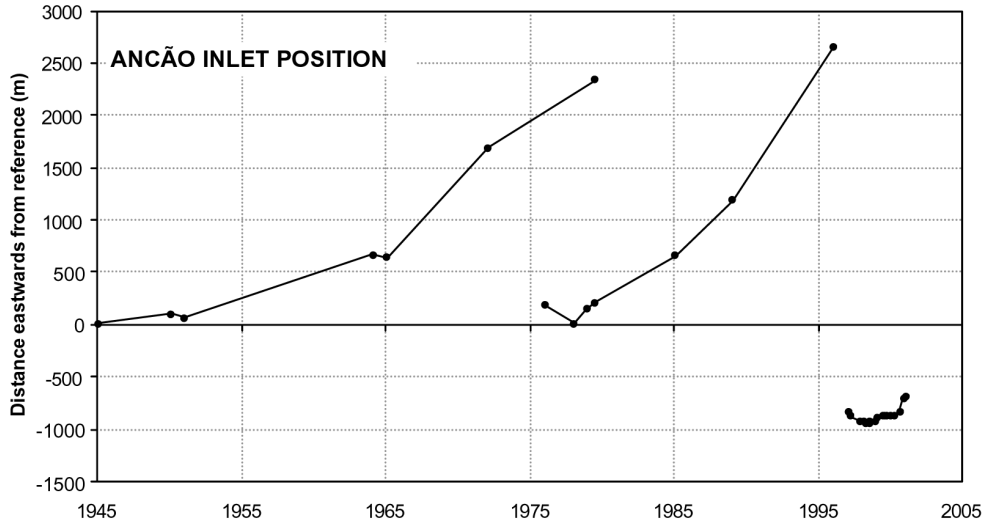

(a)

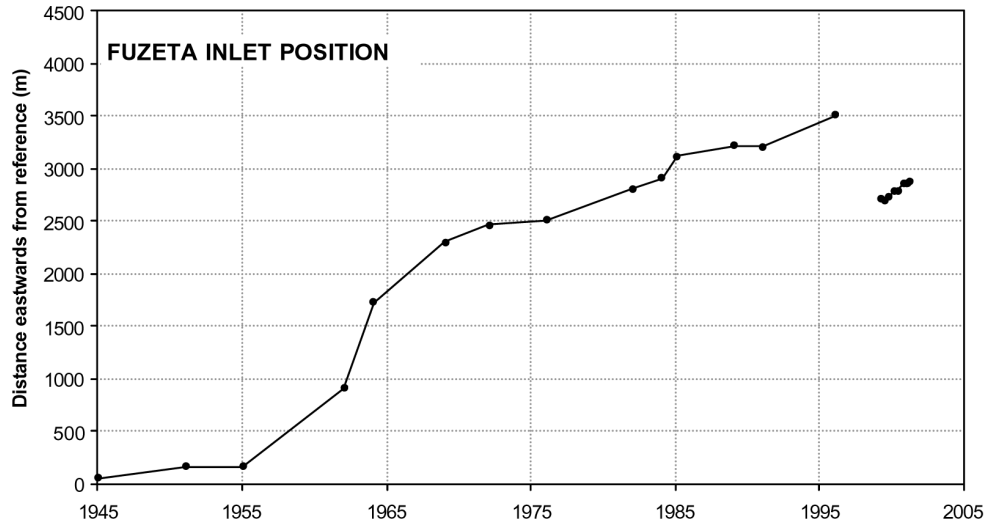

(b)

Figure 8.6: Inlet positions and migration of the natural Ancão and Fuzeta inlets for the period ∼1945-1996 compared with the positions and migration measured for the relocated inlets. Positions are relative to an arbitrary reference point that is located 10 m to the west of the westernmost position that was registered for the natural inlets between ∼1945 and 1996.

house of Fuzeta Island while leaving a safety distance in order to avoid destruction of houses in the case of a westward migration. The historical migration path that Fuzeta Inlet showed between ∼1945 and 1996 was some 3,500 m in length (see Chapter 5); and there is some evidence (Chapter 5) that indicate that the opening

of Fuzeta Inlet occurred a little before ∼1945 (Esaguy, 1985). Therefore the *NOL* is close to the position where Fuzeta Inlet was in ∼1945. In 1996 Fuzeta Inlet was showing very low efficiency, the channel was meandering and undergoing infilling processes. According to FitzGerald (1996) as the inlet migrates it elongates the channel connecting the inlet to the bay, thus increasing the friction and reducing the inlet efficiency. Therefore, it seems likely that the displacement of 800 m in the position of the inlet was not enough to attenuate the effect of the friction factors and to increase the efficiency of the inlet. Fuzeta Inlet was relocated in a position that corresponds to the historical position in about 1980 (about 2,700 m east from the *NOL*); therefore, the sediment composing the downdrift margin of the inlet was only 20 years old. Thus rapid enlargement and migration occurred without improving the efficiency of the inlet.

The location where an inlet is relocated seems to be a key factor for the success of the relocation. In the case of Ancão Inlet the relocation action can be considered as successful since the inlet reached dynamic equilibrium and started its eastward migration showing good efficiency. The Ancão Inlet relocation position is close to some of the main tidal channels of the sub-embayment. Therefore, it seems possible that the high efficiency of the inlet, even in a position that is 1,000 m away from its *NOL*, could have been enhanced due to its proximity to these tidal channels. However, some of the property and material loses could have been avoided if the inlet had been relocated in a location closer to its *NOL*. In the case of Fuzeta Inlet, the relocation in a place close to its *NOL* was completely impossible because the inlet historical migration path is presently occupied by houses. Most of these houses were illegally built during the second half of the twentieth century, however, due to several factors that are beyond the scope of this thesis the dismantling of the houses has become a difficult issue for the authorities. The case of Fuzeta Inlet relocation cannot yet be considered as a successful relocation since the inlet is presently showing the same problems (channel meandering and infilling) that caused its relocation in 1999. It seems possible that the chances for the relocation to work would have been better if the new inlet was opened in a more western location, therefore, requiring the difficult resolution of dismantling the existing houses. However, the present configuration of the backbarrier at the *NOL* shows the presence of sandy islands and sand banks that restricts the tidal currents in that area. Therefore it seems that the relocation of Fuzeta Inlet in a position close to its *NOL* would not be as successful as expected due to the lack of Ω to be captured by the inlet, unless extensive

dredging of the backbarrier area is performed.

Using the experience gained from these inlet relocations in Southern Portugal, a synthesis of recommended procedures previous to inlet relocation was made (Figure 8.7). This diagram is meant only as a theoretical guide for coastal managers or coastal engineers in the considerations prior to relocation: to decide if inlet relocation has probabilities of being successful for a specific inlet. Once inlet relocation is chosen as a real option for coastal management, the legal procedures, including environmental impact studies, should be carried out before taking the final decision.

8.3 Conclusions

It was shown in this chapter that inlet relocation can be considered as a powerful tool of soft protection for coastal management. Inlet relocation is a coastal engineering action that implies working with nature and not against it, therefore, when properly done it represents a *natural* way of either enhancing water exchange through the inlet, or of protecting coastal populations threatened by the tidal inlet. However, it is a technique that has not been widely used. Therefore, the monitoring of relocated inlets is a key element for gaining a better understanding of the processes that determine the success or failure of a relocation action as well as to determine unexpected hazards that the relocation may imply.

Two sets of monitoring data related to inlet relocation, four years for Ancão Inlet and two years for Fuzeta Inlet, were presented in this thesis. Some of the relevance of the data comes from the fact that these were some of the first relocation actions performed in the world, where the new inlet was left in a natural state, without any stabilising structures; after Tubbs Inlet (1969/70) and Captain Sam's Inlet (1983 and 1996). The two relocation actions performed in Southern Portugal had different degrees of success. According to the data presented, the position chosen for the inlet relocation seems to be the key factor for determining the success or failure of the relocation action.

Using the experience gained from the results of the monitoring of the relocated inlets, a synthesis of the procedures previous to inlet relocation was made (and is summarised in Figure 8.7):

- A study of the present hydrodynamic conditions of the system is needed. If the present hydrodynamic conditions are comparable to the historical ones,

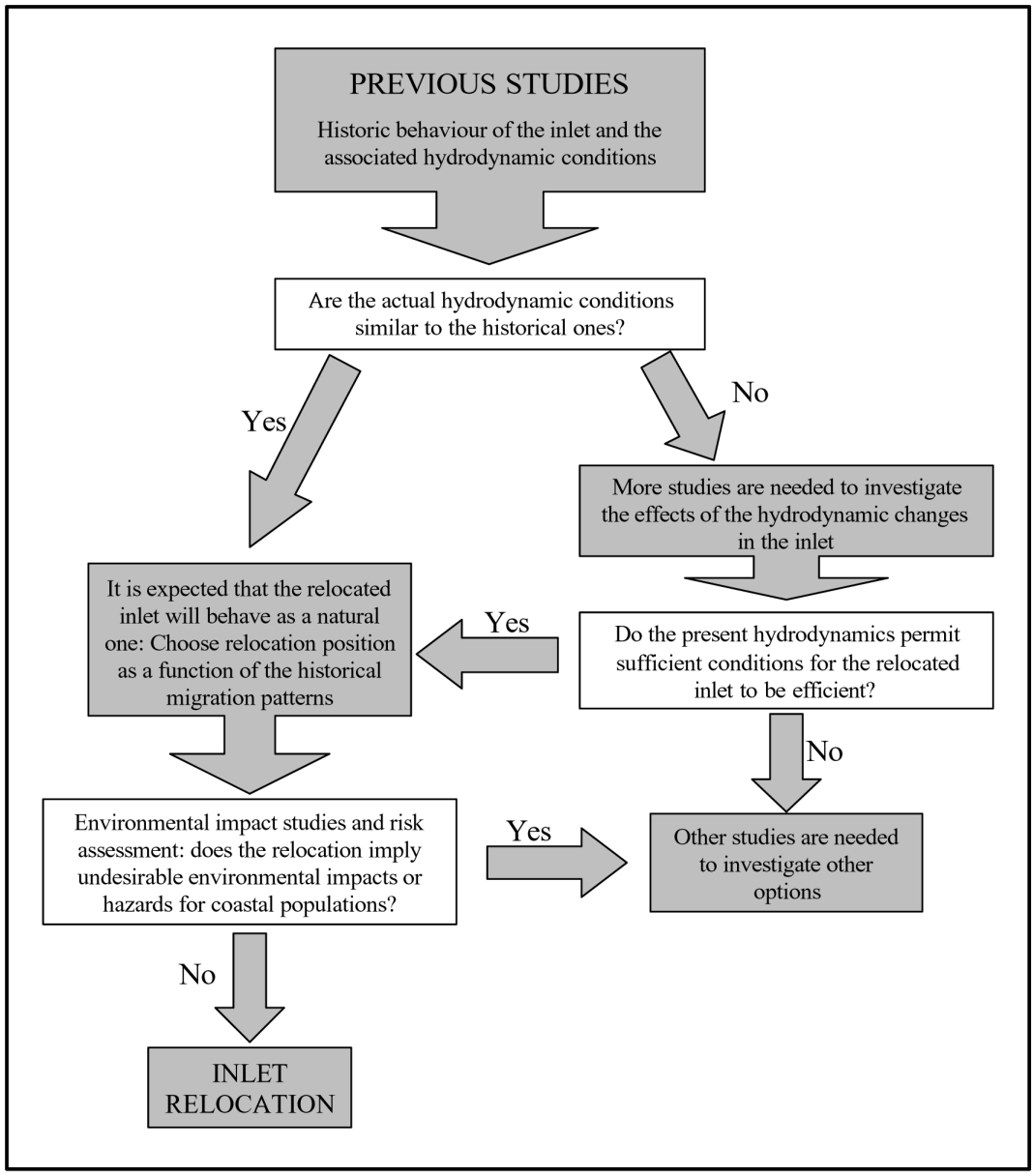

Figure 8.7: Schematic representation of the recommended theoretical procedures before an inlet relocation.

then the relocated inlet could be expected to behave as the previous natural one did. Previous studies of the historical behaviour of the natural inlet are, therefore, needed. If the present hydrodynamic conditions are not similar to the historical ones, then more hydrodynamic studies are needed in order to determine the viability of an inlet in the desired relocation position.

- If the relocation action is hydrodynamically possible, then a relocation position (where the former inlet was efficient) should be carefully chosen. Main

factors to be taken into account are: (1) The historical migration paths, and typical inlet width, of the natural inlet; (2) The hydrodynamics of the backbarrier, i.e., proximity to main tidal channels; (3) Morphology of the backbarrier, i.e., availability of space for flood-tidal delta development; (4) Proximity to adjacent tidal inlets, for multi-inlet barrier island systems only.

- Once the relocation position is chosen, environmental impact studies, taking into account hazards for the ecosystems affected by the relocation action should be made. If the environmental impact studies are not favourable, then other positions for inlet relocation or other coastal management options should be studied.

- If the environmental impact studies are favourable for inlet relocation, then the relocation can be made. A monitoring program of the relocated inlet including quantitative (surveys) data is strongly recommended in order to avoid unexpected hazards and to determine the degree of success of the relocation action.

Chapter 9

General Conclusions

"One never notices what has been done; one can only see what remains to be done."

Marie Curie, *"Letter to her brother, 1894."*

The main conclusions obtained within this thesis have been presented in the previous chapters. A set of general conclusions are presented in this chapter, mainly focusing on the tidal inlet processes where the knowledge of these processes was improved or where new results have been analysed. It also includes recommendations for further research into tidal inlets in order to fill the gaps that still exist in the knowledge of these complex systems.

The study of the historical evolution of the natural inlets in the Ria Formosa barrier island system showed that there are two typical migration patterns, one for high-energy conditions, best represented by Ancão Inlet, and one for low-energy conditions, best represented by Lacém Inlet. It is believed that these migration patterns could be applied to other migrating tidal inlets in other barrier island systems.

The effects caused by the opening and stabilisation of two inlets (Faro-Olhão and Tavira inlets) on the natural inlets of the system were analysed. Although the results presented in this thesis indicate that, aside from some decrease in inlet efficiency (i.e., Armona Inlet), the effects of the opening and stabilisation of the two inlets were not very significant over the analysed time-scale. Thus, it is believed that the system has not yet fully adapted to the new hydrodynamic conditions. Moreover, the periods in between the data-sets used did not permit, on occasions, the separation of the effects of a major storm from those directly related to the artificial opening and stabilisation, the effects of the major storms being more obvious. A decrease in the time between data-sets would greatly help to distinguish storm effects from the consequences of engineering interventions. Other factors, such as ebb/flood dominance can also affect inlet migration patterns. The study of these factors in the future would help the understanding of inlet migration patterns.

The short term studies showed that fluorescent tracers (FT) could be applied to areas far more complicated than straight beaches. It was shown that the definition of the irregular sampling grid was a very important factor for the application of fluorescent tracers in a non-straight area. Moreover, the definition of morphologically defined sectors, and the study and analysis of the FT exchanges between

them, was a key factor to overcome the complications arising from the existence of bi-directional currents. Therefore, the sediment transport patterns were determined and a semi-quantitative conceptual model was defined. Three tidal stages, associated with distinctive sediment transport patterns, were found to occur at the inlet margin during each tidal cycle. Two current gyres, one internal and anticlockwise, and one external and clockwise, were found to occur at different tidal stages. The semi-quantitative conceptual model developed explains the sediment transport paths and magnitudes that a known mass of sediment follows after its arrival at the swash platform. In terms of inlet processes, it includes the sediment accumulation on the swash platform that reflects the eastward growth of Ancão Peninsula, as well as the erosion on the internal beaches adjacent to the inlet.

The scientific contribution of the short term studies of sediment transport derives not only from the results presented, but also from the methodology developed for the analyses that makes possible the application of FT to tidal inlet studies, as well as to other areas influenced by bi-directional currents. However, more sediment transport studies at this and other inlets are needed to fully understand sediment transport pathways and magnitudes at tidal inlets. These studies should include tracer studies in other important areas of inlet systems, such as both of the deltas and the downdrift beach, as well as the study of the sediment transport pathways under high-energy conditions. The integration of these results into the transport model developed would greatly improve its accuracy and applicability.

Inlet relocation was addressed in two chapters of this thesis. Through the detailed analysis of the first two years of the evolution of Ancão Inlet, a conceptual model of the evolution of a relocated inlet was defined. This model has 4 stages, Stage 1 to Stage 3 explain the evolution of the inlet from its opening until it can be considered a *mature migrating inlet*, the fourth stage, Stage PS is related to post-storm conditions. The evolution stages in the model were determined on the basis of volumetric and morphological changes. The achievement of dynamic equilibrium, first by the inlet channel and then by the inlet deltas, together with the start of the migration, mark the transition from one evolution stage to the next. Moreover, Stage PS explains the morphologic and volumetric changes that the inlet undergoes after a storm. The conceptual model seems to be applicable to other relocated inlets with similar characteristics (i.e., Captain Sam's Inlet, South Carolina, USA). Future work will focus on applying the conceptual evolutionary model to other relocated inlets of similar characteristics as well as enhancing and

refining the model presented herein by introducing control parameters of inlet development such as tidal range, tidal prism and wave climate.

An analysis and evaluation of the two relocation actions performed in the Ria Formosa barrier island system (Ancão and Fuzeta inlets) was also made. A detailed analysis of the evolution of the two relocated inlets showed that the conceptual model defined for Ancão Inlet was applicable to Fuzeta Inlet. The relocation of Fuzeta Inlet was not as successful as the one performed at Ancão Inlet, moreover, the time needed for Fuzeta Inlet to reach each of the stages of the conceptual model was longer than the time needed for Ancão Inlet. Using the knowledge obtained from these relocations, a schematic containing the theoretical procedures to consider prior to performing an inlet relocation was defined. However, there are still several aspects of inlet relocation that need further studies. For example the ebb or flood dominance of an inlet seems to be an important factor for predicting the degree of success of a hypothetical relocation. The future monitoring of relocated inlets will provide essential information for the application of this relatively new soft protection technique in coastal engineering.

In summary, the scientific contribution of this thesis can be divided in two separated but not independent parts:

- In terms of local knowledge, it represents an in-depth study of the historic evolution and present behaviour of the tidal inlets of the Ria Formosa. Results from this thesis are believed to be useful not only for the coastal management actions to be made by the Ria Formosa Natural Park that includes these inlets, but also for the future planning of coastal engineering interventions.

- From a global point of view, there are two areas of knowledge to which this thesis represents a direct contribution: (1) Fluorescent tracers were used in a non-straight area affected by bi-directional currents. As a result, the sediment transport paths were semi-quantitatively determined for the updrift margin of an inlet. (2) The Portuguese relocations, Ancão Inlet (in June 1997) and Fuzeta Inlet (in July 1999), represent respectively the third and the fourth tidal inlet relocations found in the literature. Therefore, the studies of their evolution after the relocation represent, together with Tubbs Inlet (North Carolina, USA), Captain Sam's Inlet (South Carolina, USA) and Mason Inlet (North Carolina, USA), a reference for future relocation

interventions to be planned and performed in other barrier island systems of the world.

Chapter 10

References

Abecasis, F., Matias, M.F., Reis de Carvalho, J.J., Vera-Cruz, D., 1962. *Methods of Determining Sand and Silt Movement along the Coast, in Estuaries and in Maritime Rivers*. Laboratório Nacional de Engenharia Civil. Technical paper n. 186. Ministério de Obras Públicas, lisboa, Portugal, 25pp.

Allen, J.R., 1988. Nearshore sediment transport. *Geography Review*, 78(2), 148-157.

Andrade, C. F., 1990. *O Ambiente Barreira da Ria Formosa, Algarve-Portugal*. PhD Thesis, University Lisboa. 627 pp. (in Portuguese).

Andrade, C., Barata, A., Teles, M., 1998. An analysis of the vulnerability to overwash of the Ria Formosa barrier island system (Portugal). Using a simple multi-attribute technique (SMART) approach. *Proceedings of Littoral98 Conference* (Barcelona, Spain), 511-519.

Aubrey, D.G., 1986. Hydrodnamic controls on sediment transport in well-mixed bays and estuaries. In: J. van de Kreeke, Ed.: *Physics of Shallow Estuaries and Bays*. Coastal and Estuarine Studies, 16, 245-258.

Aubrey, D.G., McSherry, T.R., Eliet, P.P., 1993. Effects of multiple inlet morphology on tidal exhange: Waquoit Bay, Massachusetts. In: Aubrey, D.G. and Giese, G.S., Editors: *Formation and Evolution of Multiple Tidal Inlets*. Coastal and Estuarine Studies, 44, 213-235.

Bakker, W.T., de Vriend, H.J., 1995. Resonance and morphological stability of tidal basins. *Marine Geology*, 126, 5-18.

Balouin, Y., Howa, H., Michel, D., 2001. Swash platform morphology in the ebb-tidal delta of the Barra Nova Inlet, South-Portugal. *Journal of Coastal Research*, 17(4), 784-791.

Battjes, J.A., 1974. Surf similarity. *Proceedings Conference Coastal Engineering74*, 466-480.

Bettencourt, P., 1994. *Les Environnements Sedimentaires de la Côte Sotavento (Algarve, Sud Portugal) et leur Évolution Holocéne et Actuelle*, University Bordeaux I, unpublished. (in French).

Blott, S.J., Pye, K., 2001. Gradistat: a grain size distribution and statistics

package for the analysis of unconsolidated sediments. *Earth Surface Processes and Landforms*, 26, 1237-1248.

Broders, S. (2002). Masons Inlet relocation project completed. *The Seahawk. UNCW Student Newspaper*. Available at `www.surfrider.org/capefear/beachrenourishment_Masons_Inlet.htm`.

Brown, E.I., 1928. Inlets on sandy coasts. *Proceedings, American Society of Civil Engineers*, Vol. LIV, 505-553.

Bruun, P., Gerritsen, F., 1959. Natural bypassing of sand at coastal inlets. *Journal of the Waterways and Harbors Division*, ASCE, 85, 401-412.

Buonaiuto, F.S., Kraus, N.C., 2003. Limiting slopes and depths at ebb-tidal shoals. *Coastal Engineering*, 48, 51-65.

C.E.R.C.,1984. *Shore Protection Manual*. 4th edition. Coastal engineering research unit. Department of the Army Washington D.C., 354 pp.

Cialone, M.A., Seabergh, W.C., Watson, K.D., 1999. Flood shoal response to inlet modifications at Barnegat Inlet, New Jersey. *Proceedings Coastal Sediments '99 Conference (New York, U.S.A., ASCE)*, 1434-1449.

Ciavola, P., 1999. *Sediment Transport Processes on Reflective Beaches: Field Experiments in the Algarve.* PhD Thesis, University Algarve, 164 pp.

Ciavola, P., Taborda, R., Ferreira, Ó., Dias, J.A., 1997a. Field measurements of longshore sand transport and control processes on a steep meso-tidal beach in Portugal. *Journal of Coastal Research*, 13(4), 1119-1129.

Ciavola, P., Taborda, R., Ferreira, Ó., Dias, J.A., 1997b. Field observations of sand-mixing depths on steep beaches. *Marine Geology*, 141, 147-156.

Ciavola, P., Dias, N., Ferreira, Ó., Taborda, R., Dias, J.M.A., 1998. Fluorescent sands for measurements of longshore transport rates: a case study from Praia de Faro in southern Portugal. *Geo-Marine Letters*, 18, 49-57.

Ciavola, P., Vila, A., Morris, B., Davidson, M., Ferreira, Ó., Dias, J.M.A., 2000a. Wave-current interaction in the western part of the New Ancão Inlet, Algarve. *Abstracts Volume of 3rd Symposium on the Iberian Atlantic Continental Margin*

(Faro, Portugal), 143-144.

Ciavola, P., Falati, S., Calderoni, G., Tessari, U., 2000b. RUNTI: a lightweight benthic lander for the assessment of sediment transport in lagoon environments. *Proceedings of Oceanology International 2000*, Brighton, UK, Spearhead Ltd (CD-ROM), 451-460.

Cleary, W.J., 2002. Variations in inlet behaviour and shoreface san resources: factors controllling management decisions, Figure Eight Island, NC, USA. *Proceedings of International Coastal Symposium, 25th - 29th March 2002*, Templepatrick, Northern Ireland. *Journal of Coastal Research*, SI(36), 148-163.

Cleary W.J., FitzGerald, D.M., 2003. Tidal inlet response to natural sedimentation processes and dredging-induced tidal prism changes: Mason Inlet, North Carolina. *Journal of Coastal Research*. (in press).

Cleary, W.J., Jackson, C.W., Jarrett, J.T., Sault, M., Welsh, J.M., 2003. Inlet-induced shoreline changes: Bogue and New River Inlets, North Carolina. *Proceedings of Coastal Sediments03*, Sand Key, Florida, USA.

CSE, 1995. *Relocation of Captain Sams Inlet and Beach Restoration Plan. Seabrook Island, South Carolina.* Coastal Science & Engineering Inc. Technical Report CSE-738R. 153 pp.

CSE, 2001. *Seabrook Island, South Carolina. Captain Sams Inlet Relocation Project. Survey Report no.5.* Coastal Science & Engineering, Inc. Technical Report CSE-2056R. 40 pp.

Collins, M.B., Simwell, S.J., Gao, S.S., Powell, H., Hewitson, C., Taylor, J.A., 1995. Water and sediment movement in the vicinity of linear sandbanks: the Norfolk Banks, southern North Sea. *Marine Geology*, 123, 125-142.

Costa, C.L., 1994. *Final Report of Sub-Project A. Wind Wave Climatology of the Portuguese Coast.* Report PO-WAVES 6/94-A. IH/LNEC, 80 pp.

Costa, M., 1994. Agitação marítima na costa portuguesa. *Anais do Instituto Hidrográfico*, 13, 35-40. (in Portuguese).

Costa, M., Silva, R., Vitorino, J., 2002. Contribuição para o estudo do clima de agitação marítima na costa Portuguesa. *2as Jornadas Portuguesas de*

Engenharia Costeira e Portuária, Sines, Out. 2001. (in Portuguese).

Cunha, F.R., 1957. *O Clima do Algarve*. Relatório final do curso de engenheiro agrónomo. Universidade Técnica de Lisboa. Instituto Superior de Agronomia, Lisboa. 588pp. (in Portuguese)

Cunha, F.R., 1985. *O meio Físico da Ria Formosa. Aspectos Climáticos*. Cooperação Oceanográfica Luso/Francesa. Semin'ario "Sistemas Lagunares. Ria Formosa", May 1985, 16pp. (in Portuguese)

Davies, J.L., 1964. A morphogenic approach to world shorelines. *Zeits Geomorphol.*, 8, 127-142.

Davis Jr., R.A., 1994. *The Evolving Coast*. Scientific American, New York, 231pp.

Davis Jr., R.A., 1996. *Coasts*. Prentice-Hall, New Jersey, 274pp.

Davis Jr., R.A., Hayes, M.O., 1984. What is a wave-dominated coast? Hydrodynamics and sedimentation in wave-dominated coastal environments, Greenwood, B., Davis Jr., R.A., (Eds.). *Marine Geology*, 60, 313-329.

Dean, R.G., 1999. *Inlet Hydraulics and Sedimentary Considerations.* Part of a Short Course on Tidal Inlets. Coastal Sediments'99, 108pp.

Dias, J.M.A., 1988. Aspectos geológicos do litoral Algarvio. *Geonovas* (Lisboa), 10, 113-128. (in Portuguese).

Dias, J.M.A., Ferreira, Ó, Luis, J.F., Matias, A., Teixeira, S., Vila-Concejo, A., 1998. *Relatório de Monitorização da Barra Nova do Ancão*. CIACOMAR Technical Report, 29pp. (in Portuguese)

Dias, J.A., Ferreira, Ó., Sá-Pires, C., Vila-Concejo, A., 2000. *Relatório de Monitorização da Barra Nova da Fuzeta (Dezembro de 1999 a Agosto de 2000).* CIACOMAR Technical Report n. 11/00, 50pp. (in Portuguese)

Dias, J.A., Ferreira, Ó., Matias, A., Vila-Concejo, A., Sá-Pires, C., 2003. Evaluation of soft protection techniques in barrier islands by monitoring programs: case studies from Ria Formosa (Algarve-Portugal). *Journal of Coastal Research*, SI(35), (in press).

Dyer, K.R. and Huntley, D.A., 1999. The origin, classification and modelling of

sand banks and ridges. *Continental Shelf Research*, 19, 1285-1330.

Erickson, K.M., Kraus, N.C., Carr, E.E., 2003. Circulation change and ebb shoal development following relocation of Mason Inlet, North Carolina. *Proceedings of Coastal Sediments03*, Sand Key, Florida, USA.

Esaguy, A.S., 1984. *Ria de Faro, Barra da Armona. Evolução 1873-1983.* Direcção Geral de Portos Internal Report, 5 pp. (in Portuguese).

Esaguy, A.S., 1985. *Ria de Faro, Barra da Fuseta. Evolução 1944-1984.* Direcção Geral de Portos Internal Report, 11 pp. (in Portuguese).

Esaguy, A.S., 1986a. *Ria de Faro, Ilha do Ancão. Evolução 1950-1985.* Direcção Geral de Portos Internal Report, 7 pp. (in Portuguese).

Esaguy, A.S., 1986b. *Ria de Faro, Ilha de Tavira. Evolução 1950-1985.* Direcção Geral de Portos Internal Report, 8 pp. (in Portuguese).

Esaguy, A.S., 1987. *Ria de Faro, Barra de Tavira. Evolução.* Direcção Geral de Portos Internal Report, 13 pp. (in Portuguese).

Escoffier, F.F., 1940. The stability of tidal inlets. *Shore and Beach*, 8(4), 114-115.

Faria, J.M.R., Godinho, S., Almeida, M.J.R., Machado, M.S., 1981. *Estudo Hidroclimatológico da Região do Algarve.* O Clima de Portugal, Fasc. XXVII. Instituto Nacional de Meteorologia e Geofísica, 155pp. (in Portuguese)

Ferreira, Ó., Fachin, S., Coli, A., Taborda, R., Dias, J.M.A., Lontra, G., 2002. Study of a harbour infilling using sand tracer experiments. *Proceedings International Coastal Symposium*, 25th - 29th March 2002, Templepatrick, Northern Ireland. *Journal of Coastal Research*, SI(36), 283-289.

FitzGerald, D.M., 1982. Sediment bypassing at mixed energy tidal inlets. *Proceedings of Coastal Engineering Conference*, Cape Town, South Africa, 1094-1118.

FitzGerald, D.M., 1988. Shoreline erosional-depositional processes associated with tidal inlets. In: Hydrodynamics and Sediment Dynamics of Tidal Inlets. *Lecture Notes on Coastal and Estuarine Studies*, 29, 186-225.

FitzGerald, D.M., 1996. Geomorphic variability and morphologic and sedimentologic controls on tidal inlets. *Journal of Coastal Research*, SI(23), 47-71.

FitzGerald, D.M., Penland, S., Nummedal, D., 1984. Control of barrier island shape by inlet sediment bypassing: East Frisian Islands, West Germany. Greenwood, B., Davis Jr., R.A., (Eds.). *Marine Geology*, 60, 355-376.

FitzGerald, D.M., Buynevich, I.V., Fenster, M.S., McKinlay, P.A., 2000. Sand dynamics at the mouth of a rock-bound, tide-dominated estuary. *Sedimentary Geology*, 131, 25-49.

FitzGerald, D.M., Kraus, N.C., Hands, E.B., 2001. *Natural Mechanisms of Sediment Bypassing at Tidal Inlets.* ERDC/CHL CHETN-IV-30, U.S. Army Engineer Research and Development Center, Vicksburg, MS. 10 pp.

Folk, R.L., Ward, W.C., 1957. Brazos River Bar: A study in the significance of grain size parameters. *Journal of Sedimentary Petrology*, 27(1), 3-26.

Forbes, D.L., Solomon, S.M., 1999. Inlet division and coastal instability following tidal prism diversion. *Proceedings Coastal Sediments '99 Conference* (New York, U.S.A., ASCE), 1418-1433.

Galgano, F.A., Leatherman, S.P., 1999. Beach erosion, tidal inlets and politics: The Fire Island story. *Shore and Beach*, 67(2/3), 26-32.

Garcia, T., Ferreira, Ó. Matias, A., Dias, J.M.A., 2002. Recent evolution of Culatra Island (Algarve-Portugal). *Proceedings of Littoral 2002, EUROCOAST/EUCC*, Porto, Portugal, 2, 289-294.

Gaudiano, D.J., Kana, T.W., 2001. Shoal bypassing in mixed energy inlets: Geomorphic variables and empirical predictions for nine South Carolina Inlets. *Journal of Coastal Research*, 17(2), 280-291.

Gerritsen, F., Dunsbergen, D.W., 1998. Morphological-empirical relationships for ebb tidal deltas as a tool in dynamic-empirical modelling. *Proceedings of International Coastal Symposium, 1998*, Royal Palm Beach, Florida. *Journal of Coastal Research*, SI(26), 273-281.

Glaeser, J.D., 1978. Global distribution of barrier islands in terms of tectonical setting. *The Journal of Geology*, 86(3), 283-297.

Granja, H., Froidefrond, J.M., Pera, T., 1984. Processus d'evolution morphosedimentaire de la Ria Formosa (Portugal). *Bulletin Institute Geologique Bassin*

d'Aquitaine, Bordeaux, 36, 37-50. (in French).

Guza, R.T., Inman, D.L., 1975. Edge waves and beach cusps. *Journal of Geophysical Research*, 93, 9302-9314.

Hands, E.B., Shepsis, V., 1999. Cyclic channel movement at the entrance to Willapa Bay, Washington, USA. *Proceedings Coastal Sediments '99 Conference* (New York, U.S.A., ASCE), 1522-1536.

Hayes, M.O., 1975. Morphology of sand accumulations in estuaries. In: Estuarine Research, 2, L.E. Croning Ed., Academic Press, New York, 3-22.

Hayes, M.O., 1979. Barrier island morphology as a function of tidal and wave regime. *In:* Leatherman, S.P., (Ed.), *Barrier Islands: From the Gulf of St. Lawrence to the Gulf of Mexico.* Academic Press, New York, N.Y., 1-27.

Hayes, M. O. 1980. General morphology and sediment patterns in tidal inlets, *Sedimentary Geology*, 26, 139-156.

Hicks, D.M., Hume, T.M., 1997. Determining sand volumes and bathymetric change on an ebb-tidal delta. *Journal of Coastal Research*, 13(2), 407-416.

Hofstede, J.L.A., 1999. Process-response analysis for Hörnum tidal inlet in the German sector of the Wadden Sea. *Quaternary International*, 60, 107-117.

Huang, W., Sun, H., Nnaji, S., Jones, W.K., 2002. Tidal hydrodynamics in a multiple-inlet estuary: Apalachicola Bay, Florida. *Journal of Coastal Research*, 18(4), 674-684.

Hume, T.M., Herdendorf, C.E., 1992. Factors controlling tidal inlet characteristics on low drift coasts. *Journal of Coastal Research*, 8(2), 355-375.

Hume, T.M., Herdendorf, C.E., 1993. On the use of empirical stability relationships for characterising estuaries. *Journal of Coastal Research*, 9(2), 413-422.

Huntley, D.A., Nummedal, D., 1978. Velocity and stress measurements in a tidal inlet.*Proceedings 16th Coastal Engineering Conference* (New York U.S.A.), 1320-1335.

I.H., 1990. *Tabela de marés. Sotavento Algarvio. Barra de Faro-Olhão.* Instituto Hidrográfico.

I.H., 1992. *Tabela de marés. Sotavento Algarvio. Barra de Faro-Olhão.* Instituto Hidrográfico.

I.H., 1993. *Tabela de marés. Sotavento Algarvio. Barra de Faro-Olhão.* Instituto Hidrográfico.

I.H., 1996. *Tabela de marés. Sotavento Algarvio. Barra de Faro-Olhão.* Instituto Hidrográfico.

I.H., 1997. *Tabela de marés. Sotavento Algarvio. Barra de Faro-Olhão.* Instituto Hidrográfico.

I.H., 1998. *Tabela de marés. Sotavento Algarvio. Barra de Faro-Olhão.* Instituto Hidrográfico.

I.H., 1999. *Tabela de marés. Sotavento Algarvio. Barra de Faro-Olhão.* Instituto Hidrográfico.

I.H., 2000. *Tabela de marés. Sotavento Algarvio. Barra de Faro-Olhão.* Instituto Hidrográfico.

I.H., 2001. *Tabela de marés. Sotavento Algarvio. Barra de Faro-Olhão.* Instituto Hidrográfico.

I.M., 1999. *O Clima de Portugal. Normais Climatológicas da Região de 'Alentejo e Algarve', Correspondentes a 1951-1980.* Instituto Nacional de Meteorologia e Geofísica. Fascículo XLIX, Volume 4, 98pp.

Ingle, J.C., 1966. *The Movement of Beach Sand.* Elsevier Publishing, Amsterdam, 221pp.

Isla, F.I., 1999. Coastal lagoons. In Perillo, G.M.E. (ed.): *Geomorphology and Sedimentology of Estuaries. Developments in Sedimentology*, 59, 241-272.

Jaffe, B.E., List, J.H., Sallenger, Jr., A.H., 1997. Massive sediment bypassing on the lower shoreface offshore of a wide tidal inlet - Cat Island Pass, Louisiana. *Marine Geology*, 136, 131-149.

Johnsen, C.D., Cleary, W.J., Freeman, C.W., Sault, M., 1999. Inlet induced shoreline changes, high energy flank of the Cape Fear foreland, SE; NC. *Proceedings Coastal Sediments '99 Conference* (New York, U.S.A., ASCE), 1402-1417.

Johnson, D.W., 1919. *Shore Processes and Shoreline Development.* New York. John Wiley and Sons (Eds.).585 p.

Kamphuis, J.W., Davies, M.H., Nairn, R.B., Sayao, O.J., 1986. Calculation of littoral sand transport rate. *Coastal Engineering*, 10, 1-21.

Kana, T.W., 2003a. *Coastal Erosion and Solutions - A Primer.* Coastal Science and Engineering, Columbia, SC, 23pp.

Kana, T.W., Mason, J.E., 1988. Evolution of an ebb tidal-delta after an inlet relocation. *Lecture Notes on Coastal and Estuarine Studies*, 29, 382-409.

Kana T.W., McKee, P.A., 2003. Relocation of Captain Sams Inlet - 20 years later. *Proceedings of Coastal Sediments03*, Sand Key, Florida, USA.

Kana, T.W., Hayter, E.J., Work, P.A., 1999. Mesoscale sediment transport at southeastern U.S. tidal inlets: conceptual model applicable to mixed energy settings. *Journal of Coastal Research*, 15(2), 303-313.

Komar, P.D., 1977. Selective longshore transport rates of different grain-size fractions within a beach. *Journal of Sedimentary Petrology*, 47, 1444-1453.

Komar, P.D., Inman, D.L., 1970. Longhore sand transport on beaches. *Journal of Geophysical Research*, 75, 5514-5527.

Kraus, N.C., 1985. Field experiments on vertical mixing of sand in the surf zone. *Journal of Sedimentary Petrology*, 55(1), 3-14.

Kraus, N.C., Isobe, M., Igarashi, H., Sasaki, T.O. and Horikawa, K., 1982. Field experiments on longshore sand transport in the surf zone. *Proceedings Conference in Coastal Engineering'82*, Cape Town, South Africa, 969-988.

Kraus, N.C., Zarillo, G.A., Tavolaro, J.F., 2003. Hypothetical relocation of Fire Island Inlet, New York. *Proceedings of Coastal Sediments03*, Sand Key, Florida, USA.

Leatherman, S.P., 1988. *Barrier Island Handbook.* Coastal Publications Series. Laboratory for Coastal Research. The University of Maryland. Mariland. 92pp.

Lessa, G.C., 2000. Morphodynamic controls on tides and tidal currents in two macrotidal shallow estuaries, NE Australia. *Journal of Coastal Research*, 16(4),

976-989.

Machado, M.J.S.S., 1980. *Número Máximo de Dias Seguidos "sem" e "com" Precipitação em Portugal Continental*. O Clima de Portugal. Fasc. XXII. Instituto Nacional de Meteorologia e Geofísica, Lisboa, 20pp. (in Portuguese).

Madsen, O.S., 1987. Use of tracers in sediment transport studies. *Proceedings Coastal Sediments87 Conference*, 424-435.

Marden, T.P., Cleary, W.J., 1999. Barrier morphology and inlet types; low-energy flank of the Cape Fear foreland, NC. *Proceedings Coastal Sediments '99 Conference* (New York, U.S.A., ASCE), 1295-1310.

Mason, J.E., 1986. *Morphologic Evolution of a Relocated Mesotidal Inlet: Captain Sam's Inlet, South Carolina.* Technical Report, Dept. Geol., University South Carolina, Columbia, 149 pp.

Matias, A., 2000. *Estudo Morfosedimentar da Península de Cacela.* Tese de Maestrado Universidade do Algarve. CIACOMAR Technical Report n. 12/00.246pp. (in Portuguese).

Michel, M.D., 1997. *Evolution Morphodynamique d'un Littoral Sableux Situe a l'aval d'une Embochadure Lagunaire.* PhD Thesis, University Bordeaux I. 162 pp, (in French).

Morang, A., 1999. *Shinnecock Inlet, New York, Site Investigation; Report 1, Morphology and Historical Behavior.* Technical Report CHL-98-32, U.S. Army Engineer Waterways Experiment Station, Vicksburg, MS. 94 pp.

Morang, A., Parson, L.E., 2002. Coastal Morphodynamics. In: A. Morang (ed.) *Coastal Engineering Manual, Part III, Coastal Geology, Chapter IV-3*, Engineer Manual 1110-2-1100, U.S. Army Corps of Engineers, Washington, DC, 93pp.

Morris, B.D., Davidson, M.A., Huntley, D.A., 2001. Measurements of the response of a coastal inlet using video monitoring techniques. *Marine Geology*, 175, 251-272.

Morris, B.D., Davidson, M.A., Huntley, D.A., 2003. Estimates of the seasonal morphological evolution of the Barra Nova Inlet using video techniques. *Continental Shelf Research* (in review).

Nummedal, D., Fisher, I.A., 1978. Process-response models for depositional shorelines: the German and the Georgia bights. *Proceedings 16th Coastal Engineering Conference* (New York U.S.A.), 1215-1231.

O'Brien, M.P., 1969. Equilibrium flow areas of inlets on sandy coasts. Journal of Waterways and Harbors Division. *Proceedings of the American Society of Civil Engineers* 95(WW1), 43-52.

O'Brien, M.P., 1971. *A Critical Review of the E.I.Brown Analysis of "Inlets on Sandy Coasts".* University of California, Hydraulic Engineering Laboratory Technical Report HEL-24-10, 10pp.

Oertel G.F., 1972. Sediment transport of estuary entrance shoals and the formation of swash platforms. *Journal of Sedimentary Petrology*, 42(4), 857-863.

Penland, S., 1979. Influence of a jetty system on tidal inlet stability and morphology: Fort George Inlet, Florida. *Proceedings of the Specialty Conference on Coastal Structures 79*, ASCE, Virginia, USA, March 14-16, 665-689.

Pessanha, L.E.V., Pires, H.O., 1981. *Elementos sobre o Clima de Agitação Marítima na Costa Sul do Algarve.* Internal Report, Instituto Nacional de Meteorologia e Geofísica. 66 pp. (in Portuguese).

Pilkey, O.H. and Neal, W.J., 1980. Barrier island hazard mapping. *Oceanus*, 23(4), 38-46.

Pilkey, O.H. and Wright III, H.L., 1988. Seawalls versus beaches. *Journal of Coastal Research*, SI(4), 41-64.

Pilkey, O.H., Neal, W.J., Monteiro, J.H., Dias, J.M.A., 1989. Algarve barrier islands: A noncoastal-plain system in Portugal. *Journal of Coastal Research*, 5(2), 239-261.

Pires, H.O., 1998. *Project INDIA, Preliminary Report on Wave Climate at Faro.* Instituto de Meteorologia, IST, Lisbon, 36 pp.

Pita, C.A.R.M., Carvalho, M.M., 1987. *Agitação Marítima na Costa Portuguesa. Dados de Base. Temporais.* Direcção-Geral de Portos, LNEC, Internal Report, 17 pp. (in Portuguese).

Ramos, L., Dias, J.A., 2000. Overwash vulnerability attenuation in Ria Formosa system through soft interventions. *Abstracts Volume of 3rd Symposium on the Iberian Atlantic Continental Margin* (Faro, Portugal), 361-362. (in Portuguese).

Ranasinghe, R., Pattiaratchi, C., Masselink, G., 1998. Seasonal inlet closure: Governing processes. *Journal of Coastal Research*, SI(26), 32-41.

Ranasinghe, R., Pattiaratchi, C., 1999. The seasonal closure of tidal inlets: Wilson Inlet - a case study. *Coastal Engineering*, 37, 37-56.

Rosati, J.D., Kraus, N.C., 1999. Advances in coastal sediment budget methodology - with emphasis on inlets. *Shore and Beach*, 67(2&3), 56-65.

Salles, P., 2001. *Hydrodynamic Controls on Multiple Tidal Inlet Persistence.* PhD Thesis, Massachusetts Institute of Technology and Woods Hole Oceanographic Institution, 272 pp.

Seabergh, W.C., 2002. Hydrodynamics of tidal inlets. In: Vincent, L. and Demirbilek, Z. (editors), *Coastal Engineering Manual, Part II, Hydrodynamics, Chapter II-6*, Engineer Manual 1110-2-1100, U.S. Army Corps of Engineers, Washington, DC, 79pp.

Smith, N.P., 2001. Seasonal-scale transport patterns in a multi-inlet coastal lagoon. *Estuarine, Coastal and Shelf Science*, 52, 15-28.

Smith, J.B., FitzGerald, D.M., 1994. Sediment transport patterns at the Essex river inlet ebb-tidal delta, Massachusetts, U.S.A. *Journal of Coastal Research*, 10(3), 752-774.

Stauble, D., 1998. *Techniques for Measuring and Analysing Inlet Ebb Shoal Evolution.* Coastal Engineering Technical Note IV-13, U.S. Army Engineer Waterways Experiment Station, Vicksburg, MS. 12 pp.

Van de Kreeke, J., 1985. Stability of tidal inlets - Pass Cavallo, Texas. *Estuarine, Coastal and Shelf Science*, 21, 33-43.

Vila, A., Dias, J.M.A., Ferreira, Ó., Matias, A., 1999. Natural evolution of an artificial inlet. *Proceedings Coastal Sediments '99 Conference* (New York, U.S.A., ASCE), 1478-1488.

Vila-Concejo, A., Dias, J.M.A., Ferreira, Ó., Garcia, T., Matias, A., Morris, B., Sá-Pires, C., 2001. *Evolução das barras do Ancão e da Fuseta: Relatório final.* CIACOMAR Technical Report n.8/01, 106pp. (in Portuguese).

Vila-Concejo, A., Matias, A., Ferreira, Ó., Duarte, C., Dias, J.M.A., 2002. Recent evolution of the natural inlets of a barrier island system in Southern Portugal. *Proceedings of International Coastal Symposium, 25th - 29th March 2002*, Templepatrick, Northern Ireland. *Journal of Coastal Research*, SI(36), 741-752.

Vila-Concejo, A., Ferreira, Ó., Matias, A., Dias, J.M.A., 2003a. The first two years of an inlet: sedimentary dynamics. *Continental Shelf Research* (in press).

Vila-Concejo, A., Ferreira, Ó., Ciavola, P., Taborda, R., Dias, J.M.A., 2003b. Quantitative and qualitative analyses of sediment transport paths: straight beaches, inlets and harbours. *Proceedings of Coastal Sediments'03*, Sand Key, Florida USA.

Vila-Concejo, A., Ferreira, Ó., Ciavola, P., Matias, A., Dias, J.M.A., 2003c. Tracer studies on the updrift margin of a complex inlet system. *Marine Geology* (in review).

Vila-Concejo, A., Ferreira, Ó., Morris, B.D., Matias, A., Dias, J.M.A., 2003d. Lessons from inlet relocation: examples from Southern Portugal. *Coastal Engineering* (in review).

Walton, T. L. Jr. (2002). *Tidal Velocity Asymmetry at Inlets.*, ERDC/CHL CHETN IV-47. U.S. Army Engineer Research and Development Center, Vicksburg, MS. 17pp. Available at: `http://chl.wes.army.mil/library/publications/chetn`.

Walton, T.L., Adams, W.D., 1976. Capacity of inlet outer bars to store sand. *Proceedings of the 15th International Conference on Coastal Engineering*, ASCE, New York, 1919-1937.

Weidman, C.R., Ebert, J.R., 1993. Cyclic spit morphology in a developing inlet system. In: Aubrey, D.G. and Giese, G.S., Editors: *Formation and Evolution of Multiple Tidal Inlets.* Coastal and Estuarine Studies, 44, 186-212.

Weinholtz, M.B., 1964. *Contribuição para o Estudo da Evolução das Flechas de Areia na Costa Sotavento do Algarve.* Separata do Boletim Trimestral de In-

formação do D.G.S.H. 14. (in Portuguese).

White, T.E., 1998. Status of measurement techniques for coastal sediment transport. *Coastal Engineering*, 35, 17-45.

Williams, G.L., Morang, A., Lillycrop, L., 1998. *Shinnecock Inlet, New York, Site Investigation; Report 2, Evaluation of Sand Bypass Options.* Technical Report CHL-98-32, U.S. Army Engineer Waterways Experiment Station, Vic.

Williams, J.J., Arens, B., Aubrey, D., Bell, P., Bizzaro, A., Collins, M., Davidson, M., Dias, J., Ferreira, Ó., Heron, M., Howa, H., Hughes, Z., Huntley, D., Jones, M.T., O'Connor, B., Pan, S., Sarmento, A., Seabra-Santos, F., Shayler, S., Smith, J., Voulgaris, G. 1999. Inlet Dynamics Initiative: Algarve (INDIA). *Proceedings Coastal Sediments '99 Conference* (New York, U.S.A., ASCE), 612-627.

Williams, J.J., O'Connor, B.A.O., Arens, S.M., Abadie, S., Bell, P., Balouin, Y., Van Boxel, J.H., do Carmo, A.J., Davidson, M., Ferreira, Ó, Heron, M., Howa, H., Hughes, Z., Kaczmarec, L.M., Kim, H., Morris, B., Nicholson, J., Pan, S., Salles, P., Silva, A., Smith, J., Soares, C., Vila-Concejo, A., 2003. Tidal inlet function: field evidence and numerical simulation in the INDIA project. *Journal of Coastal Research*, 19(1), 189-211.

`www.coastalhazards.wcu.edu`, 2002. Department of Geosciences, Western Carolina University.

Yasso, W.E., 1965. Fluorescent tracer particle determination of the size-velocity relation for the foreshore sediment transport, Sandy Hook, New Jersey. *Journal of Sedimentary Petrology*, 64, 989-993.

Yasso, W.E., 1966. Formulations and use of fluorescent tracers coatings in sediment transport studies. *Sedimentology*, 6, 287-301.

Zenkovitch, V.P., 1960. Fluorescent substances as tracers for studying the movements of sand on the sea bed. *The Dock and Harbour Authority*, XL, 280-283.

Chapter 11

Supporting Documents

International Peer Reviewed Publications

- Vila, A., Dias, J.M.A, Ferreira, Ó., Matias, A., 1999. Natural Evolution of an Artificial Inlet. *Proceedings of 4th International Conference of Coastal Sediments*, New York 99, 2, 1478-1488.

- Vila-Concejo, A., Matias, A., Ferreira, Ó., Duarte, C., Dias, J.M.A., 2002. Recent evolution of the natural inlets of a barrier island system in Southern Portugal. *Proceedings of International Coastal Symposium, 25th - 29th March 2002*, Templepatrick, Northern Ireland. *Journal of Coastal Research*, SI(36), 741-752.

- Vila-Concejo, A., Ferreira, Ó., Ciavola, P., Taborda, R., Dias, J.M.A., 2003. Qualitative and quantitative analyses of tracer data: straight beaches, inlets and harbours. *Proceedings of Coastal Sediments 2003*.

- Dias, J.M.A., Ferreira, Ó., Matias, A., Vila-Concejo, A., Sá-Pires, C., in press. Evaluation of soft protection techniques in barrier islands by monitoring programs: case studies from Ria Formosa (Algarve-Portugal). *Journal of Coastal Research* (SI).

- Vila-Concejo, A., Ferreira, Ó., Matias, A., Dias, J.M.A., in press. The first two years of an inlet: sedimentary dynamics. *Continental Shelf Research*.

- Vila-Concejo, A., Ferreira, Ó., Ciavola, P., Matias, A., Dias, J.M.A., in review. Tracer studies on the updrift margin of a complex inlet system. *Marine Geology*.

- Vila-Concejo, A., Ferreira, Ó., Morris, B.D., Matias, A., Dias, J.M.A., in review. Lessons from inlet relocation: examples from Southern Portugal. *Coastal Engineering*.

Departmental Technical Reports

- Dias J.M.A., Ferreira, Ó., Luis, J.F., Matias, A., Teixeira, S., Vila-Concejo, A., 1998. *Relatório de Monitorização da barra Nova do Ancão.* 29pp.

- Vila-Concejo, A., Dias, J.M.A., Ferreira, Ó., 1999. *Relatório de Campo campanha AMI1.* CIACOMAR Technical Report 02/99, 20pp.

- Vila-Concejo, A., Alveirinho Dias, J.M.A., Ferreira, Ó., 1999. *Relatório de Campo campanha AMI2.* CIACOMAR Technical Report 03/99, 18pp.

- Vila-Concejo, A., Dias, J.M.A., Ferreira, Ó., 1999. *Relatório de Campo campanha AMI3.* CIACOMAR Technical Report 05/99, 19pp.

- Sá-Pires, C., Ferreira, Ó., Vila, A., 2000. *Campanhas RUI (RunUp do INDIA). Relatório de Campo.* CIACOMAR Technical Report 04/00, 22pp.

- Dias J.M.A., Ferreira, Ó, Sá-Pires, C., Vila, A., 2000. *Evolução da Barra Nova da Fuseta entre Dezembro de 1999 e Novembro de 2000.* CIACOMAR Technical Report 11/00, 50pp.

- Dias J.M.A., Ferreira, Ó., Vila-Concejo, A., Sá-Pires, C., Matias, A., Morris, B., 2001. *Evolução das Barras do Ancãoe da Fuseta: Janeiro a Maio de 2001.* CIACOMAR Technical Report 05/01, 40pp.

- Vila-Concejo, A., Dias J.M.A., Ferreira, Ó., Matias, A., Morris, B., Sá-Pires, C., 2001. *Evolução das Barras do Ancão e da Fuseta: Junho a Setembro de 2001.* CIACOMAR Technical Report 07/01, 29pp.

- Vila-Concejo, A., Dias J.M.A., Ferreira, Ó., Garcia, T., Matias, A., Morris, B., Sá-Pires, C., 2001. *Evolução das Barras do Ancão e da Fuseta durante o ano 2001.* CIACOMAR Technical Report 08/01, 106pp.

Appendix A

Topo-bathymetric Maps

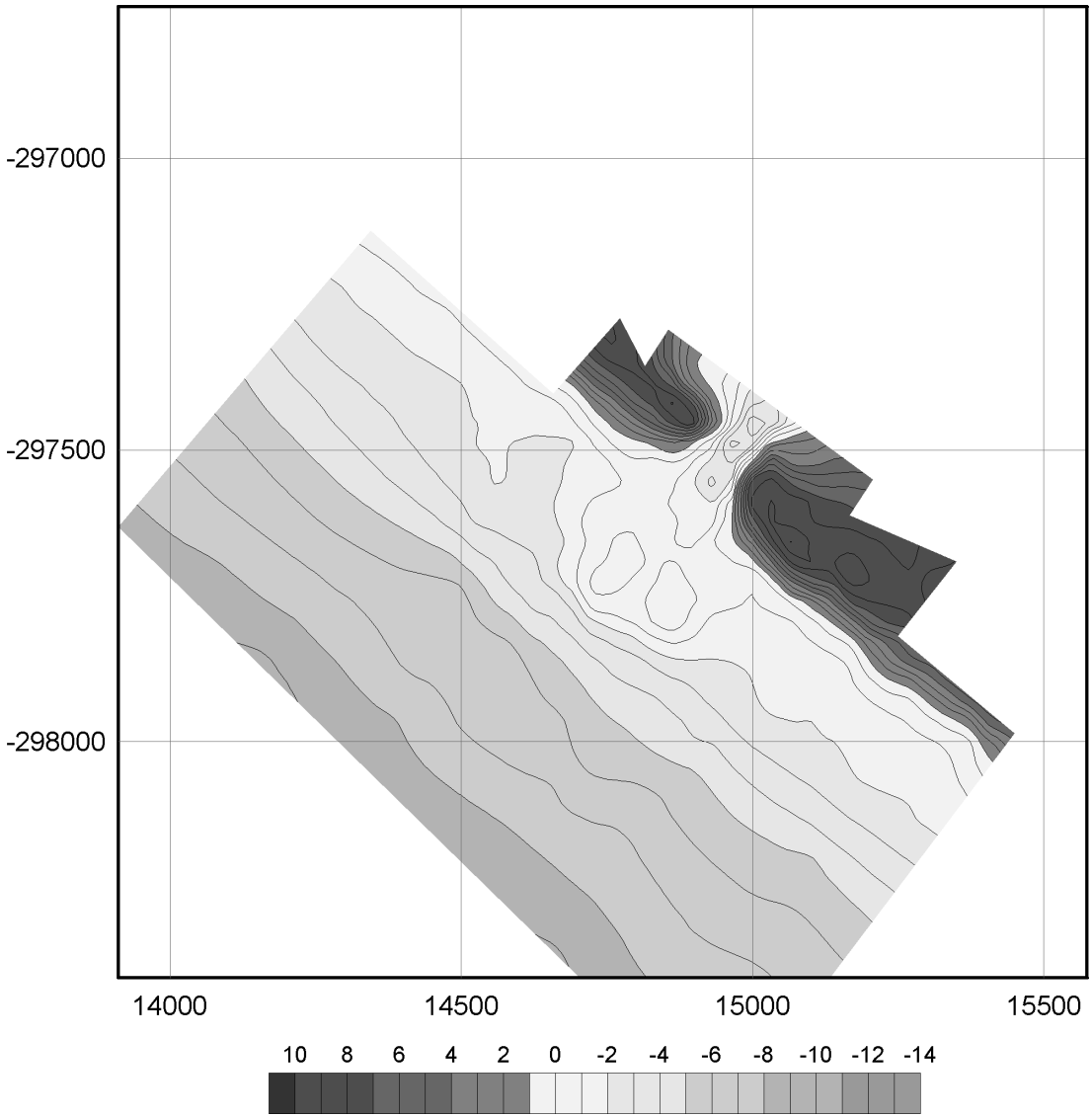

Figure A.1: Topo-bathymetric map of Ancão Inlet in August 1997. Metric coordinates refer to the Portuguese Melriça Grid. Elevation is in metres, relative to Portuguese Hydrographic Zero (Z.H.), defined as 2 m below mean sea level (MSL).

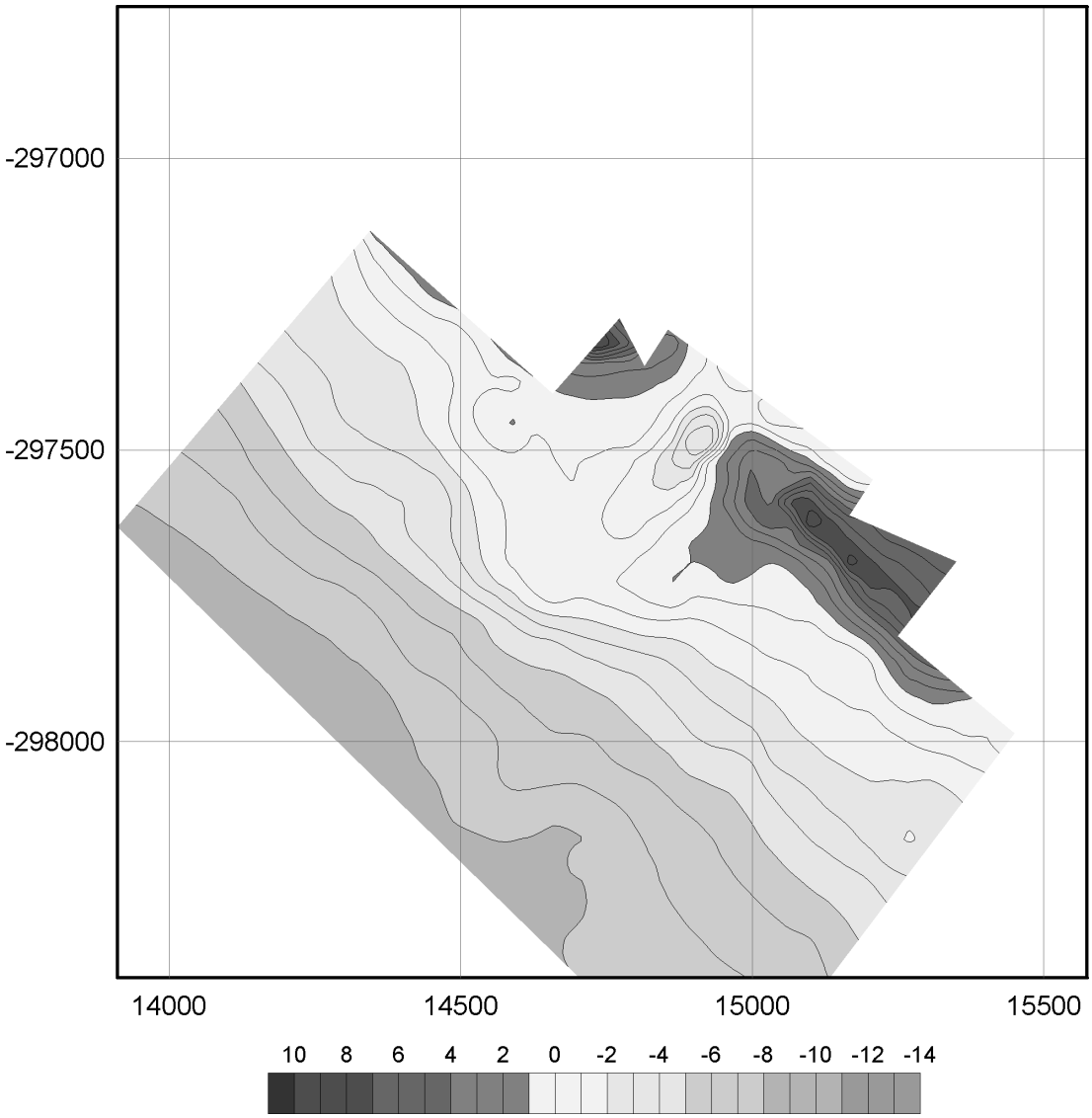

Figure A.2: Topo-bathymetric map of Ancão Inlet in April 1998. Metric coordinates refer to the Portuguese Melriça Grid. Elevation is in metres, relative to Portuguese Hydrographic Zero (Z.H.), defined as 2 m below mean sea level (MSL).

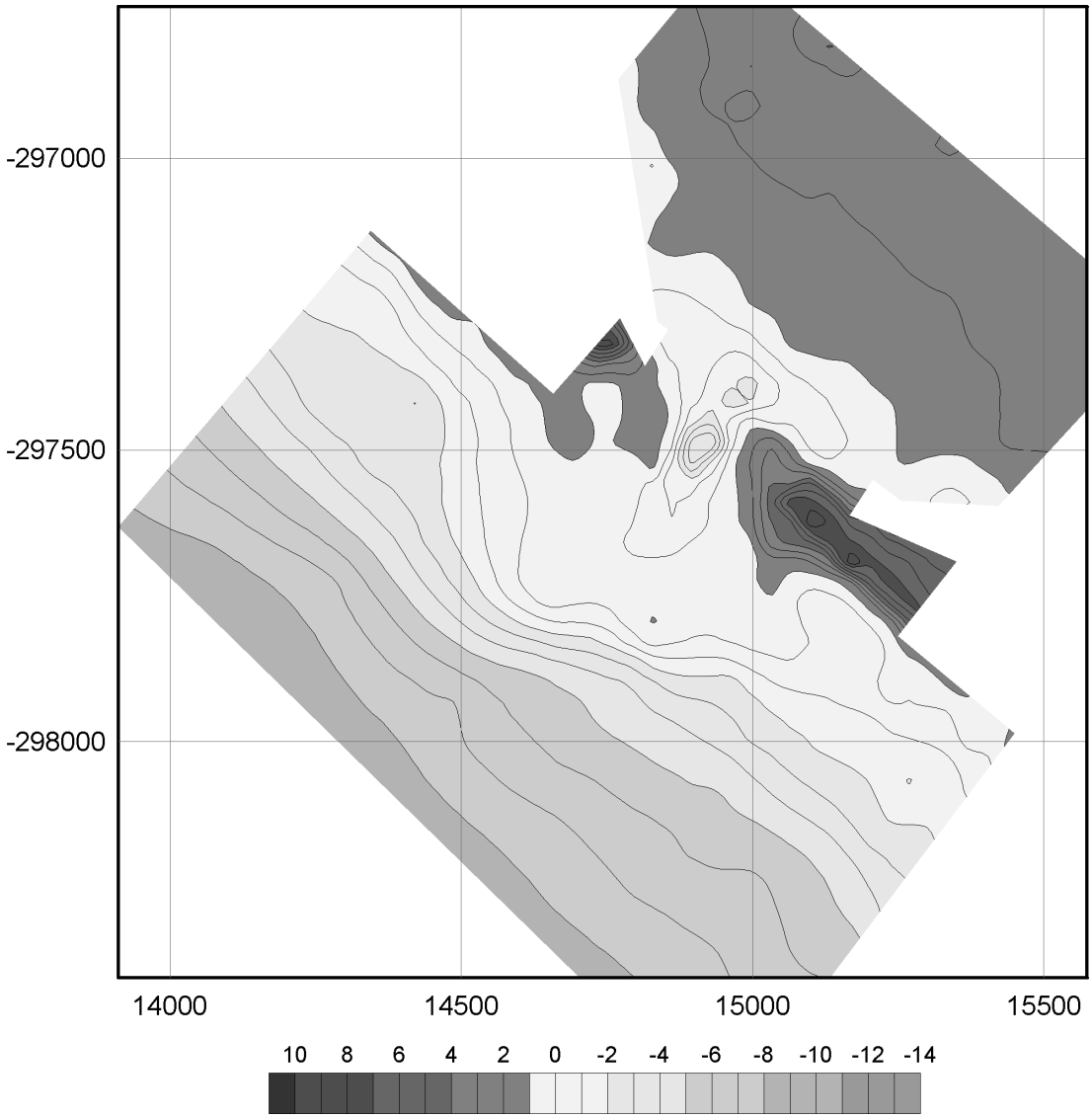

Figure A.3: Topo-bathymetric map of Ancão Inlet in July 1998. Metric coordinates refer to the Portuguese Melriça Grid. Elevation is in metres, relative to Portuguese Hydrographic Zero (Z.H.), defined as 2 m below mean sea level (MSL).

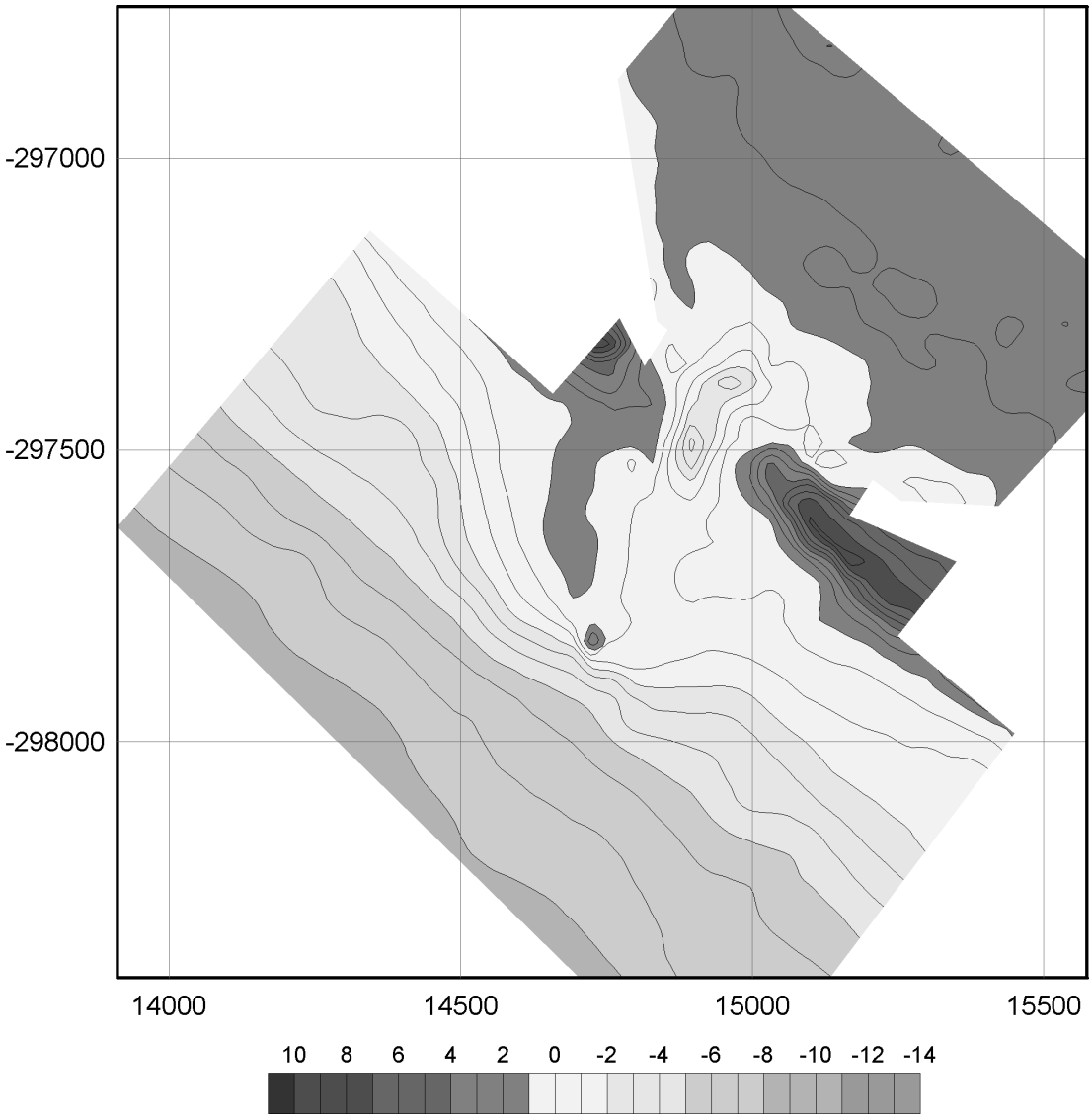

Figure A.4: Topo-bathymetric map of Ancão Inlet in October 1998. Metric coordinates refer to the Portuguese Melriça Grid. Elevation is in metres, relative to Portuguese Hydrographic Zero (Z.H.), defined as 2 m below mean sea level (MSL).

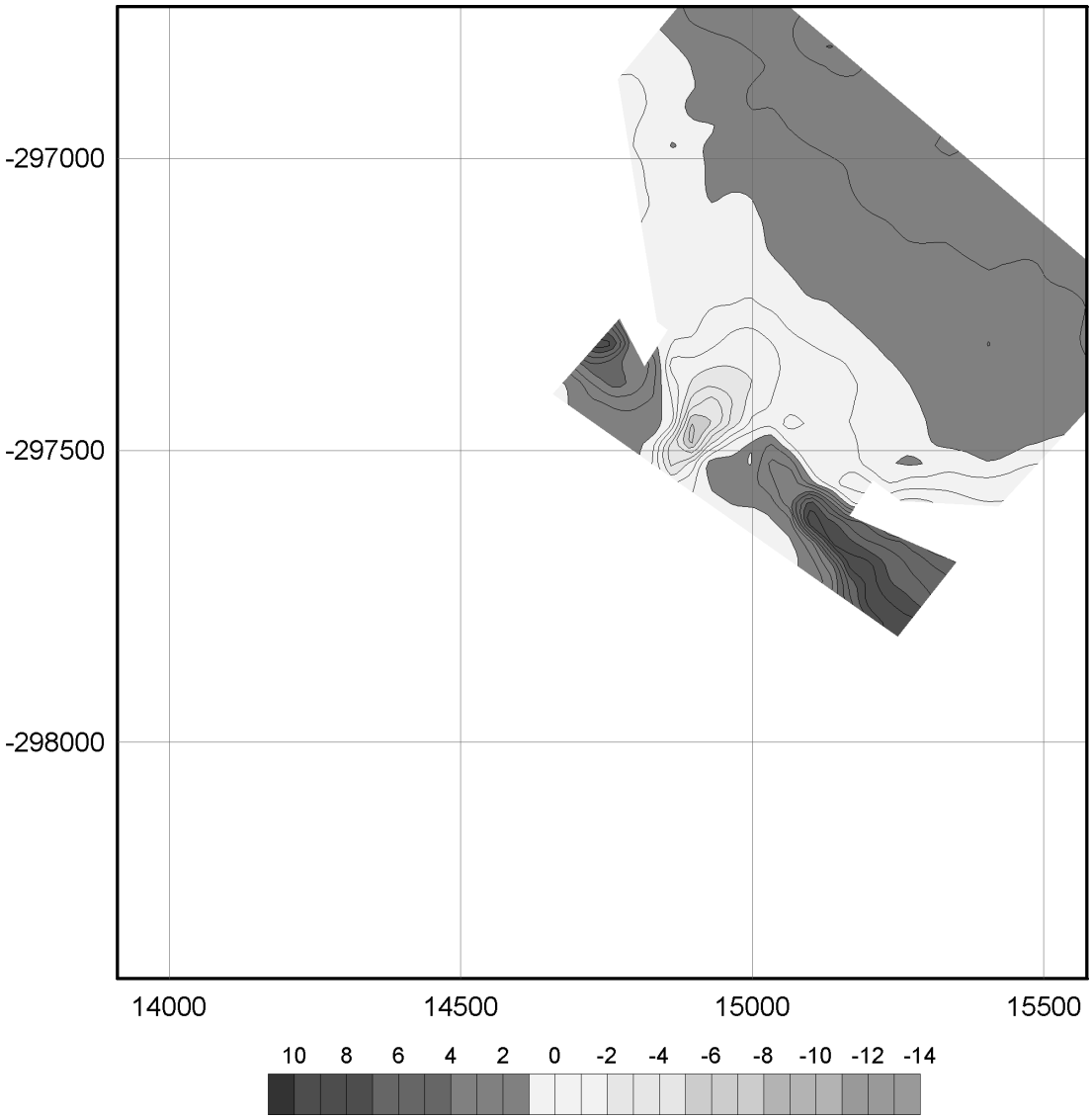

Figure A.5: Topo-bathymetric map of Ancão Inlet in December 1998. Metric co-ordinates refer to the Portuguese Melriça Grid. Elevation is in metres, relative to Portuguese Hydrographic Zero (Z.H.), defined as 2 m below mean sea level (MSL).

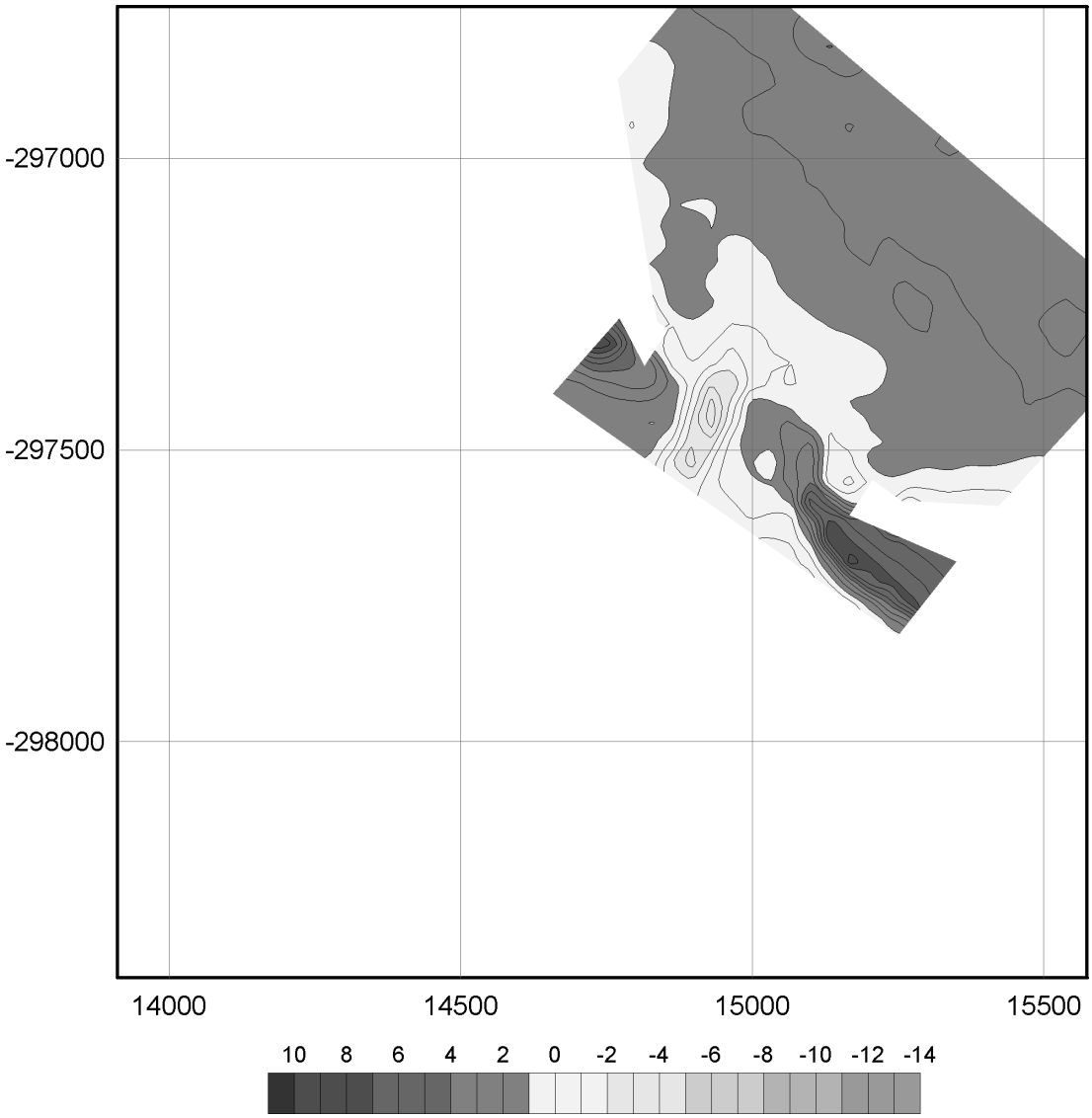

Figure A.6: Topo-bathymetric map of Ancão Inlet in January 1999. Metric coordinates refer to the Portuguese Melriça Grid. Elevation is in metres, relative to Portuguese Hydrographic Zero (Z.H.), defined as 2 m below mean sea level (MSL).

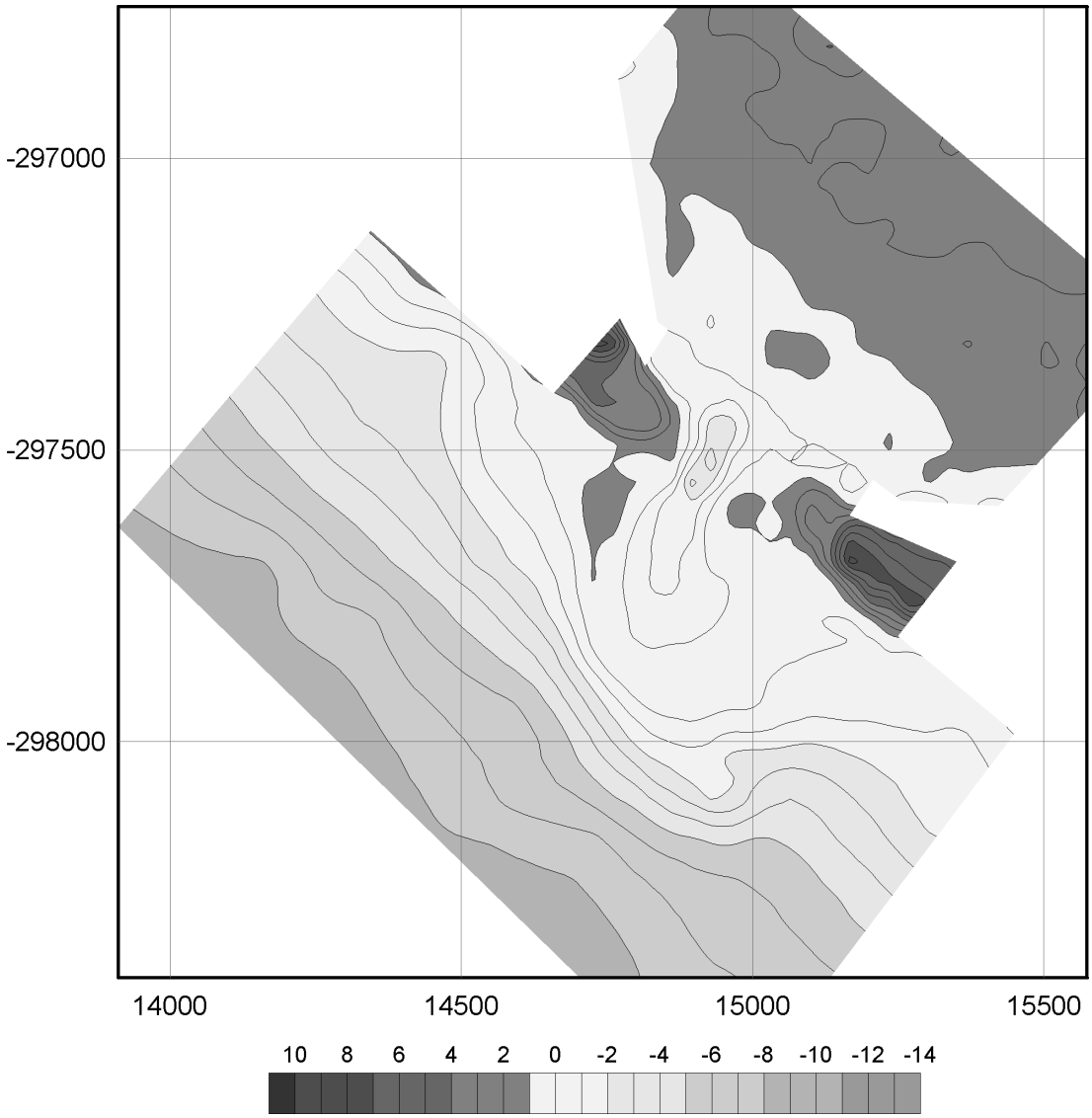

Figure A.7: Topo-bathymetric map of Ancão Inlet in May 1999. Metric coordinates refer to the Portuguese Melriça Grid. Elevation is in metres, relative to Portuguese Hydrographic Zero (Z.H.), defined as 2 m below mean sea level (MSL).

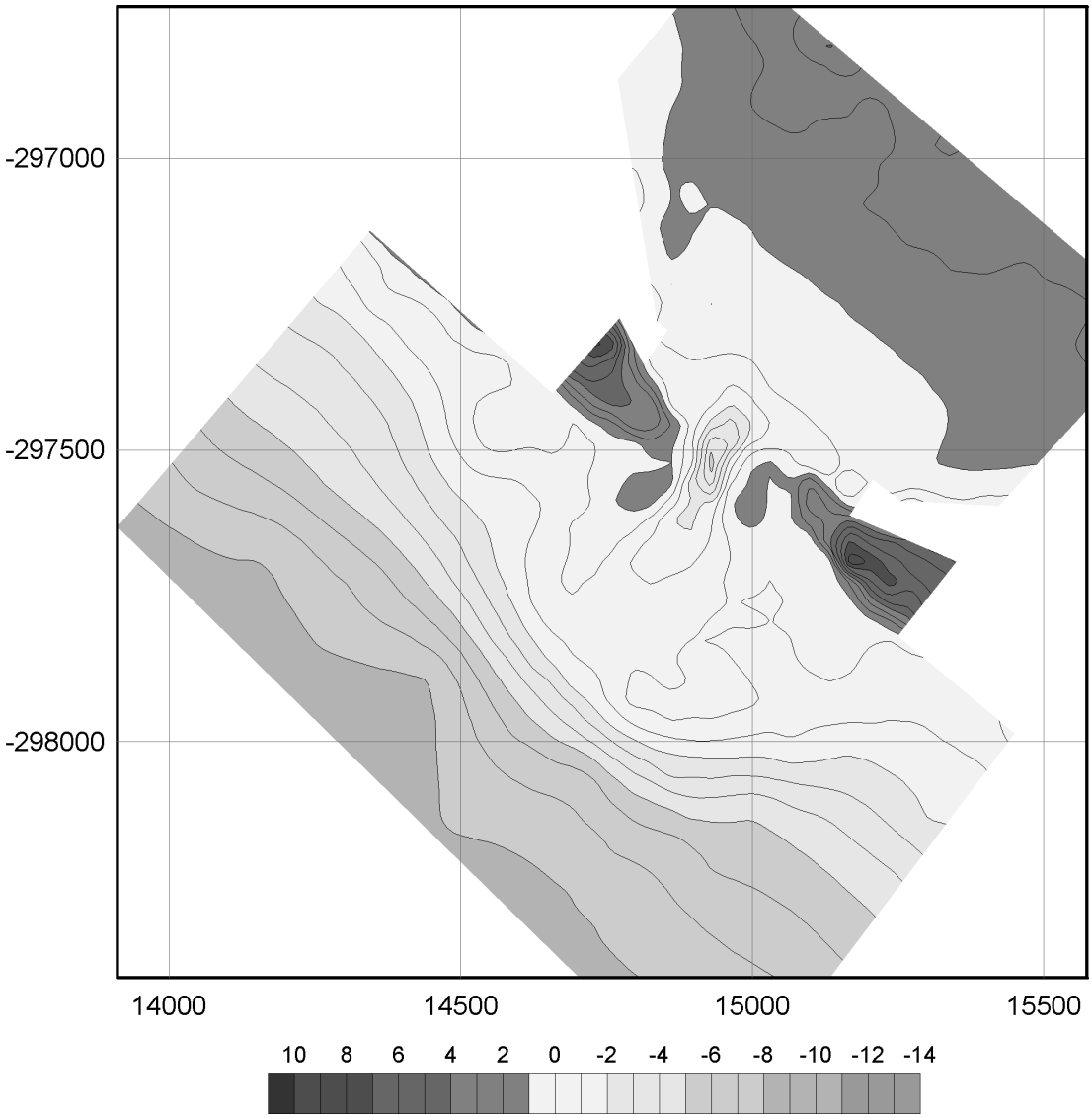

Figure A.8: Topo-bathymetric map of Ancão Inlet in July 1999. Metric coordinates refer to the Portuguese Melriça Grid. Elevation is in metres, relative to Portuguese Hydrographic Zero (Z.H.), defined as 2 m below mean sea level (MSL).

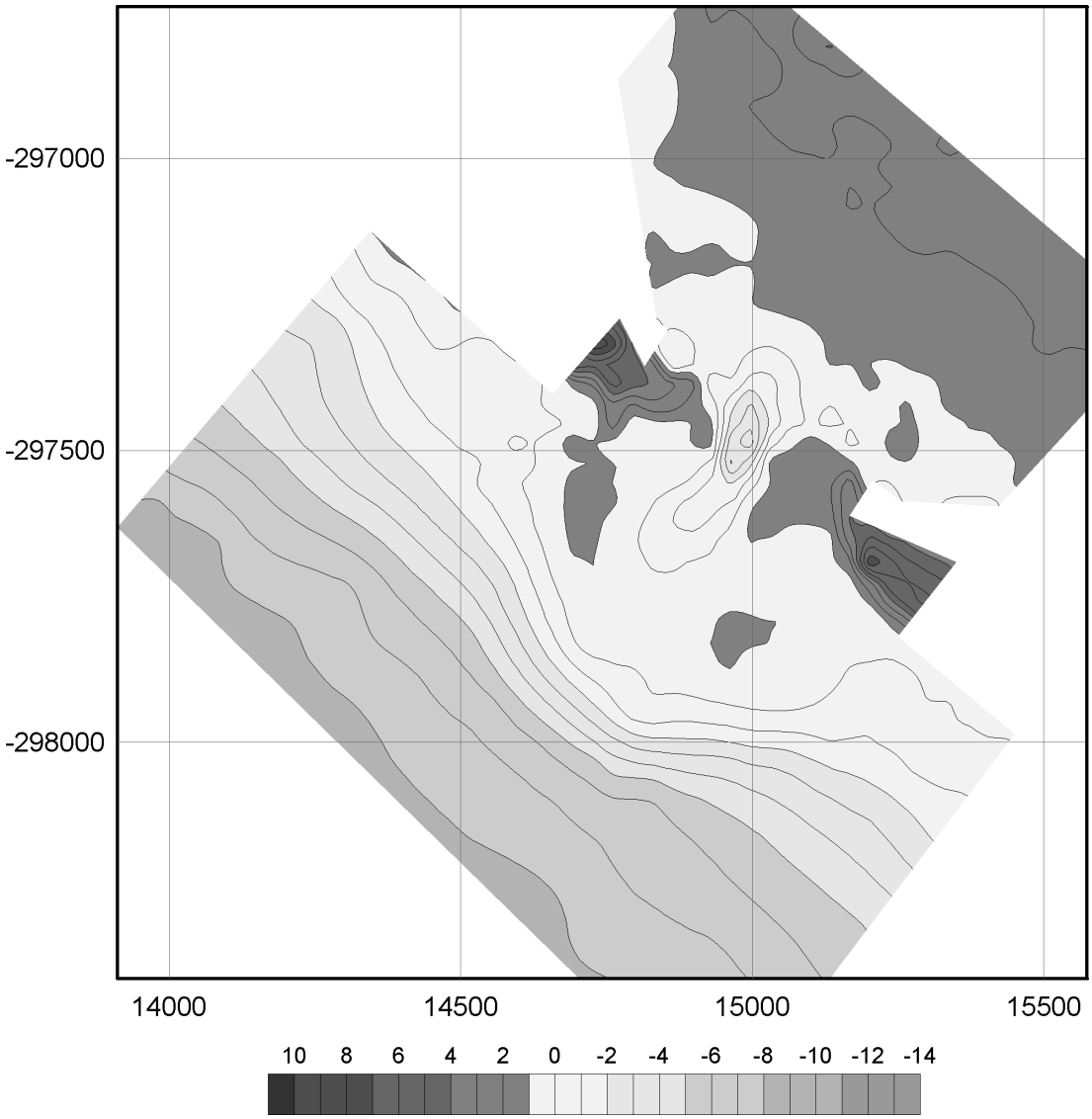

Figure A.9: Topo-bathymetric map of Ancão Inlet in November 1999. Metric co-ordinates refer to the Portuguese Melriça Grid. Elevation is in metres, relative to Portuguese Hydrographic Zero (Z.H.), defined as 2 m below mean sea level (MSL).

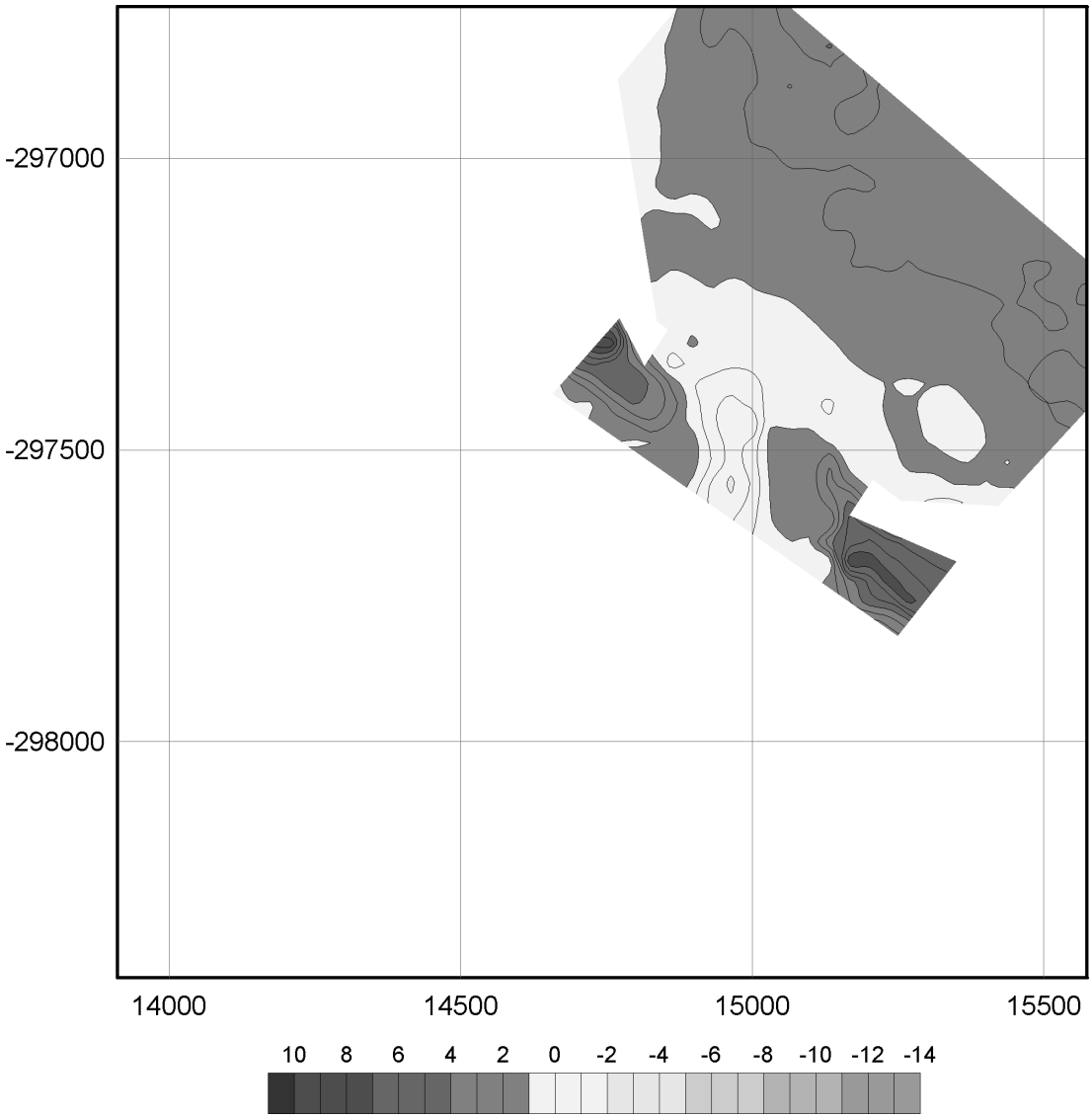

Figure A.10: Topo-bathymetric map of Ancão Inlet in January 2000. Metric coordinates refer to the Portuguese Melriça Grid. Elevation is in metres, relative to Portuguese Hydrographic Zero (Z.H.), defined as 2 m below mean sea level (MSL).

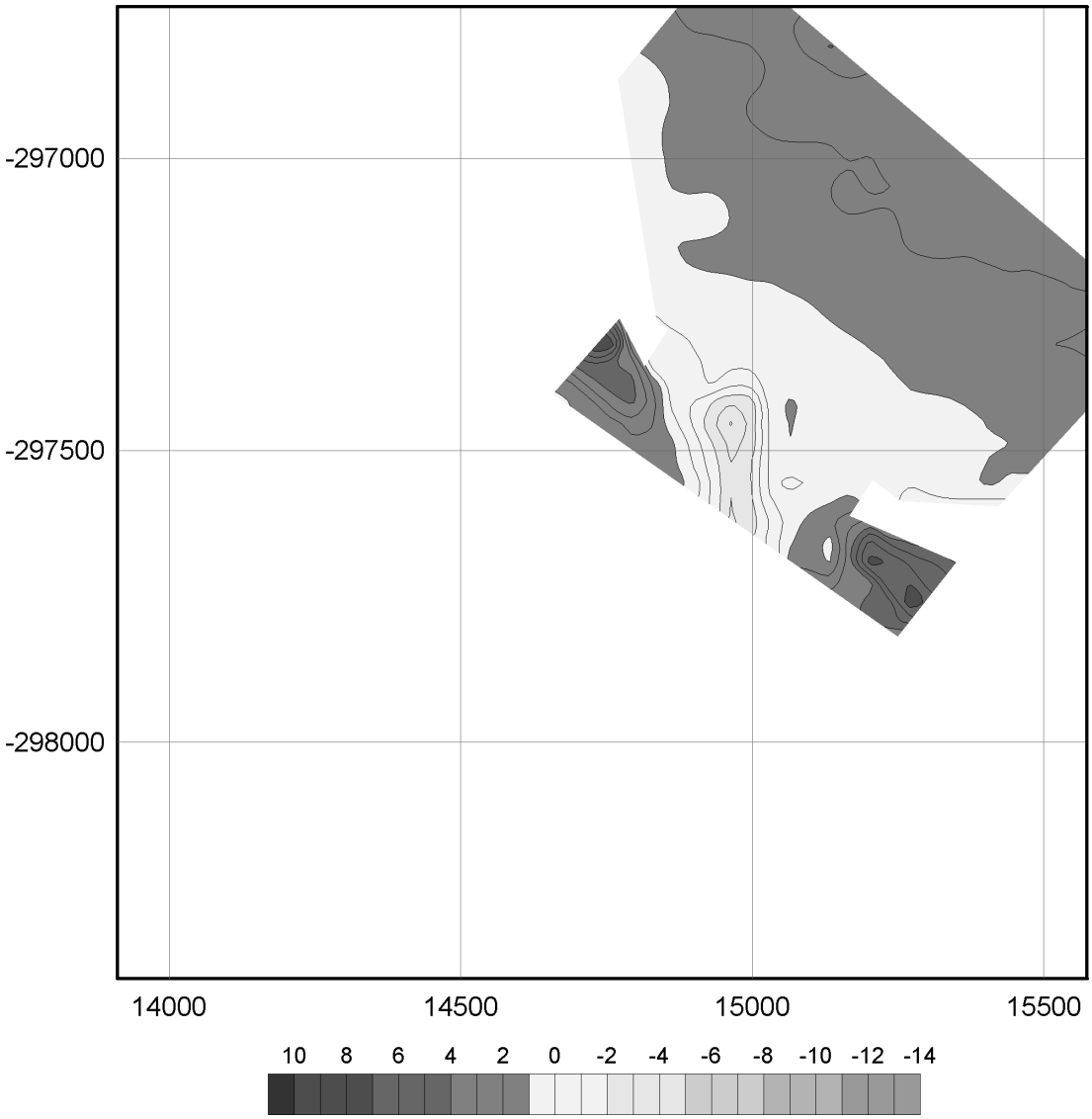

Figure A.11: Topo-bathymetric map of Ancão Inlet in March 2000. Metric coordinates refer to the Portuguese Melriça Grid. Elevation is in metres, relative to Portuguese Hydrographic Zero (Z.H.), defined as 2 m below mean sea level (MSL).

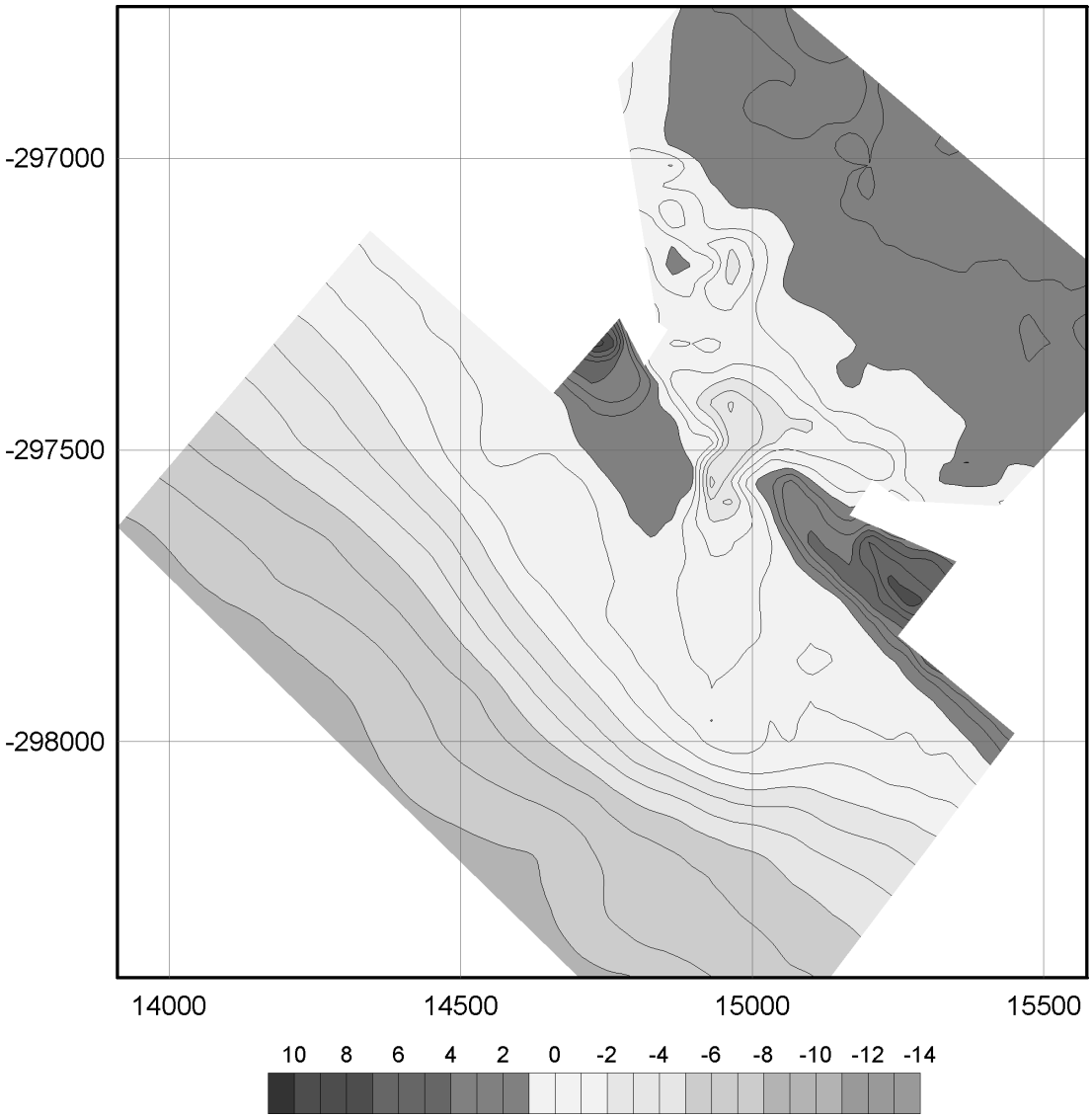

Figure A.12: Topo-bathymetric map of Ancão Inlet in June 2000. Metric coordinates refer to the Portuguese Melriça Grid. Elevation is in metres, relative to Portuguese Hydrographic Zero (Z.H.), defined as 2 m below mean sea level (MSL).

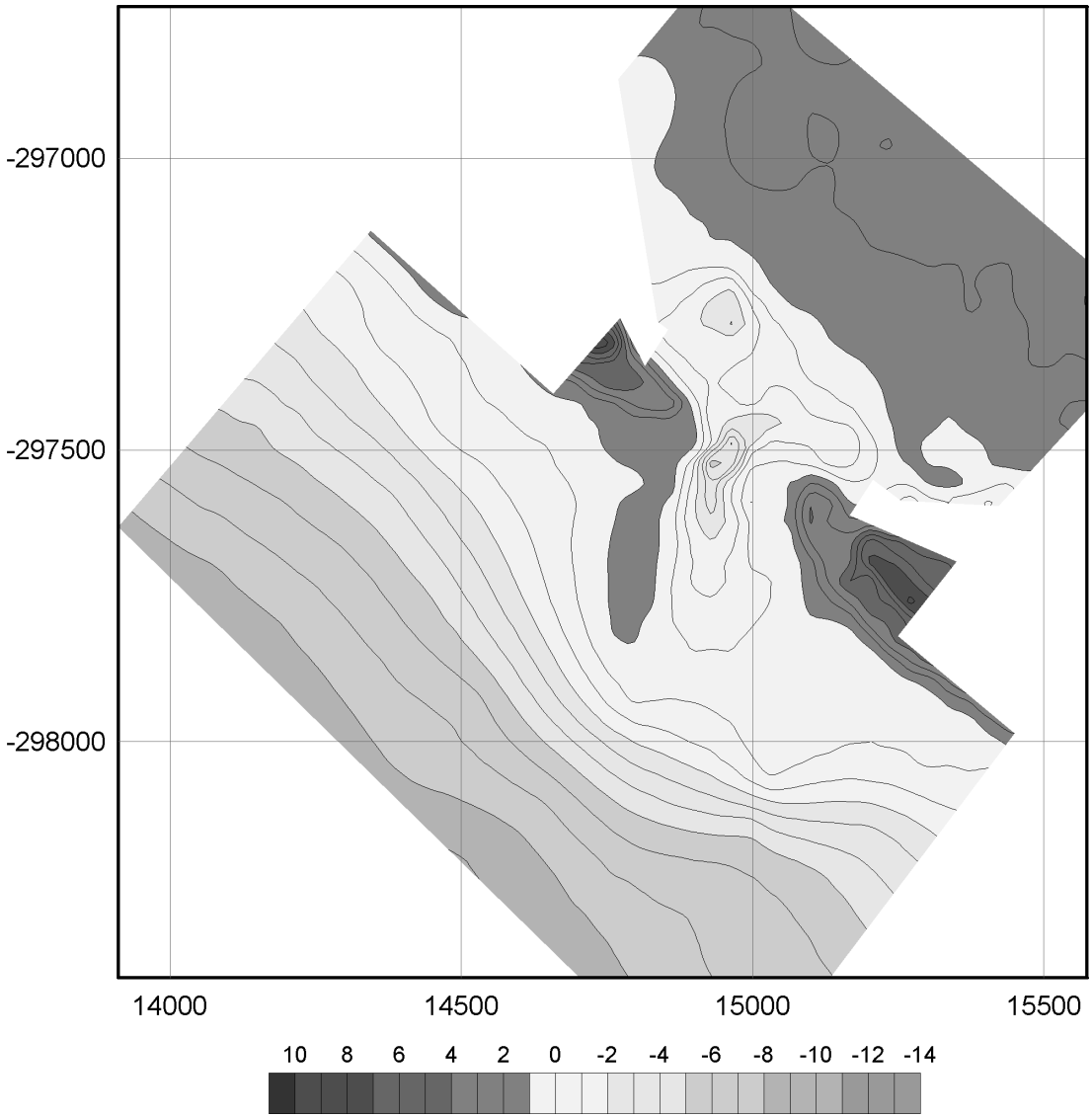

Figure A.13: Topo-bathymetric map of Ancão Inlet in September 2000. Metric co-ordinates refer to the Portuguese Melriça Grid. Elevation is in metres, relative to Portuguese Hydrographic Zero (Z.H.), defined as 2 m below mean sea level (MSL).

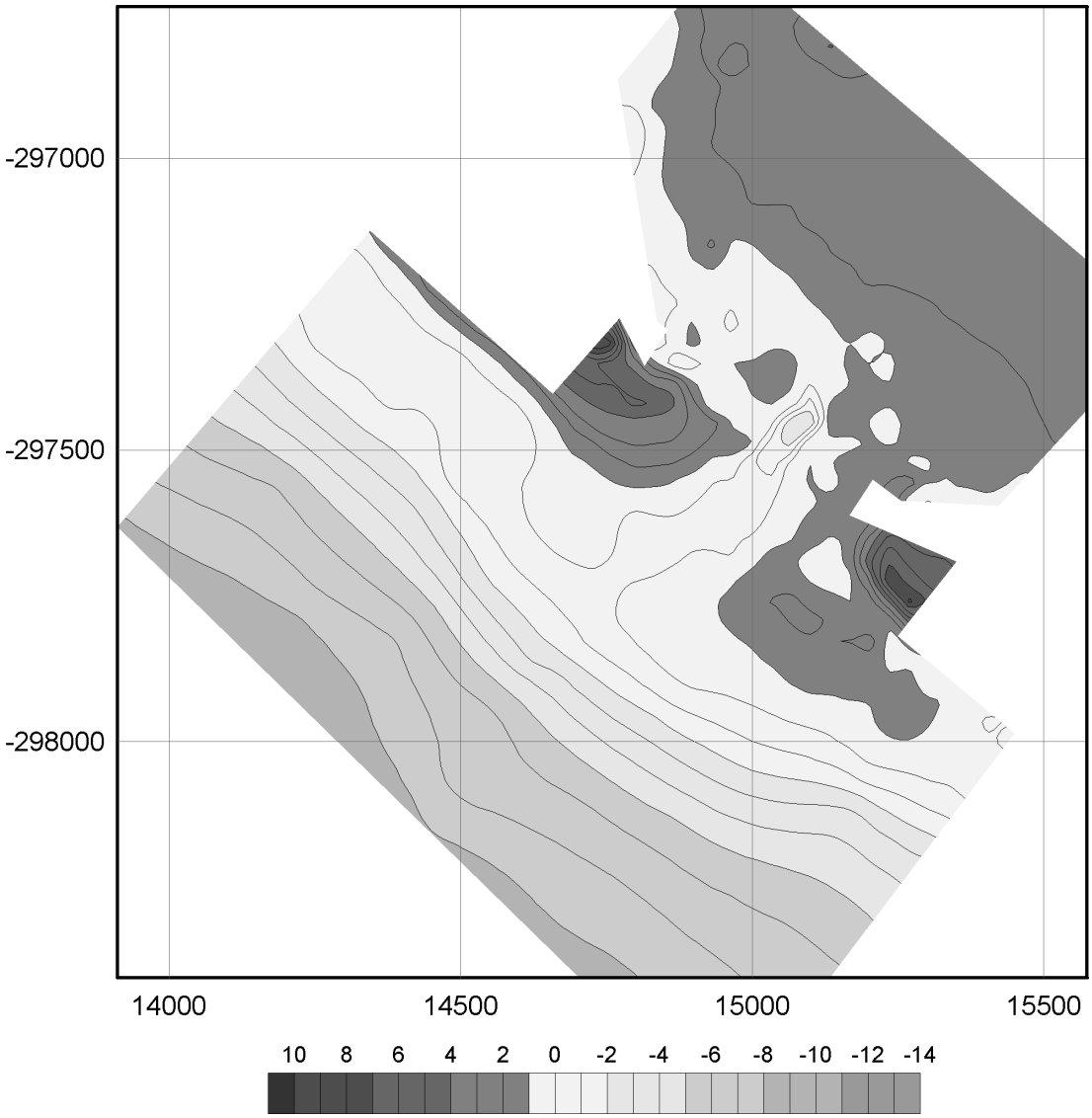

Figure A.14: Topo-bathymetric map of Ancão Inlet in January 2001. Metric coordinates refer to the Portuguese Melriça Grid. Elevation is in metres, relative to Portuguese Hydrographic Zero (Z.H.), defined as 2 m below mean sea level (MSL).

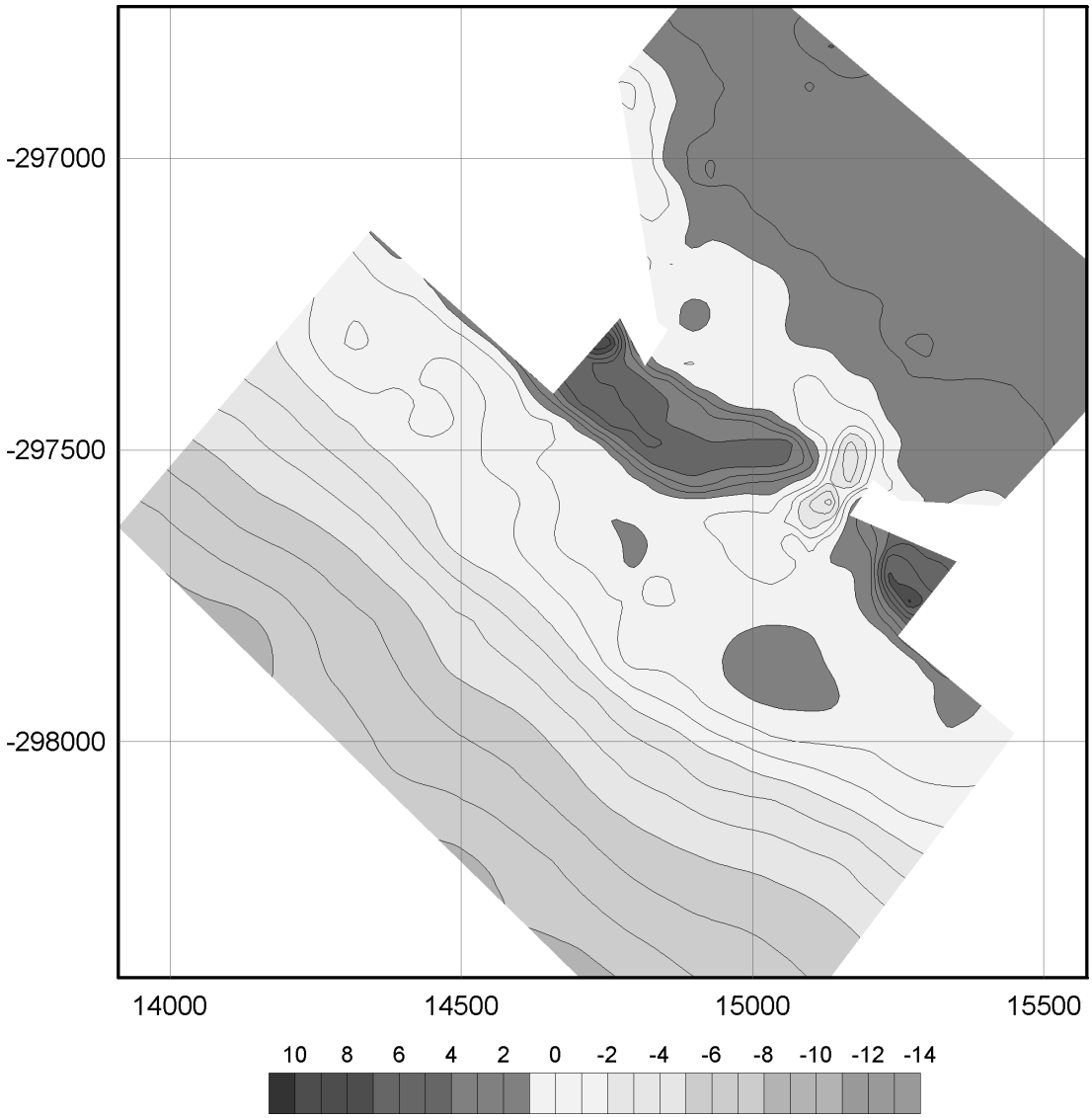

Figure A.15: Topo-bathymetric map of Ancão Inlet in April 2001. Metric coordinates refer to the Portuguese Melriça Grid. Elevation is in metres, relative to Portuguese Hydrographic Zero (Z.H.), defined as 2 m below mean sea level (MSL).

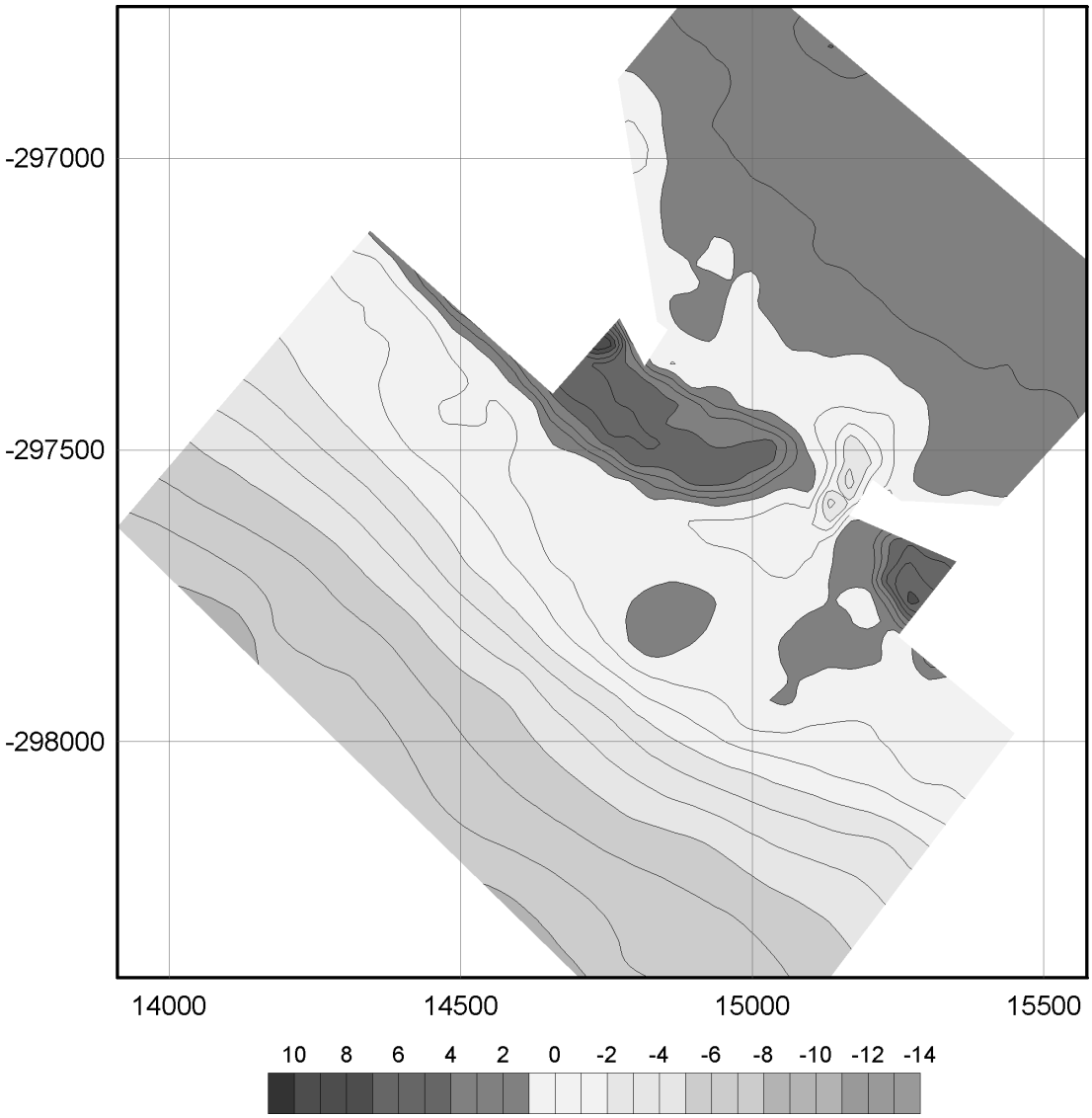

Figure A.16: Topo-bathymetric map of Ancão Inlet in July 2001. Metric coordinates refer to the Portuguese Melriça Grid. Elevation is in metres, relative to Portuguese Hydrographic Zero (Z.H.), defined as 2 m below mean sea level (MSL).

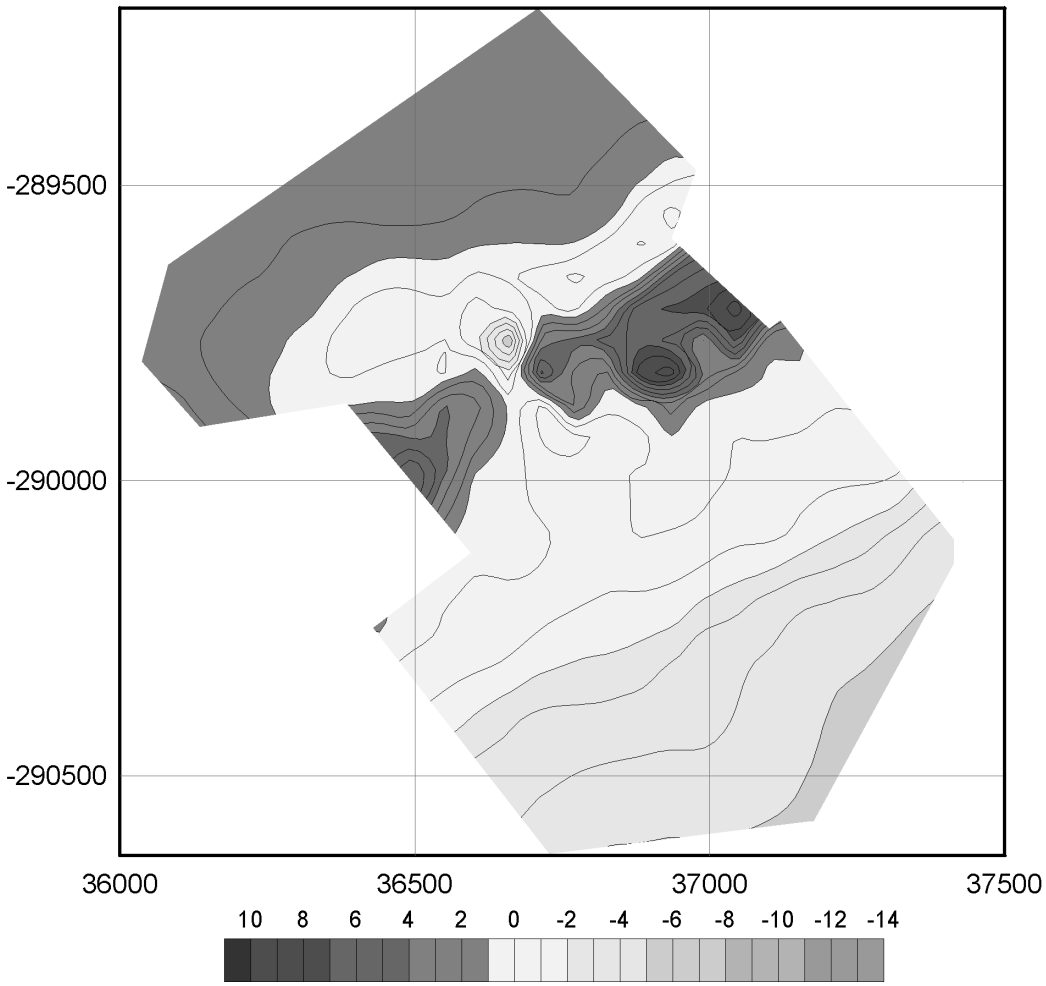

Figure A.17: Topo-bathymetric map of Fuzeta Inlet in December 1999. Metric co-ordinates refer to the Portuguese Melriça Grid. Elevation is in metres, relative to Portuguese Hydrographic Zero (Z.H.), defined as 2 m below mean sea level (MSL).

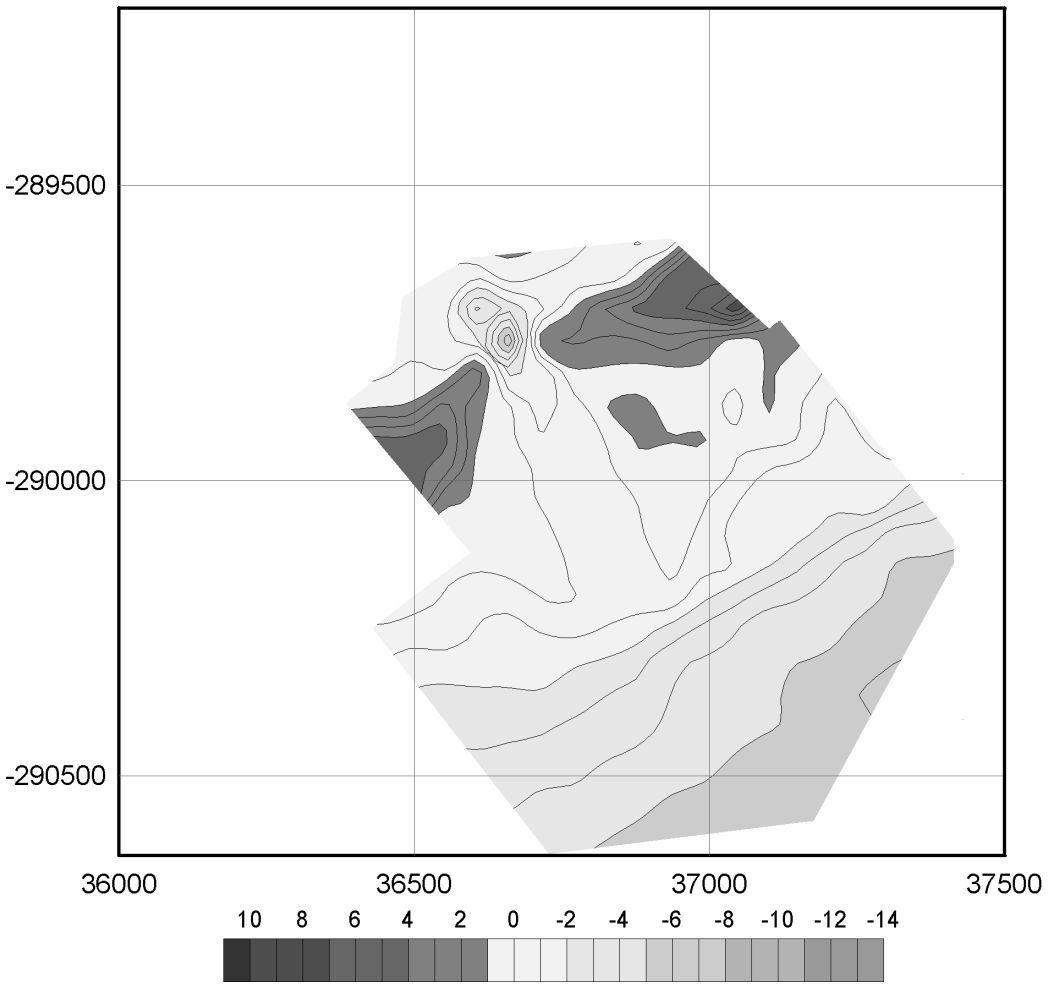

Figure A.18: Topo-bathymetric map of Fuzeta Inlet in February 2000. Metric co-ordinates refer to the Portuguese Melriça Grid. Elevation is in metres, relative to Portuguese Hydrographic Zero (Z.H.), defined as 2 m below mean sea level (MSL).

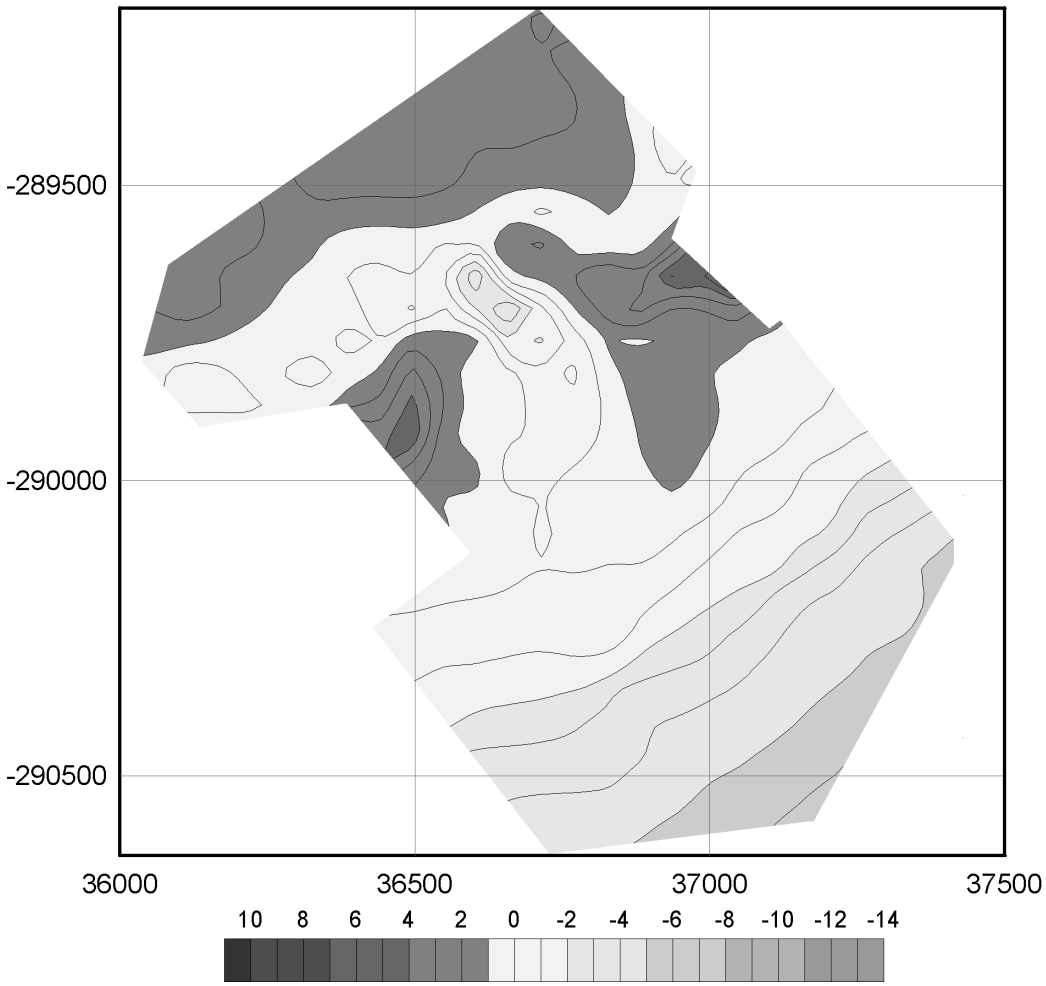

Figure A.19: Topo-bathymetric map of Fuzeta Inlet in July 2000. Metric coordinates refer to the Portuguese Melriça Grid. Elevation is in metres, relative to Portuguese Hydrographic Zero (Z.H.), defined as 2 m below mean sea level (MSL).

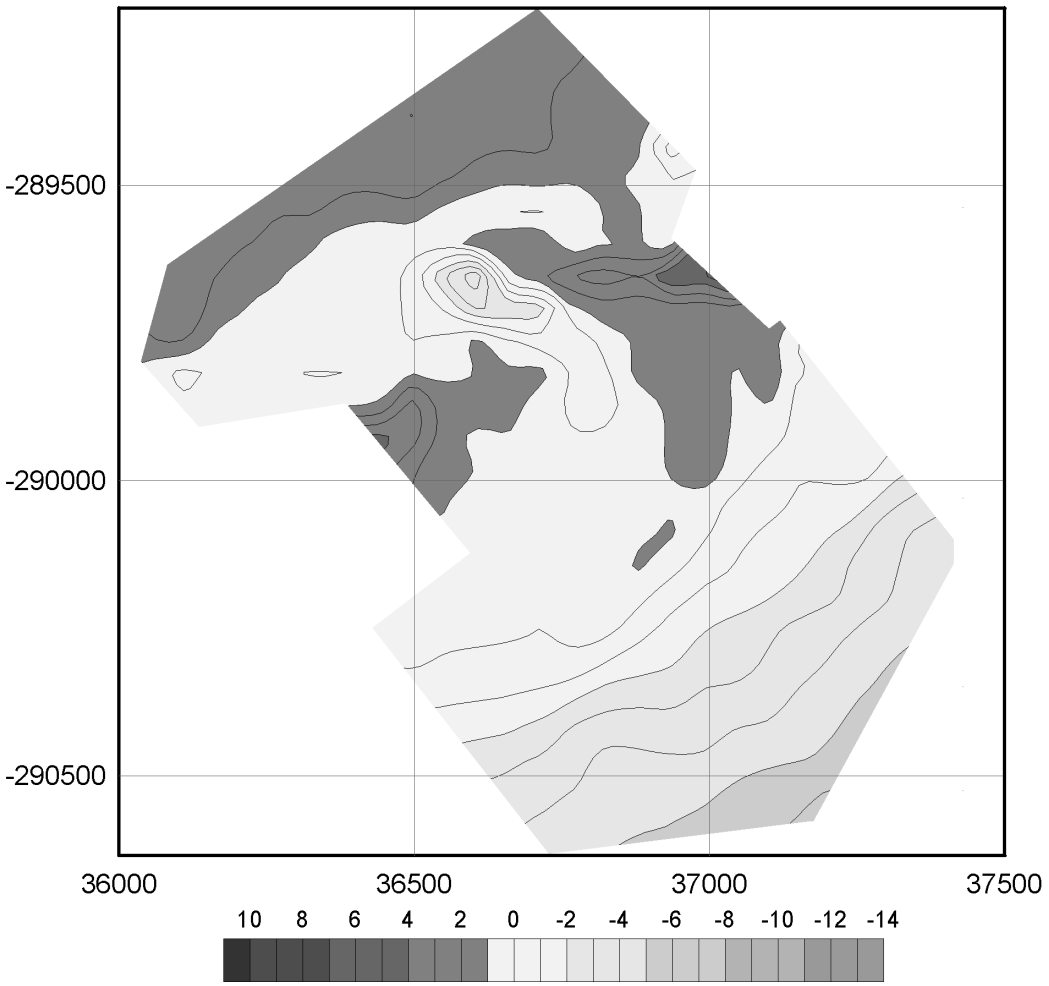

Figure A.20: Topo-bathymetric map of Fuzeta Inlet in October 2000. Metric co-ordinates refer to the Portuguese Melriça Grid. Elevation is in metres, relative to Portuguese Hydrographic Zero (Z.H.), defined as 2 m below mean sea level (MSL).

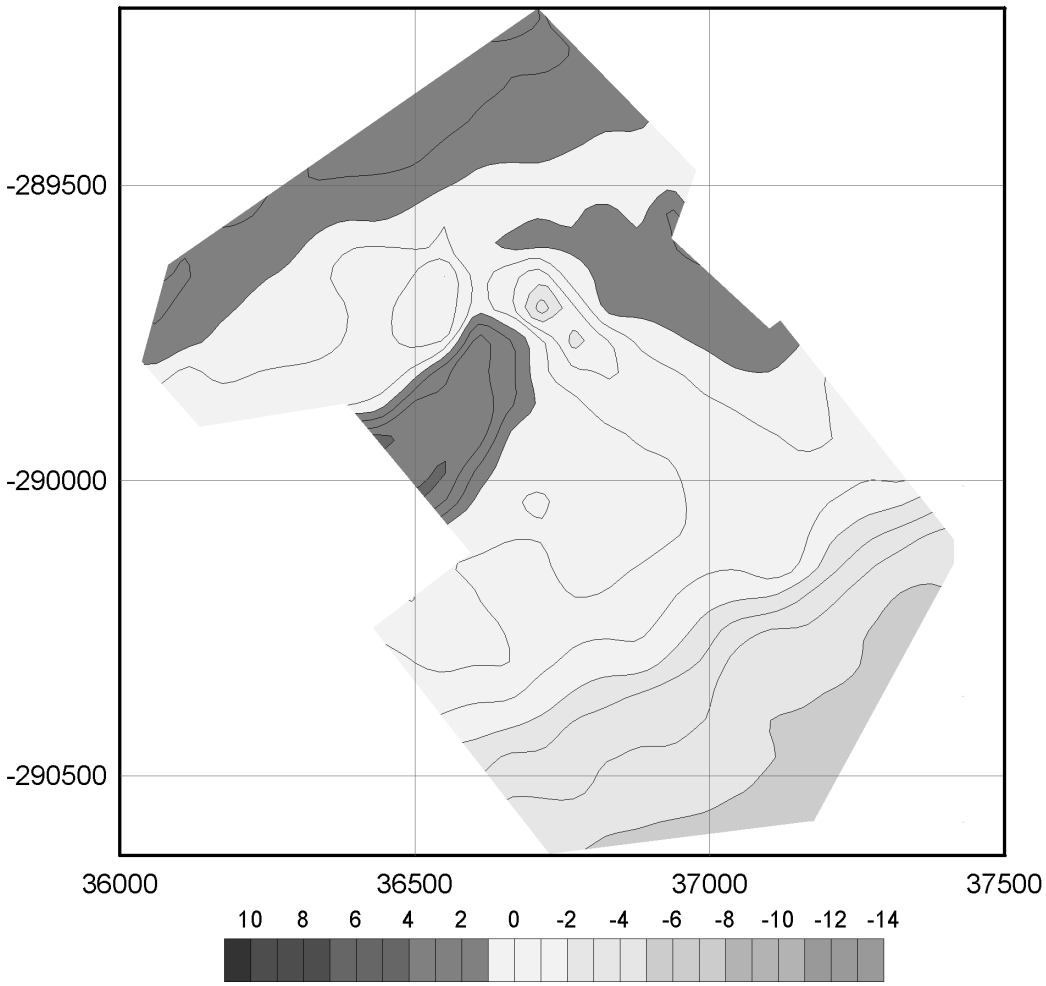

Figure A.21: Topo-bathymetric map of Fuzeta Inlet in April 2001. Metric coordinates refer to the Portuguese Melriça Grid. Elevation is in metres, relative to Portuguese Hydrographic Zero (Z.H.), defined as 2 m below mean sea level (MSL).

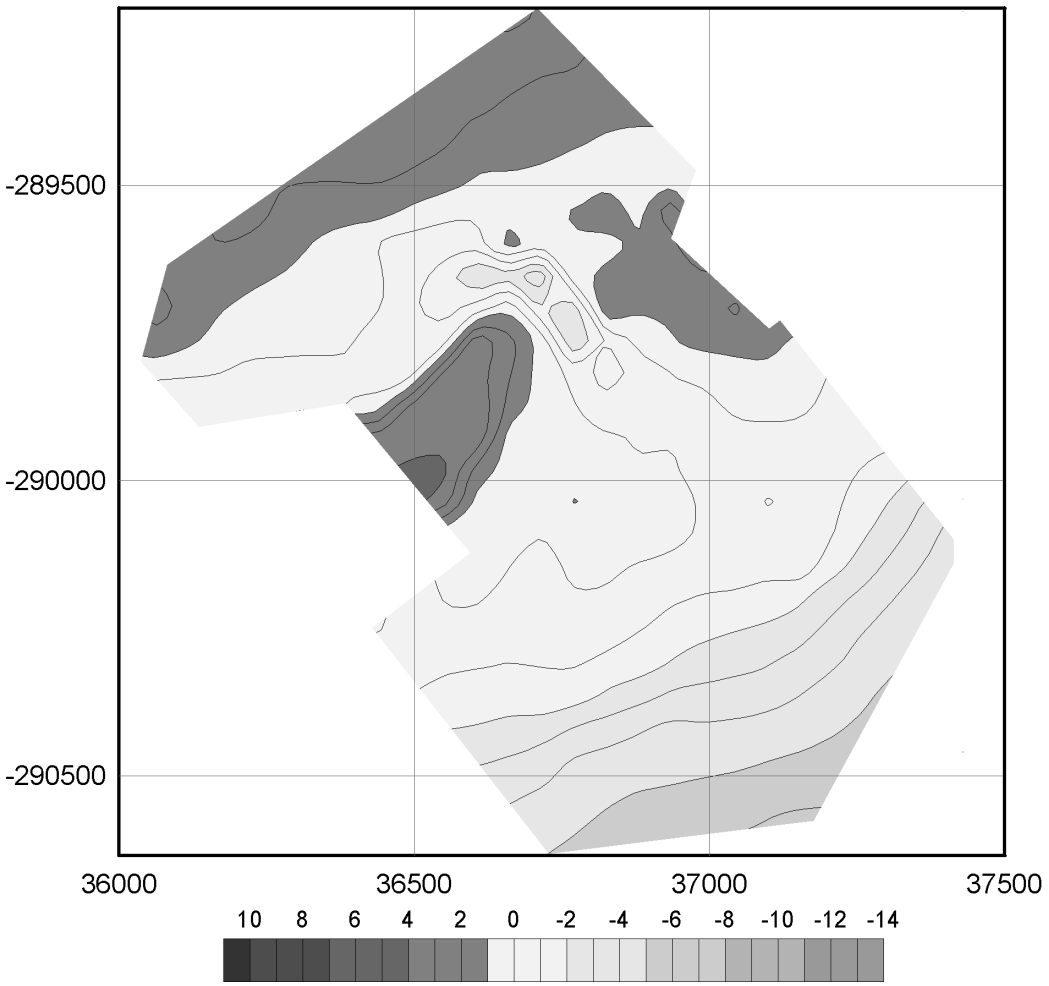

Figure A.22: Topo-bathymetric map of Fuzeta Inlet in June 2001. Metric coordinates refer to the Portuguese Melriça Grid. Elevation is in metres, relative to Portuguese Hydrographic Zero (Z.H.), defined as 2 m below mean sea level (MSL).

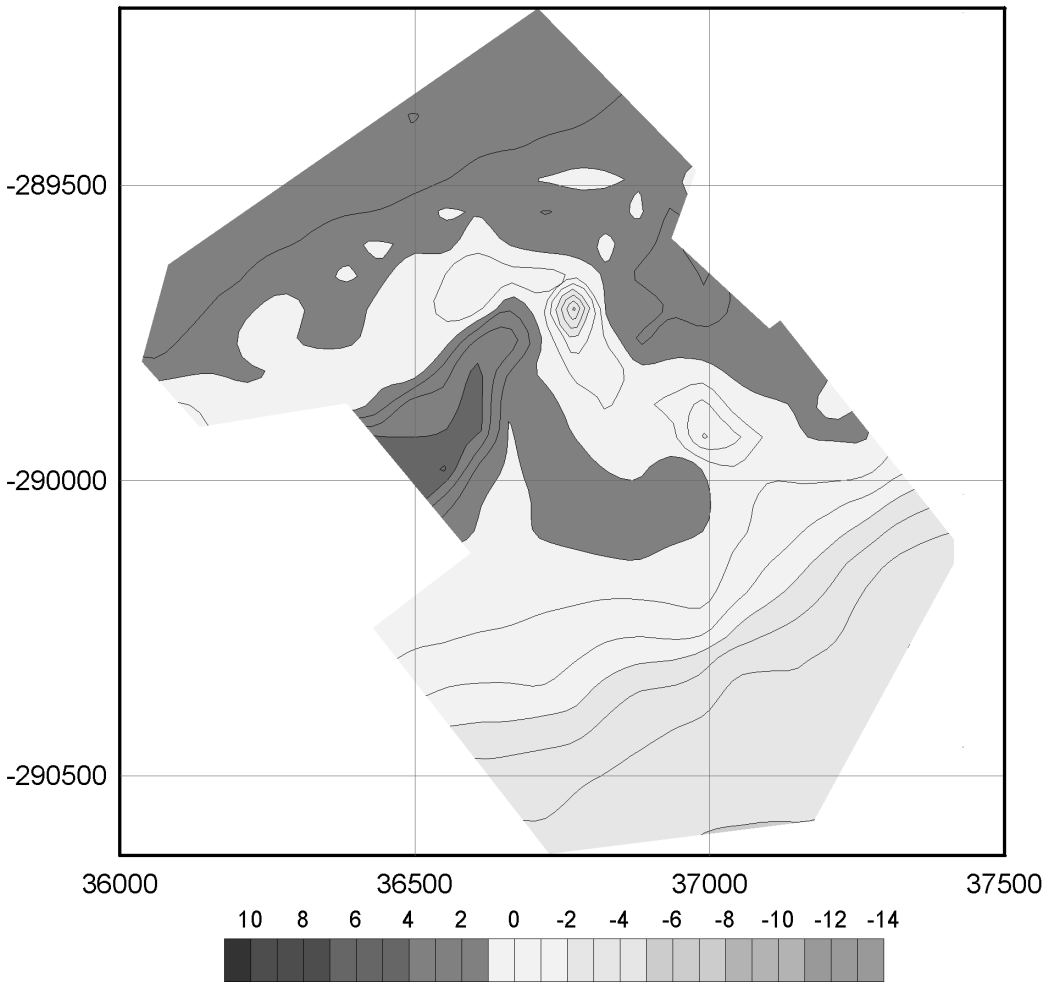

Figure A.23: Topo-bathymetric map of Fuzeta Inlet in August 2001. Metric coordinates refer to the Portuguese Melriça Grid. Elevation is in metres, relative to Portuguese Hydrographic Zero (Z.H.), defined as 2 m below mean sea level (MSL).